THE UNIVERSITY OF WARWICK

Library Declaration and Deposit Agreement

1. STUDENT DETAILS *Please*

complete the following:

Full name: .....

University ID number: .....

2. THESIS DEPOSIT

2.1 I understand that under my registration at the University, I am required to deposit my thesis with the University in BOTH hard copy and in digital format. The digital version should normally be saved as a single pdf file.

2.2 The hard copy will be housed in the University Library. The digital version will be deposited in the University's Institutional Repository (WRAP). Unless otherwise indicated (see 2.3 below) this will be made openly accessible on the Internet and will be supplied to the British Library to be made available online via its Electronic Theses Online Service (EThOS) service.
[At present, theses submitted for a Master's degree by Research (MA, MSc, LLM, MS or MMedSci) are not being deposited in WRAP and not being made available via EthOS. This may change in future.]

2.3 In exceptional circumstances, the Chair of the Board of Graduate Studies may grant permission for an embargo to be placed on public access to the hard copy thesis for a limited period. It is also possible to apply separately for an embargo on the digital version. (Further information is available in the *Guide to Examinations for Higher Degrees by Research* .)

2.4 *If you are depositing a thesis for a Master's degree by Research, please complete section (a) below. For all other research degrees, please complete both sections (a) and (b) below:*

(a) Hard Copy

I hereby deposit a hard copy of my thesis in the University Library to be made publicly available to readers (please delete as appropriate) EITHER immediately OR after an embargo period of ..... months/years as agreed by the Chair of the Board of Graduate Studies.

I agree that my thesis may be photocopied. YES / NO (*Please delete as appropriate*)

(b) Digital Copy

I hereby deposit a digital copy of my thesis to be held in WRAP and made available via EThOS.

Please choose one of the following options:

EITHER My thesis can be made publicly available online. YES / NO (*Please delete as appropriate*)

OR My thesis can be made publicly available only after ..... [date] (Please give date)
YES / NO (*Please delete as appropriate*)

OR My full thesis cannot be made publicly available online but I am submitting a separately identified additional, abridged version that can be made available online.
YES / NO (*Please delete as appropriate*)

OR My thesis cannot be made publicly available online. YES / NO (*Please delete as appropriate*)

3 GRANTING OF NON-EXCLUSIVE RIGHTS

Whether I deposit my Work personally or through an assistant or other agent, I agree to the following:

Rights granted to the University of Warwick and the British Library and the user of the thesis through this agreement are non-exclusive. I retain all rights in the thesis in its present version or future versions. I agree that the institutional repository administrators and the British Library or their agents may, without changing content, digitise and migrate the thesis to any medium or format for the purpose of future preservation and accessibility.

4 DECLARATIONS

(a) I DECLARE THAT:

- I am the author and owner of the copyright in the thesis and/or I have the authority of the authors and owners of the copyright in the thesis to make this agreement. Reproduction of any part of this thesis for teaching or in academic or other forms of publication is subject to the normal limitations on the use of copyrighted materials and to the proper and full acknowledgement of its source.
- The digital version of the thesis I am supplying is the same version as the final, hardbound copy submitted in completion of my degree, once any minor corrections have been completed.
- I have exercised reasonable care to ensure that the thesis is original, and does not to the best of my knowledge break any UK law or other Intellectual Property Right, or contain any confidential material.

I understand that, through the medium of the Internet, files will be available to automated agents, and may be searched and copied by, for example, text mining and plagiarism detection software.

(b) IF I HAVE AGREED (in Section 2 above) TO MAKE MY THESIS PUBLICLY AVAILABLE DIGITALLY, I ALSO DECLARE THAT:

- I grant the University of Warwick and the British Library a licence to make available on the Internet the thesis in digitised format through the Institutional Repository and through the British Library via the EThOS service.

If my thesis does include any substantial subsidiary material owned by third-party copyright holders, I have sought and obtained permission to include it in any version of my thesis available in digital format and that this permission encompasses the rights that I have granted to the University of Warwick and to the British Library.

5. LEGAL INFRINGEMENTS

I understand that neither the University of Warwick nor the British Library have any obligation to take legal action on behalf of myself, or other rights holders, in the event of infringement of intellectual property rights, breach of contract or of any other right, in the thesis.

Student's signature: ..... Date: .....

Organometallic Osmium Arene

Anticancer Complexes

A Thesis Submitted for the Degree of

Doctor of Philosophy

By

Ying Fu, *M. Sc.*

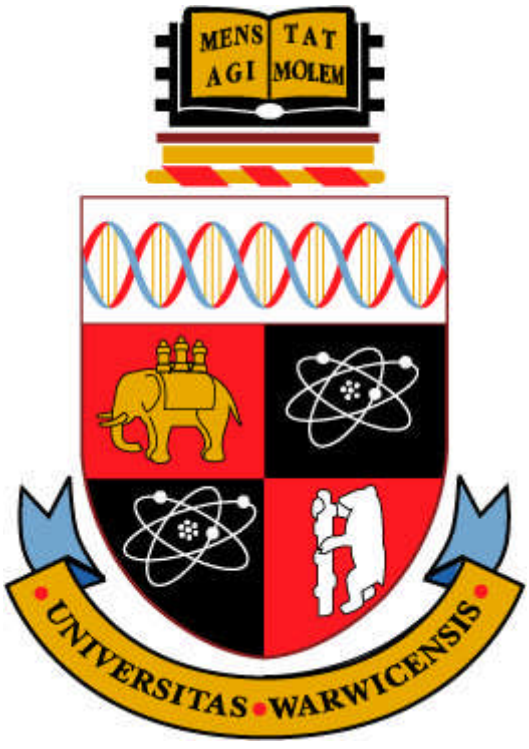

University of Warwick, Department of Chemistry

December 2011

Contents

Acknowledgements

First of all, I would like to thank Professor Peter John Sadler for his supervision and encouragement throughout my project. I really appreciate for everything that he taught me and for the opportunities and encouragement he has given me to explore different interesting areas of research. I have totally enjoyed studying and working in the PJS group.

Many thanks to the PJS group members, past and present. Thank you so much for your support in my research, I am very grateful to have made lots of friends! I would like to give me special thanks to Dr. Abraha Habtemariam for his consistent help and assistance to run this project. Special thanks also to Dr. Ana M. Pizarro, Dr. Luca Salassa, Dr. Sabine H. van Rijt, Dr. Maria J. Romero, Dr. Nicky J. Farrer, Dr. Soledad Betanzos-Lara and Dr. Jun Du for all the collaborations and discussions.

Thanks to Mr. Darren Braddick and Prof. Tim Bugg for the help with plate reader; Dr. Lijiang Song for the help with mass spectrometry; Dr. Ivan Prokes for the help with NMR; Dr. Ian J. Portman for the help with confocal microscopy; Dr. Guy J. Clarkson for solving the crystal structures reported in this thesis; Prof. Robert Cross and his group for the help with the tubulin work; Dr. Rina Soni and Prof. Martin Wills for the help with the screening of hydrogen transfer catalysts; Dr. Michael E. Snowden, Dr. Massimo Peruffo and Prof. Patrick R. Unwin for the help on the redox experiments.

Thanks to Dr. Sarah J. Farley, Khatija Bhayat and Isolda Romero for discussions on the azopyridine ligands, osmium iodide complexes and iminopyridine ligands respectively. Special thanks to two master students who worked with me: Aida Basri and Madeleine Koh for their hard work and inspirations.

Thanks to Dr. Steve Shnyder (University of Bradford) and his team for the help of *in vivo* anticancer test.

Thanks for the financial support from Prof. Peter J. Sadler and University of Warwick.

Thanks to the Chinese Society in Warwick Chemistry and Warwick Biology, special thanks to Dr. Junliang Yang, Dr. Jing Chen, Dr. Buyu Lu, Mr. Lihong Li and Mr. Qiang Zhang for discussions.

Finally special thanks to my family for all the eternal support, help and patience. Particularly a special thanks to Ke Bai for her support and encouragement, especially in the last 3 months whilst I was writing up my thesis.

Ying Fu

Oct 2011

Declaration

I hereby declare that except where specific reference is made to other sources, the work contained in this thesis is the original work of the author. It has been composed by myself and has not been submitted, in whole or in part, for any other degree, diploma, or other qualification.

Some of the work presented in this thesis has been published:

1. **Y. Fu**, A. Habtemariam and P. J. Sadler, "Osmium Anti-cancer Complexes", **2010** (***UK Patent application No 1006762.7)***

2. **Y. Fu**, A. Habtemariam, A. M. Pizarro, S. H. van Rijt, D. J. Healey, P. A. Cooper, S. D. Shnyder, G. J. Clarkson and P. J. Sadler, Organometallic osmium arene complexes with potent cancer cell cytotoxicity, *J. Med. Chem.*, **2010**, 53, 8192-8196.

3. S. D. Shnyder, **Y. Fu**, A. Habtemariam, S. H van Rijt, P. A Cooper, P. M. Loadman, P. J. Sadler, Anti-colorectal cancer activity of an organometallic osmium arene azopyridine complex, *MedChemComm*, **2011**, 2, 666-668 (***hot paper***).

4. **Y. Fu**, A. Habtemariam, A. Basri, D. Braddick, G. J. Clarkson and P. J. Sadler, Structure-Activity Relationships for Osmium Phenylazopyridine Complexes with Potent Anticancer Activity, *Dalton Trans,* **2011**, 40, 10553-10562.

Ying Fu

Oct 2011

Courses Attended

(1) Transferable skills courses in Warwick Chemistry

(2) Weekly chemical biology seminars during term time: 2008-2011

(3) PhD courses in Warwick Chemistry

Conferences and Meetings Attended

(1) Y. Fu, S. D. Shnyder, A. Habtemariam, P. A. Cooper, P. M. Loadman, P. J. Sadler, "Organometallic osmium arene anticancer complexes", 242nd ACS National Meeting, Denver, Colorado, 2011, abstract BIOL17.

(2) Y. Fu and P. J. Sadler "Novel Chemotherapeutic Anticancer Agent Using Osmium", Postgraduate Research Symposium 2011 of Warwick Chemistry. **Best Talk Prize**.

(3) Y. Fu, A. Habtemariam, A.M. Pizarro, S. Van Rijt, G. Clarkson, P. J. Sadler; "Organometallic Osmium Arene Complexes with Potent Cancer cell Cytotoxicity" ISBOMC 10, 5 International Symposium on Bioorganometallic Chemistry, Ruhr-University Bochum, Germany, 2010, abstract P13.

Abstract

The interest in the development of anticancer metal complexes for cancer therapy is growing spurred by the encouraging successful stories of platinum drugs. Osmium arene chlorido complexes had been found to show anticancer activity *in vitro*. In this thesis, the osmium arene iodido complexes were mainly explored and investigated.

It is found that iodido Os^{II} arene complexes with a general structure: $[Os(\eta^6\text{-arene})(XY)I]PF_6$ (XY = *p*-hydroxy or *p*-dimethylamino phenylazopyridine, arene = *p*-cymene or biphenyl) are potently cytotoxic at nanomolar concentrations toward a panel of human cancer cell lines. In contrast to the chlorido osmium arene anticancer complexes, the iodido complexes are stable and inert toward aquation.

More than thirty half sandwich azopyridine Os^{II} arene complexes $[Os(\eta^6\text{-arene})(azopyridine)X]^+$ (where X is chloride or iodide, the arene is *p*-cymene or biphenyl and the pyridine ring of azopyridine ligand bearing a variety of substituents) were synthesized and characterized. A preliminary structure activity relationships (SARs) were built up based on the anticancer activity towards A2780 human ovarian cancer cell line. In general, the introduction of an electron-withdrawing group (e.g. F, Cl, Br or I) at specific positions on the pyridine ring significantly increases cytotoxic activity and aqueous solubility. Changing the arene from *p*-cymene to biphenyl or the monodentate ligand (X) from chloride to iodide resulted in a significant increase in the anticancer activity. Studies in A2780 human ovarian cancer cells suggested that cellular uptake and targeting to cellular organelles play important roles in determining the anticancer activity. According to the 60 cancer cell lines screening results from National Cancer Institute (NCI), the anticancer activity achieved by the most potent Os^{II} arene azopyridine complex is 100 times more than cisplatin; 1000 times activity was

found in some cell lines. The mechanism of action may involve the inhibition of tubulin polymerization.

One iodido osmium complex was selected for anticancer efficiency evaluation *in vivo*: $[Os(\eta^6\text{-}p\text{-cym})(Azpy\text{-}NMe_2)I]PF_6$ (FY026). This complex delayed the growth of HCT116 human colon cancer xenografts in mice, with negligible toxicity. It is the first example of *in vivo* antitumour activity for an organometallic osmium arene complex. Its activity appears to involve redox mechanisms. Its potency towards A2780 ovarian and A549 lung cancer cells is increased significantly when used in combination with L-buthionine-sulfoximine (L-BSO) indicating that L-BSO can be a good candidate for combination therapy treatment with iodido osmium complexes.

Further study on the bioisosteres of FY026 was carried out by changing the azo bond (N=N) to imine bond (CH=N). Sixteen osmium arene iminopyridine complexes were synthesized, well characterized and showed good anticancer activity. Different structure-activity relationships comparing iminopyridine complexes with azopyridine complexes were identified which suggested a different anticancer mechanism. In contrast to FY026, $[Os(\eta^6\text{-}p\text{-cym})(Impy\text{-}NMe_2)I]PF_6$ (**6)** and $[Os(\eta^6\text{-}p\text{-cym})(Impy\text{-}NMe_2)Cl]PF_6$ (**14)** were found to undergo hydrolysis and the binding was observed between their hydrolyzed product (**14A**) and 9-ethylguanine.

Moreover, a hydride transfer from NADH to form an osmium hydride intermediate which is involved in a catalytic process resulting in the formation of NAD^+ was discovered. This process might be involved in the anticancer mechanism of action. A dual mechanism of action was proposed based in the interaction of these compounds with DNA nucleobase and catalytic oxidation of NADH.

Abbreviations

Å	Angstrom
Azpy	Azopyridine
bip	biphenyl
bpy	2,2' -bipyridine
ca.	*circa*
CCD	Charge-coupled Device
CCDC	Cambridge Crystallographic Data Center
CD	Circular Dichroism
CDDP	Cisplatin
$CDCl_3$	Chloroform-*d*
CNS	Central Nervous System
Da	Dalton
d	doublet
dd	doublet of doublets
DDW	Double Deionised Water
DMF	Dimethylformamide
DMSO	Dimethyl sulfoxide
DNA	Deoxyribonucleic acid
D_2O	Water-d_2
ESI	Electro-Spray Ionisation
9-EtA	9-Ethyl Adenine
9-EtG	9-Ethyl Guanine
ECACC	European Collection of Cell Cultures

FCS	Fetal Calf Serum
FDA	Food and Drug Administration
GI_{50}	50% growth inhibition concentration
GSH	Glutathione/γ-glutamylcysteinylglycine
HPLC	High Performance Liquid Chromatography
IC_{50}	50% growth inhibition concentration
ICP	Inductively Coupled Plasma
Impy	Iminopyridine
J	coupling constant
K	Kelvin
L-BSO	L-Buthionine-Sulfoximine
LC_{50}	Lethal Concentration 50
Me	Methyl
MeOD	Methanol-d4
MS	Mass Spectrometry
m	multiplet
mol equiv	Molar equivalent
m/z	mass/charge
NAC	N-Acetyl-L-Cysteine
NADH	Reduced Nicotinamide Adenine Dinucleotide
NCI	National Cancer Institute
NMR	Nuclear Magnetic Resonance
OSW	Octanol-Saturated Water
PBS	Phosphate Buffered Saline

p-cym	*para*-cymene
PDT	Photodynamic Therapy
ppb	parts per billion
ppm	parts per million
ppt	parts per trillion
q	quintet
ROS	Reactive Oxygen Species
RPMI	Roswell Park Memorial Institute medium
s	singlet
SAR	Structure Activity Relationship
SRB	Sulfurrhodamine B
t	triplet
TGI	Total Growth Inhibition
Tris	Tris(hydroxomethyl)aminoethane
UV-Vis	Ultraviolet-Visible
XRD	X-Ray Diffraction

Chapter 1
Introduction

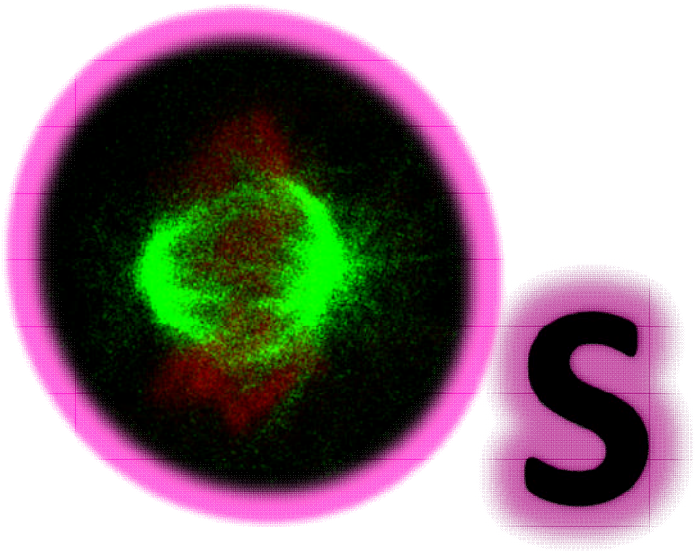

This thesis is concerned with the synthesis and elucidation of the mechanism of action of osmium(II) arene complexes and their potential application as anticancer drugs. A strong focus of this work involves looking at the structure-activity relationships with a view to improve the design and optimize the anticancer activity and increase our understanding of the mechanisms of action. This chapter introduces metallodrugs, pays special attention to cancer therapy development, novel anticancer targets for metallodrugs and the chemistry and design of osmium anticancer agents.

1.1 Cancer Therapy

It is well-known that a "war on cancer" was declared after the signing of the National Cancer Act in 1971 by Richard Nixon (the US president serving from 1969 to 1974). The progress of cancer therapy is evident and there are more anticancer drug candidates than any other disease nowadays in clinical trials. However, the success rate for anticancer drugs entering clinical development is much lower than for cardiovascular disease.[1] At a very crucial time for the war against cancer, in 2009, Barack Obama (the US president serving from 2008 to present) announced that the US would devote more than three percent of its GDP to research and development; within this budget, the US government would spend $6 billion to support cancer research. This encouraging news from the US will also attract more researchers and more public attention to the war against cancer globally.

Cancer cells are abnormal cells which grow uncontrollably at a rapid pace; they often metastasize and invade normal tissue. Cancer caused about 13% of all human deaths worldwide in 2007 (7.9 million). In the UK, about one in three will develop some form of cancer during their life time according to Cancer Research UK (CRUK 2008). The great danger and high occurrence rate make improved cancer therapy essential and in high demand.

Among all the cancer therapies, chemotherapy is the most powerful therapy. It

makes use of the ability of antineoplastic drug(s) to kill cancer cells. It also has some ability to kill cancer cells which are just starting to metastasize due to the lack of target selectivity. This method is always accompanied by serious side effects through affecting the fast-growing normal cells in humans, such as cells in the hair follicles, bone marrow and lining of the mouth and intestines. However, because the normal cells are able to recover, these side effects can be alleviated by combination treatment to lower the toxic response; they can also gradually disappear after chemotherapy, because the normal cells are capable to recover.

In the 1960s, the discovery of certain cytotoxic chemical agents facilitated the use of chemotherapy considerably. Administrations of certain combinations of cytotoxic chemical agents were able to cure some kinds of cancers, including childhood acute lymphoblastic leukemia (ALL), testicular cancer and Hodgkins disease, which were all previously considered universally fatal. In that, this discovery of cytotoxic anticancer drugs was a breakthrough in the development of anticancer medicine. Conventional cytotoxic chemotherapy has not only shown the capability to cure some types of cancer, but also proven effective in an adjuvant setting, and in reducing the risk of recurrence after surgery for high-risk breast cancer, colon and lung cancer which are still very difficult cases to treat nowadays.

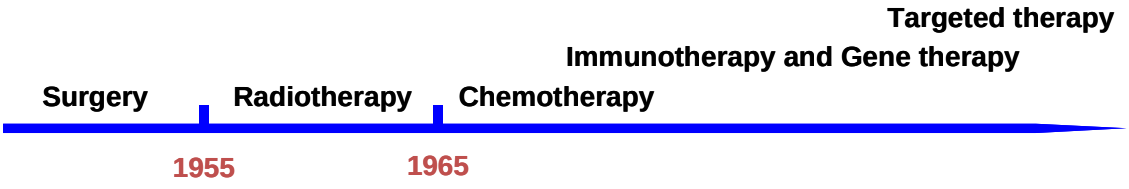

Figure 1.1. Brief timeline of the development of cancer therapy.

To avoid the drawbacks of chemotherapy, the newly developed targeted therapy seems to have a very bright future (Fig. 1.1). It moves the design and development of anticancer drugs from observation-driven to target-driven. Targeted therapy works by inhibiting the function of certain proteins that are

essential for the growth and/or proliferation of cancer cells. For example, bevacizumab (Avastin) prevents the formation of new blood vessels, which stops the tumour from growing by limiting the provision of nutrients; the mechanism of action involves blocking vascular endothelial growth factor. Another good example is erlotinib (Tarceva) which can block the epidermal growth factor receptor (EGFR), a protein that is found on the surface of cells that signals the cells to grow and divide.[2] For the cancer cells which overexpress EGFR, erlotinib can prevent their proliferation selectively.[3] Unlike anticancer drugs for conventional chemotherapy which are mostly derived from natural products or discovered by chance, development of targeted therapy drugs is mainly based on rational designs and massive screenings in order to achieve high selectivity to the target(s). However, targeted therapy does not mean no side effects, Avastin[4] (a well-known drug that blocks angiogenesis), can cause serious bleeding. Tarceva[5] (a tyrosine kinase inhibitor which acts on EGFR) can cause tiredness, diarrhea, and acne-like rash. Another bottle neck is that targeted therapies are not able to work for all patients.

Other than chemotherapy and targeted therapy, Current topics of researches on cancer therapy also include boosting the immune system, cancer vaccines, gene therapy, photodynamic therapy, radiation therapy and reoviridae[6] (Reolysin drug therapy), which also contribute for today's anticancer treatment.

1.2 Anticancer Drugs for Chemotherapy

The development of anticancer drugs plays a key role in the optimisation of cancer therapy. For several decades, the discovery of anticancer drugs was concentrating on conventional cytotoxic agents which can block essential functions of cells and target dividing cells. These drugs normally have pleiotropic effects: such as modifying DNA (CDDP[7], Fig 1.2), interfering with microtubule (Taxol[8]), influencing metabolite synthesis (Methotrexate[9]) or having an effect on chromosome topology (Rinotecan[10]). There are also some exceptions such as

oestrogen receptor modulators in the anti-hormonal therapy (e.g. Tamoxifen[11]) and epidermal growth factor receptor tyrosine kinase inhibitors (e.g. Gefitinib[12]). Among all of these, one of the most successful and commercially profitable anticancer drugs is cisplatin (CDDP[7]), a metal complex, which has been widely used for the treatment of solid malignancies for more than 30 years.

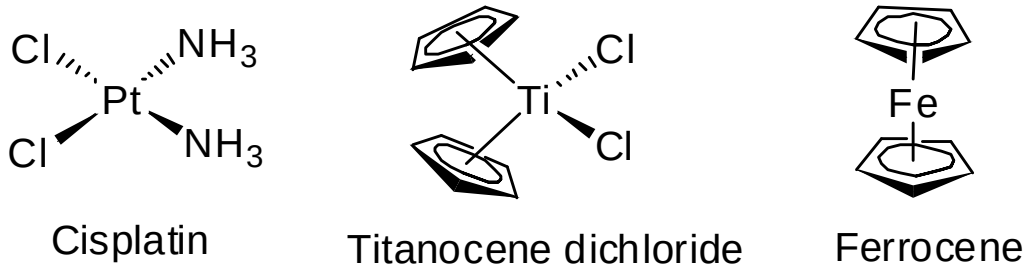

Figure 1.2. Metal complexes which can be considered to be milestones in the development of anticancer drugs.

In the early days, metals were not obvious candidates as pharmaceuticals because their compounds were generally known as toxic, not stable or have properties not suitable for drugs. In 1964, Barnett Rosenberg made a serendipitous discovery that platinum compounds can inhibit cell division when investigating the effect of electric fields on the growth of bacteria. The discovery led to the FDA approved drug cisplatin in 1978. Even though cisplatin was known for more than 100 years, the first report of its medical use was also a stimulus for researches on various metal-based anticancer compounds for clinical use. The success of cisplatin in clinical therapy of cancer has paved a way for the study of organometallic compounds which are compounds containing bonds between carbon and metal for the treatment of cancer.

From coenzyme B_{12} which is a natural organometallic compound[13] discovered in 1961 to titanocence dichloride (Fig. 1.2) which was the first anticancer non-platinum organometallic compound to achieve clinical trial in 1998,[14] bioorganometallic chemistry has developed at a very fast speed. Historically,

ferrocene (bis-cyclopentadienyl iron, Cp_2Fe, first synthesized in 1952) was the first reported anti-proliferative organometallic compound (Fig 1.2),[15] following which ruthenium and osmium organonometallic complexes all joined this field and played very active roles. Recent developments in this field have been reviewed by Metzler-Nolte et al.[16] Remarkable advances in promising areas of organometallic chemistry including catalysis, theoretical studies, mechanistic studies, "unconventional" reaction media, materials, supramolecular assemblies and bioorganometallic chemistry[17] will assist original improvements to the design of organometallic anticancer drugs.[18]

It was noticed that cisplatin was used in ca. 70% of all treatments for solid tumours. Despite the success of cisplatin in the clinic, it is also notable that it can cause general toxicity, is inactive against certain types of cancer, and leads to drug resistance and undesirable side-effects.[19-21] Even after the improvements made by second and third generations of platinum anticancer drugs (carboplatin and oxaliplatin), targeting DNA by different generations of platinum drugs[22, 23] offers an inherently limited possibility for rational improvements to increase its selectivity on cancerous cells with the aim to minimize undesired side effects. With the purpose of overcoming the drawbacks of platinum drug, it is necessary to develop a new generation of anticancer complexes of platinum and other precious metals. To avoid the similar side effects of cisplatin, it is necessary to convert the mechanism of action from the classical non-selective DNA binding to other mechanisms.[24, 25] Compared to purely organic compounds, organometallics complexes are able to obtain a greater structural variety which offers a potential to provide more possibilities to tune binding to drug targets. By the rational design of the ligand, organometallic complexes were already found to show effects through different mechanisms mainly by targeting different biomolecules. For instance, different half-sandwich ruthenium(II) complexes can act as bio-catalysts (Fig 1.3, Complex B),[26] protein kinase inhibitors[27] or DNA modifiers[28] by varying their chelating N,N-ligand.

1.3 Targets for Organometallic Anticancer Agents

DNA, proteins and redox systems are three major achievable targets for organometallic anticancer complexes; the details of successful examples of organometallic complexes are going to be discussed in this section.

1.3.1 DNA

To avoid the similar undesirable toxicity and side effects induced by cisplatin (anticancer drug targeted to DNA), organometallic complexes had shown a promising future through targeting DNA in a different way of cisplatin. For instance, other than the classical nonselective binding to DNA, organometallic ruthenium compounds had shown a potential to target topoisomerase (e.g. Fig 1.3, complex A),[29] special DNA sequence[30] or G-quadruplex[31](e.g. Fig 1.3, complex D); Control of the DNA targeting with sequence specificity was achieved by osmium compounds by targeting C5-methylated pyrimidines in DNA, this method was realized through osmium oxidation, though in the very early stage, it had shed light on the use for gene therapy in the future.[32]

1.3.2 Essential Proteins for Proliferation

In recent years, various protein targeting agents have shown promising progress on anticancer treatment: aurora-kinase inhibitors, epidermal growth factor receptor (EGFR) inhibitors and cyclin-dependent-kinase (CDK) inhibitors. EGFR has become one very important research topic in recent years. It is also note-worthy that Tarceva (erlotinib, an EGFR inhibitor), an oral anti-cancer drug developed by OSI Pharmaceuticals, Genentech and Roche, had been approved by the U S Food and Drug Administration (FDA). Tarceva is showing remarkable results for the treatment of Non-Small Cell Lung Cancer (NSCLC), however, the cost for extending life by an average of 3.3 months is so high (US$92,233) that not every patient can afford this expense.[5] An inorganic compound, ferrocene carboxaldehyde, has been found to be an EGFR inhibitor; it has the inhibition

effect on the kinase VEGFR-2 and exhibits an anticancer activity *in vitro*. Although there is still a long way to go to clinical application, ferrocene carboxaldehyde does bring a new hope to lower the price of treatment by using EGFR inhibitors by introducing a good competitor in the anticancer drug market.[33]

Other than kinase inhibitors, anti-tubulin anticancer drugs are also important for anticancer therapy in medical use. Tubulin belongs to globular proteins, the two most common types of tubulins (α-tubulin and β-tubulin) can polymerize and form microtubules which are important for spindle formation during the mitosis stage of cells. There are two classes of tubulin-polymerization-targeted drugs in clinical use, one stabilizes microtubules (eg. taxol), another destabilises like *vinca* alkaloids (eg. vincristine, vinblastine, and vinorelbine) which were discovered after taxol. Both of the two types of drugs work by interfering with the cell's ability of forming mitotic spindles appropriately, they work by inducing or preventing the normal polymerization of tubulin during the G_2/M phase of the cell cycle respectively.[34] The discovery of tubulin-targeting anticancer drugs was mainly based on natural products,[35] a lot of progress on designing inhibitors of tubulin polymerization had also been made based on organic structures,[36-40] however, there is still no report linking organometallic compounds to the inhibition of tubulin polymerization though an osmium carbonyl cluster (Fig 1.3, complex C) was reported to hyperstabilize microtubules in 2009.[35]

The mechanism of action for ruthenium(II) arene anticancer complexes was generally believed to target DNA: labile-ligand substitution can generate an active site on the ruthenium centre, it can bind to the DNA base to cause DNA damage and kill cancer cells. But recent studies of a series of ruthenium(II) arene anticancer compounds revealed that DNA was not necessarily the primary target and these compounds might prefer to bind to proteins:[41] ruthenium(II) arene RAPTA derivatives containing two chloride ligands were found to be susceptible to hydrolysis and were firstly anticipated that DNA was a primary target.[41] To

gain more insight, Messori et al. studied and found the inhibition activity of a series of RAPTA compounds towards two enzymes, i.e., cathepsin B (Cat B) and thioredoxin reductase (TrxR), which are possible targets for anticancer ruthenium(II) RAPTA complexes. However, the *in vitro* anticancer activities for these RAPTA complexes are far from reaching the activity of cisplatin; it makes them less promising for potential clinical use independently.[42]

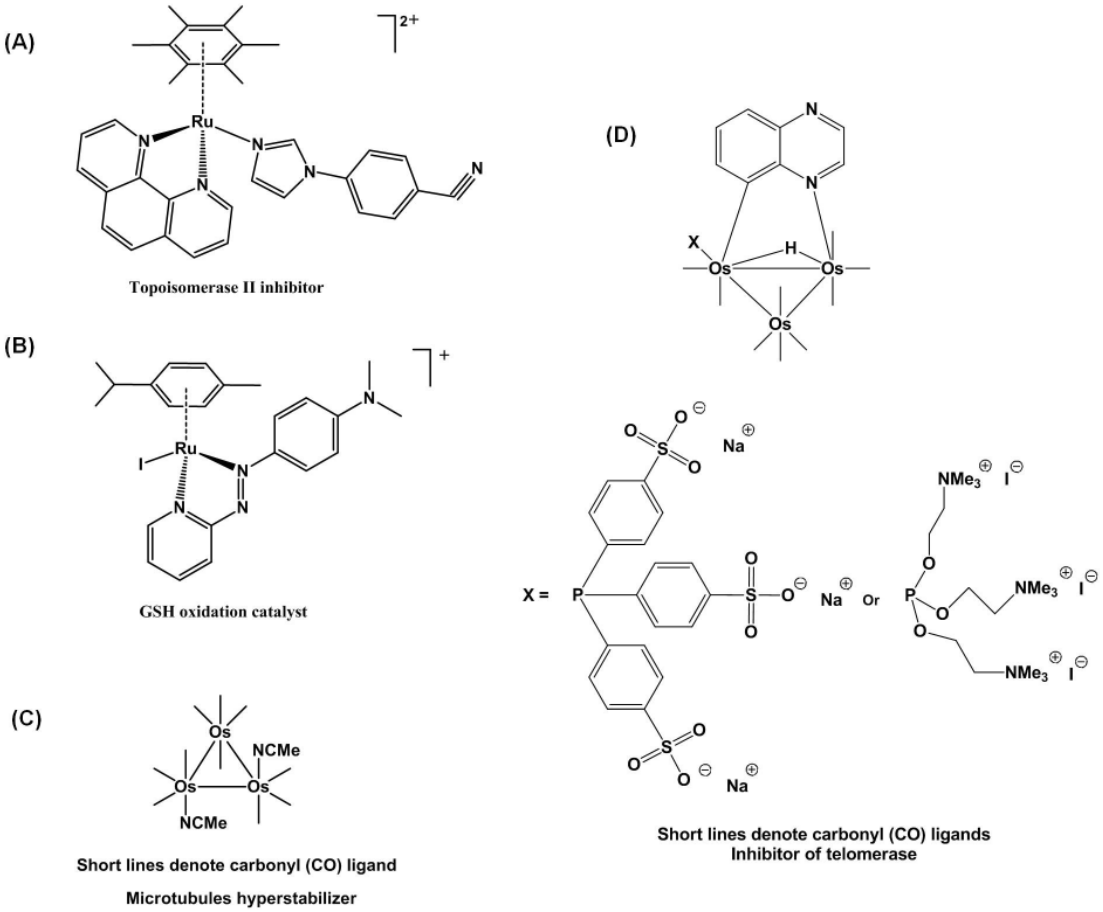

Figure 1.3. Examples of organometallic anticancer complexes.

The design and development of cytotoxic organometallic anticancer drugs are primarily observation-driven: the anticancer effect was usually found before the disclosure of the mechanism of action. However, one strategy for designing

anticancer organometallic complexes by making use of known organic anticancer drugs was newly developed. Using this strategy, Meggers' group had shown promising results for designing organometallic complexes for inhibitions of kinases.[43] The strategic procedure of making an extension from organic anticancer drugs can be summarized as follows:

1. Selection of a target and analysis of existing co-crystal structure of organic compound with the target active site. (Example: a number of the class of indolocarbazole alkaloids, which are potent ATP-competitive protein kinase inhibitors).

2. Identification of the main pharmacophore and incorporation into a ligand (for metal-binding).

3. Targeting metal complex to the active site by the incorporation of pharmacophore ligand (Additional ligand in the metal coordination sphere can form bonds to other parts of the active site to improve the biological effect and/or selectivity; and the metal can contribute coordinative binding to the active site).

The achievable advantages are summarized below:

1. The diversity of coordination numbers and geometries of metals might be used to exploit original design of pharmacophores that are not easily reached with organic elements.

2. The synthetic routes for metal complexes are generally easy. It makes the synthesis of complexes with desired features by combinatorial library design for high throughput screening (HTS) and evaluation more applicable.

3. Distinctive and tunable properties of metals can be exploited for the generation of a tailored function.

4. Crucial coordinate bonds can be achieved between metal and active binding site which are totally different from hydrogen bonds or covalent bonds which are common binding modes for organic drugs.[44]

In general, it is possible to tune the biological activity and drug properties through changing the metal`s coordination numbers, geometries, oxidation states and charges. It is also noted that the catalytic ability and other unique chemical properties of metal complexes have the potential to be developed as favorable physicochemical properties of drugs for different diseases.

1.3.3. Redox Status

The thiol/disulfide levels are closely related to the redox status in cells. Other than DNA and proteins which were mentioned above, the manipulation of thiol/disulfide levels in cells is also gaining attention as a method to kill cancer cells. There is one anticancer agent that can down-regulate thiol levels in clinical trial: L-buthionine sulfoximine (L-BSO). L-BSO is a glutathione-lowering drug which can sensitize CDDP-resistant ovarian cancer cells; it can also increase the sensitivity of antihormone-resistant human breast cancer cells to estrogen-induced apoptosis[45] and enhance apoptosis with the treatment of transforming growth factor-alpha of pancreatic cancer cells[46] (pancreatic cancer is the 5th most common cause of death from cancer in the world). Moreover, phase I study of L-BSO had proven it to be safe and well-tolerated in patients. In summary, L-BSO is a potent anticancer drug candidate with low toxicity for the combination treatment with other anticancer drugs.

To elucidate the redox status of cells, with the help of redox western analysis

and redox-sensitive green fluorescent protein assays, the following order from most reducing to most oxidizing was found:

mitochondria > nuclei > cytoplasm > endoplasmic reticulum > extracellular space.[47]

This sequence indicates that the mitochondria to be a sensitive target of oxidant-induced damage, the damage of mitochondria can lead to apoptosis and necrosis of cells. At the same time, the alkaline pH maintained by mitochondria will possibly amplify the damage.[47] The thiols' levels are important for the protection of cells against reactive oxygen species and free radicals. In that, anticancer drugs which can change the cellular thiols levels may have a potential to kill cancer cells through mitochondria-mediated cell death.

There are three major thiol/disulfide couples, namely glutathione (GSH)/glutathione disulfide (GSSG), reduced thioredoxin [Trx-$(SH)_2$]/oxidized thioredoxin (Trx-SS) and cysteine (Cys)/cystine (CySS).[48] Within these redox couples, glutathione (GSH) content is believed to play the most important role for maintaining the cellular redox status, because its concentration can range from 2 to 10 mM depending on the cell type which is much higher than other thiol/disulfide couples.[49] GSH (γ-glutamylcysteinylglycine) is an ubiquitous tri-peptide that acts as an important radical scavenger;[50, 51] it can protect the cells against reactive oxygen species (ROS). Moreover, relatively high GSH levels than normal tissues were observed in a range of human cancer tissues such as ovary,[52] breast,[53] colon,[54] lung,[55] bone marrow,[56] and larynx;[57] it was also discovered that GSH levels in tumour tissues were associated with their resistance to chemotherapy.[58]

Although ROS are generally believed to be toxic to cells, they act as a 'double-edged sword' for the proliferation of cell. In cells, when the ROS level is up-regulated on a small scale, the ROS may contribute to the proliferation; if the ROS level is raised further, it can cause DNA damage which will induce cell cycle arrest and apoptosis.[59] Therefore the selectivity to cancer cells rather than

normal cells can be achieved by increasing the ROS levels, because the basal ROS levels in cancer cells are higher than normal cells (Fig. 1.4).

Another important factor which can affect the redox status and ROS production is the cellular O_2 content. The content of oxygen in cells can regulate HIF (hypoxia-inducible factor) signal pathway. Generally due to the consequence of a poor and disorganized blood supply, solid tumours contain regions of low oxygen tension (hypoxia), which will affect neovascularization, glucose metabolism, survival and tumour spread. This pleiotropic action is orchestrated by HIF, a master transcriptional factor in nutrient stress signal pathway.[60] Overexpression of HIF is associated with increased tumour growth, vascularization and metastasis, in that, a combination therapy of HIF inhibitor with another anticancer drug which is targeting the redox system can be applicable for increasing the anticancer activity.[61]

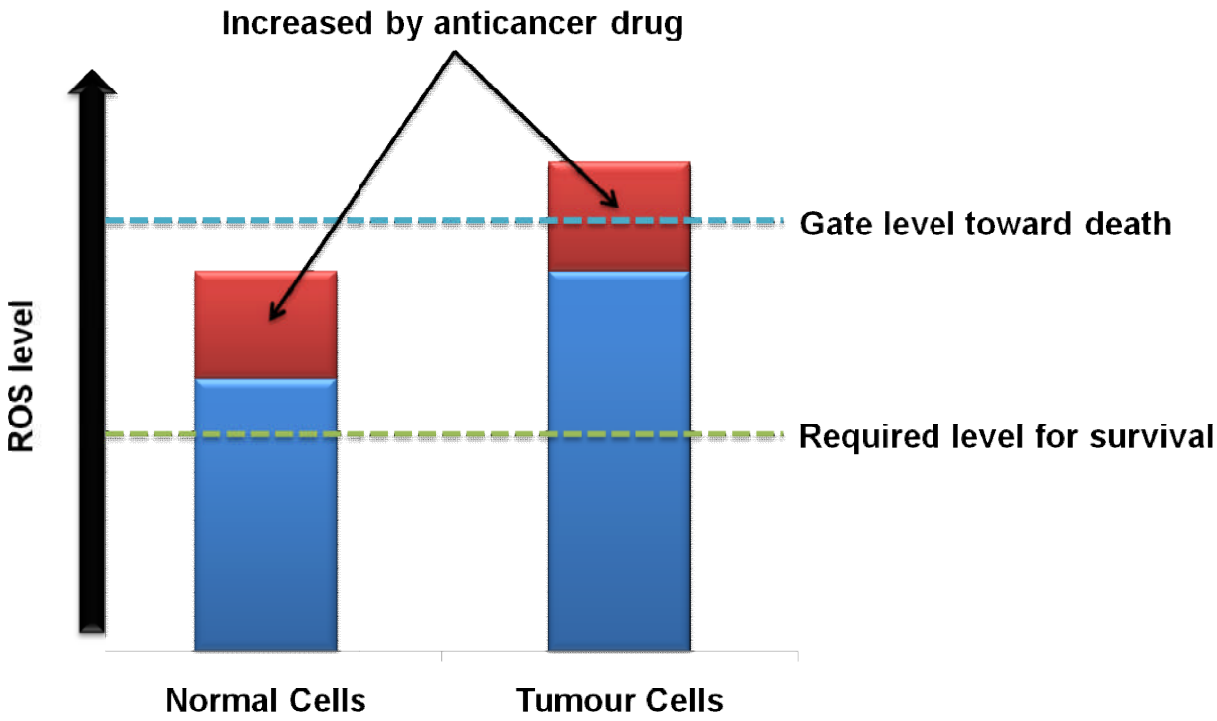

Figure 1.4. ROS level as 'double-edged sword' and the anticancer selectivity which can be achieved by increasing ROS.

There are two important families in cells contributing to the redox balance, one is thiol/disulfide couples, the other one is nicotinamide adenine dinucleotide (NADH) and its oxidised form (NAD^+) together with their phosphorylated forms NADPH/$NADP^+$. NADH is not only a reducing part of the redox system balance but also an important intermediate of mitochondrial respiration and glycolysis which are crucial processes to provide energy for cells.[62]

Early work by Steckhan[63] and Fish[64] had shown an economical process for the regeneration of NADH from NAD^+ by rhodium catalysts. Following that, ruthenium arene complexes were found to be able to regioselectivly reduce NAD^+ to NADH through transfering hydride under physiological conditions in the presence of formate.[65] However, the involvement of the reactions between NADH/NAD^+ and metal complexes in the biological environment still need further investigations.

1.4 Background of Osmium

1.4.1 Discovery of Osmium

In 1803, Smithson Tennant and William Hyde Wollaston discovered osmium in London (UK). Currently, osmium is principally acquired from the processing of platinum and nickel ores.[66] The origin of the name 'osmium' is the Greek word "osme" which means "smell". Unlike its closest relatives in the platinum group (Fig 1.5, they have similar physical and chemical properties and occur together in the same mineral deposits in most cases), osmium was not given a beautiful name such as ruthenium (in honour of Russia), palladium (namesake of the goddess Pallas Athene), iridium ("rainbow" in Greek) and rhodium ("rose").[67]

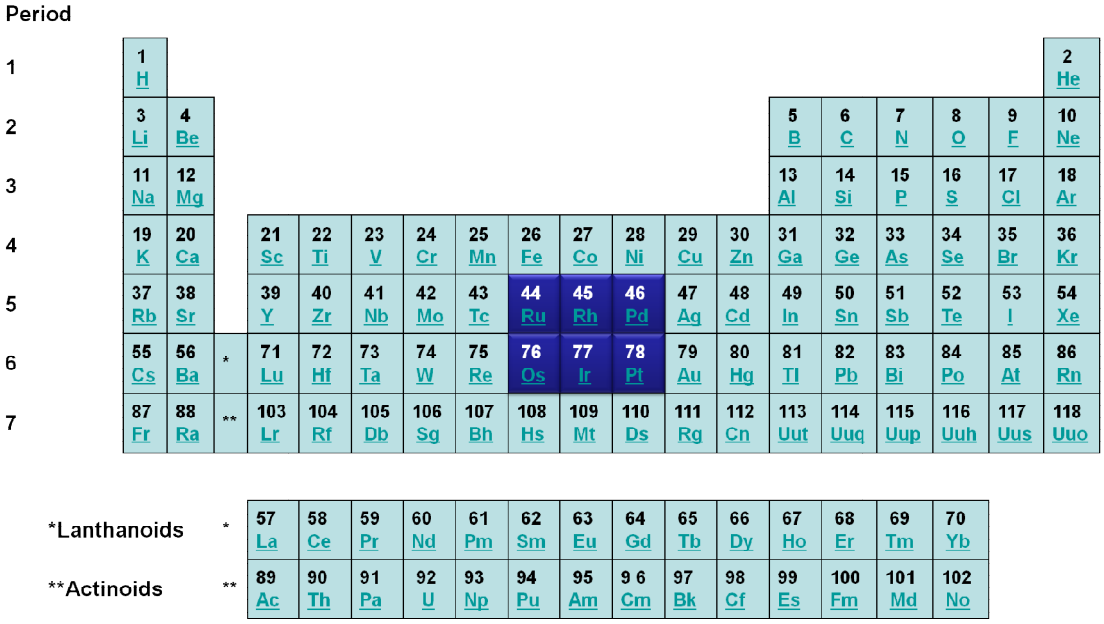

Figure 1.5. Periodic table: platinum group metals are labelled in blue.

1.4.2 Physical and Chemical Characteristics of Osmium

Osmium is an extremely dense, hard, brittle, blue-gray or blue-black transition metal in the platinum group and its atomic number is 76. It is the densest natural element, 22610 $^{kg}/_{m^3}$ (22.61 $^{g}/_{cm^3}$), slightly larger than the density of the second densest element iridium: 22560 $^{kg}/_{m^3}$ (22.56 $^{g}/_{cm^3}$).

The usual oxidation states of osmium are +4 and +3, but oxidation states from -2 to +8 are all available. There are merely two osmium compounds which have major applications: osmium tetroxide (OsO_4) which is used for staining tissue for electron microscopy and the non-volatile osmates which can act as catalysts in organic oxidation reactions.[68, 69]

1.4.3 Isotopes of Osmium

There are at least 34 isotopes of osmium, but only seven exist in nature (Table 1.2). Although it is possible to observe the NMR signal of ^{187}Os, it is one of the most insensitive nuclei, so ^{187}Os NMR is usually observed in complexes by indirect detection via proton coupling.[70]

Table 1.2. Stable isotopes of osmium.[71]

Isotopes	Natural Abundance	Nuclear Spin
^{184}Os	0.02%	0
^{186}Os	1.59%	0
^{187}Os	1.96%	1/2
^{188}Os	13.24%	0
^{189}Os	16.15%	3/2
^{190}Os	26.26%	0
^{192}Os	40.78%	0

1.5 Design of Osmium Anticancer Complexes

1.5.1 Making Extension from Ru to Os

Since osmium and ruthenium belong to the same family, making extension from one to the other can be achieved by a similar synthetic method; it may lead to novel ruthenium/osmium complexes with similar physical and biological properties. For example, the extension from OsO_4 to RuO_4 resulted in the discovery of novel ruthenium electron microscopy fixing agent (RuO_4) for cytoplasmic membranes.[72] Ruthenium and osmium complexes with similar structures may share similar anticancer mechanism of action; in that, a lot of work has been done to compare them on anticancer activity and mechanism of action (Fig. 1.6). There are also some intriguing differences have been found on the chemical properties between organometallic Ru^{II} and Os^{II} arene complexes even though their three-dimensional structures can be almost identical.[73] For instance, the two types of metal complexes have shown differences in redox potentials and photoreacitons;[74] osmium complexes are often considered to be more inert (a common characteristic of low-spin d^6 metal ions and especially 3rd row transition metals).[75, 76]

Ruthenium complexes have shown a good potential as anticancer agents. The design of osmium anticancer complexes, which are their heavier congeners, should build on knowing the role that the coordination metal played in maintaining its biological activity. When the ruthenium centre in the scaffold has a solely structural role, only the shape of the organometallic complex is responsible for its bioactivity, its osmium analogue is able to maintain the activity because the atomic radii of the two elements (Ru and Os) are almost identical due to the lanthanide contraction.[27, 77] For example, the isostructural ruthenium(II) and osmium(II) complexes were found to be good protein kinase inhibitors showing a similar potency.[78] Similarly, osmium(II) complexes with paullone derivatives (known to be potent inhibitors of cyclin-dependent kinases) as chelating ligand

have been designed to increase the solubility and bioavailability of paullone ligands; there is also no significant differences of antiproliferative activities between the osmium and ruthenium analogues.[79] In general, this method cannot improve dramatically on anticancer activity with the metal serving as a structural centre.

Other than making extension from ruthenium(II) to osmium(II), the extension from ruthenium(III) to osmium(III) showed similar/better anticancer activity as well. Although investigations are still needed to establish the mechanism of action of ruthenium anticancer complexes, two Ru(III) complexes are already undergoing clinical trials: NAMI-A and KP1091. Their anticancer mechanism of action involves the reduced Ru(II) species, however, the reason for the antimetastatic activity for NAMI-A is still unclear. This encouraging result has led to the pursuit for more novel osmium complexes with similar structures. For instance, NAMI-A type complexes of osmium have been synthesized and fully characterized in Prof. Keppler`s group.[80] In contrast to the ruthenium complexes, the osmium analogues are more inert to hydrolysis similar to the rhodium and iridium analogues which results in reduced binding to the DNA nucleobase analogue, 9-methyladenine; Osmium complexes are able to show comparable antiproliferative activity to the ruthenium congeners, and in some cases, the osmium complex is 10 times more potent than the ruthenium congeners.[80] The osmium analogue of indazolium trans-[tetrachlorobis(1H-indazole)ruthenate(III)] (KP1019) also showed promising anticancer activity.[81]

Ruthenium and osmium polypyridyl complexes have shown interesting photophysical properties[82, 83] which can be employed for anticancer treatment. There are two types of photochemistry expected which can be used for anticancer treament: (1) photo-redox processes with important biomolecules such as DNA; complexes with this type of photochemistry have the potential to become candidates for photodynamic therapy (PDT)[84] which makes use of photosensitizers to produce reactive oxygen species (ROS) to kill cancer cells;[85, 86]

(2) photo-substitution of a ligand by a biomolecule such as nucleobase; this property can be developed for photoactivated chemotherapy (PACT)[87-90] which have been highlighted recently.[74, 90] Considering the comparisons between ruthenium and osmium for PDT, there is one advantage of using osmium instead of ruthenium: osmium complexes have lower oxidizing power and undergo exclusive photoreactions from the ^{3}MLCT state, which results in a red shift in the UV–Vis spectra and indicates the possibility of using longer wavelengths[91] for PDT.[92] Other than osmium centred PDT, it is also noted that osmium-porphyrin complexes have been investigated and reviewed recently relating to the supramolecular chemistry of metalloporphyrins.[93]

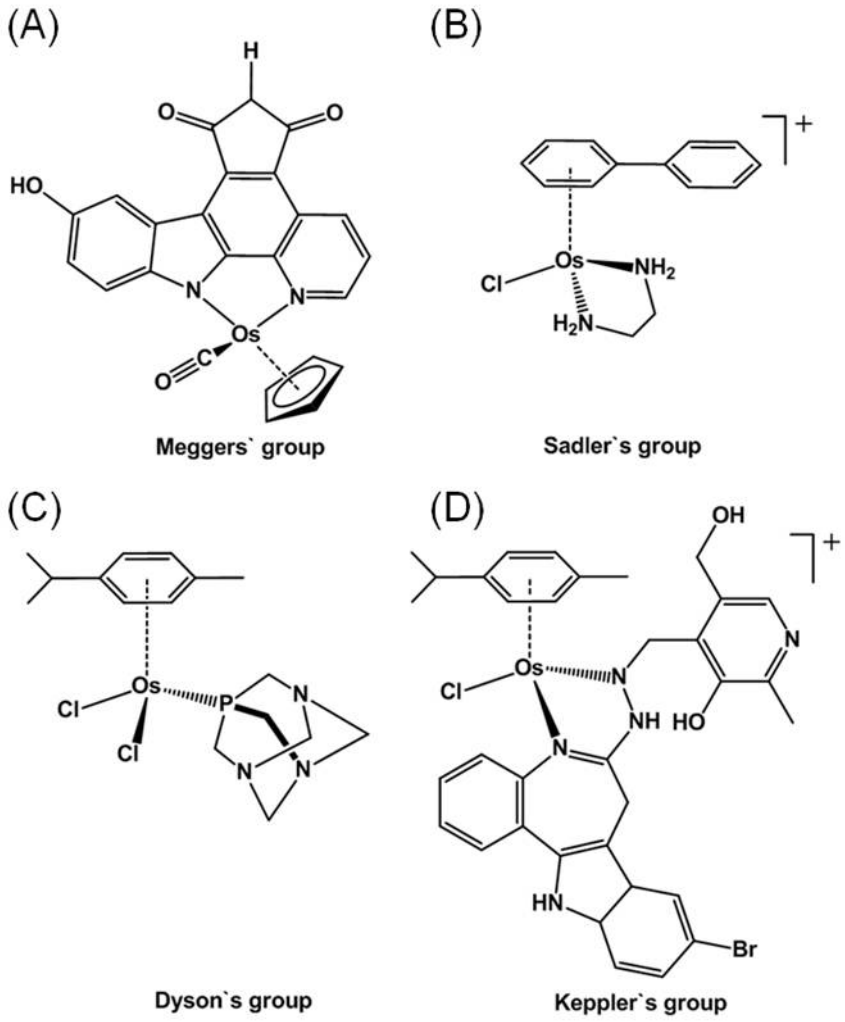

Figure 1.6. Examples of osmium anticancer complexes developed by different research groups which also have their ruthenium analogues.

1.5.2 Design of Osmium Anticancer Complexes

Osmium has a similar potential to ruthenium in binding to a variety of biomolecules such as DNA.[94-96] There are two major reasons to study osmium analogues of ruthenium: (1) to broaden the knowledge through the comparisons of the structures, spectroscopic properties, electrochemical behaviours, DNA binding properties, aqueous stabilities and reduction potentials; (2) to achieve better drug properties and anticancer activities by exploiting the differences between the two metals.

As to the clinical use of osmium, in history, the first clinical used osmium compound was osmium tetroxide (OsO_4). It was used on a limited basis for the treatment of arthritis in human about 35 years ago, principally in Europe. In 1976, a group of researchers in Switzerland reported that over 70 patients were helped by this treatment. Regarding the mechanism of action, the treatment used OsO_4 as one synovectomy agent.[97] This clinical use of osmium tetraoxide without any serious toxicity reports suggests the bio-compatibility even for osmium (VIII); the +8 oxidation state is the highest for osmium and any other chemical element. Lower than oxidation state of osmium tetraoxide, a family of nitridoosmium(VI) schiff-base complexes were reported to show anticancer activity *in vitro* and one of the complexes showed anticancer activity *in vivo* without apparent induced toxic side-effect.[98]

In order to avoid the potential of oxidizing toxicity introduced by osmium in high oxidation state, the osmium work in this thesis will concentrate on osmium complexes with lower oxidation state of osmium than OsO_4 and nitridoosmium(VI) schiff-base complexes: osmium(II). The design of the half-sandwich structure is based on the work on ruthenium complexes previously reported in Sadler`s group. Organometallic half-sandwich complexes [M(η^6-arene)(YZ)(X)], where YZ is typically a chelating diamine ligand (e.g. ethylenediamine) and X is a halide (e.g. Cl), M = Ru^{II}, were found to exhibit anticancer activity *in vitro* and *in vivo*.[99, 100] Similar to cis-platin, the target is

believed to be DNA, the labile Ru-Cl bond is able to undergo hydrolysis to form Ru-OH_2 intracellularly, whereas the hydrolysis is suppressed extracellularly.[101] The hydrolysis generates one reactive site on ruthenium which can bind to a DNA base (e.g. guanine) and lead to cell death.[102] The activity can also be tuned by changing the arene and the leaving group. Because the arene can contribute an intercalation effect to DNA binding and the leaving group modulate the hydrolysis: high activity: halide---easy hydrolysis, low activity, e.g. pyridine, inert to hydrolysis.[103, 104] Their osmium analogues were also studied and the mechanism of action which is similar to that of the ruthenium complexes was summarized below in Figure 1.7.

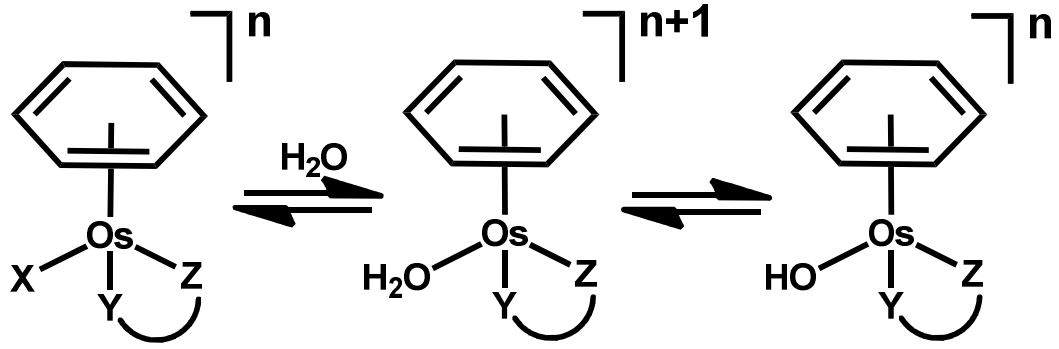

Figure 1.7. General structure of osmium anticancer complexes with piano-stool structure containing an arene, a chelating ligand YZ and a monodentate ligand X which can be labile to provide an active reactive site for the binding of biomolecules or is inert to hydrolysis to maintain its structure with anticancer activity through novel mechanisms. In water, the Os-X bond (when X is labile) is able to hydrolyse to generate the corresponding aqua product which can be deprotonated to from the hydroxo-Os adduct.

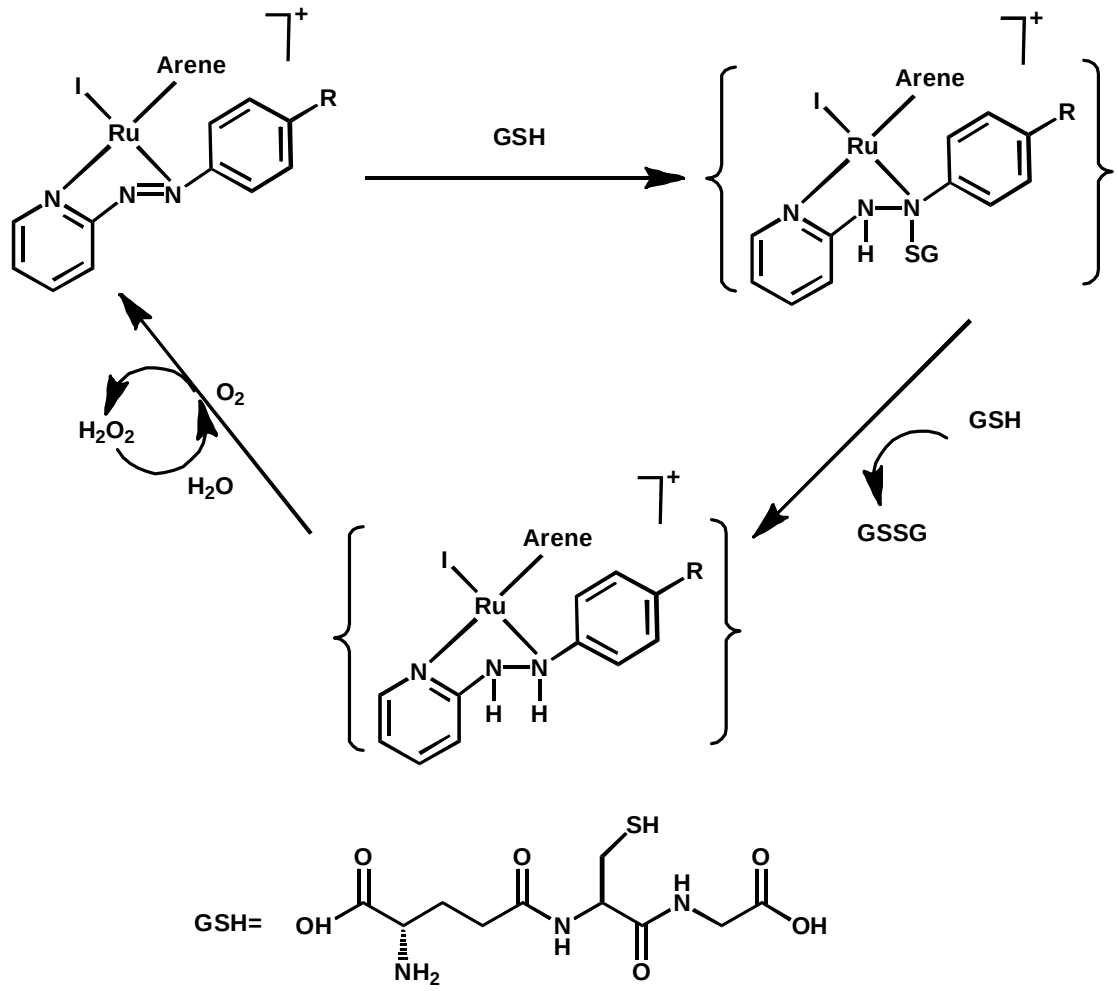

Figure 1.8. The mechanism of activity of iodido ruthenium azopyridine complexes involving catalytic oxidation of GSH.[26]

Another work on ruthenium from Sadler`s group had shown when M = Ru, XY = azopyridine chelating ligand and Z = iodide, the half-sandwich complexes were inert toward hydrolysis but could still show anticancer activities. A possible mechanism involves the iodido Ru^{II} azopyridine complexes acting as catalysts for oxidation of the tripeptide glutathione which is the major reducing agent in cells, in that, the oxidative stress will kill the cancer cells (Fig. 1.8).[26] The azopyridine ligands are well known for their strong π-acidity,[105] stabilizing the lower oxidation states of a metal. Azo compounds as ligands are very important for redox reactions of iodido Ru^{II} complexes; interestingly, the azo ligands themselves also

have a potential to oxidize GSH to GSSG which is facilitated by O_2.[106-108]

Inspired by the ruthenium work previously carried out in our group, the analogous osmium(II) complexes[109] are studied in this thesis (Fig. 1.9). The goal of anticancer research programs is to identify novel, synthetically-feasible molecules that can exhibit good anticancer activity with minimal side-effects. One efficient approach is the study of bioisosterism, a term coined to describe the modification of biological activity by isosterism.[110-112] Following this design, the general structures of osmium complexes are shown below in Figure 1.9.

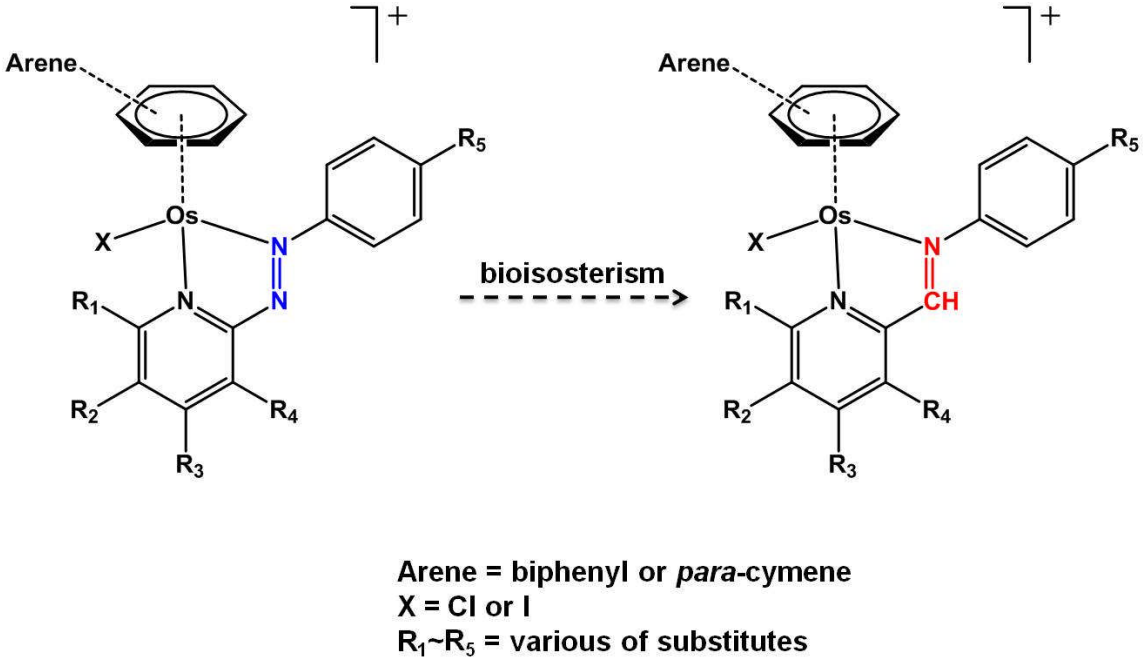

Figure 1.9. Osmium complexes designed in this thesis.

1.6 Aims

The general aim of this project is to synthesize, characterize and undertake tests on cancer cell toxicity and establish structure-activity relationships to help with the rational design and understanding of the mechanism of action on three new families of osmium(II) arene complexes which are generated by modifications on the chelating ligands. The individual aims are summarized below:

1. To gain an understanding of the aqueous solution chemistry and anticancer activity *in vitro* and *in vivo* of osmium(II) arene azopyridine complexes in relation to their chemical structures.

2. To discover the mechanism of action of osmium arene azopyridine complexes by using the structure activity relationship (SAR) of anticancer activity and combination treatments.

3. To explore the possibility of transferring hydride from NADH and investigate the mechanism of action of osmium(II) arene iminopyridine anticancer complexes.

1.7 References

1. A. Kamb, S. Wee and C. Lengauer, *Nat. Rev. Drug Discovery*, 2007, **6**, 115-120.
2. Y. Yarden, *Eur. J. Cancer*, 2001, **37**, 3-8.
3. N. G. Anderson, T. Ahmad, K. Chan, R. Dobson and N. J. Bundred, *Int. J. Cancer*, 2001, **94**, 774-782.
4. N. Ferrara, K. J. Hillan and W. Novotny, *Biochem. Biophys. Res. Commun.*, 2005, **333**, 328-335.
5. U. Gatzemeier, A. Pluzanska, A. Szczesna, E. Kaukel, J. Roubec, F. De Rosa, J. Milanowski, H. Karnicka-Mlodkowski, M. Pesek, P. Serwatowski, R. Ramlau, T. Janaskova, J. Vansteenkiste, J. Strausz, G. M. Manikhas and J. Von Pawel, *J. Clin. Oncol.*, 2007, **25**, 1545-1552.
6. M. J. V. Vähä-Koskela, J. E. Heikkilä and A. E. Hinkkanen, *Cancer Lett.*, 2007, **254**, 178-216.
7. E. R. Jamieson and S. J. Lippard, *Chem. Rev.*, 1999, **99**, 2467-2498.
8. P. B. Schiff, J. Fant and S. B. Horwitz, *Nature*, 1979, **277**, 665-667.
9. A. M. Murad, F. F. Santiago, A. Petroianu, P. R. S. Rocha, M. A. G. Rodrigues and M. Rausch, *Cancer*, 1993, **72**, 37-41.
10. D. Cunningham, Y. Humblet, S. Siena, D. Khayat, H. Bleiberg, A. Santoro, D. Bets, M. Mueser, A. Harstrick, C. Verslype, I. Chau and E. Van Cutsem, *N. Engl. J. Med.*, 2004, **351**, 337-345.
11. The Arimidex, Tamoxifen, Alone or in Combination (ATAC) Trialists' Group, *Lancet Oncol.*, 2008, **9**, 45-53.
12. J. G. Paez, P. A. Jänne, J. C. Lee, S. Tracy, H. Greulich, S. Gabriel, P. Herman, F. J. Kaye, N. Lindeman, T. J. Boggon, K. Naoki, H. Sasaki, Y. Fujii, M. J. Eck, W. R. Sellers, B. E. Johnson and M. Meyerson, *Science*, 2004, **304**, 1497-1500.
13. P. G. Lenhert and D. C. Hodgkin, *Nature*, 1961, **192**, 937-938.

14. A. Korfel, M. E. Scheulen, H. J. Schmoll, O. Grundel, A. Harstrick, M. Knoche, L. M. Fels, M. Skorzec, F. Bach, J. Baumgart, G. Sass, S. Seeber, E. Thiel and W. E. Berdel, *Clin. Cancer Res.*, 1998, **9**, 2701-2708.
15. P. Köpf-Maier, H. Köpf and E. W. Neuse, *Angew. Chem., Int. Ed.*, 1984, **23**, 456-457.
16. G. Gasser, I. Ott and N. Metzler-Nolte, *J. Med. Chem.*, 2010, **54**, 3-25.
17. C. G. Hartinger and P. J. Dyson, *Chem. Soc. Rev.*, 2009, **38**, 391-401.
18. J. Halpern, *Pure Appl. Chem.*, 2001, **73**, 209–220.
19. D. B. Zamble and S. J. Lippard, *Trends Biochem. Sci.*, 1995, **20**, 435-439.
20. K. Ishibiki, K. Kumai, S. Kodaira, O. Abe, K. Yamamoto, T. Oouchi, Y. Fukaya, K. Kimura, K. Takamatsu, E. Ootsuka, *Gan to Kagaku Ryoho*, 1989, **16**, 3185-3193.
21. G. Chu, *J .Biol. Chem.*, 1994, **269**, 787-790.
22. D. Wang and S. J. Lippard, *Nat. Rev. Drug Discovery*, 2005, **4**, 307-320.
23. B. Lippert (Ed.), Cisplatin: Chemistry and Biochemistry of a Leading Anticancer Drug, *Verlag Helvetica Chimica Acta, Postfach, Zürich, Switzerland*, 1999.
24. A. Bergamo and G. Sava, *Dalton Trans.*, 2011, **40**, 7817-7823.
25. G. Sava, A. Bergamo and P. J. Dyson, *Dalton Trans.*, 2011.*in press*.
26. S. J. Dougan, A. Habtemariam, S. E. McHale, S. Parsons and P. J. Sadler, *Proc. Natl. Acad. Sci. U. S. A.*, 2008, **105**, 11628-11633.
27. K. S. Smalley, R. Contractor, N. K. Haass, A. N. Kulp, G. E. Atilla-Gokcumen, D. S. Williams, H. Bregman, K. T. Flaherty, M. S. Soengas, E. Meggers and M. Herlyn, *Cancer Res.*, 2007, **67**, 209-217.
28. H. Chen, J. A. Parkinson, S. Parsons, R. A. Coxall, R. O. Gould and P. J. Sadler, *J. Am. Chem. Soc*., 2002, **124**, 3064-3082.
29. S. K. Singh, S. Joshi, A. R. Singh, J. K. Saxena and D. S. Pandey, *Inorg. Chem.*, 2007, **46**, 10869-10876.

30. J. Malina, M. J. Hannon and V. Brabec, *Chem. Eur. J.*, 2008, **14**, 10408-10414.

31. L. Xu, D. Zhang, J. Huang, M. Deng, M. Zhang and X. Zhou, *Chem. Commun.*, 2010, **46**, 743-745.

32. K. Tanaka, K. Tainaka, T. Umemoto, A. Nomura and A. Okamoto, *J. Am. Chem. Soc.*, 2007, **129**, 14511-14517.

33. J. Spencer, A. P. Mendham, A. K. Kotha, S. C. Richardson, E. A. Hillard, G. Jaouen, L. Male and M. B. Hursthouse, *Dalton Trans.*, 2009, 918-921.

34. J. R. Jackson, D. R. Patrick, M. M. Dar and P. S. Huang, *Nat. Rev. Cancer*, 2007, **7**, 107-117.

35. K. V. Kong, W. K. Leong and L. H. K. Lim, *Chem. Res. Toxicol.*, 2009, **22**, 1116-1122.

36. T. Beckers, T. Reissmann, M. Schmidt, A. M. Burger, H. H. Fiebig, U. Vanhoefer, H. Pongratz, H. Hufsky, J. r. Hockemeyer, M. Frieser and S. Mahboobi, *Cancer Res.*, 2002, **62**, 3113-3119.

37. J.-D. Jiang, L. Denner, Y.-H. Ling, J.-N. Li, A. Davis, Y. Wang, Y. Li, J. Roboz, L.-G. Wang, R. Perez-Soler, M. Marcelli, G. Bekesi and J. F. Holland, *Cancer Res.*, 2002, **62**, 6080-6088.

38. A. Wienecke and G. Bacher, *Cancer Res.*, 2009, **69**, 171-177.

39. J.-D. Jiang, A. S. Davis, K. Middleton, Y.-H. Ling, R. Perez-Soler, J. F. Holland and J. G. Bekesi, *Cancer Res.*, 1998, **58**, 5389-5395.

40. A. M. McElligott, E. N. Maginn, L. M. Greene, S. McGuckin, A. Hayat, P. V. Browne, S. Butini, G. Campiani, M. A. Catherwood, E. Vandenberghe, D. C. Williams, D. M. Zisterer and M. Lawler, *Cancer Res.*, 2009, **69**, 8366-8375.

41. C. Scolaro, A. Bergamo, L. Brescacin, R. Delfino, M. Cocchietto, G. Laurenczy, T. J. Geldbach, G. Sava and P. J. Dyson, *J. Med. Chem.*, 2005, **48**, 4161-4171.

42. A. Casini, C. Gabbiani, F. Sorrentino, M. P. Rigobello, A. Bindoli, T. J. Geldbach, A. Marrone, N. Re, C. G. Hartinger, P. J. Dyson and L. Messori, *J. Med. Chem.*, 2008, **51**, 6773-6781.

43. E. Meggers, *Chem. Commun.*, 2009, 1001-1010.

44. J. Singh, R. C. Petter, T. A. Baillie and A. Whitty, *Nat. Rev. Drug Discov.*, 2011, **10**, 307-317.

45. J. S. Lewis-Wambi, H. R. Kim, C. Wambi, R. Patel, J. R. Pyle, A. J. Klein-Szanto and V. C. Jordan, *Breast Cancer Res.*, 2008, **10**, R104.

46. T. Schnelldorfer, S. Gansauge, F. Gansauge, S. Schlosser, H. G. Beger and A. K. Nussler, *Cancer*, 2000, **89**, 1440-1447.

47. J. M. Hansen, Y. M. Go and D. P. Jones, *Annu. Rev. Pharmacol. Toxicol.*, 2006, **46**, 215-234.

48. D. P. Jones, Y. M. Go, C. L. Anderson, T. R. Ziegler, J. M. Kinkade, Jr. and W. G. Kirlin, *Faseb J.*, 2004, **18**, 1246-1248.

49. I. A. Cotgreave, *Biofactors*, 2003, **17**, 269-277.

50. A. Meister, *Cancer Res.*,1994, **54**, 1969-1975.

51. M. E. Anderson, *Chem.-Biol. Interact.*, 1998, **111**, 1-14.

52. M. Raderer and W. Scheithauer, *Cancer*, 1993, **72**. 3553-3563.

53. R. R. Perry, J. A. Mazetta, M. Levin and S. C. Barranco, *Cancer*, 1993, **72**, 783-787.

54. S. J. Berger, D. Gosky, E. Zborowska, J. K. Willson and N. A. Berger, *Cancer Res*, 1994, **54**, 4077-4083.

55. A. E. Oberli-Schrammli, F. Joncourt, M. Stadler, H. J. Altermatt, K. Buser, H. B. Ris, U. Schmid and T. Cerny, *Int. J. Cancer*, 1994, **59**, 629-636.

56. F. Joncourt, A. E. Oberli-Schrammli, M. Stadler, K. Buser, L. Franscini, M. F. Fey and T. Cerny, *Leuk. Lymphoma*, 1995, **17**, 101-109.

57. T. P. Mulder, J. J. Manni, H. M. Roelofs, W. H. Peters and A. Wiersma, *Carcinogenesis*, 1995, **16**, 619-624.

58. C. P. Schroder, A. K. Godwin, P. J. O'Dwyer, K. D. Tew, T. C. Hamilton and R. F. Ozols, *Cancer Invest.*, 1996, **14**, 158-168.

59. B. Halliwell, *Biochem J.*, 2007, **401**, 1-11.

60. J. Pouyssegur, F. Dayan and N. M. Mazure, *Nature*, 2006, **441**, 437-443.

61. G. L. Semenza, *Nat. Rev. Cancer*, 2003, **3**, 721-732.

62. W. Ying, *Antioxid. Redox Signaling*, 2008, **10**, 179-206.

63. E. Steckhan, S. Herrmann, R. Ruppert, E. Dietz, M. Frede and E. Spika, *Organometallics*, 1991, **10**, 1568-1577.

64. H. C. Lo, C. Leiva, O. Buriez, J. B. Kerr, M. M. Olmstead and R. H. Fish, *Inorg. Chem.*, 2001, **40**, 6705-6716.

65. Y. Yan, M. Melchart, A. Habtemariam, A. Peacock and P. Sadler, *J. Biol. Inorg. Chem.*, 2006, **11**, 483-488.

66. M. W. George, *U.S. Geological Survey Mineral Commodity Summaries (USGS Mineral Resources Program)*, 2008.

67. S. I. Venetskii, *Metallurgist*, 1974, **18**, 155–157.

68. H. C. Kolb, M. S. VanNieuwenhze and K. B. Sharpless, *Chem. Rev.*, 1994, **94**, 2483–2547.

69. T. J. Colacot, *Platinum Met. Rev.*, 2002, **46**, 82-83.

70. J. C. Gray, A. Pagelot, A. Collins, F. P. A. Fabbiani, S. Parsons and P. J. Sadler, *Eur. J. Inorg. Chem.*, 2009, **18**, 2673-2677.

71. J. W. Arblaster, *Platinum Met. Rev.*, 2004, **48**, 173-179.

72. P. Gaylarde and I. Sarkany, *Science*, 1968, **161**, 1157-1158.

73. M. Jasna, S. W. Douglas, G. E. Atilla-Gokcumen, S. M. S. Keiran, J. C. Patrick, D. W. Richard, F. Panagis, K. Stefan, H. Meenhard and M. Eric, *Chem.--Eur. J.*, 2008, **14**, 4816-4822.

74. C. Moucheron, A. Kirsch-De Mesmaeker and J. M. Kelly, *J. Photochem. Photobiol., B*, 1997, **40**, 91-106.

75. A. Dorcier, W. H. Ang, S. Bolano, L. Gonsalvi, L. Juillerat-Jeannerat, G. b. Laurenczy, M. Peruzzini, A. D. Phillips, F. Zanobini and P. J. Dyson, *Organometallics*, 2006, **25**, 4090-4096.

76. M. A. Esteruelas, H. Werner, *J. Organomet. Chem.*, 1986, **303**, 221-231.

77. L. Zhang, P. Carroll and E. Meggers, *Org. Lett.*, 2004, **6**, 521-523.

78. J. Maksimoska, D. S. Williams, G. E. Atilla-Gokcumen, K. S. Smalley, P. J. Carroll, R. D. Webster, P. Filippakopoulos, S. Knapp, M. Herlyn and E. Meggers, *Chem.--Eur. J.*, 2008, **14**, 4816-4822.

79. W. F. Schmid, R. O. John, G. Mühlgassner, P. Heffeter, M. A. Jakupec, M. Galanski, W. Berger, V. B. Arion and B. K. Keppler, *J. Med. Chem.*, 2007, **50**, 6343-6355.

80. B. Cebrián-Losantos, A. A. Krokhin, I. N. Stepanenko, R. Eichinger, M. A. Jakupec, V. B. Arion and B. K. Keppler, *Inorg. Chem.*, 2007, **46**, 5023-5033.

81. G. E. Bu̇chel, I. N. Stepanenko, M. Hejl, M. A. Jakupec, B. K. Keppler and V. B. Arion, *Inorg. Chem.*, 2011, **50**, 7690–7697.

82. H.-J. Yu, H. Chao, L. Jiang, L.-Y. Li, S.-M. Huang and L.-N. Ji, *Inorg. Chem. Commun.*, 2008, **11**, 553-556.

83. S. Dhar, D. Senapati, P. K. Das, P. Chattopadhyay, M. Nethaji and A. R. Chakravarty, *J. Am. Chem. Soc.*, 2003, **125**, 12118-12124.

84. S. B. Brown, E. A. Brown and I. Walker, *Lancet Oncol.*, 2004, **5**, 497-508.

85. A. A. Holder, D. F. Zigler, M. T. Tarrago-Trani, B. Storrie and K. J. Brewer, *Inorg. Chem.*, 2007, **46**, 4760-4762.

86. S.-W. Lai, Q. K. W. Chan, N. Zhu and C.-M. Che, *Inorg. Chem.*, 2007, **46**, 11003-11016.

87. R. R. Allison, G. H. Downie, R. Cuenca, X.-H. Hu, C. J. H. Childs and C. H. Sibata, *Photodiagnosis Photodyn. Ther.*, 2004, **1**, 27-42.

88. D. Kessel, *Photodiagnosis Photodyn. Ther.*, 2004, **1**, 3-7.

89. R. R. Allison, H. C. Mota and C. H. Sibata, *Photodiagnosis Photodyn. Ther*., 2004, **1**, 263-277.

90. N. J. Farrer, L. Salassa and P. J. Sadler, *Dalton Trans.*, 2009, 10690-10701.

91. L. Brancaleon and H. Moseley, *Laser. Med. Sci.*, 2002, **17**, 173-186.

92. R. E. Holmlin, E. D. A. Stemp and J. K. Barton, *J. Am. Chem. Soc.*, 1996, **118**, 5236-5244.

93. I. Beletskaya, V. S. Tyurin, A. Y. Tsivadze, R. Guilard and C. Stern, *Chem. Rev.*, 2009, **109**, 1659-1713.

94. A. F. Peacock and P. J. Sadler, *Chem-Asian J.*, 2008, **3**, 1890-1899.

95. S. H. van Rijt, A. F. Peacock, R. D. Johnstone, S. Parsons and P. J. Sadler, *Inorg. Chem*., 2009, **48**, 1753-1762.

96. S. H. van Rijt, A. J. Hebden, T. Amaresekera, R. J. Deeth, G. J. Clarkson, S. Parsons, P. C. McGowan and P. J. Sadler, *J. Med. Chem.*, 2009, **52**, 7753-7764.

97. I. Boussina, R. Lagier, H. Ott and G. H. Fallet, *Scand. J. Rheumatol*., 1976, **5**, 53-59.

98. W.-X. Ni, W.-L. Man, M. T.-W. Cheung, R. W.-Y. Sun, Y.-L. Shu, Y.-W. Lam, C.-M. Che and T.-C. Lau, *Chem. Commun.*, 2011, **47**, 2140-2142.

99. R. E. Morris, R. E. Aird, P. del Socorro Murdoch, H. Chen, J. Cummings, N. D. Hughes, S. Parsons, A. Parkin, G. Boyd, D. I. Jodrell and P. J. Sadler, *J. Med. Chem.*, 2001, **44**, 3616-3621.

100. R. E. Aird, J. Cummings, A. A. Ritchie, M. Muir, R. E. Morris, H. Chen, P. J. Sadler and D. I. Jodrell, *Br. J. Cancer*, 2002, **86**, 1652-1657.

101. F. Wang, H. Chen, S. Parsons, I. D. H. Oswald, J. E. Davidson, P. J. Sadler, *Chem.- Eur. J.*, 2003, **9**, 5810-5820.

102. O. Novakova, J. Kasparkova, O. Vrana, P. M. van Vliet, J. Reedijk and V. Brabec, *Biochemistry*, 1995, **34**, 12369-12378.

103. A. F. A. Peacock, A. Habtemariam, R. Fernandez, V. Walland, F. P. A. Fabbiani, S. Parsons, R. E. Aird, D. I. Jodrell and P. J. Sadler, *J. Am. Chem. Soc.*, 2006, **128**, 1739-1748.

104. A. F. A. Peacock, S. Parsons and P. J. Sadler, *J. Am. Chem. Soc.*, 2007, **129**, 3348-3357.

105. R. A. Krause and K. Krause, *Inorg. Chem.*, 2002, **19**, 2600–2603.

106. E. M. Kosower and N. S. Kosower, *Nature*, 1969, **224**, 117-120.

107. M. F. Renschler, *Eur. J. Cancer*, 2004, **40**, 1934-1940.

108. E. M. Kosower and T. Miyadera, *J. Med. Chem.*, 1972, **15**. 307-312.

109. B. K. Ghosh, A. Mukhopadhyay, S. Goswami, S. Ray and A. Chakravorty, *Inorg. Chem.*, 2002, **23**, 4633–4639.

110. Y. C. Martin, *J. Med. Chem.*, 1981, **24**, 229-237.

111. K. Birchall, V. J. Gillet, P. Willett, P. Ducrot and C. Luttmann, *J. Chem. Inf. Model.*, 2009, **49**, 1330-1346.

112. G. A. Patani and E. J. LaVoie, *Chem. Rev.*, 1996, **96**, 3147-3176.

Chapter 2
Materials and Methods

In this chapter, the general techniques and instrumentation used in this thesis are described. More details of individual experiments are described in each appropriate chapter. The synthesis and characterization of osmium iodido dimers used as starting materials are also included.

2.1 Materials and Synthesis

2.1.1 Materials

$OsCl_3 \cdot 3H_2O$ and osmium Specpure Plasma Standard were purchased from Alfa-Aesar. Ethanol and methanol were dried over Mg/I_2 or anhydrous quality was used (Aldrich). All other reagents used were obtained from commercial suppliers and used as received. The preparations of the starting materials $[Os(\eta^6\text{-bip})Cl_2]_2$ and $[Os(\eta^6\text{-}p\text{-cym})Cl_2]_2$ have been previously reported.[1] The synthesis method of the azopyridine ligands has been previously described.[2] The A2780 human ovarian carcinoma cell line and A549 human lung adenocarcinoma epithelial cell line were purchased from the European Collection of Animal Cell Cultures (Salisbury, UK), RPMI-1640 media and trypsin were purchased from Invitrogen, bovine serum from Biosera, penicillin, streptomycin, trichloroacetic acid (TCA) and sulforhodamine B (SRB) from Sigma-Aldrich, and tris[hydroxymethyl]aminomethane (Tris) from Formedium.

$[Os(\eta^6\text{-bip})I_2]_2$. The dimer $[Os(\eta^6\text{-bip})Cl_2]_2$ (100.4 mg, 0.12 mmol) was stirred at 353 K for 1 h suspended in water (200 mL). The solution then hot-filtered and KI (1039.8 mg, 6.26 mmol) was added to the solution. A deep orange precipitate was formed immediately. The solution was left in the fridge (277K) for 2 h. The precipitate was collected by filtration and washed with cold ethanol and diethyl ether, then dried in a desiccator overnight. Yield: 95.4 mg (66.0%). Anal. ^{1}H NMR(DMSO-d_6) δ 7.74 (d, 4H), 7.45 (m, 6H), 6.84 (d, 4H), 6.56 (d, 2H), 6.34 (d, 4H). CHN analysis: Found C, 24.33 %; H, 1.64 %, Calcd for $C_{24}H_{20}I_4Os_2$: C, 24.09 %; H, 1.68 %.

[Os(η^6-*p*-cym)I_2]$_2$. The dimer [Os(η^6-*p*-cym)Cl_2]$_2$ (103.8 mg, 0.135 mmol) was stirred at 353 K for 1 h to allow it dissolved in water (50 mL). Then KI (2683.9 mg, 16.18 mmol) was added to the solution and heated under reflux for 1 h. A deep orange precipitate was formed immediately. The solution was left in a fridge (277K) for 2 h. The precipitate was collected by filtration and washed with cold ethanol and diethyl ether, then dried in a desiccator overnight. Yield: 112.6 mg (67.9%). Anal. ^{1}H NMR (DMSO-d_6) δ 6.10 (dd, 8H), 3.04 (m, 2H), 2.43 (s, 6H), 1.25 (d, 12H). CHN analysis: Found: C, 20.78 %; H, 2.35 %, Calcd for $C_{20}H_{28}I_4Os$: C, 20.77 %; H, 2.44 %.

2.1.2 Synthesis

Osmium complexes studied in this thesis were synthesized through one general method: stirring osmium dimer with chelating ligand in methanol or methanol/water mixture at ambient temperature or 353K for a period of time, then an excess of NH_4PF_6 was added to the solution, the precipitate (product) was collected by filtration and washed with cold ethanol and diethyl ether, finally dried under vacuum. The general synthesis route was summarized below in Chart 2.1.

Chart 2.1. Synthesis route for osmium complexes studied in this thesis.

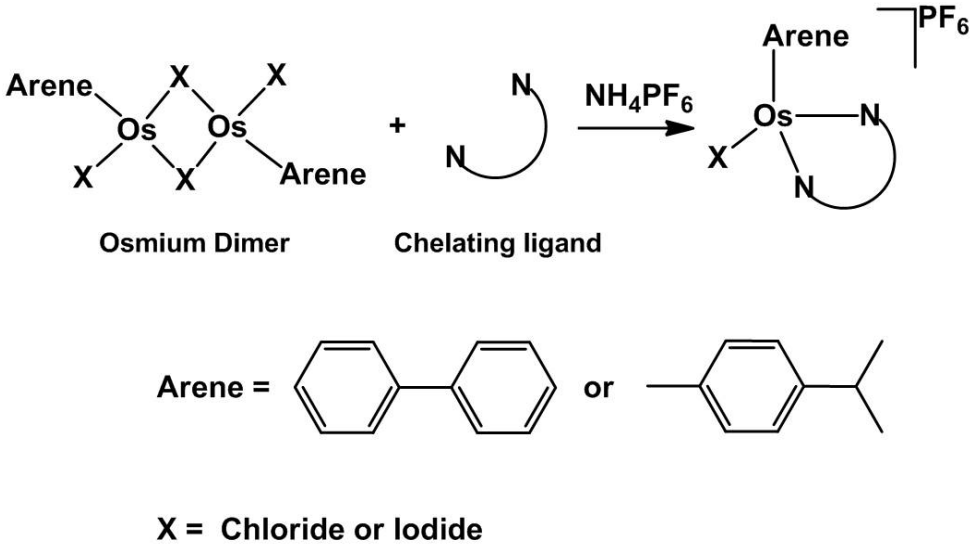

2.2 Instrumentation and Methods

2.2.1 NMR Spectroscopy[3]

^{1}H NMR spectra were acquired in 5 mm NMR tubes at 298K or 310K on either Bruker DPX-400, Bruker DRX-500, Bruker AV III 600 or Bruker AV II 700 spectrometers. ^{1}H NMR chemical shifts were internally referenced to acetone (2.09 ppm), 1, 4-dioxane (3.71 ppm), $CHCl_3$ (7.27 ppm) or DMSO (2.50 ppm). A lot of NMR were performed in aqueous solutions so as to be biological relevant. The use of aqueous solutions results in a huge HOD signal which can obscure other proton peaks in the ^{1}H spectrum. To minimize this effect, the HOD signal can be suppressed by presaturation.[4] This technique involves the saturation of the HOD peak by irradiation of the frequency of water between pulse sequences. The disadvantage of this technique is that the signals close to HOD peak are also reduced in terms of intensity. All data processing was carried out using MestReC or TOPSPIN version 2.0 (Bruker U.K. Ltd.).

2.2.2 Electrospray Ionisation Mass Spectrometry (ESI-MS)

Spectra were obtained by preparing the samples in 50% CH_3CN and 50% H_2O (v/v) and infusing into the mass spectrometer (Varian 4000). The mass spectra were recorded with a scan range of m/z 500-1000 for positive ions. Data were processed using Data Analysis version 3.3 (Bruker Daltonics).

2.2.3 Elemental Analysis

Elemental analysis (carbon, hydrogen, and nitrogen) was carried out through Warwick Analytical Service using an Exeter analytical elemental analyzer (CE440).

2.2.4 UV-Vis Spectroscopy

UV-Vis spectra were recorded on a Cary 50-Bio spectrophotometer using 1-cm path-length quartz cuvettes (0.5 mL) and a PTP1 Peltier temperature controller. Spectra were recorded at 310 K from 800 to 200 nm. All data processing was carried out using Excel 2007 (Microsoft, USA) or Origin 7.5 (Origin, USA).

2.2.5 pH^* Measurements

pH^* (pH meter reading from D_2O solution without correction for effects of deuterium on glass electrode) values were measured at ambient temperature before the NMR spectra were recorded, using a Corning 240 pH meter equipped with a microcombination electrode calibrated with Aldrich buffer solutions at pH 4, 7 and 10. The pH^* values were adjusted with dilute NaOH or HNO_3 solutions in D_2O.

2.2.6 Calculations of pK_a^* Values

^1H NMR spectra were recorded when the pH^* values of aqua complexes in D_2O were varied from ca. 1 to 12 in pH^* by adjusting with diluted NaOH or HNO_3 solutions in D_2O. The chemical shifts of the ligands were plotted against pH^* values. The curve from the pH^* titration was fitted to the Henderson-Hasselbalch equation[5] using ORIGIN 7.5, with the assumption that the observed chemical shifts are weighted averages according to the populations of the protonated and deprotonated species. These pK_a^* values can be coverted to pK_a values by using the equation $pK_a = 0.929pK_a^* + 0.42$ as suggested by Krezel and Bal.[6]

The Henderson-Hasselbalch Equation: $pH = pK_a + \log_{10}([A^-]/[HA])$

When half is dissocated: $[HA] = [A^-]$ and $pH = pK_a$

When δ_{obs} is the chemical shift of observation at a given pH and δ_{HA} and δ_{A^-} are the chemical shifts at low and high pH respectively, the Henderson-Hasselbalch equation can be modified as below[7]:

$$\delta_{obs} = [\delta_{HA} + \delta_{A^-} \times 10\ (pK_a^* - pH^*)]/[1 + 10\ (pK_a^* - pH^*)]$$

2.2.7 X-ray Crystallography

X-ray diffraction data were generally obtained on an Oxford Diffraction Gemini four-circle system with a Ruby CCD area detector using Mo Kα radiation.[8] Absorption corrections were applied using ABSPACK. The crystals were mounted in oil and held at 100(2) K with the Oxford Cryosystem Cryostream Cobra. The structures were solved by direct methods using SHELXS (TREF) with additional light atoms found by Fourier methods.[9] Refinement used SHELXL 97.[10] H atoms were placed at geometrically calculated positions and refined riding on their parent atoms. All the data collection and solution of crystal structures were carried out by Dr. Guy Clarkson from Department of Chemistry, University of Warwick. Details of the acquisition and solving the individual crystal structures are explained in the corresponding chapters.

2.2.8 Electrochemistry

The electrochemical study was carried out using the similar conditions as for the ruthenium analogues reported previously.[2] It was performed with a CHI730A bipotentiostat (CH Instrument, USA) system. All of the electrochemical techniques used a three-electrode configuration with all the electrodes in solution, one 2 mm diameter platinum disc electrode was used as the working electrode with a chloridized silver wire as the quasi-reference electrode and a Pt counter electrode (CH Instrument, USA). The reference electrode was Ag/AgCl in a solution of 0.1 M [TBA][BF_4] in DMF against which $E_{1/2}$ for the ferrocenium/ferrocene couple was measured to be +0.55 V.

2.2.9 Cell Cultures

A549 non-small cell lung and A2780 ovarian human cell lines (ECACC, Salisbury, UK) were cultured in RPMI 1640 cell culture medium supplemented with 1 mM sodium pyruvate, 2 mM L-glutamine and 10% fetal bovine serum.

2.2.10 Determination of IC_{50} Values

The concentrations of the osmium complexes that inhibit 50% of the proliferation of human ovarian A2780 cancer cells were determined using the sulforhodamine B assay (Fig. 2.1).[11] A2780 cells were seeded in 96-well plates (Falcon) at 5000 cells/well, after incubation for 48 h. The complexes were solubilised in DMSO (Sigma) to provide 10 mM stock solutions. These were serially diluted with cell culture media to give concentrations four-fold greater than the final concentrations for the assay. The complexes diluted in cell culture media were added to the 96-well plates with cells in triplicate. The final DMSO concentration in each well was no more than 1% (v/v). The media containing the complexes were removed after 24 h. The cells were washed with phosphate buffered saline once and cell culture medium was added (150 µL/well). The cells were then allowed to grow for a further 72 h. The surviving cells were fixed by adding 150 µL/well of 50% (w/v) trichloroacetic acid and incubated for 1 h in a refrigerator (277 K). The plates were washed with tap water three times and dried under a flow of warm air, 0.4% sulforhodamine B (Sigma) solution (100 µL/well) was added, followed by washing with 1% acetic acid five times and drying under a flow of warm air. The dye was dissolved in 10 mM Tris buffer (200 µL/well). The absorbance of each well was determined using a Multiskan Ascent plate reader (Labsystems) at 540 nm. The absorbance of SRB in each well is directly proportional to the cell number. Then the absorbance was plotted against concentration and the IC_{50} determined by using Origin software (version 7.5).

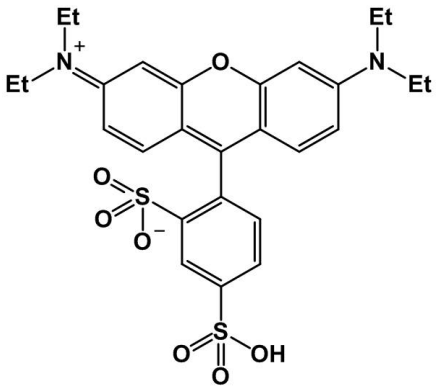

Sulforhodamine B

Figure 2.1 Chemical structure of SRB

2.2.11 NAC and L-BSO Combination Treatments

A2780 cells or A549 cells were treated with 50 μM NAC or L-BSO and various concentrations of osmium complexes for 24 h. Then NAC/L-BSO and osmium complexes were removed at the same time and the cells were washed with PBS once, then incubated for a further 72 h for recovery. Cell viability was determined by using the SRB assay as described above.

2.2.12 Inductively Coupled Plasma Mass Spectroscopy (ICP-MS)

ICP-MS analyses were carried out on an Agilent Technologies 7500 series ICP-MS instrument. The water used for ICP-MS analysis was double deionized using a USF Elga UHQ PS water deionizer. To make the stock solution of osmium standard, the osmium Specpure plasma standard was diluted in double deionized water to 20 ppm; the osmium standards for calibration were freshly prepared by diluting this stock solution with 3.6 % HNO_3 in double deionized water. The concentrations used were 400, 200, 100, 50, 25, 10, 5, 1, 0.5 and 0.1 ppb of ^{189}Os. In this thesis, ICP-MS was employed to analyze the osmium concentration in water solution, cell samples and tissue samples after digestions. All the water used for ICP-MS was double deionised by using USF Elgar UHQ water system.

2.2.13 Determination of Partition Coefficient (log P)

Octanol-saturated water and water-saturated octanol were prepared by stirring the mixtures of octanol and water for 24 h. Aliquots of stock solutions of osmium complexes in octanol-saturated water (2 mL) were added to the same volumes of water-saturated octanol (2 mL), and the solutions were shaken in an IKA Vibrax VXC basic shaker for 4 h at the speed of 500 g/min after partition. The aqueous layer was transferred into test tubes for osmium analysis. Aqueous samples before and after partitioning were diluted with 3.6 % HNO_3 to the appropriate range for the analysis by ICP-MS calibrated with aqueous standards (osmium, 0.1-400 ppb). These procedures were carried out at ambient temperature (ca. 298 K). Log P values for osmium complexes were calculated using the equation log P_{oct} = log($[Os]_{oct}/[Os]_{aq}$).[12]

2.2.14 Cellular Uptake

A2780 cells were seeded at the concentration of 10^6 cells/well in 6-well plates. After 24 h incubation, cells were exposed to osmium complex. After drug exposure, the drug-containing medium was removed. Then samples were washed with PBS twice, trypsinized, collected and stored at 253 K until ICP-MS analysis for osmium content. The numbers of cells were counted using a cytometer. The whole cell pellets were digested as described above. Firstly, 0.5 mL of freshly distilled 72% HNO_3 was added to each 1 mL cells pellets, and the samples were transferred into Wheaton V-Vials. The vials were heated in an oven at 373 K for 16 h to digest the samples fully, allowed to cool, and then transferred to Falcon tubes. The vials were washed with double deionized water three times and diluted 10 times with double deionized water to obtain 6% HNO_3 sample solutions. A blank and the standards were loaded into the sample tray and were run from the lowest to the highest concentration in a ‘no gas’ mode, followed by the samples.

2.2.15 Separation of Cell Fractions

The A2780 cells were seeded into Petri dishes at a concentration of 5×10^6 cells/dish. After 24 h incubation, osmium compounds were added. The cells were harvested after a further incubation with osmium compound for 24 h. Then the four cell fractions (cytosol, membrane plus particulate fraction, nucleus and cytoskeleton) were separated following the protocol described for the kit (Biovision, Inc, USA). The concentrations of osmium in different fractions were measured by ICP-MS after digestion following the same method as for the cellular uptake study.

2.2.16 Detection of ROS

To detect changes in general oxidative stress,[13] the level of ROS (including O_2^-, $OH^{\cdot}$, H_2O_2) in A2780 cells was determined using the probe 2′,7′-dichlorodihydrofluorescein-diacetate (DCFH-DA, Figure 2.2). When taken up by live cells, DCFH-DA hydrolyzes to 2′,7′-dichlorodihydrofluorescein (DCFH), which in turn is oxidized to 2′,7′-dichlorofluorescein (DCF) in the presence of ROS and detected by its intense fluorescence.[14, 15]

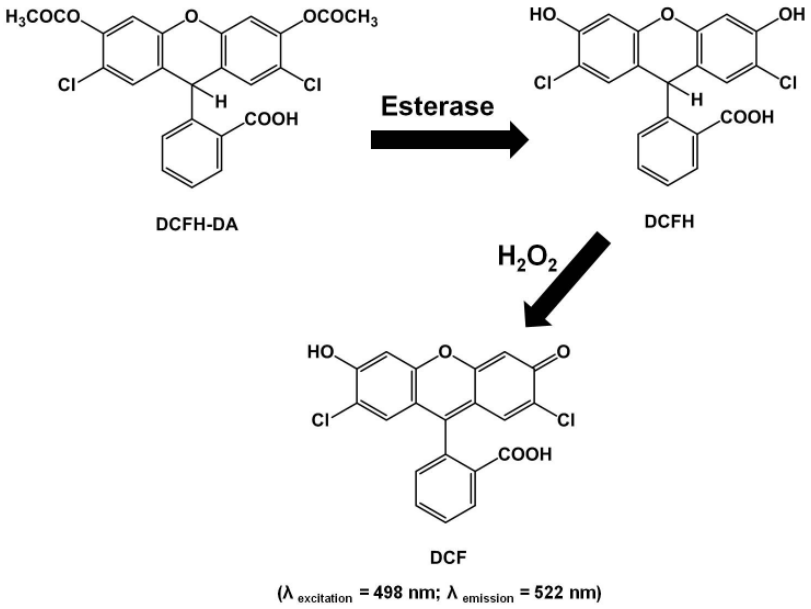

Figure 2.2 Mechanism of de-esterification from DCFH-DA to DCFH, which is oxidized to fluorescent DCF.

The vial of DCFH-DA was opened under N_2 protection, and contents were dissolved in DMSO to give a 10 mM stock solution. A2780 cells were seeded (5000 cells/well) into black 96-well plates and incubated for 24 h at 310 K, 5% CO_2, high humidity. Cells were loaded with DCFH-DA (10 μM) and incubated for 30 min. The probe was removed and PBS was used to wash the cells twice. The cells were then kept in PBS solution and osmium compound was added. Hydrogen peroxide was also added as the positive control. The fluorescence was recorded over a period of 4 h at 310 K by excitation at 480 nm and emission at 530 nm on a TECAN plate reader.

2.2.17 Cell Cycle Analysis[16]

To analyze the cell cycle distributions, propidium iodide (Fig. 2.3) is used as one fluorescent probe for cell cycle and apoptosis analysis.[17] It can be excited with 488 nm wavelength light then show red fluorescence. It binds to DNA by intercalating between the nucleobases with little sequence preference, it can also bind to RNA, so it is necessary to use RNAse to treat the cell samples to avoid this effect before analyzing cell cycle. Once the PI dye is bound to nucleic acids, its fluorescence is enhanced 20~30 fold which makes it more sensitive for detection. PI is membrane impermeant, in that, for the cell cycle analysis, all the cells should be fixed or treated by permeabilizing agent (eg. Triton X-100) to make sure PI can get through cellular membrane.

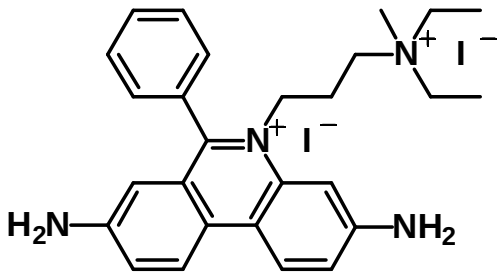

Propidium iodide (PI)

Figure 2.3 Chemical structure of PI.

A2780 cells were incubated with osmium complex of various concentrations for 24 h and then harvested. Then the collected cells were washed with PBS and fixed in 70% ethanol (253 K). The fixed cells were centrifuged and washed once with PBS, followed by resuspension in PBS containing 7.5 µM propidium iodide (PI) and 100 µg/ml RNase A. They were analyzed by flow cytometry (FACS-Calibur, Beckton Dickenson). The cell cycle distribution was evaluated using the Flow Jo 7.0 (Tree Star, USA).

2.2.18 Tubulin Polymerization Assay

A cytoskeleton tubulin polymerization assay kit (Cytoskeleton, USA catalogue no BK004) was used in the tubulin polymerization study. Briefly, 10 µL of general tubulin buffer (80 mM PIPES, pH 6.9, 2 mM $MgCl_2$ and 0.5 mM EGTA) containing osmium compound, colchicine or taxol was pipetted into the prewarmed 96 well microplate. Tubulin (defrosted to room temperature from -80 °C and then placed on ice before use) was diluted with tubulin polymerization buffer with 1 mM GTP to a final concentration of 4 mg mL^{-1}. Diluted tubulin (100 µL) was added into the wells containing osmium compound, colchicine or taxol. Diluted tubulin (100 µL) mixed with general tubulin buffer (10 µL) served as control. The absorbance at 340 nm was read immediately with a Tecan microplate reader (TECAN, Switzerland).

2.2.19 Immunofluorescence by Confocal Microscopy[18]

A2780 Cells were seeded on Lab-TekTM Chamber Slides (Thermo Scientific Nunc, UK) 10,000 cells/chamber, after 24 h incubation, osmium compound at different concentrations were added and incubated for another 24 h. Cells were fixed with 4% formaldehyde in PBS (20 min, 310 K), then rinsed with PBS (3 × 2 mL×2 min), and permeabilized with 0.1% Triton X-100 solution (PBS solution) for 15 min at ambient temperature. The cells were blocked with blocking buffer (2 mg/ mL BSA, overnight at 269 K), and then, the cell monolayers were incubated

(1 h, 310 K) with monoclonal anti-α-tubulin-Alexa 488 (4 µg/mL) (Invitrogen Molecular Probles, Catalog No. 32-2588) and PI (7.5 µM). The structure of Alexa 488 was shown in Figure 2.4. After the incubation, the cells were washed with PBS and the immunofluorescence was detected using a Leica SP5 fluorescence confocal microscope, with 100× objective.

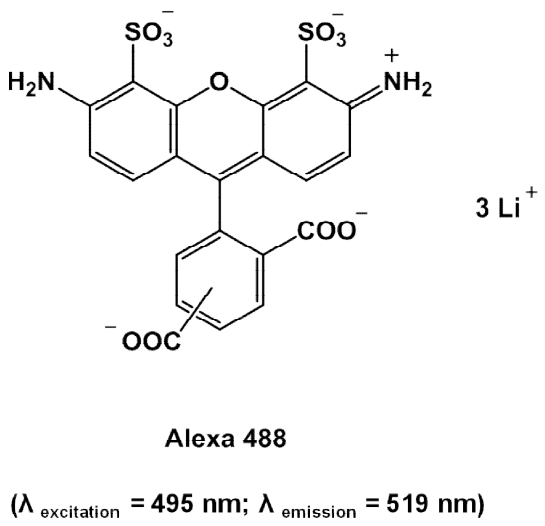

Figure 2.4 Chemical structure of Alexa 488.

2.3 References

1. A. F. A. Peacock, A. Habtemariam, S. A. Moggach, A. Prescimone, S. Parsons and P. J. Sadler, *Inorg. Chem.*, 2007, **46**, 4049-4059.
2. S. J. Dougan, A. Habtemariam, S. E. McHale, S. Parsons and P. J. Sadler, *Proc. Natl. Acad. Sci. U. S. A.*, 2008, **105**, 11628-11633.
3. P. J. Hore, ed., *Nuclear Magnetic Resonance*, Oxford University Press Inc, New York, 2001.
4. G. Wider, S. Macura, A. Kumar, R. R. Ernst and K. Wüthrich, *J. Magn. Reson.*, 1984, **56**, 207-234.
5. H. N. Po and N. M. Senozan, *J. Chem. Educ.*, 2001, **78**, 1499-1503.
6. A. Krezel and W. Bal, *J. Inorg. Biochem.*, 2004, **98**, 161-166.
7. R. Tribolet and H. Sigel, *Eur. J. Biochem.*, 1987, **163**, 353-363.
8. *CrysAlis PRO*, Oxford Diffraction Ltd., Abington, Oxfordshire, U.K., 2007.
9. G. M. Sheldrick, Acta Crystallogr., Sect. A: Found. Crystallogr., 1990, **46**, 467–473
10. G. M. Sheldrick, SHELX97, Programs for Crystal Structure Analysis (Release 97-92), University of Göttingen, Germany, 1997.
11. V. Vichai and K. Kirtikara, *Nat. Protocols*, 2006, **1**, 1112-1116.
12. A. Leo, C. Hansch and D. Elkins, *Chem. Rev.*, 1971, **71**, 525-616.
13. B. Halliwell and M. Whiteman, *Br. J. Pharmacol.*, 2004, **142**, 231-255.
14. H. Wang and J. A. Joseph, *Free Radical BioMed.*, 1999, **27**, 612-616.
15. A. Gomes, E. Fernandes and J. L. F. C. Lima, *J. Biochem. Biophys. Methods*, 2005, **65**, 45-80.
16. I. Nicoletti, G. Migliorati, M. C. Pagliacci, F. Grignani and C. Riccardi, *J. Immunol. Methods*, 1991, **139**, 271-279.
17. C. Riccardi and I. Nicoletti, *Nat. Protocols*, 2006, **1**, 1458-1461.
18. M. A. Jordan and L. Wilson, *Nat. Rev. Cancer*, 2004, **4**, 253-265.

Chapter 3
Os^{II} Arene Azopyridine-R Complexes

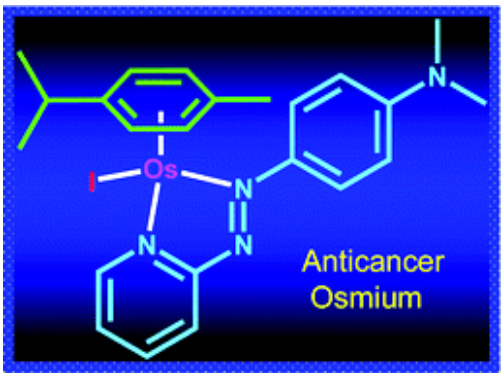

3.1 Introduction

The success of platinum complexes (e.g. cisplatin and carboplatin) as anticancer drugs is well known, however, these drugs have a limited spectrum of activity, can have severe toxic side-effects, and tumours often develop resistance.[1, 2] A number of ruthenium-based compounds have been reported to display promising anticancer activity[3-6] and two octahedral ruthenium(III) complexes have reached clinical trials.[7, 8] The Ru^{III} complexes are thought to be reduced to active Ru^{II} species *in vivo*. Ruthenium(II) can be stabilized by π-bonded arene ligands and a range of Ru^{II} arene complexes of the type [Ru(η^6-arene)(XY)Z)] where XY = diamine chelate and Z = Cl, show *in vitro* and *in vivo* anticancer activity.[9, 10] These complexes can undergo activation via hydrolysis and bind strongly to DNA, a potential target.[11]

Arene complexes of the heavier congener osmium(II) display similar structures in the solid state to those of Ru^{II} but are subtly different with regard to their chemical reactivity. For example, Os^{II} arene ethylenediamine chlorido complexes hydrolyze ca. 40x more slowly and the related aqua adducts have pK_a values for Os–OH_2/OH which are ca. 1.5 pK_a units lower (more acidic) than those of the analogous Ru^{II} complexes.[9, 12] Faster ligand exchange in Os^{II} complexes can be achieved by incorporating oxygen-containing chelating ligands, e.g. picolinates.[13, 14] Several examples of Os^{II} arene complexes which exhibit cancer cell cytotoxicity have now been reported.[15-19]

The introduction of strong π-acceptor chelating (XY) ligands such as bipyridine or azopyridine (Azpy), dramatically changes the properties of the Os and Ru complexes.[11, 16, 20] For example, Ru complexes of the type [Ru(η^6-biphenyl)(Azpy)I]$^+$ are relatively inert towards ligand substitution and appear to kill tumour cells by ligand-centered redox-mediated mechanisms.[21] Here we report the synthesis of a range of osmium complexes of formula [Os(η^6-arene)(azopyridine-R)Z]$^+$ where arene = *p*-cymene (*p*-cym) or biphenyl (bip), R =

hydrogen (H), hydroxyl (OH) or dimethylamino (NMe_2), and Z = chloride or iodide (Chart **3.1**). The X-ray crystal structures of five complexes are reported and their chemical reactivity is investigated. Surprisingly, several of these Os^{II} azopyridine complexes are an order of magnitude more potent than the clinically-used drug cisplatin towards a range of human cancer cell lines. An evaluation of their toxicity in mice bearing xenografted colon tumours is also reported.

3.2 Experimental Section

3.2.1 Synthesis of Azo Ligands. Syntheses of azpy ligands were based on literature reports.[11]

3.2.2 Synthesis of Complexes

Complexes **1** – **12** were prepared by the same general method: reaction of the appropriate azopyridine derivative with the dimers; $[Os(\eta^6\text{-bip})Cl_2]_2$, $[Os(\eta^6\text{-bip})I_2]_2$, $[Os(\eta^6\text{-}p\text{-cym})Cl_2]_2$ or $[Os(\eta^6\text{-}p\text{-cym})I_2]_2$. The purities of all compounds prepared were determined to be ≥95% by elemental analysis.

$[Os(\eta^6\text{-bip})(Azpy)I]PF_6$ (1)

$[Os(\eta^6\text{-bip})I_2]_2$ (30 mg, 0.025 mmol) in methanol (30 mL) and water (10 mL) was heated under reflux at 353 K under nitrogen for 2 h. Azpy (9.15 mg, 0.05 mmol) in methanol (10 mL) was added drop-wise. The solution-colour changed from orange to red immediately. After heating under reflux for another 2 h; the solution was hot-filtered and the volume was reduced to about 10 mL on a rotary evaporator. Ammonium hexafluorophosphate (40.0 mg. 0.25 mmol) was added. The solution was left in the fridge for 2 h. A brown powder precipitated out. The powder was collected by filtration and washed with little cold ethanol and diethyl ether, then dried in a dessicator overnight. Yield: 20 mg (61.1%). Anal. ESI-MS Calcd for $C_{23}H_{19}IN_3Os$: m/z 656.0, found 655.9. ^{1}H NMR($(CD_3)_2CO$) δ 9.44 (d,

1H, J = 8 Hz), 9.01 (d, 1H, J = 8 Hz), 8.38 (t, 1H, J = 8 Hz), 7.98 (d, 2H, J = 8 Hz), 7.76 (m, 3H), 7.47 (m, 6H), 7.12 (d, 1H, J = 6 Hz), 6.98 (t, 1H, J = 6 Hz), 6.83 (m, 2H), 6.72 (t, 1H, J = 5 Hz). CHN analysis Found: C, 35.41%; H, 2.40%; N, 5.55%, Calcd for $C_{23}H_{19}F_6IN_3OsP$: C, 34.55 %; H, 2.40 %; N, 5.26 %.

[Os(η^6-*p*-cym)(Azpy)I]PF_6 (2)

[Os(η^6-*p*-cym)I_2]$_2$ (30.5 mg, 0.0264 mmol) was dissolved in methanol (20 mL) and Azpy (9.6mg, 0.053 mmol) in methanol (10 mL) was added drop-wise. The solution-colour changed from yellow to brown gradually and was stirred at ambient temperature for 3 h. The volume was reduced to about 10 mL by removal of methanol on a rotary evaporator. Ammonium hexafluorophosphate (17.7 mg. 0.11 mmol) was added. Then the solution was left in the freezer for 24 h; a dark coloured powder precipitated, which was collected by filtration and washed with cold ethanol and diethyl ether, then finally dried in vacuum. Yield: 14.5 mg (35.3%). Anal. Calcd for $C_{21}H_{23}IN_3Os$: m/z 636.1, found 636.0. ^{1}H NMR($(CD_3)_2CO$) δ 9.66 (d, 1H, J = 6 Hz), 9.04 (d, 1H, J = 8 Hz), 8.41 (t, 1H, J = 8 Hz), 8.20-8.19 (m, 2H), 7.87-7.75 (m, 4H), 6.77 (d, 1H, J = 6 Hz), 6,43 (d, 1H, J = 6 Hz), 6.38 (d, 1H, J = 5 Hz), 6.32 (d, 1H, J = 5 Hz), 2.67 (s, 3H), 2.62 (m, 1H), 1.04 (d, 3H, J = 7 Hz), 1.02 (d, 3H, J = 7 Hz). CHN analysis Found: C, 32.19%; H, 2.85%; N, 5.34%, Calcd for $C_{21}H_{23}F_6IN_3OsP$: C, 32.36%; H, 2.97%; N, 5.39%. Single crystals suitable for X-ray diffraction were obtained by slow evaporation of a methanol solution of complex **2** at ambient temperature.

[Os(η^6-bip)(Azpy-OH)I]PF_6 (3)

[Os(η^6-bip)I_2]$_2$ (86.1 mg, 0.072 mmol) in methanol (30 mL) and water (10 mL) mixture was heated under reflux at 353 K under nitrogen for 2 h. Azpy-OH (19.0 mg, 0.096 mmol) in methanol (10 mL) was added drop-wise, the solution colour changed from orange to red immediately, the solution was heated to reflux for further 2 h, hot-filtered, and the volume was reduced to about 10 mL by removal

of methanol on a rotary evaporator. Ammonium hexafluorophosphate (118.5 mg, 0.73 mmol) was added and the solution was left in the fridge for 2 h. A deep brown powder precipitated which was filtered off and washed with cold ethanol and diethyl ether, then dried in a dessicator overnight. Yield: 63.1 mg (53.7%). Anal. ESI-MS Calcd for $C_{23}H_{19}IN_4OOs$: m/z 672.02, found 671.9. ^1H NMR($(CD_3)_2CO$) δ 9.30 (d, 1H, J = 9 Hz), 8.80 (d, 1H, J = 8 Hz), 8.31-9.27 (m, 1H), 8.02 (d, 2H, J = 9 Hz), 7.66-7.63 (m, 1H), 7.46 (m, 5H), 7.01 (d, 1H, J = 6 Hz), 6.93 (d, 2H, J = 6 Hz), 6.82 (m, 2H), 6.72 (t, 1H, J = 6 Hz), 6.66 (d, 1H, J = 6 Hz). CHN analysis Found: C, 34.07%; H, 2.34%; N, 5.03%, Calcd for $C_{23}H_{19}F_6IN_4OOsP$: C, 33.87%; H, 2.34%; N, 5.03%. Single crystals of [(η^6-bip)Os(azpy-O)I]·$0.5H_2O$ suitable for X-ray diffraction were obtained by slow evaporation of a methanol solution of complex 3^* at ambient temperature.

[Os(η^6-*p*-cym)(Azpy-OH)I]PF_6 (4)

[Os(η^6-*p*-cym)I_2]$_2$ (50.5 mg, 0.0437 mmol) was dissolved in methanol (50 mL); Azpy-OH (17.4 mg, 0.087 mmol) in methanol (10 mL) was added drop-wise; The solution was stirred at ambient temperature for 24 h with 10 drops of 1 M HCl solution; The volume was reduced to about 2 mL by removal of methanol on a rotary evaporator. The complex was purified by chromatography on a Sephadex LH20 column. Ammonium hexafluorophosphate (28.6 mg. 0.18 mmol) was added. Then the solution was left in the fridge for 0.5 h. A dark coloured powder precipitated out, which was collected by filtration and washed with cold ethanol and diethyl ether, then finally dried in vacuum. Yield: 30.6 mg (43.2%). Anal. ESI-MS Calcd for $C_{21}H_{23}IN_3Os$: m/z 652.1, found 652.0. ^1H NMR($(CD_3)_2CO$) δ 9.75 (bs, 1H), 9.58 (d, 1H, J = 6 Hz), 9.93 (d, 1H, J = 8 Hz), 8.40-8.38 (m, 1H), 8.19 (d, 2H, J = 9 Hz), 7.83-7.82 (m, 1H), 7.15 (d, 2H, J = 9 Hz), 6.72 (d, 1H, J = 6 Hz), 6.43 (m, 2H), 6.34 (d, 1H, J = 6 Hz), 3.35 (s, 3H), 2.63 (m, 1H), 1.04 (d, 3H, J = 7 Hz), 1.02 (d, 3H, J = 7 Hz). CHN analysis Found: C, 31.04%; H, 3.05%; N, 5.28%, Calcd for $C_{21}H_{23}F_6IN_3OOsP$: C, 31.71%; H, 2.91%; N, 5.28%.

[Os(η^6-bip)(azpy-NMe_2)I]PF_6 (5)

[Os(η^6-bip)I_2]$_2$ (100 mg, 0.037 mmol) in methanol (30 mL) and water (10 mL) was heated under reflux at 348 K under nitrogen for 2 h. Azpy-NMe_2 (37.9 mg, 0.074 mmol) in methanol (10 mL) was then added drop-wise, the solution-colour changed from orange to dark red immediately, then gradually turned to deep blue. It was further heated to reflux for 1 h, hot-filtered and the volume was reduced to about 10 mL by removal of methanol on a rotary evaporator, and ammonium hexafluorophosphate (135.1 mg. 0.37 mmol) was added. Then the solution was left in the fridge for 1 h. A dark colored powder precipitated and was collected by filtration, washed with cold ethanol and diethyl ether, then dried under vacuum. Yield: 22 mg (42.6%). Anal. ESI-MS Calcd for $C_{25}H_{24}IN_4Os$: m/z 699.07, found 699.0, ^{1}H NMR($(CD_3)_2CO$) δ 9.12 (d, 1H, J = 6 Hz), 8.54 (d, 2H, J = 8 Hz), 8.14 (m, 3H), 7.49-7.40 (m, 6H), 7.02 (d, 1H, J = 6 Hz), 6.82 (d, 2H), 6.77 (d, 1H), 6.75-6.67 (m, 2H), 3.40 (s, 6H). CHN analysis Found: C, 36.22%; H, 2.93%; N, 6.81%, Calcd for $C_{25}H_{24}F_6IN_4OsP$: C, 35.65%; H, 2.87%; N, 6.65%. Single crystals of suitable for X-ray diffraction were obtained by slow evaporation of a methanol solution of complex **5** at ambient temperature.

[Os(η^6-*p*-cym)(Azpy-NMe_2)I]PF_6 (6)

[Os(η^6-*p*-cym)I_2]$_2$ (100.0 mg, 0.086 mmol) was dissolved in methanol (50 mL) at 313 K; Azpy-NMe_2 (39.5mg, 0.175 mmol) in methanol (10 mL) was added drop-wise, the solution-colour changed from orange to blue immediately. The solution was stirred at ambient temperature for 3 h; The volume was reduced to about 10 mL by removal of methanol on a rotary evaporator, and ammonium hexafluorophosphate (141.8 mg. 0.87 mmol) was added. Then the solution was left in the freezer for 24 h; Dark colour powder was precipitated which was collected by filtration, washed with cold ethanol and diethyl ether, then finally dried in vacuum. Yield: 122.7 mg (86.7%). Anal. ESI-MS Calcd for $C_{23}H_{28}IN_4Os$:

m/z 679.1, found 679.0. ^{1}H NMR($(CD_3)_2CO$) δ 9.43 (d, 1H, J = 6 Hz), 8.65 (d, 1H, J = 8 Hz), 8.29-8.22 (m, 3H), 7.64 (m, 1H), 6.97 (d, 2H, J = 9 Hz), 6.59 (d, 1H, J = 6 Hz), 6.30 (m, 3H), 3.41 (s, 3H), 2.80 (s, 6H), 2.63-2.56 (m, 1H), 1.02 (d, 3H, J = 7 Hz), 0.98 (d, 3H, J = 7 Hz).. CHN analysis Found: C, 33.42%; H, 3.28%; N, 6.72%, Calcd for $C_{23}H_{28}F_6IN_4OsP$: C, 33.58% H, 3.43% N, 6.81%.

[Os(η^6-bip)(Azpy)Cl]PF$_6$ (7)

$[Os(\eta^6\text{-bip})Cl_2]_2$ (100.7 mg, 0.121 mmol) in methanol (40 mL) and water (10 mL) was heated under reflux under nitrogen for 2 h. The solution was hot-filtered to remove black residue, then azpy (55 mg, 0.3 mmol) in methanol (5 mL) was added drop-wise, the solution colour changed from orange to black immediately. The solution was stirred and left to cool down to room temperature for 1 h. The volume was reduced to about 10 mL by removal of methanol on a rotary evaporator and ammonium hexafluorophosphate (215.0 mg. 1.32 mmol) was added. The solution was left in the fridge overnight. A brown powder precipitated, which was filtered off, washed with diethyl ether, then dried in a dessicator overnight. Yield: 109.4 mg (77.9%). Anal. ESI-MS Calcd for $C_{23}H_{19}ClN_3Os$: m/z 564.09, found 564.0. ^{1}H NMR($(CD_3)_2CO$) δ 9.47 (d, 1H, J = 6 Hz), 8.98 (d, 1H, J = 8 Hz), 8.46 (t, 1H, J = 6 Hz), 7.97 (d, 2H, J = 8 Hz), 7.97 (t, 1H, J = 8 Hz), 7.74 (t, 1H, J = 8 Hz), 7.61 (m, 4H), 7.51 (m, 3H), 6.96 (d, 1H, J = 6 Hz), 6.89 (d, 1H, J = 6 Hz), 6.77 (t, 1H, J = 6 Hz), 6.70 (t, 1H, J = 6 Hz), 6.45 (t, 1H, J = 6 Hz). CHN analysis Found: C, 39.56%; H, 2.90%; N, 6.48%, Calcd for $C_{23}H_{19}F_6ClN_3OsP$: C, 39.80%; H, 3.07%; N, 5.81%.

[Os(η^6-*p*-cym)(Azpy)Cl]PF$_6$ (8)

$[Os(\eta^6\text{-}p\text{-cym})Cl_2]_2$ (40.7 mg, 0.0515 mmol) was dissolved in methanol (20 mL). Azpy (21.1mg, 0.116 mmol) in 5 mL of methanol was added drop-wise. The solution colour changed from yellow to brown gradually, it was stirred at ambient temperature for 1 h; The volume was reduced to about 10 ml by removal of

methanol on a rotary evaporator. Ammonium hexafluorophosphate (52.2 mg. 0.32 mmol) was added. Then the solution was left in the freezer for 24 h; Dark colour powder precipitated out, which was filtered off, washed with cold ethanol and diethyl ether, then finally dried in vacuum. Yield: 60.5 mg (85.4%). Anal. ESI-MS Calcd for $C_{21}H_{23}ClN_3Os$: m/z 544.1, found 544.1. ^{1}H NMR($(CD_3)_2CO$) δ 9.65 (d, 1H, J = 6 Hz), 9.01 (d, 1H, J = 9 Hz), 8.50-8.48 (m, 1H), 8.16 (d, 2H, J = 8 Hz), 8.02-7.99 (m, 1H), 7.78 (m, 3H), 6.79 (d, 1H, J = 6 Hz), 6,39 (d, 1H, J = 6 Hz), 6.32 (m, 2H), 2.54 (m, 1H), 2.43 (s, 3H), 1.00 (d, 3H, J = 7 Hz), 0.96 (d, 3H, J = 7 Hz).. CHN analysis Found: C, 36.61%; H, 3.21%; N 6.10%, Calcd for $C_{21}H_{23}F_6ClN_3OsP$: C, 36.66%; H, 3.37%; N, 6.61%. Single crystals suitable for X-ray diffraction were obtained by slow evaporation of a methanol solution of complex **8** at ambient temperature.

[Os(η^6-bip)(azpy-OH)Cl]PF_6 (9)

$[Os(\eta^6\text{-bip})Cl_2]_2$ (51 mg, 0.061 mmol) in methanol (40 mL) and water (10 mL) was heated under reflux under nitrogen for 2 h. Azpy-OH (30.1 mg, 0.15 mmol) in methanol (2 mL) was added, the solution turned from orange to deep brown-red. Then the solution was hot-filtered and left to cool down to ambient temperature while stirring for 1 h. The volume was reduced to about 10 ml by removal of methanol on a rotary evaporator. Ammonium hexafluorophosphate (100.6 mg. 1.11 mmol) was added. The solution was left in the fridge for 0.5 h. A brown solid precipitated which was collected by filtration, washed with diethyl ether and dried overnight in a dessicator. Yield: 42.0 mg (47.9%). Anal. ESI-MS Calcd for $C_{23}H_{19}ClN_3Os$: m/z 580.08, found 580.0. ^{1}H NMR($(CD_3)_2CO$) δ 9.37 (d, 1H, J = 9 Hz), 8.83 (d, 1H, J = 8 Hz), 8.39-8.34 (m, 1H), 8.01 (d, 2H, J = 9 Hz), 7.80-7.50 (m, 1H), 7.61-7.59 (m, 2H), 7.50 (m, 3H), 7.02 (d, 2H, J = 6 Hz), 6.86 (d, 1H, J = 6 Hz), 6.76 (d, 1H, J = 6 Hz), 6.72 (m, 2H), 6.45 (t, 1H). CHN analysis Found: C, 38.15%; H, 3.04%; N, 5.19%, Calcd for $C_{23}H_{19}F_6ClN_3OOsP$: C, 38.15%; H, 2.64%; N, 5.80%.

[Os(η^6-*p*-cym)(Azpy-OH)Cl]PF_6 (10)

[Os(η^6-*p*-cym)Cl_2]$_2$ (50.1 mg, 0.063 mmol) was dissolved in methanol (50 mL). Azpy-OH (32.8mg, 0.16 mmol) in methanol (10 mL) was added drop-wise. The solution was stirred at ambient temperature for 24h with 4 drops of 1M HCl. The complex was purified by chromatography on a Sephadex LH20 column. Ammonium hexafluorophosphate (54.3 mg. 0.33 mmol) was added. The solvent was removed on a rotary evaporator. A brown solid was collected by filtration and washed with cold ethanol and diethyl ether, then finally dried under vacuum. Yield: 16.5 mg (18.6%). Anal. ESI-MS Calcd for $C_{21}H_{23}ClN_3OOs$: m/z 560.1, found 560.1. ^{1}H NMR($(CD_3)_2CO$) δ 9.58 (d, 1H, J = 6 Hz), 9.93 (d, 1H, J = 8 Hz), 8.39 (t, 1H, J = 8 Hz), 8.19 (d, 2H, J = 9 Hz), 7.82 (t, 1H, J = 6 Hz), 7.15 (d, 2H, J = 9 Hz), 6.72 (d, 1H, J = 6 Hz), 6.43 (m, 2H), 6.34 (d, 1H, J=6 Hz), 3.35 (s, 3H), 2.63 (m, 1H), 1.02 (d, 3H, J = 7 Hz), 0.98 (d, 3H, J = 7 Hz). CHN analysis Found: C, 35.13%; H, 3.40%; N, 4.84%, Calcd for $C_{21}H_{23}F_6ClN_3OsP$: C, 35.82%; H, 3.29%; N, 5.97%.

[Os(η^6-bip)(azpy-NMe_2)Cl]PF_6 (11)

[Os(η^6-bip)Cl_2]$_2$ (104 mg,0.12 mmol) was dissolved in methanol (40 mL) and water (10 mL), the solution was heated to refluxed under nitrogen for 2 h at 248 K. Then azpy-NMe_2 (70.626 mg, 0.3121 mmol) in 5mL of methanol was added drop-wise. The solution turned from orange to purple, it was hot-filtered and left to cool to ambient temperature while stirring for 1 h. Then the solvent was evaporated on a rotary evaporator and ammonium hexafluorophosphate (182.23 mg. 1.11 mmol) was added. The solution was left in the fridge overnight. A purple solid precipitated and filtered off, washed with diethyl ether and dried overnight in a dessicator. Yield:135.5 mg (89%). Anal. ESI-MS Calcd for $C_{25}H_{24}ClN_4Os$: m/z 607.13, found 607.0. ^{1}H NMR($(CD_3)_2CO$) δ 9.16 (d, 1H, J = 6 Hz), 8.51 (d, 1H, J = 8 Hz), 8.23-8.20 (m, 1H), 8.14 (d, 2H, J = 6 Hz), 7.69-7.47 (m, 6H), 6.94 (d, 1H,

J = 6 Hz), 6.87 (d, 2H, J = 6 Hz), 6.77 (d, 1H, J = 6 Hz), 6.68-6.63 (m, 2H), 6.44 (t, 1H, J = 6 Hz), 3.40 (s, 6H). CHN analysis Found: C, 39.99%; H, 3.16%; N, 7.45%, Calcd for $C_{25}H_{24}F_6ClN_4OsP$: C, 39.98%; H, 3.22%; N, 7.46%. Single crystals suitable for X-ray diffraction were obtained diffusion of diethyl ether into a solution of complex **11** in methanol at 277 K.

[Os(η^6-*p*-cym)(Azpy-NMe_2)Cl]PF_6 (12)

[Os(η^6-*p*-cym)Cl_2]$_2$ (100.0 mg, 0.126 mmol) is dissolved in methanol (40 mL). Azpy-NMe_2 (57.4 mg, 0.254 mmol) in methanol (5mL) was added drop-wise. The solution-colour changed from yellow to blue immediately, it was stirred at ambient temperature for 1 h. The volume was reduced to about 10 mL by removal of methanol on a rotary evaporator. Ammonium hexafluorophosphate (205.8 mg. 1.26 mmol) was added. Then the solution was left in the freezer for 24h; A dark colour powder precipitated, which was colleted by filtration and washed with cold ethanol and diethyl ether, then finally dried in vacuum. Yield: 148.5 mg (80.6%). Anal. ESI-MS Calcd for $C_{23}H_{28}ClN_4Os$: m/z 587.2, found 587.4. ^{1}H NMR($(CD_3)_2CO$) δ 9.04 (d, 1H, J = 6 Hz), 8.58 (d, 1H, J = 8 Hz), 8.31-8.23 (m, 3H), 7.70 (m, 3H), 6.58 (d, 1H, J = 6 Hz), 6.32-6.26 (m, 3H), 2.80 (s, 6H), 2.48-2.45 (m, 1H), 2.47 (s, 3H), 0.98 (d, 3H, J = 7 Hz), 0.94 (d, 3H, J = 7 Hz). CHN analysis Found: C, 37.72%; H, 3.72%; N, 7.69%, Calcd for $C_{23}H_{28}F_6ClN_4OsP$: C, 37.78 %; H, 3.86%; N, 7.66 %.

3.2.3 Stability and Hydrolysis. Aqueous solutions of osmium complexes **6, 8** and **12 (**50 µM) in 5% MeOD-d_4/ 95% deuterated phosphate buffer (10 mM, pH^*=7.0) were monitored for 24 h at 310 K by ^{1}H NMR spectroscopy. The stability of **6** was further investigated by monitoring the UV-vis spectrum of a ca. 30 µM solution in 5% methanol/95% water at various time intervals over 24 h at 310 K.

3.2.4 Study of Complex 6 with N-Acetyl-L-Cysteine (NAC). The ^{1}H NMR spectrum of a solution containing 1.0 mM [(η^6-*p*-cym)Os(Azpy-NMe_2)I]PF_6 (**6**) and 7.35 mM NAC in 30% acetone-d_6 and 70% phosphate buffer (7.35 mM, pH^*=7.0) was monitored for a period of 24 h at 310 K.

3.2.5 GSH Reaction. A solution containing [Os(η^6-*p*-cym)(Azpy-NMe_2)I]PF_6 (**6**) (100 μM) and GSH (10 mM) was incubated at 310 K in 95% D_2O phosphate buffer (10 mM) and 5% methanol-D_4 and was monitored by ^{1}H-NMR spectroscopy for a period of 24 h.

3.2.6 Reaction with Silver Nitrate. Complex **12** (25 mg, 0.034 mmol) and silver nitrate (5.8 mg, 0.034 mmol) were heated under reflux overnight at 1:1 mol ratio in a mixture of methanol (10 mL) and water (10 mL). The mass spectrum was recorded to monitor the product.

3.2.7 ROS Detection. DCFH-DA was handled under an N_2 atmosphere, dissolved in DMSO to give a 10 mM stock solution. A2780 cells were seeded at 5000 cells/well into black 96-well plate and incubated for 24 h at 310 K, 5% CO_2, and high humidity. Cells were incubated for 20 min with DCFH-DA (10 μM). To remove extracellular probe, the cells were washed twice with PBS. The cells were then kept in PBS solution and either the osmium complex, or osmium complex plus L-BSO (50 μM), or hydrogen peroxide (50 μM, as the positive control) were added. The fluorescence was recorded over a period of 4 h at 310 K by excitation at 480 nm and emission at 530 nm using a TECAN plate reader.

3.2.8 X-ray Crystallography. X-ray crystallographic data for compounds **2, 3*, 5, 8, 11** and **14** have been deposited in the Cambridge Crystallographic Data Centre with CCDC references numbers 776271, 776270, 776273, 776268, 776269 and 776272, respectively. The collection and structure solution were carried out by Dr. Guy J. Clarkson.

3.2.9 ICP-MS. ICP-MS analyses were carried out on an Agilent Technologies 7500 Series ICP-MS instrument. The water used for ICP-MS analysis was double deionised (DDW) using a USF Elga UHQ water deionizer. The osmium Specpure plasma standard (Alfa Aesar, 1000 ppm in 5% HCl) was diluted with DDW to 20 ppm. The standards for calibration were freshly prepared by diluting this stock solution with 3% HNO_3 in DDW. The concentrations used were 100, 60, 20, 10, 5, 4, 2, 1, 0.4 and 0.1 ppb.

3.2.10 Combination Treatment with 6 and L-BSO. To determine the effect of decreased GSH levels on the cytotoxicity of **6,** A2780 human ovarian and A549 human lung cancer cells were co-incubated with 50 μM L-BSO and various concentrations of **6** for 24 h. Cell viability was then determined using the sulforhodamine (SRB) assay.

3.2.11 Animals. Six to ten week old female BALB/cOlaHsd-Foxn1^{nu} mice (Harlan, Blackthorn, UK), maintained with food (Teklad 2018 diet, Harlan) and water *ad libitum*, were used according to UKCCCR guidelines for the welfare of animals[2]. Regulated procedures were carried out under a UK Home Office Project License. This work was carried out by Dr. Steve Shnyder (University of Bradford) and his team.

3.2.12 Tumour System. HCT-116 (human colon adenocarcinoma line) tumours were excised from a donor animal, placed in sterile physiological saline containing antibiotics and cut into small fragments of approximately 2 mm^3. Under brief general inhalation anaesthesia, fragments were implanted in the left flank of each mouse using a trocar. Once the tumours could accurately be measured by calipers (mean tumour volume of 32mm^3), the mice were allocated

into groups by restricted randomisation to keep group mean tumour size variation to a minimum. This work was carried out by Dr. Steve Shnyder (University of Bradford) and his team.

3.2.13 Plasma and Tissue Distribution Studies. Tumour-bearing mice (n=3 per time point) were sacrificed at 5 min, 60 min and 240 min following intravenous administration of a single 10 mg kg^{-1} dose of FY026 (**6**). Tumour, liver, lung, kidneys and plasma were collected, weighed and stored at 193 K until analyzed. Osmium concentrations in different samples were measured by ICP-MS using the methodology described above. Tumour and tissue samples were homogenized in phosphate buffered saline, and digested in HNO_3 at 353 K overnight to give clear solutions. These were then diluted as appropriate for evaluation by ICP-MS.

3.2.14 Chemotherapy Studies. Compounds were administered by single injection, with the day of therapy designated day 0. The maximum soluble dose of FY026 when administered as a single intravenous injection was established as 40 $mgkg^{-1}$. The efficacy of FY026 was compared with the standard anticancer agent cisplatin which was administered as a single dose intraperitoneally at its maximum tolerated dose of 8 mg kg^{-1}. The effects of therapy were assessed as previously described.[22] Briefly, daily 2-dimensional caliper measurements of the tumours were taken, with volumes calculated using the formula $(a^2 \times b) / 2$, where a is the smaller and b the larger diameter of the tumour. Tumour volume was then normalised to the respective volume on day 0, and semi-log plots of relative tumour volume (RTV) versus time were made. Mann-Whitney U tests were performed to determine the statistical significance of any differences in growth rate (based on tumour volume doubling time) between control and treated groups, and between the 2 compounds. This work was carried out by Dr. Steve Shnyder (University of Bradford) and his team.

3.3 Results and Discussions

Previously Peacock et al. reported the synthesis of the Os^{II} azopyridine complexes $[Os(\eta^6\text{-arene})(Azpy\text{-}NMe_2)Cl]PF_6$ with arene = biphenyl (**11**) and *p*-cymene (**12**).[16] Cytotoxicity tests for these complexes were hampered by their low solubility and the occurrence of precipitation under the test conditions used. No activity towards human A549 lung cancer cells was detected up to concentrations of 100 μM. In the present chapter, the similar Os^{II} azopyridine complexes with iodido replacing chlorido (Z), and with azpy-R (R = H, OH, and NMe_2) were explored. The complexes remained in solution under the cell testing conditions with no apparent precipitation (vide infra).

3.3.1 Chemistry

Six novel cationic iodido osmium arene complexes containing chelating azopyridine ligands (azpy, azpy-OH and azpy-NMe_2) were synthesized where PF_6 acts as the counter ion. In general, they have poor aqueous solubility ($\leq$ 0.2 mM), with the biphenyl complexes being less water-soluble than the *p*-cymene complexes. The structures of the iodido complexes with azpy (**2**), azpy-OH (**3**) and azpy-NMe_2 (**5**) (Chart 3.1) were determined by X-ray crystallography. For comparison, six chlorido analogues were synthesized and the structures of the azpy complex **8** and azpy-NMe_2 complex **11** were also determined by X-ray crystallography. The X-ray structure of **12** has been reported previously.[16] The structure of the dimer $[Os(\eta^6\text{-}p\text{-cym})I_2]_2$ which is an important synthetic intermediate in this work was also determined by X-ray crystallography (Fig. 3.1).

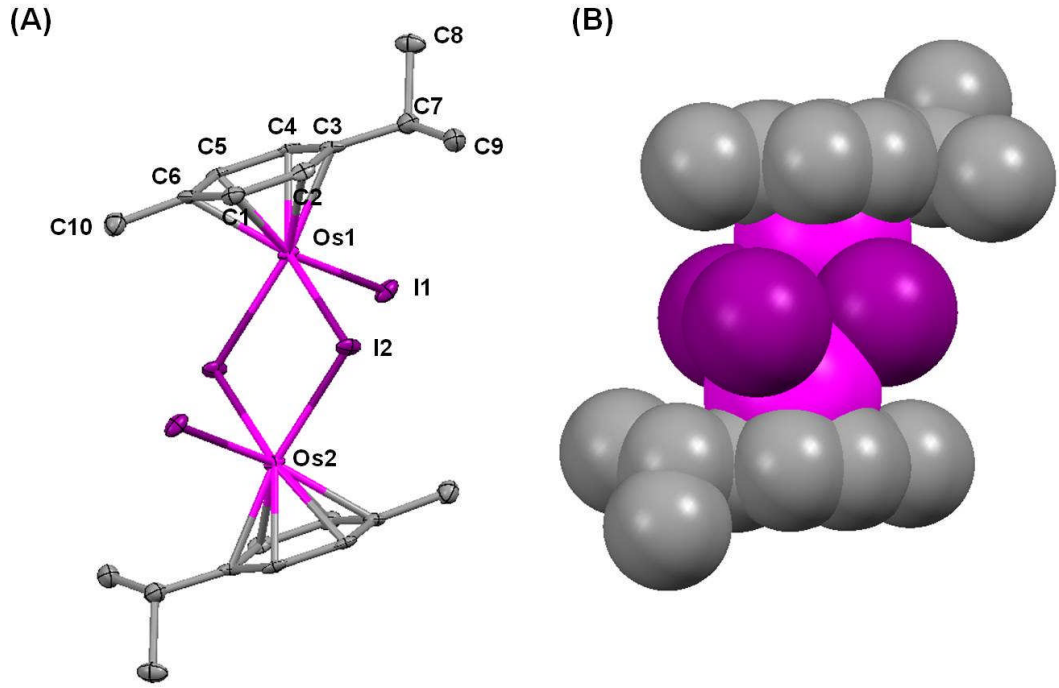

Figure 3.1. The dimer $[Os(\eta^6\text{-}p\text{-cym})I_2]_2$ lies on an inversion centre between the two bridging iodides; only the asymmetric unit is labelled. (A) X-ray structure with thermal ellipsoids drawn at 50% probability, the hydrogen atoms were omitted for clarity. (B) Crystallographic space-filling view. Salient bond lengths (Å) and angles (deg): Os1−(*para*-cymene centroid): 1.665; Os1−I1: 2.7250(4); Os1−I2: 2.7347(4); I2−Os1−I1: 88.319(12); Os1-I2-Os2: 97.484(11).

Chart 3.1. Osmium azopyridine arene complexes studied in this chapter.

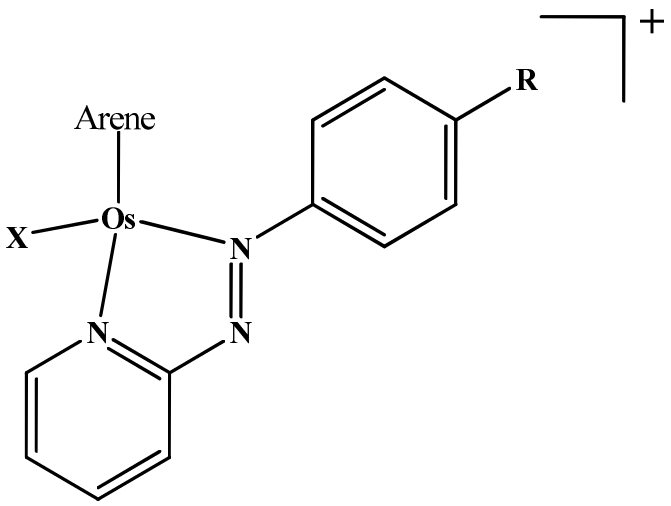

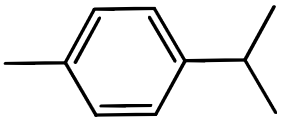

p-cym

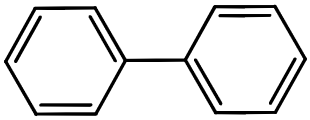

bip

Complex	Arene	R	X
1	bip	H	I
2	*p*-cym	H	I
3	bip	OH	I
4	*p*-cym	OH	I
5	bip	NMe_2	I
6	*p*-cym	NMe_2	I
7	bip	H	Cl
8	*p*-cym	H	Cl
9	bip	OH	Cl
10	*p*-cym	OH	Cl
11	bip	NMe_2	Cl
12	*p*-cym	NMe_2	Cl

All the osmium complexes adopt the familiar pseudo-octahedral 'piano-stool' structure (Fig. 3.2), with bond lengths and angles within the expected ranges.[16] The crystal of the neutral complex $[Os(\eta^6\text{-bip})(Azpy\text{-}O)I]\cdot 0.5H_2O$ (**3***) was obtained by slow evaporation of a methanolic solution of complex **3** $[Os(\eta^6\text{-bip})(Azpy\text{-}OH)I]PF_6$. **3*** has a relatively short O15–C12 bond length (1.258(4) Å) indicating deprotonation of the OH group, with the iodido ligand balancing the charge on Os^{II} to afford a neutral complex. A water molecule in the lattice forms a short H-bond with the phenoxide group and bridges two phenoxides of neighboring complexes (Fig. 3.3). The pK_a of the azpy-OH ligand in **3** was determined to be ca 6.9 (comparable with a value of 6.48 for the ruthenium analogue)[11] and so the complex would be expected to be deprotonated under the conditions of the cytotoxicity assays (pH = 7.4), as shown in the X-ray structure. Selected bond lengths and angles for these structures are listed in Table 3.1.

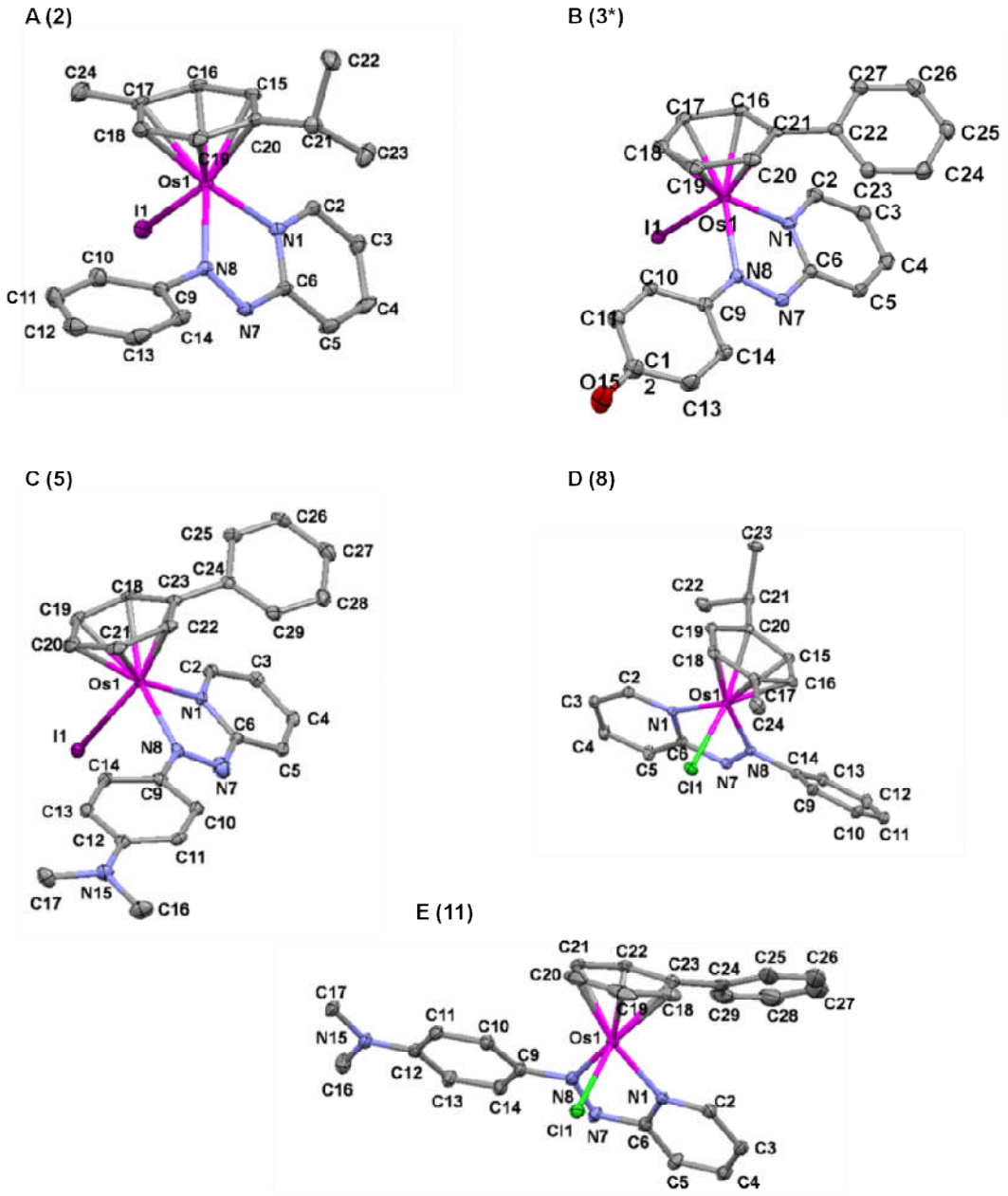

Figure 3.2. X-ray crystal structures (A) [Os(η^6-*p*-cym)(Azpy)I]$^+$ (**2**), (B) [Os(η^6-bip)(Azpy-O)I] (**3***), (C) [Os(η^6-bip)(Azpy-NMe$_2$)I]$^+$ (**5**), (D) [Os(η^6-*p*-cym)(Azpy)Cl]$^+$ (**8**), and (E) [Os(η^6-bip)(Azpy-NMe$_2$)Cl]$^+$ (**11**), with thermal ellipsoids drawn at 50% probability. The hydrogen atoms, counterions (PF_6) and solvent water molecules have been omitted for clarity.

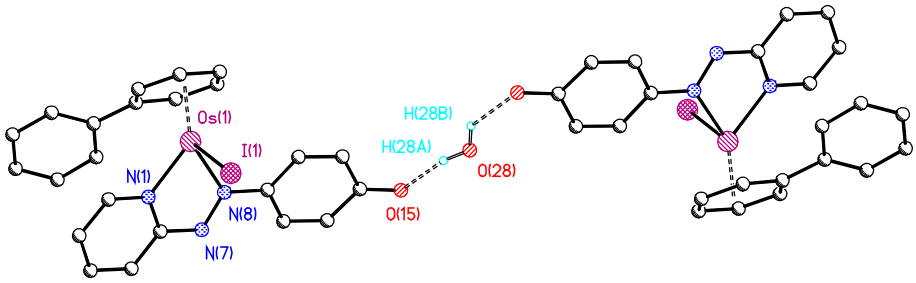

Figure 3.3. Hydrogen bond formation between water and the phenoxide ligand in the x-ray crystal structure of [Os(η^6-bip)(Azpy-O)I]·0.5H_2O.

Table 3.1. Selected bond lengths (Å) and angles (deg) for [Os(η^6-*p*-cym)(Azpy)I]PF_6 (**2**), [Os(η^6-bip)(Azpy-O)I]·0.5H_2O (**3**), [Os(η^6-bip)(Azpy-NMe_2)I]PF_6 (**5**), [Os(η^6-*p*-cym)(Azpy)Cl]PF_6 (**8**), [Os(η^6-bip)(Azpy-NMe_2)Cl]PF_6 (**11**).

(A)

bond length/angle	**2**	**3**	**5**
Os(1)-N(8)	2.010(3)	2.080(2)	2.1017(18)
Os(1)-N(1)	2.052(3)	2.054(2)	2.0804(18)
Os(1)-C(15)	2.186(3)	2.206(3)	2.189(2)
Os(1)-C(19)	2.206(3)	2.211(3)	2.199(2)
Os(1)-C(18)	2.225(3)	2.211(3)	2.205(2)
Os(1)-C(16)	2.244(3)	2.215(3)	2.206(2)
Os(1)-C(20)	2.246(3)	2.217(3)	2.211(2)
Os(1)-C(17)	2.284(3)	2.225(3)	2.222(2)
Os(1)-I(1)	2.6856(3)	2.7185(2)	2.70798(19)
N(7)-N(8)	1.293(4)	1.323(3)	1.314(3)
N(8)-Os(1)-N(1)	74.85(11)	75.12(9)	76.74(7)
N1-Os-I	87.81(8)	87.59(6)	86.00(5)
I-Os-N8	83.07(8)	87.83(6)	86.60(5)

Table 3.1. Selected bond lengths (Å) and angles (deg) for [Os(η^6-*p*-cym)(Azpy)I]PF_6 (**2**), [Os(η^6-bip)(Azpy-O)I]·0.5H_2O (**3**), [Os(η^6-bip)(Azpy-NMe_2)I]PF_6 (**5**), [Os(η^6-*p*-cym)(Azpy)Cl]PF_6 (**8**), [Os(η^6-bip)(Azpy-NMe_2)Cl]PF_6, [Os(η^6-bip)(Azpy-NMe_2)Cl]PF_6 (**11**).

(B)

bond length/angle	**8**	**11**
Os(1)-N(8)	2.0225(15)	2.072(2)
Os(1)-N(1)	2.0543(15)	2.049(2)
Os(1)-C(15)	2.1843(18)	2.198(3)
Os(1)-C(19)	2.2196(18)	2.205(3)
Os(1)-C(18)	2.2313(18)	2.205(3)
Os(1)-C(16)	2.2381(18)	2.214(3)
Os(1)-C(20)	2.2474(19)	2.218(3)
Os(1)-C(17)	2.2619(18)	2.218(2)
Os(1)-Cl(1)	2.3817(5)	2.3992(6)
N(7)-N(8)	1.290(2)	1.297(3)
N(8)-Os(1)-N(1)	74.84(6)	75.23(9)
N1-Os-Cl	84.35(5)	85.12(6)
Cl-Os-N8	86.59(5)	83.82(6)

3.3.2 Cytotoxicity

In contrast to previous studies on complexes **11** and **12**,[16] the complexes were soluble in the culture medium at the concentrations tested and no precipitation was observed after 24 h. None of the azopyridine ligands themselves showed cytotoxic activity against A2780 human ovarian cancer cells at concentrations up to 100 μM. The IC_{50} values of the osmium azopyridine complexes (Table 3.2) ranged from 0.14 μM for the iodido biphenyl complexes **3** and **5** with azpy-OH and azpy-NMe_2 ligands, to > 50 μM for the chlorido complex **8** containing azpy in the human ovarian cell line A2780 (Table 3.2A). According to these preliminary results, three complexes (**3**, **6** and **12**) were selected for further evaluation against a cisplatin-resistant sub-line of A2780, A2780/cis, and also against a panel of human cancer cell lines of differing histiotype. Complexes **3** and **6** (Table 3.2B) showed at least 10-fold greater potency than cisplatin against all cell lines tested apart from RT-112 (bladder), which demonstrated a 3-fold difference for complex **3**. Complex **12** showed similar potency to cisplatin over the cell line panel. The highest activity in comparison to the reference cisplatin for all three complexes was seen for the PC-3 (prostate) cell line. Interestingly, complexes bearing electron-donating hydroxyl or dimethylamino substituents on the phenyl ring of the azopyridine ligands are an order of magnitude more active compared to complexes bearing unsubstituted azpy ligands. This may indicate that redox processes associated with the chelated ligand[21] are important for activity. In contrast octahedral Ru^{II} complexes such as $[Ru(azpy)_2Cl_2]$ containing two unsubstituted azpy ligands have been reported to be as active as cisplatin against A2780 cells.[23]

The high potency of the organometallic iodido osmium complexes reported here, with IC_{50} values within the nanomolar range, is notable. This is unprecedented for cytotoxic organometallic osmium arene complexes, for which activities generally fall in the micromolar range.[16, 18, 19] In addition, their ruthenium analogues were significantly less cytotoxic (7 to more than 56 times

less active) in the A2780 ovarian cancer cell line.[21] In particular, the Ru analogue of complex **3** ([Ru(η^6-bip)(Azpy-OH)I]PF_6) is 35 times less active.

Table 3.2. (A) IC_{50} values for complexes **1–12** in human ovarian cell line A2780; (B) IC_{50} values for **3**, **12**, **6** in A2780/cis ovarian, A549 lung, HCT-116 colon, MCF-7 breast, PC-3 prostate and RT-112 bladder human cancer cell lines.

(A)

Complex		**IC_{50}(μM)**
[Os(η^6-bip)(Azpy)I]PF_6	**1**	5.4(±0.8)
[Os(η^6-*p*-cym)(Azpy)I]PF_6	**2**	10.3(±0.1)
[Os(η^6-bip)(Azpy-OH)I]PF_6	**3**	0.14(±0.01)
[Os(η^6-*p*-cym)(Azpy-OH)I]PF_6	**4**	0.32(±0.2)
[Os(η^6-bip)Os(Azpy-NMe_2)I]PF_6	**5**	0.14(±0.01)
[Os(η^6-*p*-cym)(Azpy-NMe_2)I]PF_6	**6**	0.18(±0.01)
[Os(η^6-bip)(Azpy)Cl]PF_6	**7**	13.9(±3.8)
[Os(η^6-*p*-cym)(Azpy)Cl]PF_6	**8**	>50
[Os(η^6-bip)(Azpy-OH)Cl]PF_6	**9**	0.84(±0.1)
[Os(η^6-*p*-cym)(Azpy-OH)Cl]PF_6	**10**	1.3(±0.2)
[Os(η^6-bip)(Azpy-NMe_2)Cl]PF_6	**11**	3.9(±0.3)
[Os(η^6-*p*-cym)(Azpy-NMe_2)Cl]PF_6	**12**	1.8(±0.1)
Cisplatin		1.8(±0.1)

(B)

Complex/ IC_{50}(μM)	**A2780/cis**	**A549**	**HCT-116**	**MCF-7**	**PC-3**	**RT-112**
3	<0.3	0.4	<0.3	0.25	<0.3	0.4
6	<0.3	<0.3	<0.3	0.079	0.6	<0.3
12	1.8	5.2	0.9	1.1	6.8	2.2
Cisplatin	4	4.1	2.6	3	21.5	1.4

3.3.4 Stability and Hydrolysis

The hydrolysis (aquation) of the azopyridine complexes was investigated since this is a potential mechanism for activation of halido osmium arene complexes in their interaction with possible biological targets such as DNA.[16, 24]

The aqueous behavior of the highly active complexes [Os(η^6-*p*-cym)(Azpy-NMe_2)I]PF_6 **6** (IC_{50} = 0.2 μM), moderately active complex [Os(η^6-*p*-cym)(Azpy-NMe_2)Cl]PF_6 **12** (IC_{50} = 1.8 μM) and inactive complex [Os(η^6-*p*-cym)(Azpy)Cl]PF_6 **8** (IC_{50} > 50 μM) against A2780, was studied at 310 K over 24 h by ^{1}H NMR.

The ^{1}H NMR spectra of a 50 μM solution of inactive complex **8** in 10 mM phosphate buffer 95% D_2O/5% MeOD-d_4 over 24 h showed the disappearance of the peaks corresponding to the bound azopyridine and *p*-cymene ligands (Fig. 3.3) suggesting that this complex is not stable under aqueous conditions. Similar behavior has been observed for the ruthenium analogue [Ru(η^6-*p*-cym)(azpy)Cl]PF_6.[11] In contrast, complexes **6** and **12** did not show ligand loss, neither did they hydrolyze as judged by their ^{1}H NMR spectra, which remained unchanged (Fig. 3.3). In addition, ESI-MS analyses showed ions corresponding to the chlorido and iodido complexes only, and UV-vis spectra in 10% methanol/90% water, showed no change over 24 h (Fig. 3.4). An attempt to remove the chloride from the aqueous solution of **12** by reacting it with silver nitrate under reflux overnight, did not result in the expected aqua product. The chlorido complex was the only species detected by MS (Fig. 3.5), indicating a strong Os–Cl bond.

These observations suggest that active complexes **6** and **12** are stable under the biologically-relevant testing conditions. In addition, the inertness of the Os–I bond suggests that hydrolysis process is not critical for the activation of these complexes and it is consistent with previous observations of the analogous Ru^{II} azpy complexes,[21] implying that the azpy ligand plays an important role in the activity.

(A)

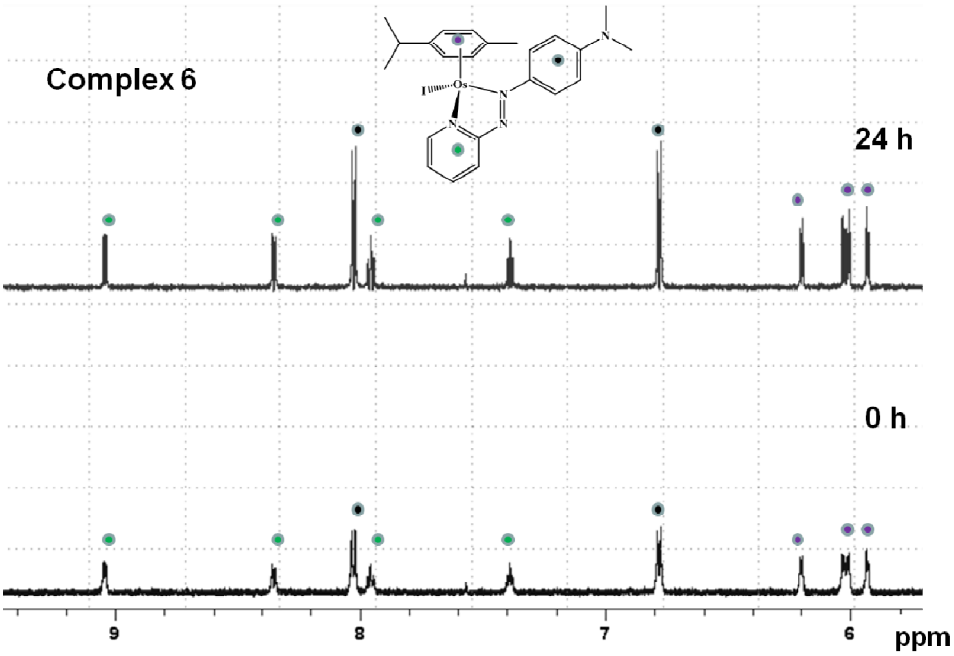

(B)

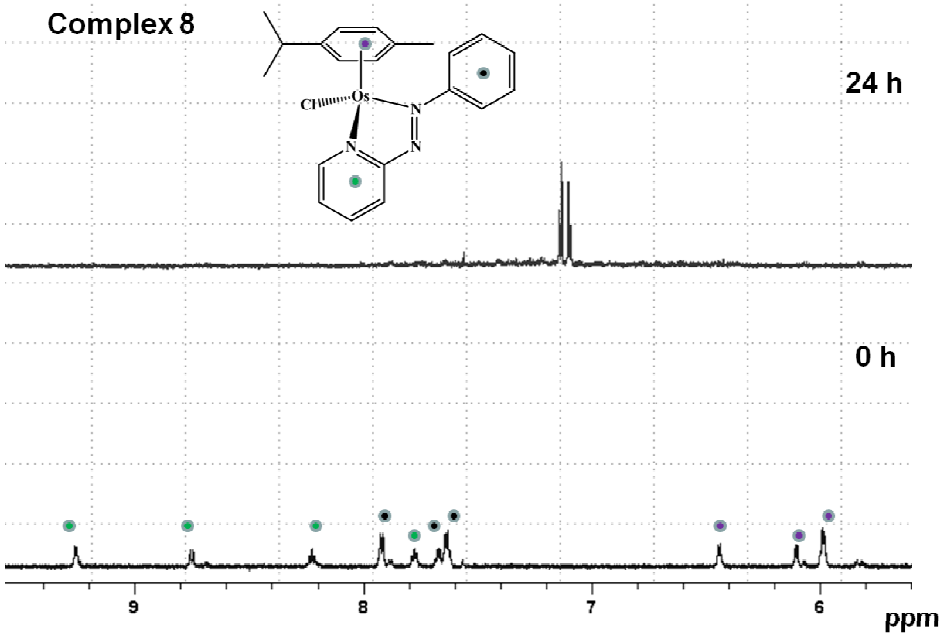

(C)

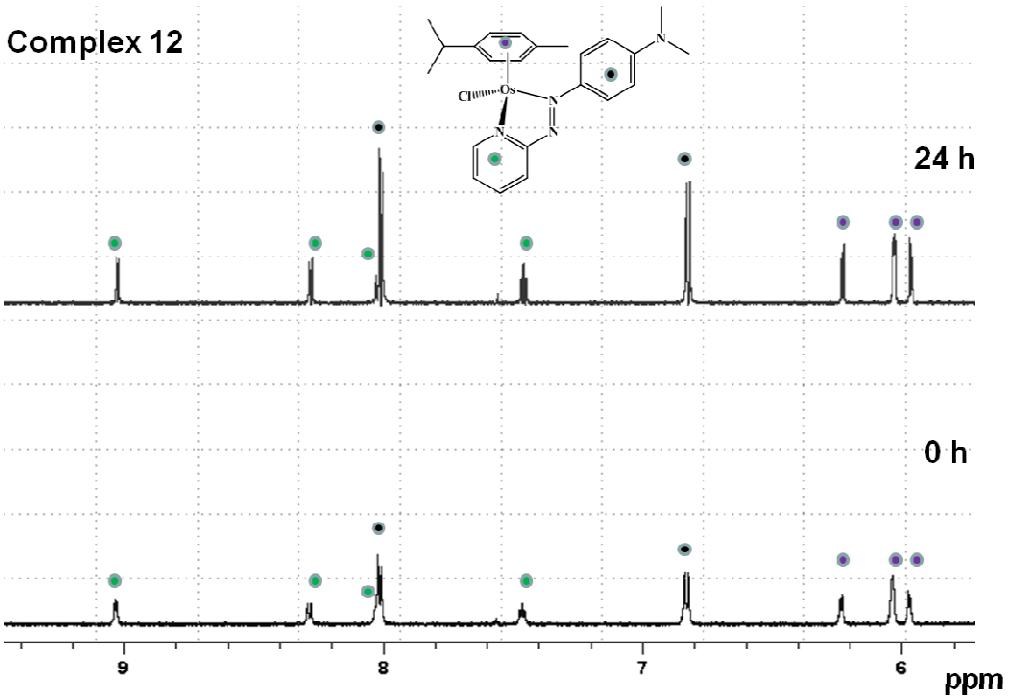

Figure 3.3. Hydrolysis and stability experiments of osmium complexes **6**, **8** and **12**. ^{1}H-NMR spectra of (A) [Os(η^{6}-*p*-cym)(Azpy-NMe$_2$)I]PF$_6$ **(6)**, (B) [Os(η^{6}-*p*-cym)(Azpy)Cl]PF$_6$ **(8)** and (C) [Os(η^{6}-*p*-cym)(Azpy-NMe$_2$)Cl]PF$_6$ **(12)** were recorded before and after 24 h incubation at 310 K.

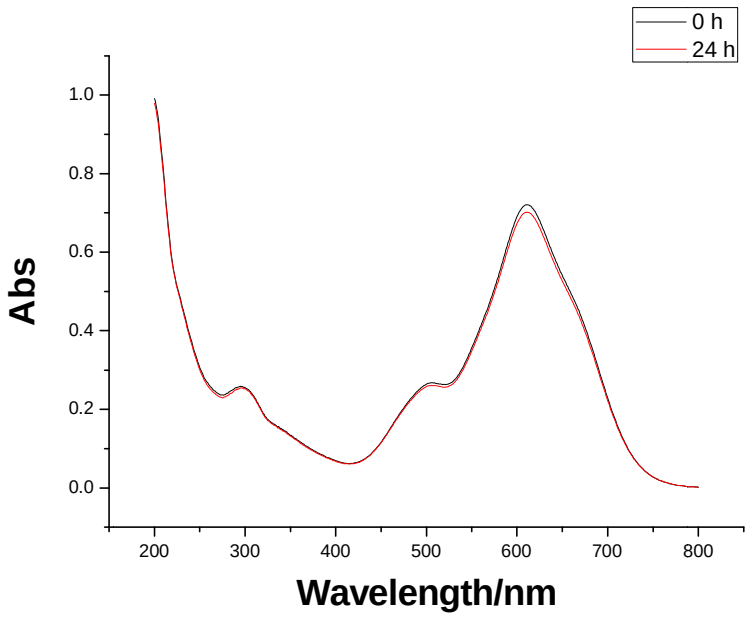

Figure 3.4. UV-Vis spectra of [Os(η^6-*p*-cym)(Azpy-NMe_2)I]PF_6 (33.3 µM) in 10% methanol and 90% water soon after dissolution (black curve) and after 24 h incubation at 310 K (red curve).

Figure 3.5. Positive-ion mass-spectrum of the solution resulting from the reaction of complex **12** with 1 mol equiv silver nitrate for 24 h at 353 K. Only peaks from [Os(η^6-*p*-cym)(Azpy-NMe_2)Cl] (**12**) were detected, suggesting that no aqua product was formed.

3.3.5 Effect of N-acetyl-L-cysteine (NAC) on cytotoxicity

Pre-treatment of cells with NAC can block cisplatin-dependent caspase-3 activation and apoptosis by inhibiting the accumulation of intracellular reactive oxygen species (ROS) and maintaining intracellular GSH levels.[25] In order to investigate possible involvement of ROS in the cytotoxicity of azopyridine Os^{II} arene complexes, the effect of pre-treatment of cells with NAC was investigated. Cisplatin was used as the positive control, whereas cells not treated with osmium complexes served as the negative control.

A2780 cells were treated with the iodido complexes **3**, **5** and **6** and chlorido complex **12** at concentrations that were 1.2–1.8x their respective IC_{50} values and for cisplatin a concentration 2.5x its IC_{50} value was used. These doses reduced cell growth to <30% of the control value (Fig. 3.6). Pre-treatment with 5 mM NAC for 2 h and co-treatment with osmium complexes for 24 h was employed to increase the intracellular glutathione concentration,[21] resulted in the inhibition of the antiproliferation effects of iodido complexes **3**, **5** and **6**. This was shown by their growth levels of >70% when pre-treated with NAC. For chlorido complex **12**, the NAC pre-treatment and co-treatment had only a small effect on restoring growth (Fig. 3.6). These results suggest that, unlike the azopyridine osmium arene iodido complexes or cisplatin, the cytotoxicity associated with osmium chlorido complex **12** does not appear to depend on the production of reactive oxygen species (ROS), but may be explained by a different mechanism of cytotoxic activity.

In order to investigate the possibility that the complexes might react directly with NAC and that the effects are not merely due to thiol levels in cells, a solution containing 1.0 mM $[(\eta^6\text{-}p\text{-cym})Os(Azpy\text{-}NMe_2)I]PF_6$ (**6**) and excess (7.35 mM) NAC in 30% acetone-d_6 and 70% phosphate buffer (10 mM; pH 7.0) was

monitored by ^{1}H NMR spectroscopy for 24 h at 310 K. No new peaks appeared in the ^{1}H NMR spectrum (Fig. 3.7), suggesting that complex **6** and possibly the other iodido complexes do not readily react with NAC.

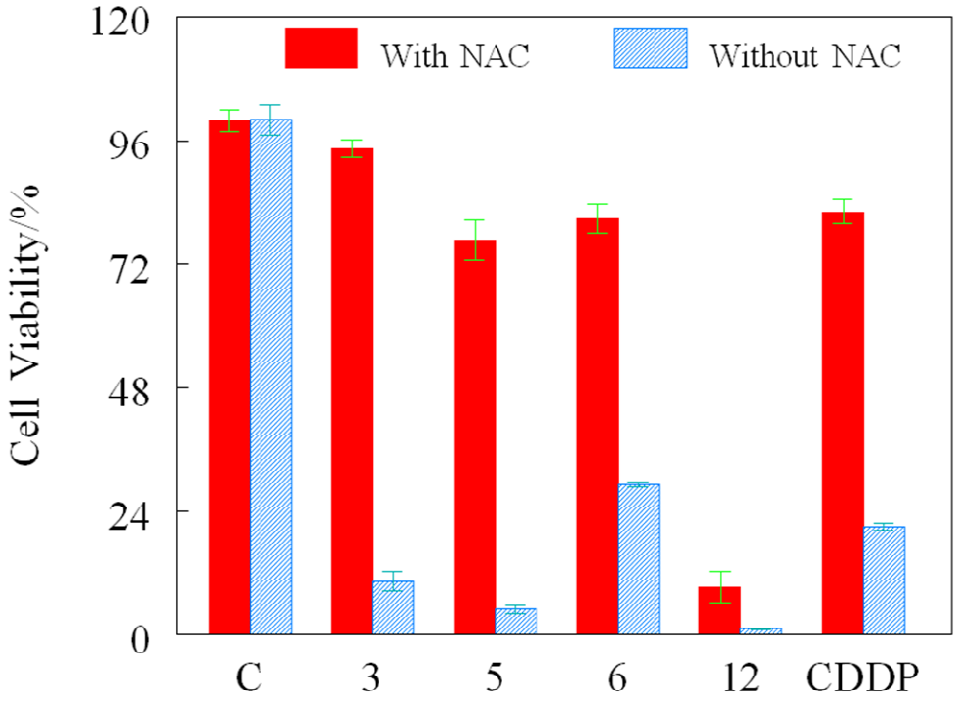

Figure 3.6. Cell viability of A2780 human ovarian cancer cells after 24 h exposure to osmium complexes or cisplatin followed by 72 h recovery (red bars), and cell viability for cells that were pre-treated with 5 mM of NAC for 2 h prior to the addition of the osmium complexes or cisplatin (blue bars). Doses of complexes: [Os(η^6-bip)(Azpy-OH)I]PF_6 (**3**), 0.25 μM; [Os(η^6-bip)(Azpy-NMe_2)I]PF_6 (**5**), 0.25 μM; [Os(η^6-*p*-cym)(Azpy-NMe_2)I]PF_6 **(6)**, 0.25 μM; [Os(η^6-*p*-cym)(Azpy-NMe_2)Cl]PF_6 (**12**), 2.5 μM; CDDP (cisplatin), 5 μM. The error bars are standard deviations of six replicates. C = control

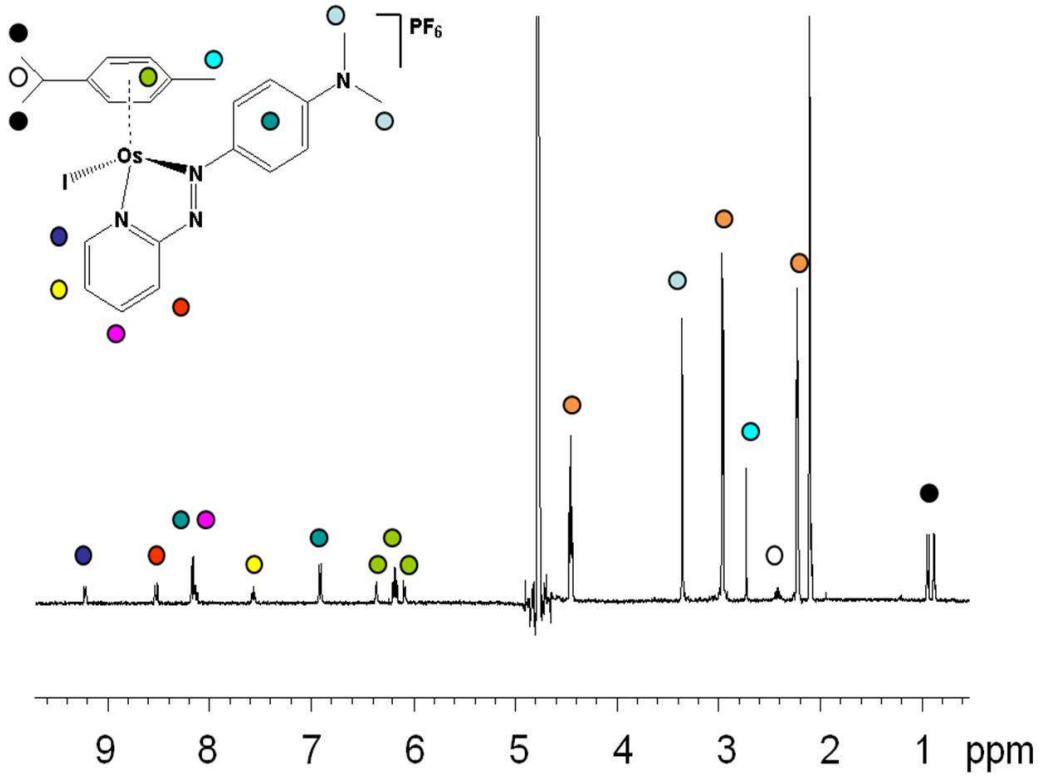

Figure 3.7. ^{1}H NMR spectrum of a solution containing 1.0 mM [Os(η^6-*p*-cym)(Azpy-NMe$_2$)I]PF$_6$ (**6**) and 7.35 mM NAC in 30% acetone-d$_6$ and 70% phosphate buffer (10 mM, pH=7.0) after incubation for 24 h at 310 K. Peak assignments: NAC, orange; complexes, other colours as indicated on the structure.

3.3.6 Reactions with Glutathione (GSH)

Since some azopyridine ruthenium arene complexes appear to oxidize GSH catalytically to form GSSG,[21] similar reactions were studied for the osmium analogues. The ^{1}H NMR spectrum of a solution containing the highly cytotoxic iodido complex [Os(η^6-*p*-cym)(Azpy-NMe$_2$)I]PF$_6$ (**6**) (100 μM) and a 100-fold molar excess of GSH (10 mM, to mimic intracellular conditions) showed little change over a period of 24 h (Fig 3.8). This suggests that complex **6** does not catalytically oxidize GSH, unlike the analogous Ru^{II} complex.

The mechanism of cytotoxic activity for these Os^{II} azopyridine complexes therefore appears to be different from that of the Ru^{II} analogues, and also different from those bearing hydrolysable Ru/Os–Cl bonds, perhaps indicating why the Os^{II} complexes are more potent.

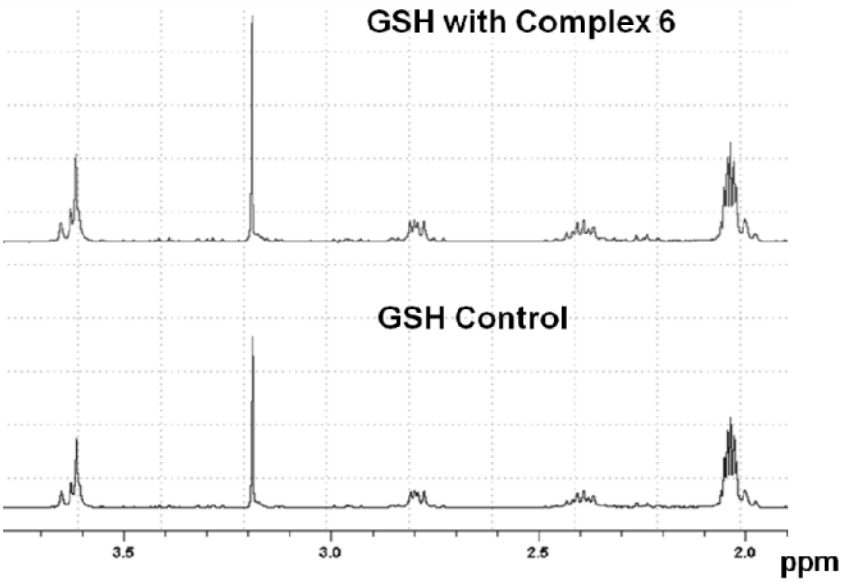

Figure 3.8. Reaction of complex **6** with GSH. ^{1}H NMR spectrum of 10 mM GSH (bottom) and in the presence of 100 μM [Os(η^6-*p*-cym)(Azpy-NMe$_2$)I]PF$_6$ (**6**) for 24 h at 310 K (top).

3.3.7 Evaluation of *in vivo* toxicity

Complexes **3** and **6** were selected for further *in vivo* evaluation based on their promising activity *in vitro*. On evaluation of their toxicity in a nude mouse tumour HCT-116 xenograft model, the complexes demonstrated negligible deleterious effects at doses up to and including their maximum soluble dose of 40 $mg \cdot kg^{-1}$. This dose is approximately six times higher than the maximum tolerated dose of cisplatin in the same tumour model, and suggests that with the comparative lack of toxicity of the complexes there is likely to be a much broader therapeutic window (Fig. 3.9). This will be investigated further in extensive *in vivo* pharmacokinetic and efficacy studies.

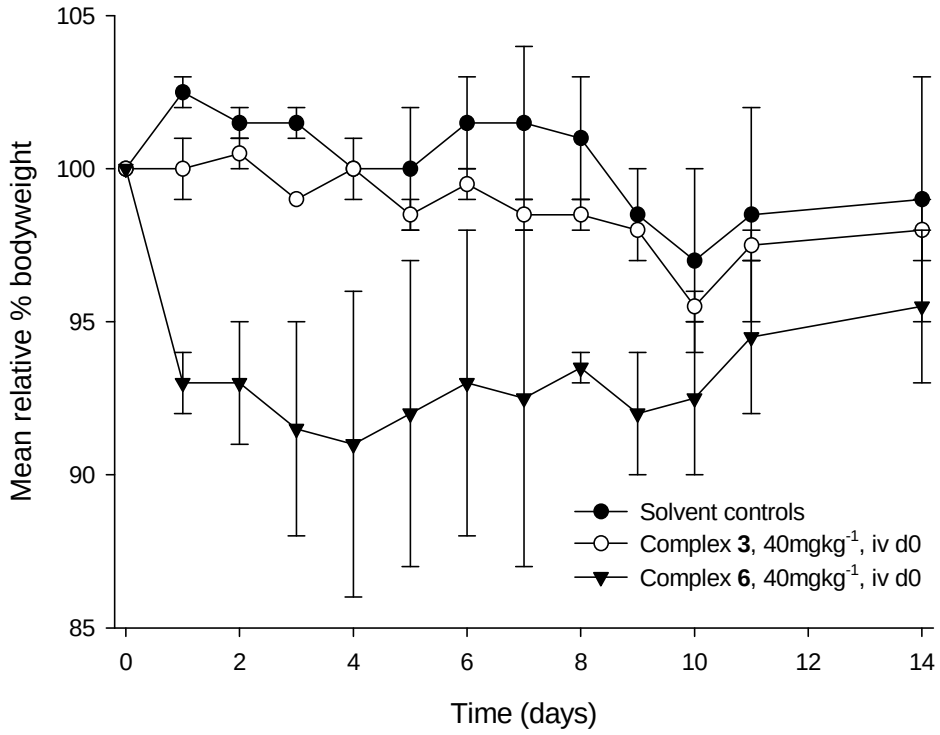

Figure 3.9. Mean relative body weight curves for **3** and **6** administered intravenously as a single dose on day 0 at their maximum soluble dose of 40 $mg \cdot kg^{-1}$ to mice bearing HCT-116 human tumour xenografts (n = 2). Fluctuations in body weight are well within the normal limits suggesting that neither complex is toxic.

3.3.8 Evaluation of the *in vivo* efficacy

First the anticancer efficacy of complex **6** (FY026, Fig. 3.10) *in vivo* versus the subcutaneously implanted HCT-116 xenograft model, when administered as a single intravenous injection at its maximum soluble dose of 40 mg/kg was studied. The agent had negligible toxicity, with an observed maximum weight loss well within the normal limits. Complex **6** was seen to induce a statistically significant tumour growth delay in the HCT-116 model compared to the untreated control ($p<0.01$). The positive control compound the standard agent cisplatin was employed and administered i.p (standard route for this model) at its MTD in this mouse model ($p<0.05$, Figure. 3.11 and Table 3.3). The maximum weight loss observed with complex **6** was 8%, indicating a lack of toxicity. This combined with the favourable tumour distribution reported below, would suggest that there is significant scope to administer this compound on a repeat-dose schedule to enhance its therapeutic activity.

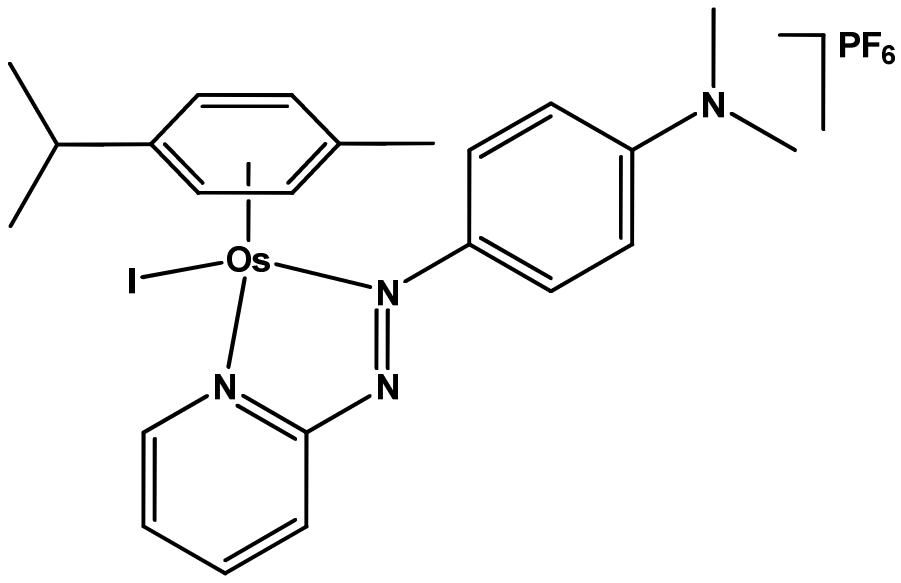

Figure 3.10. The structure of complex **6** (**FY026**)

Table 3.3. Evaluation of the *in vivo* efficacy of **6** in the HCT-116 colon adenocarcinoma s.c. xenograft model.

Compound (dose in mg kg^{-1})	Mean tumour doubling time (days)	Significance	Maximum % weight loss (day)
Untreated controls	3.9		8 (8)
Complex **6** (40.0)	6.5	$p<0.01$	8 (1)
Cisplatin (8.0)	6.4	$p=0.05$	8 (6)

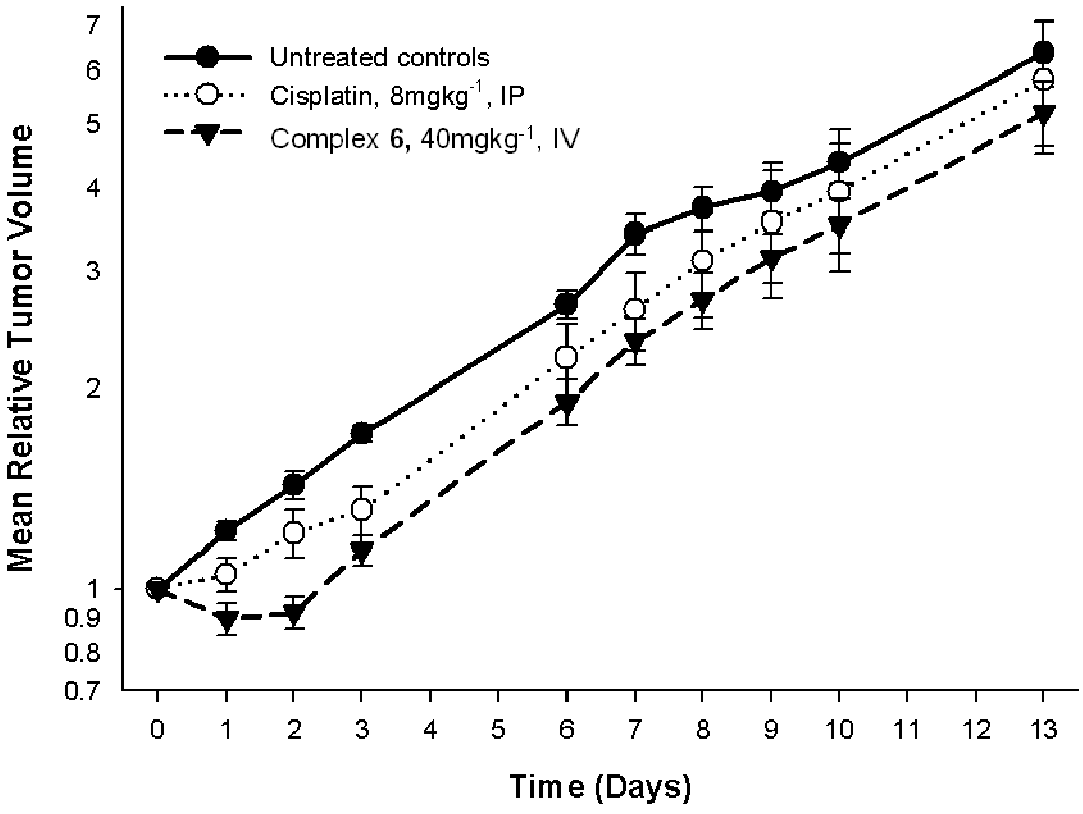

Figure 3.11. Evaluation of the *in vivo* efficacy of complex **6** when administered as a single intravenous injection at its maximum soluble dose of 40 mg kg^{-1} in the subcutaneously implanted HCT-116 human colon adenocarcinoma model. Complex **6** shows a greater efficacy than the standard agent cisplatin administered at its maximum tolerated dose in this model. Points represent mean ± S.D. (n=8).

3.3.9 Distribution of Osmium after Administration of Complex 6

In HCT116 xenograft-bearing mice, the distribution of **6** was analysed in the liver, kidneys, tumour, lungs and plasma, 5, 60 and 240 min after administration. The results are shown in Table 3.4 and Figure 3.12. Osmium was detected in the tumour and all tissues over the time period of analysis. The amount of osmium in the plasma was surprisingly low after just 5 min, suggesting a large volume of distribution or high level of tissue distributions (mainly in kidney).

Table 3.4. Tumour, normal tissue and plasma distribution of osmium from **6** following i.v. administration of a single dose of 10 mg kg^{-1}.

	μg Os / g tissue				
Time/min	Kidney	Lungs	Liver	Plasma	Tumour
5	1259.7 (± 66.6)	5.81 (± 4.18)	88.6 (± 57.9)	19.6 (± 23.3)	11.9 (± 2.22)
60	513.5 (± 208.5)	40.3 (± 15.0)	136.4 (± 4.96)	21.8 (± 2.54)	8.80 (± 1.24)
240	418.6 (± 103.3)	28.3 (± 3.49)	77.2 (±10.5)	19.0 (± 10.6)	6.68 (± 2.77)

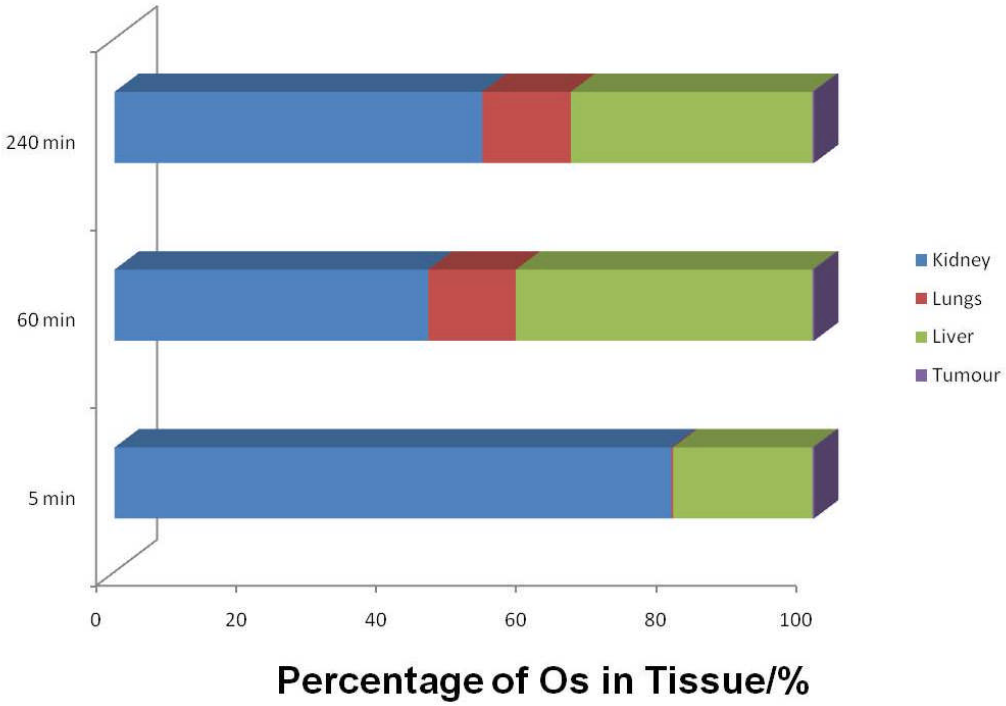

Figure 3.12. Percentage of Os distributions in kidney, lungs, liver and tumour. Points represent the mean concentration for three mice.

3.3.10 Combination treatment with L-BSO

The azopyridine complex **6** is relatively inert. For example, it does not readily undergo hydrolysis in aqueous solution or bind to DNA bases, unlike chlorido diamine Os^{II} arene complexes. Our initial studies on iodido azopyridine Os^{II} arene complexes suggested that their cytotoxic activity might involve redox mechanisms. Here we have investigated the ability of complex **6** to generate reactive oxygen species (ROS) in cancer cells. ROS play important roles in regulating cell proliferation, death, and senescence. The redox system is also a significant target for anticancer treatment.[26] Targeting the redox system can induce selective cell death in malignant cells and spare normal cells due to the higher baseline level of ROS in cancer cells.

The level of ROS induced in A2780 human ovarian cancer cells by complex **6** was determined using the probe 2′,7′-dichlorodihydrofluorescein-diacetate (DCFH-DA). This is taken up by live cells, hydrolyzed to 2′,7′-dichlorodihydrofluorescein (DCFH), and in turn oxidized to 2′,7′-dichlorofluorescein (DCF) in the presence of ROS and exhibits a green fluorescence.[27] Using this probe, we determined the level of general oxidative stress induced in cells by **6**. The effect of combined exposure to **6** and L-buthionine-sulfoximine (L-BSO) was investigated. L-BSO, a specific inhibitor of γ-glutamyl-cysteine synthetase, depletes intracellular glutathione (GSH). Gutathione plays a central role in a wide range of cellular functions, including protection, detoxification, transport, and metabolism. A2780 cells were pre-incubated for 20 min with 10 μM DCFH-DA. The relative increase in DCF fluorescence was then detected over a period of 4 h after treatment of the cells with 1 μM **6**, or 1 μM **6** plus 50 μM L-BSO, or 50 μM H_2O_2 (Figure 3.13). On treatment with **6** alone, the ROS level increased by 21% compared to the control. This level increased further to 50% in the presence of L-BSO in addition to **6**. The mode of interference by **6** in the redox balance in cells and the production of ROS is not yet clear. Complex **6** underwent an electrochemical reduction in

dimethylformamide with an associated half-wave potential of -0.64 V (vs. Ag/AgCl). This reduction can be associated with addition of an electron into the π* orbital centred on the azo group of the azopyridine ligand to form an azo anion radical, a process previously detected for the Ru^{II} analog, although occurring more readily in the latter case at a potential of -0.40 V. Unlike the Ru complex, **6** does not react catalytically with GSH.

These data suggested that L-BSO might enhance the cytotoxicity of complex **6** towards cancer cells. As can be seen from Figure 3.14, L-BSO alone at a dose of 50 μM had no significant effect of the growth of either A2780 human ovarian cells or A549 human lung cancer cells, but greatly enhanced the cytotoxicity of complex 6 at doses of 0.1 and 1 μM for A2780 cells, and 1 and 5 μM for A549 cells. These results imply that combination treatment with **6** and L-BSO may have potential as a therapeutic strategy. Clinical trials of L-BSO are currently in progress on combinations with melphalan in patients with persistent or recurrent stage III malignant melanoma.[28]

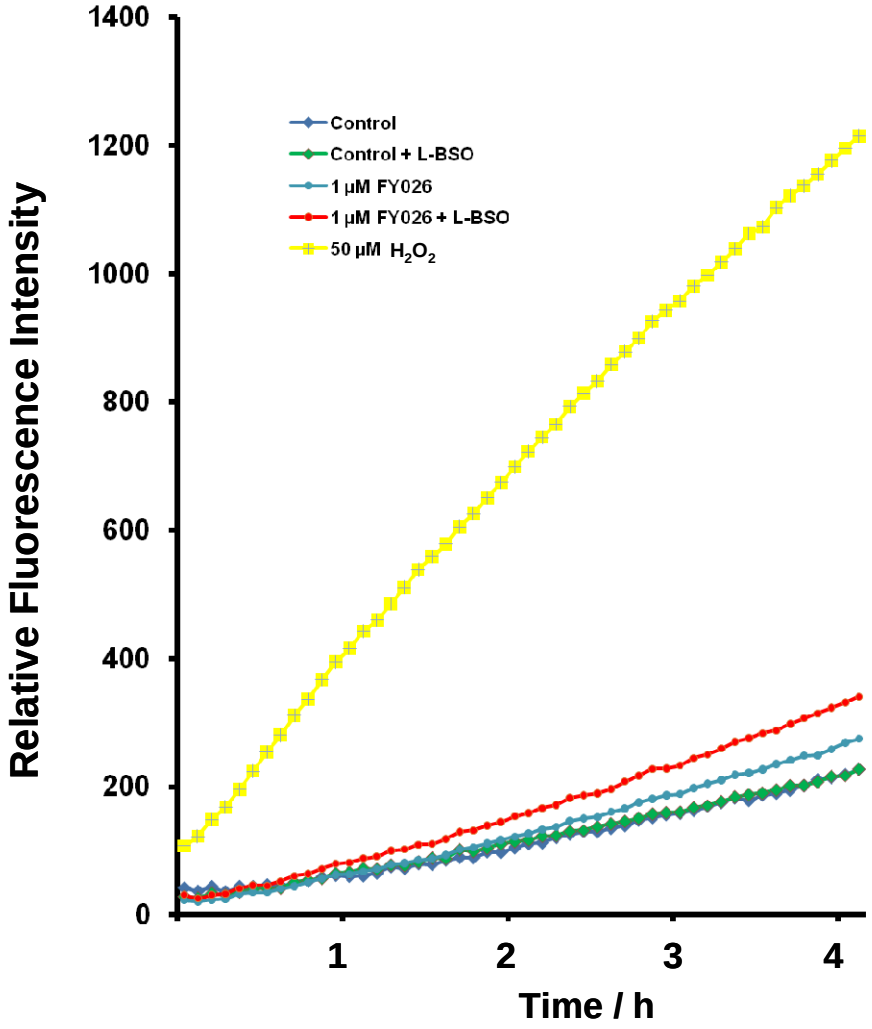

Figure 3.13. Relative changes in DCF fluorescence detected over time after exposure to 1 µM complex **6** (FY026), 1 µM **6** with 50 µM L-BSO, and 50 µM H_2O_2. For each experiment the fluorescence was averaged over 8 wells.

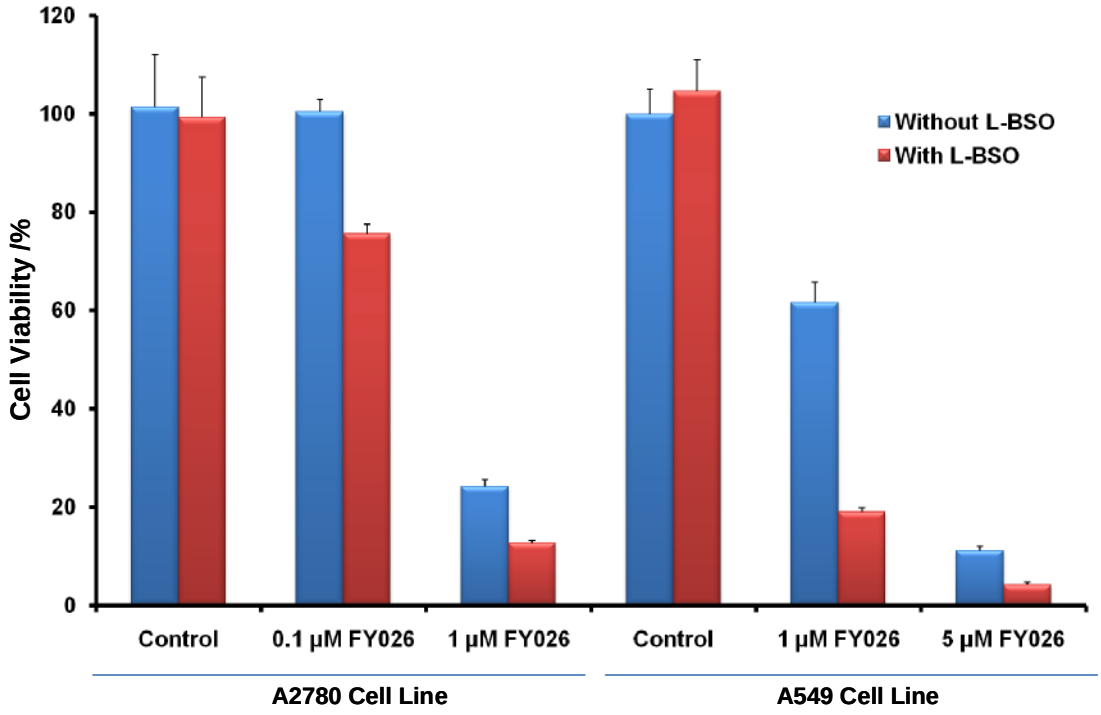

Figure 3.14. Percentage cell survival after 24 h exposure to osmium complex **6** (FY026) with or without 50 µM L-BSO. Left: A2780 ovarian cancer cells. Right: A549 lung cancer cells. Previously determined IC_{50} values are 0.2 µM for A2780 cells (24 h exposure to **6** followed by 72 h recovery period), and 0.4 µM for A549 cells (24 h exposure, 96 h recovery period).

3.4 Conclusions

Pseudo-octahedral 'piano-stool' organometallic osmium arene complexes have the potential for exploration as anticancer complexes. They are attractive since they provide a hydrophobic arene face amenable to a wide variety of substitutions together with three other variable coordination positions. Both the arene and the other ligands can have a major effect on determining the electron distribution within the complex, controlling their rates of ligand substitution and their redox properties (metal- or ligand-centered). In this chapter, the chelated azopyridine ligand is both a σ-donor and a strong π-acceptor, i.e. there is a strong back-donation of electrons from Os^{II} onto the azopyridine ligand producing a large effect on overall reactivity. Iodido complexes were more cytotoxic than the analogous chlorido complexes. In addition, iodido complexes containing *p*-hydroxyl or *p*-dimethylamino substituents on the azopyridine chelating ligand (e.g. complexes **3** and **6**) were cytotoxic at nanomolar concentrations towards ovarian, lung, breast, colon, prostate, and bladder human cancer cells, an order of magnitude more potent than cisplatin, and (unexpectedly) than their Ru^{II} analogues. These iodido complexes are also inert towards hydrolysis. Interestingly, their cytotoxicity was inhibited by pre-treatment of the cells wth N-acetyl-L-cysteine suggesting that reactive oxygen species (ROS) are involved in their mechanism of action, although, unlike their Ru^{II} arene azopyridine analogues, the Os^{II} complexes investigated here do not oxidize GSH catalytically. More encouragingly, these Os^{II} complexes exhibited low toxicity and negligible deleterious effects in a HCT-116 tumour xenograft model indicating that they may exhibit a broad therapeutic window.

The organometallic osmium arene azopyridine complex **6**, which has nanomolar activity *in vitro* in a panel of human cancer cell lines, exhibits acivity *in vivo* against HCT116 human colon cancer xenografts in mice, with negligible toxicity. This appears to be the first demonstration of significant anticancer activity *in viv*o for organometallic half-sandwich osmium complexes. Studies on

the plasma, tumour and normal tissue distribution of **6** suggest that there is scope to optimize the therapeutic activity using multiple-dose schedules without the risk of off-target toxicity.

3.5 Summary

Iodido osmium(II) complexes $[Os(\eta^6\text{-arene})(XY)I]^+$, XY = *p*-hydroxy or *p*-dimethylamino azopyridine, arene = *p*-cymene or biphenyl, are potently cytotoxic at nanomolar concentrations towards a panel of human cancer cell lines. They exhibit low toxicity and negligible deleterious effects in a colon cancer xenograft model, giving rise to the possibility of a broad therapeutic window. The most active complexes are stable and inert towards aquation. Their cytotoxic activity appears to involve redox mechanisms. The activity of a potent complex **6** (FY026) *in vivo* versus HCT116 human colon cancer xenografts and the distribution of osmium in plasma and tissues were investigated. Further insight into the mechanism of action of **6** (FY026) was obtained from studies of its redox potential, its ability to generate Reactive Oxygen Species (ROS) in cells, and the effect of L-buthionine-sulfoximine (L-BSO), a specific inhibitor of γ-glutamyl-cysteine synthetase known to reduce intracellular thiol levels,[29] on the cytotoxicity of the complex.

3.6 References

1. L. Kelland, *Nat. Rev. Cancer*, 2007, **7**, 573-584.
2. Z. H. Siddik, *Oncogene*, 2003, **22**, 7265-7279.
3. I. Bratsos, S. Jedner, T. Gianferrara and E. Alessio, *Chimia*, 2007, **61**, 692-697.
4. M. A. Jakupec, M. Galanski, V. B. Arion, C. G. Hartinger and B. K. Keppler, *Dalton Trans.*, 2008, 183-194.
5. Ott. I. Gust. R, *Arch. Pharm.*, 2007, **340**, 117– 126.
6. Y. K. Yan, M. Melchart, A. Habtemariam and P. J. Sadler, *Chem. Commun.*, 2005, 4764-4776.
7. C. G. Hartinger, S. Zorbas-Seifried, M. A. Jakupec, B. Kynast, H. Zorbas and B. K. Keppler, *J. Inorg. Biochem.*, 2006, **100**, 891-904.
8. J. M. Rademaker-Lakhai, D. van den Bongard, D. Pluim, J. H. Beijnen and J. H. Schellens, *Clin. Cancer Res.*, 2004, **10**, 3717-3727.
9. F. Wang, A. Habtemariam, E. P. van der Geer, R. Fernandez, M. Melchart, R. J. Deeth, R. Aird, S. Guichard, F. P. Fabbiani, P. Lozano-Casal, I. D. Oswald, D. I. Jodrell, S. Parsons and P. J. Sadler, *Proc. Natl. Acad. Sci. U. S. A.*, 2005, **102**, 18269-18274.
10. R. E. Aird, J. Cummings, A. A. Ritchie, M. Muir, R. E. Morris, H. Chen, P. J. Sadler and D. I. Jodrell, *Br. J. Cancer*, 2002, **86**, 1652-1657.
11. S. J. Dougan, M. Melchart, A. Habtemariam, S. Parsons and P. J. Sadler, *Inorg. Chem.*, 2006, **45**, 10882-10894.
12. A. F. A. Peacock, A. Habtemariam, R. Fernandez, V. Walland, F. P. A. Fabbiani, S. Parsons, R. E. Aird, D. I. Jodrell and P. J. Sadler, *J. Am. Chem. Soc.*, 2006, **128**, 1739-1748.
13. A. F. A. Peacock and P. J. Sadler, *Chem. Asian J.*, 2008, **3**, 1890-1899.

14. S. H. van Rijt, A. F. A. Peacock, R. D. L. Johnstone, S. Parsons and P. J. Sadler, *Inorg. Chem.*, 2009, **48**, 1753-1762.

15. A. Dorcier, W. H. Ang, S. Bolano, L. Gonsalvi, L. Juillerat-Jeannerat, G. Laurenczy, M. Peruzzini, A. D. Phillips, F. Zanobini and P. J. Dyson, *Organometallics*, 2006, **25**, 4090-4096.

16. A. F. A. Peacock, A. Habtemariam, S. A. Moggach, A. Prescimone, S. Parsons and P. J. Sadler, *Inorg. Chem.*, 2007, **46**, 4049-4059.

17. W. F. Schmid, R. O. John, V. B. Arion, M. A. Jakupec and B. K. Keppler, *Organometallics*, 2007, **26**, 6643-6652.

18. S. H. van Rijt, A. J. Hebden, T. Amaresekera, R. J. Deeth, G. J. Clarkson, S. Parsons, P. C. McGowan and P. J. Sadler, *J. Med. Chem.*, 2009, **52**, 7753-7764.

19. S. H. van Rijt, A. Mukherjee, A. M. Pizarro and P. J. Sadler, *J. Med. Chem.*, 2010, **53**, 840-849.

20. A. H. Velders, H. Kooijman, A. L. Spek, J. G. Haasnoot, D. de Vos and J. Reedijk, *Inorg. Chem.*, 2000, **39**, 2966-2967.

21. S. J. Dougan, A. Habtemariam, S. E. McHale, S. Parsons and P. J. Sadler, *Proc. Natl. Acad. Sci. U. S. A.*, 2008, **105**, 11628-11633.

22. S. D. Shnyder, P. A. Cooper, N. J. Millington, G. R. Pettit, M. C. Bibby and P. Y. E. Auristatin, *Int. J. Oncol.*, 2007, **31**, 353-360.

23. A. C. G. Hotze, S. E. Caspers, D. De Vos, H. Kooijman, A. L. Spek, A. Flamigni, M. Bacac, G. Sava, J. G. Haasnoot and J. Reedijk, *J. Biol. Inorg. Chem.*, 2004, **9**, 354-364.

24. H. Kostrhunova, J. Florian, O. Novakova, A. F. A. Peacock, P. J. Sadler and V. Brabec, *J. Med. Chem.*, 2008, **51**, 3635-3643.

25. J. P. Godbout, J. Pesavento, M. E. Hartman, S. R. Manson and G. G. Freund, *J. Biol. Chem.*, 2002, **277**, 2554-2561.

26. D. Trachootham, J. Alexandre and P. Huang, *Nat. Rev. Drug Discov.*, 2009, **8**, 579-591.

27. B. Halliwell and M. Whiteman, *Br. J. Pharmacol.*, 2004, **142**, 231-255.

28. H. Bailey, R. Mulcahy, K. Tutsch, R. Arzoomanian, D. Alberti, M. Tombes, G. Wilding, M. Pomplun and D. Spriggs, *J. Clin. Oncol.*, 1994, **12**, 194-205.

29. J. E. Biaglow, M. E. Varnes, S. W. Tuttle, N. L. Oleinick, K. Glazier, E. P. Clark, E. R. Epp and L. A. Dethlefsen, *Int. J. Radiat. Oncol. Biol. Phys.*, 1986, **12**, 1139-1142.

Chapter 4
Os^{II} Arene R-azopyridine Complexes

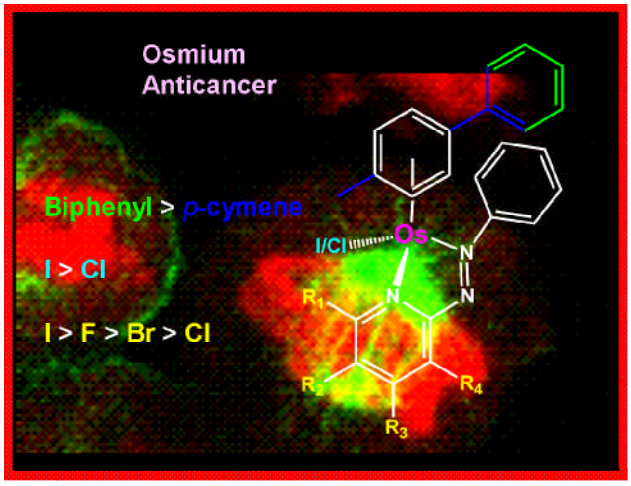

4.1 Introduction

The only recognised clinical use of osmium appears to be for synovectomy in arthritic patients in Scandinavia.[1-3] This involves the local administration of osmium tetroxide (OsO_4), usually considered to be a highly toxic compound. The lack of reports of long term side effects suggests that osmium itself can be biocompatible, although clearly this might be dependent on the exact nature of the compound administered. Osmium carbohydrate polymers (osmarins) have been also investigated as potential antiarthritic agents.[4]

Recently, non-organometallic osmium(VI) complexes were reported to show anticancer activity *in vivo*.[5] In previous chapter, certain half-sandwich organometallic iodido osmium azopyridine arene complex (FY026) was found to be able to exhibit potent *in vitro* and *in vivo* anticancer activity; FY026 showed much higher activity than the clinical drug cisplatin to a panel of cancer cell lines *in vitro*.[6, 7] Similar to Ru^{II},[8] the introduction of the strong π-acceptor azopyridine as a ligand in organometallic Os^{II} complexes has a major effect on their chemical and biological properties.[5]

For Os^{II} arene picolinate complexes, log P values correlate with cellular uptake, which indicates that increased lipophilicity favours uptake by cancer cells, probably through a passive diffusion pathway, and results in an increase in anticancer activity.[9] However, increasing lipophilicity to improve anticancer activity can result in difficulties with clinical formulation and lower bioavailability[10]. Hence there is a need for rational design aimed at tuning lipophilicity while maintaining anticancer activity.

The goal of anticancer research programs is to identify novel, synthetically-feasible molecules that exhibit useful anticancer activity with minimal side-effects. One efficient approach is the study of bioisosterism, a term coined to describe the modification of biological activity by isosterism.[11-13] In this chapter, a series of

bioisosteres of Os^{II} arene complexes containing chelated azopyridines with various substitutents on the pyridine ring were studied. Cellular reactive oxygen species (ROS) were found to accumulate but do not lead to the death of cancer cells, suggesting a mechanism different from that for related complexes with an unsubstituted pyridine ring and a substitutent on the phenyl ring. In addition, it is found that down-regulation of the cellular GSH level results in lowering of anticancer activity, a property which has been found only for the anticancer drug taxol, which kills cancer cells in a GSH-dependent manner.[14]

4.2 Experimental

4.2.1 X-ray Crystallography

X-ray diffraction data for $[Os(\eta^6\text{-bip})(1\text{-Cl-Azpy})Cl]PF_6$ (**7**) $[Os(\eta^6\text{-bip})(2\text{-F-Azpy})Cl]PF_6$ (**10**, $[Os(\eta^6\text{-bip})(2\text{-Cl-Azpy})I]PF_6$ (**13**), $[Os(\eta^6\text{-}p\text{-cym})(2\text{-Cl-Azpy})I]PF_6$ (**14**), $[Os(\eta^6\text{-}p\text{-cym})(2\text{-Cl-Azpy})Cl]PF_6$ (**16**), $[Os(\eta^6\text{-}p\text{-cym})(2\text{-Br-Azpy})I]PF_6$ (**18**), $[Os(\eta^6\text{-bip})(2\text{-Br-Azpy})Cl]PF_6$ (**19**), $[Os(\eta^6\text{-}p\text{-cym})(2\text{-Br-Azpy})Cl]PF_6$ (**20**), $[Os(\eta^6\text{-}p\text{-cym})(3\text{-Cl-Azpy})I]PF_6$ (**24**) and $[Os(\eta^6\text{-}p\text{-cym})(3\text{-Cl-Azpy})Cl]PF_6$ (**26**) were obtained on an Oxford Diffraction Gemini four-circle system with a Ruby CCD area detector using Mo Kα radiation.[15] Absorption corrections were applied using ABSPACK. The crystals were mounted in oil and held at 100(2) K with the Oxford Cryosystem Cryostream Cobra, except compound **7** for which data was collected at ambient temperature. The structures were solved by direct methods using SHELXS (TREF) with additional light atoms found by Fourier methods.[16] Refinement used SHELXL 97.[17] H atoms were placed at geometrically calculated positions and refined riding on their parent atoms. X-ray crystallographic CIF files for complexes **18**, **16**, **14**, **13**, **19**, **10**, **7**, **24**, **20**, and **26** have been deposited in the CCDC with reference numbers 821519 –

821528, respectively. The collection and structure solution were carried out by Dr. Guy J. Clarkson.

4.2.2 Synthesis and Characterization

[Os(η^6-bip)(1-CF$_3$-4-Cl-Azpy)I]PF$_6$ (1). [Os(η^6-bip)I$_2$]$_2$ (50.0 mg, 0.042 mmol) was dissolved in methanol (40 mL) at 353 K. 1-CF$_3$-4-Cl-azpy (24.0 mg, 0.084 mmol) in methanol (10 mL) was added drop-wise. The solution was stirred at 353 K for 16 h. The volume was reduced to about 10 mL by removal of methanol on a rotary evaporator, and ammonium hexafluorophosphate (27.7 mg, 0.17 mmol) was added. The solution was then left in a freezer at 253 K for 24 h. The dark coloured precipitate was collected by filtration, washed with cold ethanol and diethyl ether, then finally dried *in vacuo*. Yield: 43.1 mg (57.1 %). ESI-MS Calcd for $C_{24}H_{17}ClF_3IN_3Os$: m/z 758.0, found 757.8. ^{1}H NMR((CD$_3$)$_2$CO): δ 9.80 (s, 1H), 8.71 (d, 1H, J = 2 Hz), 7.96 (d, 2H, J = 8 Hz), 7.72 (t, 1H, J = 8 Hz), 7.56-7.44 (m, 6H), 7.42-7.38(m, 2H), 7.27 (t, 1H, J = 6 Hz), 7.22 (d, 1H, J = 6 Hz), 6.98 (t, 1H, J = 6 Hz), 6.88 (d, 1H, J = 6 Hz), 6.77 (t, 1H, J = 6 Hz), CHN analysis: Found: C, 31.98%; H, 2.08%; N, 4.34%. Calcd for $C_{24}H_{17}ClF_9IN_3OsP$: C, 31.96% H, 1.90% N, 4.66%.

[Os(η^6-*p*-cym)(1-CF$_3$-4-Cl-Azpy)I]PF$_6$ (2). [Os(η^6-*p*-cym)I$_2$]$_2$ (50.0 mg, 0.043 mmol) was dissolved in methanol (40 mL). 1-CF$_3$-4-Cl-azpy (24.6 mg, 0.086 mmol) in methanol (10 mL) was added drop-wise, the solution-colour changed from yellow to red brown immediately. The solution was stirred at ambient temperature for 72 h. The volume was reduced to about 10 mL by removal of methanol on a rotary evaporator, and ammonium hexafluorophosphate (28.0 mg. 0.17 mmol) was added. The solution was then left in a freezer (253 K) for 24 h. Dark coloured crystals formed which were collected by filtration, washed with cold ethanol and diethyl ether, then finally dried *in vacuo*. Yield: 54.4 mg (71.7 %). ESI-MS Calcd for $C_{22}H_{21}ClF_3IN_3Os$: m/z 738.0, found 737.8. ^{1}H

MR($(CD_3)_2CO$): δ 8.91 (s, 1H), 8.41 (d, 2H, , J = 6 Hz), 8.06-7.79 (m, 6H), 7.07 (d, 2H, , J = 6 Hz), 6.46-6.40 (m, 3H), 6.16 (d, 2H, , J = 6 Hz), 2.77 (s, 3H), 2.62-2.52 (m, 1H), 0.93 (d, 3H, J = 7 Hz), 0.88 (d, 3H, J = 7 Hz). CHN analysis: Found: C, 29.91%; H, 2.38%; N, 4.83%. Calcd for $C_{22}H_{21}ClF_9IN_3OsP$: C, 29.96%; H, 2.40%; N, 4.76%.

[Os(η^6-bip)(1-CF_3-4-Cl-Azpy)Cl]PF_6 (3). [Os(η^6-bip)Cl_2]$_2$ (50.0 mg, 0.06 mmol) was dissolved in methanol (40 mL) at 353 K. 1-CF_3-4-Cl-azpy (34.3 mg, 0.12 mmol) in methanol (10 mL) was added drop-wise. The solution was stirred at 353 K for 2 h. The volume was reduced to about 10 mL by removal of methanol on a rotary evaporator, and ammonium hexafluorophosphate (39.1 mg, 0.24 mmol) was added. The solution was then left in a freezer (253 K) for 24 h. The dark coloured precipitate was collected by filtration, washed with cold ethanol and diethyl ether, then finally dried *in vacuo*. Yield: 71.9 mg (88.7 %). ESI-MS Calcd for $C_{24}H_{17}Cl_2F_3N_3Os$: m/z 666.0, found 666.0. ^{1}H NMR($(CD_3)_2CO$): δ 9.55 (s, 1H), 8.84 (d, 1H, J = 2 Hz), 7.99 (d, 2H, J = 8 Hz), 7.76 (t, 1H, J = 8 Hz), 7.66-7.54 (m, 6H), 7.50-7.47(m, 2H), 7.07 (d, 1H, J = 6 Hz), 6.98-6.92 (m, 3H), 6.54-6.49 (m, 1H). CHN analysis: Found: C, 36.43%; H, 2.07%; N, 5.17%. Calcd for $C_{24}H_{17}Cl_2F_9N_3OsP$: C, 35.56%; H, 2.11%; N, 5.18%.

[Os(η^6-*p*-cym)(1-CF_3-4-Cl-Azpy)Cl]PF_6 (4). [Os(η^6-*p*-cym)Cl_2]$_2$ (50.0 mg, 0.063 mmol) was dissolved in methanol (40 mL). 1-CF_3-4-Cl-azpy (36.1 mg, 0.126 mmol) in methanol (10 mL) was added drop-wise, the solution-colour changed from yellow to red brown immediately. The solution was stirred at ambient temperature for 12 h. The volume was reduced to about 10 mL by removal of methanol on a rotary evaporator, and ammonium hexafluorophosphate (41.2 mg, 0.25 mmol) was added. The solution was then left in the freezer (253 K) for 24 h. The dark coloured precipitate was collected by filtration, washed with cold ethanol and diethyl ether, then finally dried *in vacuo*. Yield: 69.2 mg (69.5 %). ESI-MS Calcd for $C_{22}H_{21}Cl_2F_3N_3Os$: m/z 646.1, found 646.0. ^{1}H

NMR($(CD_3)_2CO$): δ 9.80 (s, 1H), 8.88 (s, 1H), 8.18 (m, 2H), 7.96-7.81 (m, 3H), 7.03 (d, 1H, J = 8 Hz), 6.68 (d, 1H, J = 8 Hz), 6.56 (m, 2H), 2.80 (s, 3H), 2.58-2.49 (m, 1H), 1.00 (d, 3H, J = 7 Hz), 0.96 (d, 3H, J = 7 Hz). CHN analysis: Found: C, 33.26%; H, 2.59%; N, 5.24%. Calcd for $C_{22}H_{21}Cl_2F_9N_3OsP$: C, 33.43%; H, 2.68%; N, 5.32%.

[Os(η^6-*p*-cym)(1-Cl-Azpy)I]PF$_6$ (5). [Os(η^6-*p*-cym)I_2]$_2$ (50.0 mg, 0.043 mmol) was dissolved in methanol (30 mL). 1-Cl-azpy (18.7 mg, 0.086 mmol) in methanol (10 mL) was added drop-wise. The solution was stirred at 353 K for 4 h. The volume was reduced to about 10 mL by removal of methanol on a rotary evaporator, and ammonium hexafluorophosphate (28.0 mg, 0.17 mmol) was added. The solution was then left in the freezer (253 K) for 24 h. The dark coloured precipitate was collected by filtration, washed with cold ethanol and diethyl ether, then finally dried *in vacuo*. Yield: 28.0 mg (40.0 %). ESI-MS Calcd for $C_{21}H_{22}ClIN_3Os$: m/z 670.0, found 669.9. ^{1}H NMR($(CD_3)_2CO$): δ 9.01 (d, 1H, J = 6 Hz), 8.20 (d, 1H, J = 8 Hz), 8.14-8.02 (m, 3H), 7.81 (m, 1H), 7.14 (d, 2H, J = 9 Hz), 6.61 (m, 2H), 6.46 (d, 1H, J = 6 Hz), 6.16 (m, 4H), 2.39 (s, 3H), 2.69-2.64 (m, 1H), 1.05 (d, 3H, J = 7 Hz), 1.01 (d, 3H, J = 7 Hz). CHN analysis: Found: C, 30.38%; H, 2.62%; N, 5.11%. Calcd for $C_{21}H_{22}ClF_6IN_3OsP$: C, 30.99%; H, 2.72%; N, 5.16%.

[Os(η^6-bip)(1-Cl-Azpy)I]PF$_6$ (6). [Os(η^6-bip)I_2]$_2$ (30.0 mg, 0.025 mmol) was dissolved in methanol (40 mL) at 353 K. 1-Cl-azpy (10.8 mg, 0.050 mmol) in methanol (10 mL) was added drop-wise. The solution was stirred at 353 K for 2 h. The volume was reduced to about 10 mL by removal of methanol on a rotary evaporator, and ammonium hexafluorophosphate (16.3 mg, 0.10 mmol) was added. The solution was then left in a freezer (253 K) for 24 h. The dark coloured precipitate was collected by filtration, washed with cold ethanol and diethyl ether, then finally dried *in vacuo*. Yield: 22.0 mg (52.8 %). ESI-MS Calcd for $C_{23}H_{18}ClIN_3Os$: m/z 690.0, found 689.9. ^{1}H NMR($(CD_3)_2CO$): δ 8.56 (d, 1H, J =

6 Hz), 8.33 (t, 1H, J = 8 Hz), 8,19 (d, 1H, J = 6 Hz), 7.87 (d, 2H, J = 8 Hz), 7.66 (t, 1H, J = 8 Hz), 7.52-7.39 (m, 7H), 7.19 (d, 1H, J = 6 Hz), 7.00 (t, 2H, J = 6 Hz), 6.99-6.78 (m, 2H). CHN analysis: Found: C, 32.82%; H, 2.08%; N, 4.75%. Calcd for $C_{23}H_{18}ClF_6IN_3OsP$: C, 33.12%; H, 2.18%; N, 5.04%.

[Os(η^6-*p*-cym)(1-Cl-Azpy)Cl]PF_6 (7). [Os(η^6-*p*-cym)Cl_2]$_2$ (50.0 mg, 0.063 mmol) was dissolved in methanol (30 mL). 1-Cl-azpy (27.4 mg, 0.126 mmol) in methanol (10 mL) was added drop-wise, the solution-colour changed from yellow to red immediately. The solution was stirred at ambient temperature for 4 h. The volume was reduced to about 10 mL by removal of methanol on a rotary evaporator, and ammonium hexafluorophosphate (41.2 mg, 0.25 mmol) was added. The solution was then left in the freezer (253 K) for 24 h. The dark coloured precipitate which was collected by filtration, washed with cold ethanol and diethyl ether, then finally dried *in vacuo*. Yield: 86.3 mg (94.8 %). ESI-MS Calcd for $C_{21}H_{22}Cl_2N_3Os$: m/z 578.1, found 578.1. ^{1}H NMR($(CD_3)_2CO$): δ 8.94 (d, 1H, J = 8 Hz), 8.41 (t, 1H, J = 8 Hz), 8.30(d, 1H, J = 8 Hz), 8.13(d, 2H, J = 8 Hz), 7.76 (m, 3H), 7.06 (d, 1H, J = 6 Hz), 6.42 (d, 1H, J = 6 Hz), 6.37 (d, 1H, J = 6 Hz), 6.16 (d, 1H, J = 6 Hz), 2.62-2.54 (m, 1H), 2.46 (s, 3H), 1.01 (d, 3H, J = 7 Hz), 0.97 (d, 3H, J = 7 Hz). CHN analysis: Found: C, 34.91%; H, 3.02%; N, 5.75%. Calcd for $C_{21}H_{22}Cl_2F_6N_3OsP$: C, 34.91%; H, 3.07%; N, 5.82%.

[Os(η^6-bip)(1-Cl-Azpy)Cl]PF_6 (8). [Os(η^6-bip)Cl_2]$_2$ (50.0 mg, 0.060 mmol) was dissolved in methanol (40 mL) at 353 K. 1-Cl-azpy (26.1 mg, 0.12 mmol) in methanol (10 mL) was added drop-wise. The solution was stirred at 353 K for 1 h. The volume was reduced to about 10 mL by removal of methanol on a rotary evaporator, and ammonium hexafluorophosphate (39.1 mg, 0.24 mmol) was added. The solution was then left in the freezer (253K) for 24 h. Dark coloured powder was precipitated which was collected by filtration, washed with cold ethanol and diethyl ether, then finally dried *in vacuo*. Yield: 27.8 mg (31.2 %). ESI-MS Calcd for $C_{23}H_{18}Cl_2N_3Os$: m/z 598.0, found 598.0. ^{1}H NMR($(CD_3)_2CO$):

^{1}H NMR($(CD_3)_2CO$): δ 8.92 (d, 1H, J = 6 Hz), 8.43 (t, 1H, J = 8 Hz), 8,26 (d, 1H, J = 6 Hz), 7.94 (d, 2H, J = 8 Hz), 7.72 (t, 1H, J = 8 Hz), 7.62-7.35 (m, 7H), 7.06 (t, 11H, J = 6 Hz), 6.94 (t, 2H, J = 6 Hz), 6.74 (t, 1H, J = 6 Hz), 6.50 (t, 1H, J = 6 Hz), CHN analysis: Found: C, 36.95%; H, 2.39%; N, 5.59%. Calcd for $C_{23}H_{18}Cl_2F_6N_3OsP$: C, 37.20%; H, 2.44% ; N, 5.66%.

[Os(η^6-bip)(2-F-Azpy)I]PF_6 (9). [Os(η^6-bip)I_2]$_2$ (25.0 mg, 0.021 mmol) was dissolved in methanol (20 mL) at 313 K. 2-F-Azpy (8.4 mg, 0.042 mmol) in methanol (10 mL) was added drop-wise, the solution-colour changed from yellow to brown immediately. The solution was heated under reflux (353K) for 12 h. The volume was reduced to about 10 mL by removal of methanol on a rotary evaporator, and ammonium hexafluorophosphate (13.7 mg, 0.084 mmol) was added. The solution was then left in a freezer (253 K) for 24 h. Dark coloured powder precipitated which was collected by filtration, washed with cold ethanol and diethyl ether, then finally dried *in vacuo*. Yield: 15.5 mg (45.0 %). ESI-MS Calcd for $C_{23}H_{18}FIN_3Os$: m/z 674.0, found 674.1. ^{1}H NMR($(CD_3)_2CO$): δ 9.50 (t, 1H, J = 2 Hz), 8.88 (d of d, 1H), 8,91 (d of d, 2H), 8,32(d of t, 1H), 8,02 (d of d, 1H), 7.95-7.92 (m, 2H), 7.73-7.41 (m, 5H), 7.13-7.09 (m, 2H), 6.96 (t, 1H, J = 7 Hz). 6.79 (d, 1H, J = 7 Hz), 6.65 (t, 1H, J = 7 Hz). CHN analysis: Found: C, 34.17%; H, 2.28%; N, 5.04%. Calcd for $C_{23}H_{18}F_7IN_3OsP$: C, 33.79%; H, 2.22%; N, 5.14%.

[Os(η^6-bip)(2-F-Azpy)Cl]PF_6 (10) [Os(η^6-bip)Cl_2]$_2$ (50.0 mg, 0.06 mmol) was dissolved in methanol (40 mL) and water (10 mL) mixture at 353 K. 2-F-Azpy (24.1 mg, 0.12 mmol) in methanol (10 mL) was added drop-wise. The solution was heated under reflux (353K) for 4 h. The volume was reduced to about 10 mL by removal of methanol on a rotary evaporator, and ammonium hexafluorophosphate (97.8mg, 0.6 mmol) was added. The solution was then left in a freezer (253 K) for 24 h. Dark coloured powder precipitated which was collected by filtration, washed with cold ethanol and diethyl ether, then finally

dried *in vacuo*. Yield: 37.5 mg (86.1 %). ESI-MS Calcd for $C_{23}H_{18}ClFN_3Os$: m/z 582.1, found 582.0. ^{1}H NMR($(CD_3)_2CO$): δ 9.53 (t, 1H, J = 2 Hz), 9.08 (d of d, 1H), 8,40 (d of t, 2H), 7.94 (d, 2H J = 8 Hz), 7.73 (t, 1H, J = 8 Hz), 7.63-7.48 (m, 7H), 7.97-7.32 (m, 2H), 6.87 (t, 1H, J = 6 Hz). 6.78 (d, 1H, J = 6 Hz), 6.47 (t, 1H, J = 6 Hz). CHN analysis: Found: C, 37.69%; H, 2.33%; N, 5.87%. Calcd for $C_{23}H_{18}ClF_7N_3OsP$: C, 38.05%; H, 2.50%; N, 5.79%.

[Os(η^6-*p*-cym)(2-F-Azpy)I]PF$_6$ (11). [Os(η^6-*p*-cym)I$_2$]$_2$ (50.0 mg, 0.043 mmol) was dissolved in methanol (40 mL) at 313 K. 2-F-azpy (34.8 mg, 0.17 mmol) in methanol (10 mL) was added drop-wise. The solution was stirred at 313 K for 4 h. The volume was reduced to about 10 mL by removal of methanol on a rotary evaporator, and ammonium hexafluorophosphate (70.0 mg, 0.43 mmol) was added. The solution was then left in a freezer (253 K) for 24 h. Dark coloured powder precipitated which was collected by filtration, washed with cold ethanol and diethyl ether, then finally dried *in vacuo*. Yield: 38.7 mg (48.5 %). ESI-MS Calcd for $C_{21}H_{22}FIN_3Os$: m/z 654.0, found 654.0. ^{1}H NMR($(CD_3)_2CO$): δ 9.70 (s, 1H), 9.13 (d, 1H, J = 6 Hz), 8.34 (t, 1H, J = 6 Hz), 8.17 (d, 2H, J = 6 Hz), 7.82-7.73 (m, 3H), 6.84 (d, 1H, J = 6 Hz), 6.52 (d, 1H, J = 6 Hz), 6.45 (d, 1H, J = 6 Hz), 6.35 (d, 1H, J = 6 Hz), 2.83 (s, 3H), 2.65-2.61 (m, 1H), 1.04 (d, 3H, J = 7 Hz), 1.00 (d, 3H, J = 7 Hz). CHN analysis: Found: C, 32.27%; H, 2.81%; N, 5.21%. Calcd for $C_{21}H_{22}F_7IN_3OsP$: C, 31.63%; H, 2.78%; N, 5.27%.

[Os(η^6-*p*-cym)(2-F-Azpy)Cl]PF$_6$ (12). [Os(η^6-*p*-cym)Cl$_2$]$_2$ (25.0 mg, 0.032 mmol) was dissolved in methanol (20 mL) at 313 K. 2-F-azpy (12.7 mg, 0.063 mmol) in methanol (10 mL) was added drop-wise. The solution was stirred at ambient temperature for 4 h. The volume was reduced to about 10 mL by removal of methanol on a rotary evaporator, and ammonium hexafluorophosphate (20.5 mg, 0.13 mmol) was added. The solution was then left in the freezer (253 K) for 24 h. Dark coloured powder was precipitated which was collected by filtration, washed with cold ethanol and diethyl ether, then finally dried *in vacuo*. Yield: 11.9 mg

(52.7 %). ESI-MS Calcd for $C_{21}H_{22}ClFN_3Os$: m/z 561.1, found 561.0. ^{1}H NMR($(CD_3)_2CO$): δ 9.70 (s, 1H), 9.12 (d, 1H, J = 6 Hz), 8.43 (t, 1H, J = 6 Hz), 8.17 (d, 2H, J = 6 Hz), 7.65-7.58 (m, 3H), 6.87 (d, 1H, J = 6 Hz), 6.80 (d, 1H, J = 6 Hz), 6.51 (d, 1H, J = 6 Hz), 6.42 (d, 1H, J = 6 Hz), 2.81 (s, 3H), 2.53-2.49 (m, 1H), 0.99 (d, 3H, J = 7 Hz), 0.94 (d, 3H, J = 7 Hz). CHN analysis: Found: C, 35.07%; H, 2.98%; N, 5.71%. Calcd for $C_{21}H_{22}ClF_7N_3OsP$: C, 35.72%; H, 3.14%; N, 5.95%.

[Os(η^6-bip)(2-Cl-Azpy)I]PF$_6$ (13). [Os(η^6-bip)I_2]$_2$ (30.0 mg, 0.025 mmol) was dissolved in methanol (10 mL) at 353 K and heated under reflux for 1 h. 2-Cl-azpy (10.8mg, 0.050 mmol) in methanol (10 mL) was added drop-wise. The solution was stirred at 353 K for 2 h. The volume was reduced to about 10 mL by removal of methanol on a rotary evaporator, and ammonium hexafluorophosphate (16.3 mg, 0.10 mmol) was added. The solution was then left in the freezer (253 K) for 24 h. Dark coloured crystalline precipitated which was collected by filtration, washed with cold ethanol and diethyl ether, then finally dried *in vacuo*. Yield: 24.5 mg (29.3 %). ESI-MS Calcd for $C_{23}H_{18}ClIN_3Os$: m/z 690.0, found 689.9. ^{1}H NMR($(CD_3)_2CO$): δ 9.46 (d, 1H, J = 3 Hz), 8.99 (d, 1H, J = 9 Hz), 8,40 (d of d, 1H), 7.91 (d, 2H, J = 8 Hz), 7.69 (t, 1H, J = 8 Hz), 7.55-7.47 (m, 3H), 7.44-7.39(m, 4H), 7.13 (d, 1H, J = 6 Hz), 7.09 (t, 1H, J = 6 Hz), 6.89 (t, 1H, J = 6 Hz), 6.82 (d, 1H, J = 6 Hz), 6.72 (t, 1H, J = 6 Hz). CHN analysis: Found: C, 32.92%; H, 2.06%; N, 5.03%. Calcd for $C_{23}H_{18}ClF_6IN_3OsP$: C, 33.21%; H, 2.18%; N, 5.04%.

[Os(η^6-*p*-cym)(2-Cl-Azpy)I]PF$_6$ (14). [Os(η^6-*p*-cym)I_2]$_2$ (50.0 mg, 0.043 mmol) was dissolved in methanol (40 mL) at 313 K. 2-Cl-azpy (18.8 mg, 0.0865 mmol) in methanol (10 mL) was added drop-wise, the solution-colour changed from yellow to red immediately. The solution was stirred at ambient temperature for 3 h. The volume was reduced to about 10 mL by removal of methanol on a rotary evaporator, and ammonium hexafluorophosphate (28.2 mg, 0.173 mmol) was added. The solution was then left in a freezer (253 K) for 24 h. The dark coloured

precipitate was collected by filtration, washed with cold ethanol and diethyl ether, then finally dried *in vacuo*. Yield: 45.7 mg (64.8 %). ESI-MS Calcd for $C_{21}H_{22}ClIN_3Os$: m/z 670.0, found 669.9. ^{1}H NMR($(CD_3)_2CO$): δ 9.71 (s, 1H), 9.05 (d, 1H, J = 9 Hz), 8.45 (d, 1H, J = 6 Hz), 8.16 (d, 2H, J = 6 Hz), 7.83-7.71 (m, 3H), 6.88 (d, 1H, J = 6 Hz), 6.57 (d, 1H, J = 6 Hz), 6.47 (d, 1H, J = 6 Hz), 6.35 (d, 1H, J = 6 Hz), 2.78 (s, 3H), 2.69-2.65 (m, 1H), 1.02 (d, 3H, J = 7 Hz), 0.97 (d, 3H, J = 7 Hz). CHN analysis: Found: C, 30.95%; H, 2.60%; N, 5.12%. Calcd for $C_{21}H_{22}ClF_6IN_3OsP$: C, 30.99%; H, 2.72%; N, 5.16%.

[Os(η^6-bip)(2-Cl-Azpy)Cl]PF_6 (15). [Os(η^6-bip)Cl_2]$_2$ (50.0 mg, 0.060 mmol) was dissolved in methanol (20 mL) at 353 K and heated under reflux and N_2 for 1 h. 2-Cl-azpy (26.1 mg, 0.120 mmol) in methanol (10 mL) was added drop-wise. The solution was stirred at 353 K for 1 h. The volume was reduced to about 10 mL by removal of methanol on a rotary evaporator, and ammonium hexafluorophosphate (39.1 mg, 0.24 mmol) was added. The solution was then left in a freezer (253 K) for 24 h. Dark coloured crystals formed which were collected by filtration, washed with cold ethanol and diethyl ether, then finally dried *in vacuo*. Yield: 41.3 mg (46.3 %). ESI-MS Calcd for $C_{23}H_{18}Cl_2N_3Os$: m/z 598.0, found 598.0. ^{1}H NMR($(CD_3)_2CO$): δ 9.49 (d, 1H, J = 3 Hz), 8.97 (d, 1H, J = 9 Hz), 8,48 (d of d, 1H), 7.92 (d, 2H, J = 8 Hz), 7.70 (t, 1H, J = 8 Hz), 7.61-7.46 (m, 3H), 7.44-7.38(m, 4H), 6.96 (d, 1H, J = 6 Hz), 6.89 (d, 1H, J = 6 Hz), 6.85 (t, 1H, J = 6 Hz), 6.79 (t, 1H, J = 6 Hz), 6.46 (t, 1H, J = 6 Hz). CHN analysis: Found: C, 36.92%; H, 2.32%; N, 5.56%. Calcd for $C_{23}H_{18}Cl_2F_6N_3OsP$: C, 37.20%; H, 2.44%; N, 5.66%.

[Os(η^6-*p*-cym)(2-Cl-Azpy)Cl]PF_6 (16). [Os(η^6-*p*-cym)Cl_2]$_2$ (50.0 mg, 0.063 mmol) was dissolved in methanol (40 mL) at 313 K. 2-Cl-azpy (27.5 mg, 0.126 mmol) in methanol (10 mL) was added drop-wise, the solution-colour changed from yellow to red immediately. The solution was stirred at ambient temperature for 24 h. The volume was reduced to about 10 mL by removal of methanol on a rotary evaporator, and ammonium hexafluorophosphate (41.2 mg, 0.253 mmol)

was added. The solution was then left in a freezer (253 K) for 24 h. Dark coloured crystals formed which were collected by filtration, washed with cold ethanol and diethyl ether, then finally dried *in vacuo*. Yield: 41.2 mg (45.2 %). ESI-MS Calcd for $C_{21}H_{22}Cl_2N_3Os$: m/z 578.1, found 578.0. ^{1}H NMR($(CD_3)_2CO$): δ 9.68 (s, 1H), 9.01 (d, 1H, J = 9 Hz), 8.45 (d of d, 1H), 8.13 (d, 2H, J = 6 Hz), 7.83-7.51 (m, 3H), 6.89 (d, 1H, J = 6 Hz), 6.52 (d, 1H, J = 6 Hz), 6.39-6,34 (m, 2H), 2.80 (s, 3H), 2.54-2.46 (m, 1H), 1.00 (d, 3H, J = 7 Hz), 0.96 (d, 3H, J = 7 Hz). CHN analysis: Found: C, 34.80%; H, 2.98%; N, 5.78%. Calcd for $C_{21}H_{22}Cl_2F_6N_3OsP$: C, 34.91%; H, 3.07% N, 5.82%.

[Os(bip)(2-Br-Azpy)I]PF_6 (17). $[Os(bip)I_2]_2$ (30.0 mg, 0.025 mmol) was dissolved in methanol (30 mL) and water (10 mL), and the solution was heated under reflux (T=353 K) for 1.5 h. 2-Br-azpy (13.1 mg, 0.05 mmol) in methanol (10 mL) was added drop-wise, the solution-colour changed from orange to brown immediately. The solution was stirred and heated under reflux for 1.5 h further. The volume was reduced to about 10 mL by removal of methanol on a rotary evaporator, and ammonium hexafluorophosphate (16.4 mg, 0.2 mmol) was added. The solution was then left in a fridge for 24 h. The dark coloured precipitate was collected by filtration, washed with cold ethanol and diethyl ether, then finally dried *in vacuo*. Yield: 22.5 mg (51.2 %). ESI-MS Calcd for $C_{23}H_{18}BrIN_3Os$: m/z 733.9, found 733.7. ^{1}H NMR($(CD_3)_2CO$): δ 9.50 (d, 1H, J = 2 Hz), 8.91 (d, 1H, J = 9 Hz), 8,52 (d of d, 1H), 7.92 (d, 2H, J = 8 Hz), 7.69 (t, 1H, J = 8 Hz), 7.55-7.44 (m, 2H), 7.43-7.39 (m, 5H), 7.16-7.19 (m, 2H), 6.87 (t, 1H, J = 6 Hz), 6.81 (d, 1H, J = 6 Hz), 6.71 (t, 1H, J = 6 Hz). CHN analysis: Found: C, 31.94%; H, 1.97%; N, 4.74%. Calcd for $C_{23}H_{18}BrF_6IN_3OsP$: C, 31.45%; H, 2.07% N, 4.78%.

[Os(η^6-*p*-cym)(2-Br-Azpy)I]PF_6 (18). $[Os(\eta^6\text{-}p\text{-cym})I_2]_2$ (20.0 mg, 0.017 mmol) was dissolved in methanol (40 mL). 2-Br-Azpy (9.3 mg, 0.035 mmol) in methanol (10 mL) was added drop-wise. The solution colour changed from yellow to dark red immediately, it was stirred at ambient temperature for 16 h. The volume was

reduced to ca 5 mL by removal of methanol on a rotary evaporator and ammonium hexafluorophosphate (11.3 mg, 0.069 mmol) was added. Then the solution was left in a freezer (253 K) for 24 h. A dark coloured solid precipitated, which was filtered off, washed with diethyl ether, dried *in vacuo*. Yield: 16.2 mg (54.7%). Anal. ESI-MS Calcd for $C_{21}H_{22}BrIN_3Os$: m/z 714.0, found 713.9. ^{1}H NMR($(CD_3)_2CO$) δ 9.79 (s, 1H), 8.95 (d, 1H, J = 9 Hz), 8.67 (d, 1H, J = 6 Hz), 8.16 (d, 1H, J = 7 Hz), 7.86-7.78 (m, 3H), 6.93 (d, 1H, J = 6 Hz), 6.57 (d, 1H, J = 6 Hz), 6.39 (m, 2H), 2.56-2.53 (m, 1H), 2.46 (s, 3H), 1.02 (d, 3H, J = 7 Hz), 0.96 (d, 3H, J = 7 Hz). CHN analysis Found: C, 29.98%; H, 2.85%; N, 4.72%, Calcd for $C_{21}H_{22}BrIF_6N_3OsP$: C, 29.38%; H, 2.58%; N, 4.90%.

[Os(bip)(2-Br-Azpy)Cl]PF$_6$ (19). $[Os(bip)Cl_2]_2$ (30.0 mg, 0.036 mmol) was dissolved in methanol (30 mL) and water (10 mL), and the solution was heated under reflux (T=353 K) for 1 h. 2-Br-azpy (18.9 mg, 0.072 mmol) in methanol (10 mL) was added drop-wise, the solution-colour changed from orange to brown immediately. The solution was stirred and heated under reflux for 1 h further. The volume was reduced to about 10 mL by removal of methanol on a rotary evaporator, and ammonium hexafluorophosphate (59.0 mg, 0.36 mmol) was added. The solution was then left in a fridge for 24 h. The dark coloured precipitate was collected by filtration, washed with cold ethanol and diethyl ether, then finally dried *in vacuo*. Yield: 19.2 mg (33.8 %). ESI-MS Calcd for $C_{23}H_{18}BrClN_3Os$: m/z 642.0, found 641.9. ^{1}H NMR($(CD_3)_2CO$): δ 9.54 (d, 1H, J = 2 Hz), 8.88 (d, 1H, J = 9 Hz), 8,61 (d of d, 1H), 7.72 (d, 2H, J = 8 Hz), 7.61 (t, 1H, J = 8 Hz), 7.50-7.44 (m, 2H), 7.43-7.36 (m, 5H), 6.98 (d, 1H, J = 6 Hz), 7.89-7.80 (m, 3H), 6.47 (t, 1H, J = 6 Hz). CHN analysis: Found: C, 34.84%; H, 2.15%; N, 5.29%. Calcd for $C_{23}H_{18}BrClF_6N_3OsP$: C, 35.10%; H, 2.31% N, 5.34%.

[Os(η^6-*p*-cym)(2-Br-Azpy)Cl]PF$_6$ (20). $[Os(\eta^6\text{-}p\text{-cym})Cl_2]_2$ (30.0 mg, 0.038 mmol) was dissolved in methanol (20 mL) ; 2-Br-Azpy (20.0 mg, 0.076 mmol) in methanol (10 mL) was added drop-wise, the solution colour changed from yellow

to dark red immediately. The solution was stirred at ambient temperature for 3 h. The volume was reduced to ca. 5 mL by removal of methanol on a rotary evaporator and ammonium hexafluorophosphate (24.7 mg, 0.15 mmol) was added. Then the solution was left in the freezer (253 K) for 24 h; A dark colour crystalline precipitated which was filtered off and washed with diethyl ether, then dried *in vacuo*. Yield: 39.2 mg (67.3%). Anal. ESI-MS Calcd for $C_{21}H_{22}BrClN_3Os$: m/z 622.0, found 622.1. ^{1}H NMR($(CD_3)_2CO$) δ 9.83 (s, 1H), 9.00 (d, 1H, J = 9 Hz), 8.61 (d, 1H, J = 6 Hz), 8.22 (d, 1H, J = 6 Hz), 7.80-7.78 (m, 3H), 6.94 (d, 1H, J = 6 Hz), 6.63 (d, 1H, J = 6 Hz), 6.41 (d, 1H, J = 6 Hz), 6.39 (d, 1H, J = 6 Hz), 2.80 (s, 3H), 2.67-2.64 (m, 1H), 1.04 (d, 3H, J = 7 Hz), 0.99 (d, 3H, J = 7 Hz). CHN analysis Found: C, 32.85%; H, 2.82%; N, 5.39%, Calcd for $C_{21}H_{22}BrClF_6N_3OsP$: C, 32.89%; H, 2.89%; N, 5.48%.

[Os(η^6-bip)(2-I-Azpy)I]PF$_6$ (21). [Os(η^6-bip)I_2]$_2$ (26.0 mg, 0.022 mmol) was dissolved in methanol (20 mL) and water (5 mL), and the solution was heated under reflux (T=353 K) for 1 h. 2-Br-azpy (13.4 mg, 0.043 mmol) in methanol (5 mL) was added drop-wise, the solution-colour changed from orange to brown immediately. The solution was stirred and heated under reflux for 1 h further. The volume was reduced to about 10 mL by removal of methanol on a rotary evaporator, and ammonium hexafluorophosphate (14.3 mg, 0.088 mmol) was added. The solution was then left in a fridge (253 K) for 24 h. Dark coloured powder precipitated which was collected by filtration, washed with cold ethanol and diethyl ether, then finally dried *in vacuo*. Yield: 19.2 mg (52.0 %). ESI-MS Calcd for $C_{23}H_{18}F_6IN_3Os$: m/z 781.9, found 781.8. ^{1}H NMR($(CD_3)_2CO$): δ 9.54 (d, 1H, J = 2 Hz), 8.74 (d, 1H, J = 9 Hz), 8,64 (d of d, 1H), 7.92 (d, 2H, J = 8 Hz), 7.70 (t, 1H, J = 8 Hz), 7.52-7.46 (m, 3H), 7.44-7.41(m, 4H), 7.15 (d, 1H, J = 6 Hz), 7.09 (d, 1H, J = 6 Hz), 6.83-6.78 (m, 2H), 6.69 (t, 1H, J = 6 Hz). CHN analysis: Found: C, 29.90%; H, 1.87%; N, 4.51%. Calcd for $C_{23}H_{18}F_6I_2N_3OsP$: C, 29.85%; H, 1.96% N, 4.54%.

[Os(η^6-*p*-cym)(2-I-Azpy)I]PF$_6$ (22). [Os(η^6-*p*-cym)I$_2$]$_2$ (25.0 mg, 0.022 mmol) was dissolved in methanol (40 mL) at 313 K. 2-I-Azpy (13.4 mg, 0.043 mmol) in methanol (10 mL) was added drop-wise, the solution-colour changed from orange to blue immediately. The solution was stirred at ambient temperature for 4 h. The volume was reduced to about 10 mL by removal of methanol on a rotary evaporator, and ammonium hexafluorophosphate (14.0 mg, 0.086 mmol) was added. The solution was then left in a freezer (253 K) for 24 h. Dark coloured powder precipitated which was collected by filtration, washed with cold ethanol and diethyl ether, then finally dried *in vacuo*. Yield: 27.4 mg (70.4 %). ESI-MS Calcd for $C_{21}H_{22}F_6IN_3Os$: m/z 762.0, found 761.8. ^{1}H NMR($(CD_3)_2CO$): δ 9.89 (s, 1H), 9.13 (m, 1H), 8.71 (d of d, 1H), 8.18 (m, 2H), 7.82-7.73 (m, 2H), 6.91 (d, 1H, J = 6 Hz), 6.59 (d, 1H, J = 6 Hz), 6.41 (d, 1H, J = 6 Hz), 6.35 (d, 1H, J = 6 Hz), 2.83 (s, 3H), 2.65-2.61 (m, 1H), 1.04 (d, 3H, J = 7 Hz), 0.99 (d, 3H, J = 7 Hz). CHN analysis: Found: C, 27.62%; H, 2.27%; N, 4.64%. Calcd for $C_{21}H_{22}F_6I_2N_3OsP$: C, 27.86%; H, 2.45% N, 4.64%.

[Os(η^6-bip)(3-Cl-Azpy)I]PF$_6$ (23). [Os(η^6-bip)I$_2$]$_2$ (30.0 mg, 0.025 mmol) in methanol (30 mL) and water (10 mL) was heated under refluxed (T=348 K) for 1.5 h. 3-Cl-Azpy (11.2 mg, 0.052 mmol) in methanol (10 mL) was added drop-wise. The solution colour changed from orange to dark red immediately, it was stirred at 348 K for 1.5 h. The volume was reduced to ca. 10 mL by removal of methanol on a rotary evaporator and ammonium hexafluorophosphate (41.0 mg, 0.25 mmol) was added. Then the solution was left in a fridge for 24 h. A dark colour powder precipitated, which was filtered off, washed with cold methanol and diethyl ether, dried *in vacuo*. Yield: 28.4 mg (68.1%). Anal. ESI-MS Calcd for $C_{23}H_{18}ClIN_3Os$: m/z 690.0, found 689.9. ^{1}H NMR($(CD_3)_2CO$) δ 9.41 (d, 1H, J = 6 Hz), 9.14 (d, 1H, J = 2 Hz), 7.96-7.90 (m, 3H), 7.74 (t, 1H, J = 5 Hz), 7.59-7.41 (m, 7H), 7.13 (d, 1H, J = 6 Hz), 7.05 (t, 1H, J = 6 Hz), 6.92-6.85 (m, 2H),

6.74 (t, 1H, J = 6 Hz). CHN analysis Found: C, 33.12%; H 2.18%; N 5.04%, Calcd for $C_{23}H_{18}ClF_6IN_3OsP$: C, 32.89%; H, 2.89%; N, 5.48%.

[Os(η^6-*p*-cym)(3-Cl-Azpy)I]PF$_6$ (24). [Os(η^6-*p*-cym)I$_2$]$_2$ (30.0 mg, 0.026 mmol) was dissolved in methanol (50 mL) . 3-Cl-Azpy (12.5 mg, 0.058 mmol) in methanol (10 mL) was added drop-wise. The solution colour changed from yellow to dark red immediately. It was then stirred at ambient temperature for 5 h. The volume was reduced to ca. 10 mL by removal of methanol on a rotary evaporator and ammonium hexafluorophosphate (41.8 mg, 0.26 mmol) was added. Then the solution was left in a freezer (253 K) for 24 h. Dark coloured crystals formed, which were filtered off, washed with diethyl ether, finally dried *in vacuo*. Yield: 28.4 mg (67.1%). Anal. ESI-MS Calcd for $C_{21}H_{22}ClIN_3Os$: m/z 670.0, found 670.0. ^{1}H NMR((CD$_3$)$_2$CO) δ 9.59 (d, 1H, J = 6 Hz), 9.16 (s, 1H), 8.18 (m, 2H), 7.96 (m, 1H), 7.84 (s, 1H), 7.76 (t, 3H), 6.82 (d, 1H, J = 6 Hz), 6.48-6.45 (m, 2H), 6.36 (d, 1H, J = 6 Hz), 2.73 (s, 3H), 2.66 (m, 1H), 1.05 (d, 3H, J = 7 Hz), 0.99 (d, 3H, J = 7 Hz). CHN analysis Found: C, 30.94%; H, 2.60%; N, 5.12%; Calcd for $C_{21}H_{22}ClF_6IN_3OsP$: C, 30.99%; H, 2.72%; N, 5.16%. Single crystals suitable for X-ray diffraction were obtained by slow evaporation of a methanol solution of complex 10 at 277 K.

[Os(η^6-bip)(3-Cl-Azpy)Cl]PF$_6$ (25). [Os(η^6-bip)Cl$_2$]$_2$ (30.0 mg, 0.036 mmol) in methanol (30 mL) and water (10 mL) was heated under reflux (T=348 K) for 1 h. 3-Cl-Azpy (16.1 mg, 0.073 mmol) in methanol (10 mL) was added drop-wise, the solution colour changed from orange to dark red immediately. The solution was stirred at 348 K for 2 h. The volume was reduced to ca. 10 mL by removal of methanol on a rotary evaporator and ammonium hexafluorophosphate (59.0 mg, 0.36 mmol) was added. Then the solution was left in the fridge for 24 h; A dark coloured powder precipitated, which was filtered off and washed with cold methanol and diethyl ether, then dried *in vacuo*. Yield: 31.0 mg (57.9%). Anal. ESI-MS Calcd for $C_{23}H_{18}Cl_2N_3Os$: m/z 597.6, found 598.0. ^{1}H NMR((CD$_3$)$_2$CO)

δ 9.05 (d, 1H, J = 6 Hz), 8.87 (s, 1H), 7.73 (d, 1H, J = 6 Hz), 7.39 (d, 2H, J = 6 Hz), 7.28 (m, 1H), 7.17 (t, 2H, J = 6 Hz), 7.08-7.02 (m, 5H), 6.49 (d, 1H, J = 6 Hz), 6.46 (d, 1H, J = 6 Hz), 6.33 (t, 1H, J = 6 Hz), 6.18 (t, 1H, J = 6 Hz), 5.86 (t, 1H, J = 6 Hz). CHN analysis Found: C, 37.06%; H, 2.38%; N, 5.58%, Calcd for $C_{23}H_{18}Cl_2F_6N_3OsP$: C, 37.20%; H, 2.44%; N, 5.66%.

[Os(η^6-*p*-cym)(3-Cl-Azpy)Cl]PF$_6$ (26). [Os(η^6-*p*-cym)Cl$_2$]$_2$ (30.0 mg, 0.038 mmol) was dissolved in methanol (20 mL); 3-Cl-Azpy (16.7 mg, 0.077 mmol) in methanol (10 mL) was added drop-wise, the solution colour changed from yellow to dark red immediately. The solution was stirred at ambient temperature for 3 h. The volume was reduced to ca. 5 mL by removal of methanol on a rotary evaporator and ammonium hexafluorophosphate (25.0 mg, 0.15 mmol) was added. Then the solution was left in the freezer (253 K) for 24h; Dark coloured crystals formed which were filtered off and washed with diethyl ether, dried *in vacuo*. Yield: 39.1 mg (71.2%). Anal. ESI-MS Calcd for $C_{21}H_{22}Cl_2N_3Os$ [M] m/z 578.1, found 578.1. ^{1}H NMR((CD$_3$)$_2$CO) δ 9.60 (d, 1H, J = 6 Hz), 9.13 (s, 1H), 8.15 (d, 2H, J = 7 Hz), 8.11 (m, 1H), 7.86-7.79 (m, 3H), 6.84 (d, 1H, J = 6 Hz), 6.46 (d, 1H, J = 6 Hz), 6.38 (s, 2H), 2.56-2.53 (m, 1H), 2.43 (s, 3H), 1.02 (d, 3H, J = 7 Hz), 0.98 (d, 3H, J = 7 Hz). CHN analysis Found: C, 34.80%; H, 2.96%; N, 5.79%, Calcd for $C_{21}H_{22}Cl_2F_6N_3OsP$: C, 34.91%; H, 3.07%; N, 5.82%.

[Os(η^6-bip)(Abpy)I]PF$_6$ (27). [Os(η^6-bip)I$_2$]$_2$ (50.1 mg, 0.0418 mmol) and Abpy (19.5 mg, 0.105 mmol) were dissolved methanol (30 mL) and heated under reflux at 353 K for 3 h. The volume was reduced to ca. 10 mL by removal of methanol on a rotary evaporator. Ammonium hexafluorophosphate (29.3 mg, 0.16 mmol) was added. Then the solution was left in a freezer (253 K) for 24 h. A dark coloured precipitate formed, which was filtered off, washed with cold ethanol and diethyl ether, finally dried *in vacuo*. Yield: 48.2 mg (72.0%). Anal. ESI-MS Calcd for $C_{22}H_{18}IN_4Os$: m/z 657.0, found 656.9. ^{1}H NMR((CD$_3$)$_2$CO) δ 9.44 (d, 1H J = 6 Hz), 9.07 (m, 1H), 8.76 (d, 1H J = 6 Hz), 8.38 (t, 1H, J = 8 Hz), 8.14 (m, 2H),

7.76 (m, 2H), 7.61 (m, 2H), 7.45 (m, 3H). 7.25 (d, 1H, J = 6 Hz), 7.13 (d, 1H, J = 6 Hz), 7.03 (t, 1H, J = 6 Hz), 6.95 (t, 1H, J = 6 Hz), 6.82 (t, 1H, J = 6 Hz). CHN analysis Found: C, 32.59%; H, 2.17%; N, 7.07%, Calcd for $C_{20}H_{22}F_6IN_4OsP$: C, 33.01%; H, 2.27%; N, 7.00%.

[Os(η^6-*p*-cym)(Abpy)I]PF_6 (28). [Os(η^6-*p*-cym) I_2]$_2$ (40.0 mg, 0.035 mmol) was dissolved in 50 mL of methanol at 313 K; Abpy (16.1 mg, 0.087 mmol) in methanol (5 mL) was added drop-wise, the solution colour changed from orange to pink immediately; and was stirred at ambient temperature for 16 h. The volume was reduced to ca. 10 mL by removal of methanol on a rotary evaporator. Ammonium hexafluorophosphate (56.2 mg, 0.35 mmol) was added. Then the solution was left in a freezer (253 K) for 24 h. A dark coloured precipitate formed, which was filtered off, washed with cold ethanol and diethyl ether, then finally dried *in vacuo*. Yield: 35.2 mg (64.5%). Anal. ESI-MS Calcd for $C_{20}H_{22}IN_4Os$: m/z 637.0, found 637.0. H NMR($(CD_3)_2CO$) δ 9.74 (d, 1H, J = 6 Hz), 9.12 (m, 1H), 8.90 (d, 1H, J = 5 Hz), 8.41 (m, 1H), 8.22 (m, 2H), 7.86 (m, 2H), 6.78 (d, 1H, J = 6 Hz), 6.72 (d, 1H, J = 6 Hz), 6.57 (d, 1H, J = 6 Hz), 6.51 (d, 1H, J = 6 Hz), 2.72 (s, 3H), 2.39 (m, 1H), 0.95 (d, 3H, J = 7 Hz), 0.91 (d, 3H, J = 7 Hz). CHN analysis Found: C, 30.91%; H, 2.74%; N, 7.28%, Calcd for $C_{20}H_{22}F_6IN_4OsP$: C, 30.78%; H, 2.84%; N, 7.18%.

[Os(η^6-bip)(Abpy)Cl]PF_6 (29). [Os(η^6-bip)Cl_2]$_2$ (51.0 mg, 0.064 mmol) and Abpy (32.0 mg, 0.17 mmol) were dissolved in methanol (30 mL) and heated under refluxed (T=348 K) for 4 h. The solution colour changed from orange to pink immediately. The volume was reduced to ca. 10 mL by removal of methanol on a rotary evaporator and ammonium hexafluorophosphate (40.0 mg, 0.24 mmol) was added. Then the solution was left in a freezer (253 K) for 24 h. A black crystalline product precipitated, which filtered off and washed with cold methanol and diethyl ether, then dried *in vacuo*. Yield: 56.4 mg (62.6%). Anal. ^{1}H NMR($(CD_3)_2CO$) δ 9.49 (d, 1H, J = 6 Hz), 9.05 (m, 1H), 8.80 (d, 1H, J = 8 Hz),

8.46 (t, 1H, , J = 8 Hz), 8.17 (m, 2H), 7.82 (m, 2H), 7.66 (d, 2H, J = 6 Hz), 7.48 (m, 3H). 7.14 (d, 1H, J = 6 Hz), 6.97 (d, 2H, J = 3 Hz), 6.82 (t, 1H, J = 6 Hz), 6.53 (m, 1H). CHN analysis Found: C, 36.91%; H, 2.42%; N, 8.25%, Calcd for $C_{20}H_{22}ClF_6N_4OsP$: C, 37.27%; H, 2.56%; N, 7.90%.

[Os(η^6-*p*-cym)(Abpy)Cl]PF$_6$ (30). [Os(η^6-*p*-cym)Cl$_2$]$_2$ (35.2 mg, 0.0445 mmol) was dissolved in methanol (25 mL) at RT. Abpy (20.4 mg, 0.11 mmol) in methanol (5 mL) was added drop-wise, the solution colour changed from orange to pink immediately. The solution was stirred at RT for 1 h. The volume was reduced to ca 10 mL by removal of methanol on a rotary evaporator. Ammonium hexafluorophosphate (73.0 mg, 0.45 mmol) was added. Then the solution was left in the freezer (253 K) for 24 h. The dark coloured precipitate was filtered off and washed with cold ethanol and diethyl ether, then finally dried *in vacuo*. Yield: 41.5 mg (67.7%). Anal. ESI-MS Calcd for $C_{20}H_{22}ClN_4Os$: m/z 545.1, found 545.0. ^{1}H NMR((CD$_3$)$_2$CO) δ 9.72 (d, 1H, J = 5 Hz), 9.07 (m, 1H), 8.94 (d, 1H, J = 4 Hz), 8.49 (t, 1H, J = 8 Hz), 8.25 (m, 2H), 7.88 (m, 2H), 6.93 (d, 1H, J = 6 Hz), 6.74 (d, 1H, J = 6 Hz), 6.49 (d, 1H, J = 6 Hz), 6.40 (d, 1H, J = 6 Hz), 2.58 (m, 1H), 2.39 (s, 3H), 0.97 (d, 3H, J = 7 Hz), 0.93 (d, 3H, J = 7 Hz). CHN analysis Found: C, 34.69%; H, 3.08%; N, 8.20%, Calcd for $C_{20}H_{22}ClPN_4OsF_6$: C, 34.86%; H, 3.22%; N, 8.13%.

[Os(η^6-*p*-cym)(OH-Azpy-NO$_2$)I]PF$_6$ (31). [Os(η^6-*p*-cym)I$_2$]$_2$ (23.8 mg, 0.020 mmol) was dissolved in methanol (30 mL) . OH-Azpy-NO$_2$ (10.5mg, 0.043 mmol) in methanol (5 mL) was added drop-wise. The solution was stirred at ambient temperature for 48 h with 7 drops of HCl (1 M). The volume was reduced to ca. 2 mL by removal of methanol on a rotary evaporator. The complex was purified by chromatography on a Sephadex LH20 column. Ammonium hexafluorophosphate (10.0 mg, 0.61 mmol) was added. Then the solution was left in the fridge for 0.5 h. The dark coloured precipitate was filtered off, washed with cold ethanol and diethyl ether, then finally dried *in vacuo*. Yield: 12.7 mg (37.8%). Anal. ESI-MS

Calcd for $C_{21}H_{22}IN_4O_3Os$: m/z 697.0, found 696.9. ^{1}H NMR($(CD_3)_2CO$) δ 9.87 (d, 1H, J = 2 Hz), 9.68 (d, 1H, J = 9 Hz), 9.39 (d, 2H, J = 9 Hz), 9.73 (d, 2H, J = 9 Hz), 8.57 (m, 1H), 7.38 (d, 1H, J = 8 Hz), 7.04 (d, 1H, J = 8 Hz), 6.57 (s, 1H), 4.50 (m, 1H), 3.60 (s, 3H), 0.89 (d, 3H, J = 7 Hz), 0.84 (d, 3H, J = 7 Hz). CHN analysis Found: C, 31.06%; H, 2.83%; N, 6.44%, Calcd for $C_{21}H_{22}F_6IN_4O_3OsP$: C, 30.01%; H, 2.64%; N, 6.67%.

[Os(η^6-*p*-cym)(OH-Azpy-NO_2)Cl]PF_6 (32). [Os(η^6-*p*-cym) Cl_2]$_2$ (31.5 mg, 0.040 mmol) was dissolved in methanol (30 mL). OH-Azpy-NO_2 (19.7 mg, 0.081 mmol) in methanol (10 mL) was added drop-wise, the solution colour changed from yellow to brown immediately. The solution was stirred at ambient temperature for 4 h. The volume was reduced to about 2 mL by removal of methanol on a rotary evaporator. The complex was purified by chromatography on a Sephadex LH20 column. Ammonium hexafluorophosphate (26.2 mg, 0.16 mmol) was added. Then the solution was left in the freezer (253 K) for 1 h. The dark coloured precipitate was filtered off, washed with diethyl ether, and finally dried *in vacuo*. Yield: 25.1 mg (41.8%). Anal. ESI-MS Calcd for $C_{21}H_{22}ClN_4O_3Os$: 605.1, found 605.1. ^{1}H NMR($(CD_3)_2CO$) δ 9.06 (d, 1H, J = 2 Hz), 8.79 (d, 1H, J = 9 Hz), 8.56 (d, 2H, J = 9 Hz), 8.33 (d, 2H, J = 9 Hz), 7.80 (d, 1H, J = 8 Hz), 6.74 (d, 1H, J = 8 Hz), 6.36 (d, 2H, J = 8 Hz), 6.22 (d, 1H, J = 8 Hz), 2.57-2.52 (m, 1H), 2.47 (s, 3H), 1.02 (d, 3H, J = 7 Hz), 0.98 (d, 3H, J = 7 Hz). CHN analysis Found: C, 34.35%; H, 2.95%; N, 7.35%, Calcd for $C_{21}H_{22}ClF_6N_4O_3OsP$: C, 33.67%; H, 2.96%; N, 7.48%.

4.2.3 Determination of IC_{50} Values

The concentrations of the osmium complexes that inhibit 50% of the proliferation of human ovarian A2780 cancer cells were determined using the sulforhodamine B assay.[18] A2780 cells were seeded in 96-well plate (Falcon) at 5000 cells/well, after the incubation for 48 h. The complexes were solubilised in DMSO (Sigma)

to provide 10 mM stock solutions. These were serially diluted by cell culture media to give concentrations four-fold greater than the final concentrations for the assay. The complexes diluted in cell culture media were added to the 96-well plate with cells in triplicate. The final DMSO concentration in each well was no more than 1% (v/v). The media containing the complexes were removed after 24 h. The cells were washed with phosphate buffered saline once and cell culture medium was added (150 µL/well). The cells were then allowed to grow for a further 72 h. The surviving cells were fixed by adding 150 µL/well of 50% (w/v) trichloroacetic acid and incubated for 1 h in a refrigerator (277 K). The plates were washed with tap water three times and dried under a flow of warm air, 0.4% sulforhodamine B (Sigma) solution (100 µL/well) was added, followed by washing with 1% acetic acid five times and drying under a flow of warm air. The dye was dissolved in 10 mM Tris buffer (200 µL/well). The absorbance of each well was determined using a Multiskan Ascent plate reader (Labsystems) at 540 nm. The absorbance of SRB in each well is directly proportional to the cell number. Then the absorbance was plotted against concentration and the IC_{50} determined by using Origin software.

4.2.4 NAC or L-BSO Combination Treatments

A2780 cells were treated with 50 µM NAC or L-BSO and various concentrations of osmium complexes for 24 h. Then NAC/L-BSO and osmium complexes were removed at the same time and cells washed with PBS once, then incubated for a further 72 h for recovery. Cell viability was determined using the SRB assay as described above.

4.2.5 Cellular Uptake

A2780 cells were seeded 10^6 cells/well in 6-well plates. After 24 h incubation, cells were exposed to 4 μM osmium complex. After 1 h, 2 h, 4 h and 24 h of drug exposure, the drug-containing medium was removed. Then samples were washed with PBS twice, trypsinized, collected and stored at 253 K until ICP-MS analysis for osmium content. The numbers of cells were counted using a cytometer. The whole cell pellets were digested as described below. Firstly, 0.5 mL of freshly distilled 72% HNO_3 was added to each 1 mL cells pellets, and the samples were transferred into Wheaton V-Vials The vials were heated in an oven at 373 K for 16 h to digest the samples fully, allowed to cool, and then transferred to Falcon tubes. The vials were washed with double deionized water three times and diluted 10 times with double deionized water to obtain 6% HNO_3 sample solutions. A blank and the standards were loaded into the sample tray and were run from the lowest to the highest concentration in a 'no gas' mode, followed by the samples.

4.2.6 Separation of Cell Fractions

The A2780 cells were seeded into Petri dishes at a concentration of 5×10^6 cells/dish. After 24 h incubation, osmium compounds **9** (4 μM) and **23** (4 μM) were added. The cells were harvested after a further incubation with osmium compound for 24 h. Then the four cell fractions (cytosol, membrane plus particulate fraction, nucleus and cytoskeleton) were separated following the protocol described for the kit (BioVision, Inc, USA). The concentrations of osmium in different fractions were measured by ICP-MS after digestion following the same method as for the cellular uptake study. The ICP-MS analysis was helped by Aida Basri.

4.2.7 Detection of ROS

The vial of DCFH-DA was opened under N_2 protection, and contents dissolved in DMSO to give a 10 mM stock solution . A2780 cells were seeded (5000 cells/well) into black 96-well plates and incubated for 24 h at 310 K, 5% CO_2, high humidity.

Cells were loaded with DCFH-DA (10 μM) and incubated for 30 min. The probe was removed and PBS was used to wash the cells twice. The cells were then kept in PBS solution and osmium compound **9** (4 μM), or NAC (50 μM) with **9** (4 μM)**,** or L-BSO (50 μM) with **9** (4 μM) were added. Hydrogen peroxide (50 μM) was added as the positive control. The fluorescence was recorded over a period of 4 h at 310 K by excitation at 480 nm and emission at 530 nm on a TECAN plate reader.

4.2.8 Tubulin Polymerization Assay

A cytoskeleton tubulin polymerization assay kit (catalog no BK004) was used in the tubulin polymerization study. Briefly, 10 μL of general tubulin buffer (80 mM PIPES, pH 6.9, 2 mM $MgCl_2$ and 0.5 mM EGTA) containing osmium compound **9**, colchicine or taxol was pipetted into the prewarmed 96 well microplate. Tubulin (defrosted to room temperature from -80 °C and then placed on ice before use) was diluted with tubulin polymerization buffer with 1 mM GTP to a final concentration of 4 mg mL^{-1}. Diluted tubulin (100 μL) was added into the wells containing osmium compound **9**, colchicine or taxol. Diluted tubulin (100 μL) mixed with general tubulin buffer (10 μL) served as control. The absorbance at 340 nm was read immediately with a Tecan microplate reader.

4.2.9 Cell Cycle Analysis

A2780 cells were incubated with osmium compounds **9** or **23** at various concentrations for 24 h and then harvested. Detached and adherent cells were washed with PBS and fixed in 70% ethanol. The fixed cells were centrifuged and washed once with PBS, followed by resuspension in PBS–EDTA containing 7.5 μM propidium iodide (PI) and 10 μg/ml RNase A. After the cells had stood at room temperature for 30 min, they were analyzed by flow cytometry with

CellQuest Pro Software (Beckton Dickenson, USA). The cell cycle distribution was evaluated using the Flowjo 7.6 (Beckton Dickenson, USA).

4.2.10 Immunofluorescence by Confocal Microscopy

A2780 Cells were seeded on Lab-TekTM Chamber Slides (Thermo Scientific Nunc) 10,000 cells/chamber, after 24 h incubation, osmium compound **9** at different concentrations were added and incubate for another 24 h. Cells were fixed with 4% formaldehyde in PBS (20 min, 310 K), then rinsed with PBS (3 × 2 mL×2 min) and permeabilized with 0.1% Triton X-100 solution (PBS solution) for 15 min at ambient temperature. The cells were blocked with blocking buffer (2 mg/ mL BSA, overnight at 269 K), and then, the cell monolayers were incubated (1 h, 310 K) with monoclonal anti-α-tubulin-Alexa 488 (4 μg/mL) (Invitrogen Molecular Probles, Catalog No. 32-2588) with PI (7.5 μM). After the incubation, the cells were washed with PBS and the immunofluorescence was detected using a Leica SP5 fluorescence confocal microscope, with 100× objective.

4.3 Results

In the previous chapter, the synthesis and cancer cell cytotoxicity of twelve osmium(II) azopyridine complexes containing various substituents on the phenyl ring were reported.[6] The least active compounds in this class contained unsubstituted one phenyl ring in the chelating ligand.[6] In this chapter, an investigation of whether the latter complexes can be activated by introducing substituents (R) into the pyridine ring in the class $[Os(\eta^6\text{-}p\text{-cym})(R\text{-Azpy})X]PF_6$ was carried out. The effect of changing the arene ligand (from *p*-cymene to biphenyl) and the monodentate ligand (X) from Cl to I was also studied. The exploration of such a family of bioisosteres may allow optimisation of properties and allow discovery of candidates (‘hits’) suitable for preclinical development.

In total, 32 novel complexes with nine types of azopyridine chelating ligands were synthesized in good yields, with PF_6^- as the counter anion, and characterized by elemental analysis, ESI-MS and NMR spectroscopy (Chart 4.1). For ten complexes, X-ray crystal structures were determined.

Chart 4.1. Osmium azopyridine arene complexes studied in this chapter.

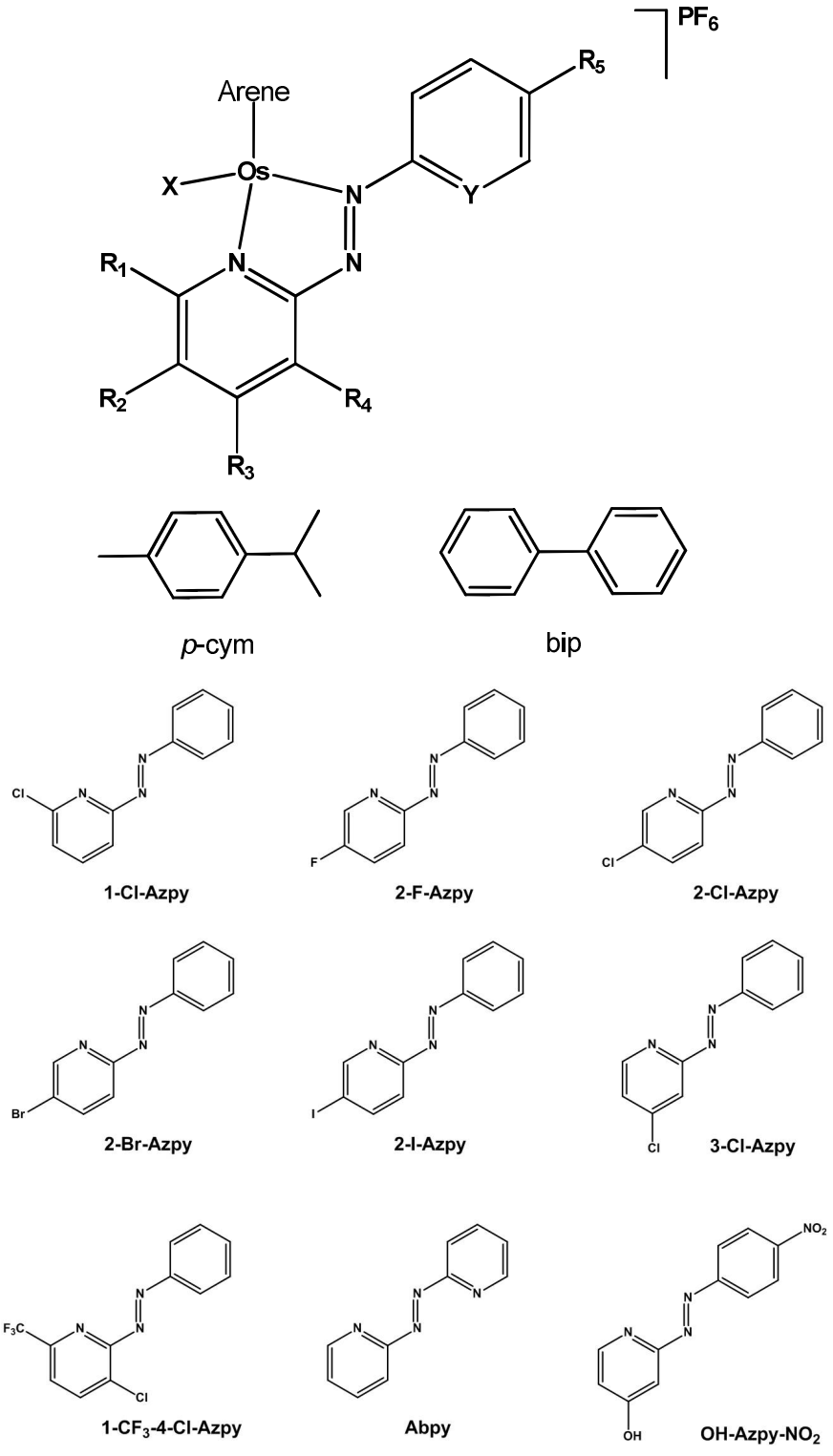

Complex	Arene	R_1	R_2	R_3	R_4	R_5	X	Y
1	bip	CF_3	H	H	Cl	H	I	C
2	*p*-cym	CF_3	H	H	Cl	H	I	C
3	bip	CF_3	H	H	Cl	H	Cl	C
4	*p*-cym	CF_3	H	H	Cl	H	Cl	C
5	bip	Cl	H	H	H	H	I	C
6	*p*-cym	Cl	H	H	H	H	I	C
7*	bip	Cl	H	H	H	H	Cl	C
8	*p*-cym	Cl	H	H	H	H	Cl	C
9	bip	H	F	H	H	H	I	C
10*	bip	H	F	H	H	H	Cl	C
11	*p*-cym	H	F	H	H	H	I	C
12	*p*-cym	H	F	H	H	H	Cl	C
13*	bip	H	Cl	H	H	H	I	C
14*	*p*-cym	H	Cl	H	H	H	I	C
15	bip	H	Cl	H	H	H	Cl	C
16*	*p*-cym	H	Cl	H	H	H	Cl	C
17	bip	H	Br	H	H	H	I	C
18*	*p*-cym	H	Br	H	H	H	I	C
19*	bip	H	Br	H	H	H	Cl	C
20*	*p*-cym	H	Br	H	H	H	Cl	C
21	bip	H	I	H	H	H	I	C
22	*p*-cym	H	I	H	H	H	I	C
23	bip	H	H	Cl	H	H	I	C
24*	*p*-cym	H	H	Cl	H	H	I	C
25	bip	H	H	Cl	H	H	Cl	C
26*	*p*-cym	H	H	Cl	H	H	Cl	C
27	bip	H	H	H	H	H	I	N
28	*p*-cym	H	H	H	H	H	I	N
29	bip	H	H	H	H	H	Cl	N
30	*p*-cym	H	H	H	H	H	Cl	N
31	*p*-cym	H	H	OH	H	NO_2	I	C
32	*p*-cym	H	H	OH	H	NO_2	Cl	C

* X-ray structure determined

4.3.1 X-ray Crystal Structures

Eighteen novel iodido osmium complexes were synthesized and the structures of [Os(η^6-bip)(2-Cl-Azpy)I]PF_6 (**13**), [Os(η^6-*p*-cym)(2-Cl-Azpy)I]PF_6 (**14**), [Os(η^6-*p*-cym)(2-Br-Azpy)I]PF_6 (**18**) and [Os(η^6-*p*-cym)(3-Cl-Azpy)I]PF_6 (**24**) were determined by X-ray crystallography. For comparison, fourteen chlorido analogues were synthesized and the structures of the complexes [Os(η^6-bip)(1-Cl-Azpy)Cl]PF_6 (**7**), [Os(η^6-bip)(2-F-Azpy)Cl]PF_6 (**10**), [Os(η^6-*p*-cym)(2-Cl-Azpy)Cl]PF_6 **(16)**, [Os(η^6-bip)(2-Br-Azpy)Cl]PF_6 (**19**), [Os(η^6-*p*-cym)(2-Br-Azpy)Cl]PF_6 (**20**) and [Os(η^6-*p*-cym)(3-Cl-Azpy)Cl]PF_6 (**26**) were also determined by X-ray crystallography (Fig 4.1, Tables 4.1 and 4.2). All the X-ray crystal structures adopt the familiar half-sandwich 'piano-stool' geometry.

Figure 4.1. X-ray crystal structures of the cations of [Os(η^6-bip)(1-Cl-Azpy)Cl]PF_6 (**7**) [Os(η^6-bip)(2-F-Azpy)Cl]PF_6 (**10**), [Os(η^6-bip)(2-Cl-Azpy)I]PF_6 (**13**), [Os(η^6-*p*-cym)(2-Cl-Azpy)I]PF_6 (**14**), [Os(η^6-*p*-cym)(2-Cl-Azpy)Cl]PF_6 (**16**), [Os(η^6-*p*-cym)(2-Br-Azpy)I]PF_6 (**18**), [Os(η^6-bip)(2-Br-Azpy)Cl]PF_6 (**19**), [Os(η^6-*p*-cym)(2-Br-Azpy)Cl]PF_6 (**20**), [Os(η^6-*p*-cym)(3-Cl-Azpy)I]PF_6 (**24**) and [Os(η^6-*p*-cym)(3-Cl-Azpy)Cl]PF_6 (**26**) with thermal ellipsoids drawn at 50% probability. The hydrogen atoms, counterions (PF_6^-) and solvent water molecules have been omitted for clarity.

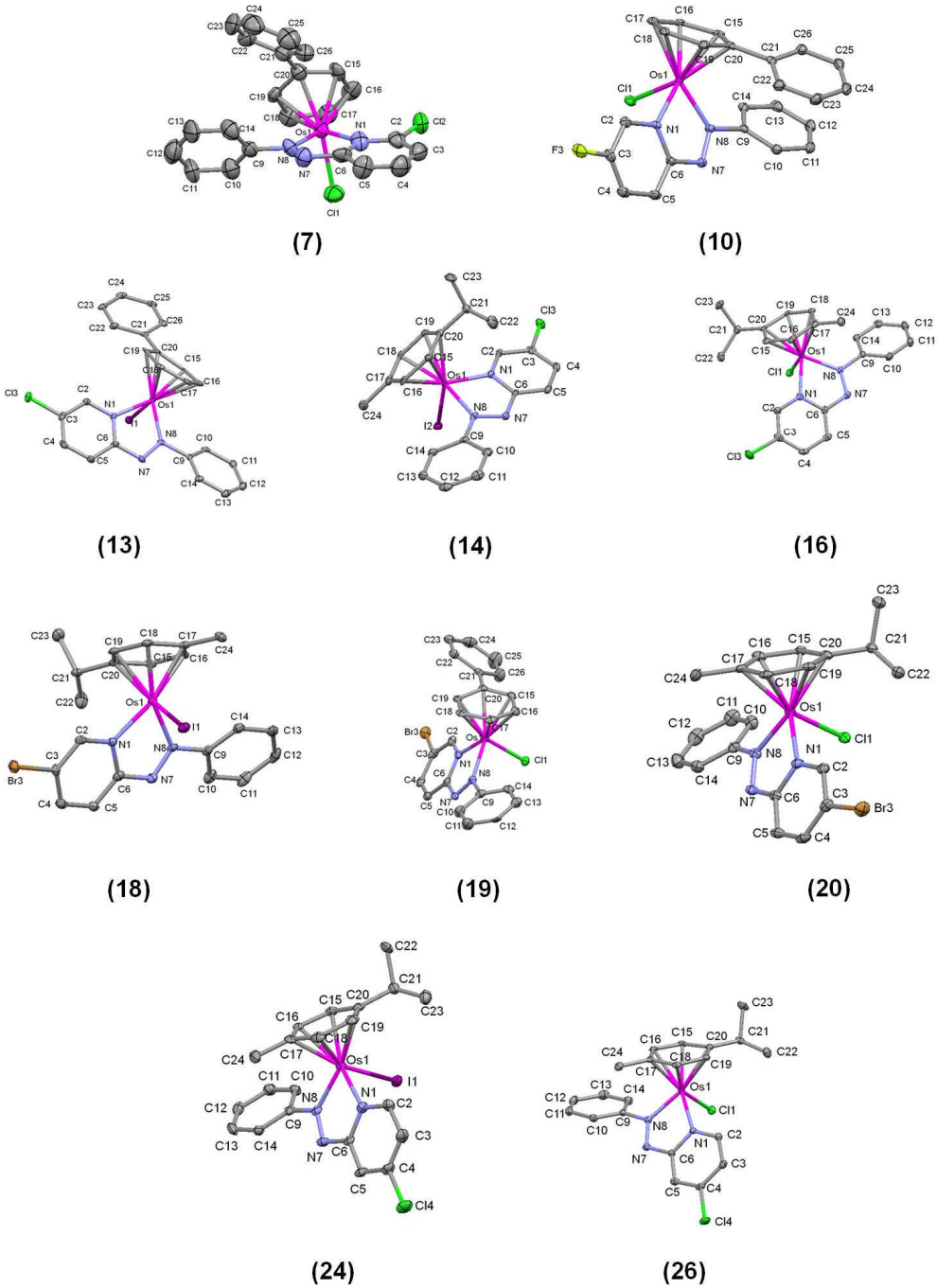

Table 4.1

(A) X-ray crystallographic data for compounds **7**, **10**, **13** and **14**.

	7	**10**	**13**	**14**
Formula	$C_{23}H_{18}Cl_2F_6N_3OsP$	$C_{23}H_{18}ClF_7N_3OsP$	$C_{23}H_{18}ClF_6IN_3OsP$	$C_{21}H_{22}ClF_6IN_3OsP$
Molar mass	742.47	726.02	833.92	813.94
Crystal system	Monoclinic	Triclinic	Monoclinic	Triclinic
Crystal size /mm	0.35 x 0.25 x 0.08	0.40 x 0.16 x 0.16	0.25 x 0.10 x 0.10	0.50 x 0.40 x 0.08
Space group	P2(1)/c	P-1	P2(1)/n	P-1
Crystal	black block	brown block	black block	purple block
a / Å	7.6240(5)	7.4624(2)	6.9574(2)	7.6626(5)
b / Å	28.9718(19)	10.8856(4)	16.7829(6)	11.9693(8)
c / Å	11.0421(14)	14.5449(5	20.7297(7	13.6120(6)
α / deg	90	81.182(3)	90	99.966(5)
β / deg	94.240(8)	84.223(2)	93.182(3)	102.906(5)
γ / deg	90	82.970(3)	90	91.374(5)
T / K	298(2)	100(2)	100(2)	100(2)
Z	4	2	4	2
R [F > 4σ (F)][a]	0.0654	0.0249	0.023	0.0323
R_w[b]	0.1996	0.0569	0.0484	0.0779
GOF[c]	1.044	0.998	1.008	1.018
Δρ max and min/ eÅ^{-3}	3.453 and -4.967	1.152 and -1.411	0.718 and -0.747	1.683 and -1.828

[a] $R = \Sigma||Fo| - |Fc||/\Sigma|Fo|$. [b] $R_w = [\Sigma w(Fo^2 - Fc^2)^2/\Sigma wFo^2)]^{1/2}$. [c] GOF = $[\Sigma w(Fo^2 - Fc^2)^2/(n-p)]^{1/2}$. Where n = number of reflections and p = number of parameters.

(B) X-ray crystallographic data for compounds **16**, **18** and **19**.

	16	**18**	**19**
Formula	$C_{21}H_{22}Cl_2F_6N_3OsP$	$C_{21}H_{22}BrF_6IN_3OsP$	$C_{23}H_{18}BrClF_6N_3OsP$
Molar mass	722.49	858.4	786.93
Crystal system	Triclinic	Triclinic	Triclinic
Crystal size /mm	0.22 x 0.18 x 0.16	0.20 x 0.14 x 0.12	0.40 x 0.18 x 0.05
Space group	P-1	P-1	P-1
Crystal	green block	black block	brown block
a / Å	9.1784(2)	7.8035(3)	8.8866(5)
b / Å	10.6711(3)	11.9630(5)	10.0428(4)
c / Å	12.2921(4)	13.6394(6)	14.1695(7
α / deg	93.579(2)	100.216(4)	103.452(4)
β / deg	93.460(2)	102.863(4)	94.374(4)
γ / deg	96.430(2)	90.779(3)	100.802(4)
T / K	100(2)	100(2)	100(2)
Z	2	2	2
R [F > 4σ (F)][a]	0.0214	0.0264	0.0257
R_w[b]	0.0424	0.0608	0.0567
GOF[c]	0.977	1.034	0.99
Δρ max and min/ eÅ^{-3}	0.800 and -0.759	2.450 and -0.866	1.113 and -1.144

[a] $R = \Sigma||Fo| - |Fc||/\Sigma|Fo|$. [b] $R_w = [\Sigma w(Fo^2 - Fc^2)^2/\Sigma wFo^2)]^{1/2}$. [c] GOF = $[\Sigma w(Fo^2 - Fc^2)^2/(n-p)]^{1/2}$. Where n = number of reflections and p = number of parameters.

(C) X-ray crystallographic data for compounds **20**, **24** and **25**

	20	**24**	**26**
Formula	$C_{21}H_{22}BrClF_6N_3OsP$	$C_{22}H_{27}ClF_6IN_3O_{1.50}Os$	$C_{21}H_{22}Cl_2F_6N_3OsP$
Molar mass	766.95	854.99	722.49
Crystal system	Monoclinic	Orthorhombic	Triclinic
Crystal size /mm	0.30 x 0.10 x 0.05	0.32 x 0.32 x 0.18	0.20 x 0.12 x 0.05
Space group	P2(1)/n	Pbca	P-1
Crystal	black block	black block	black block
a / Å	16.6936(5)	19.4975(4)	7.2224(2)
b / Å	9.0505(3)	14.2729(3)	10.6661(4)
c / Å	16.9583(5)	20.3022(3)	15.8327(6)
α / deg	90	90	79.383(3)
β / deg	107.970(3)	90	78.400(3)
γ / deg	90	90	85.931(3)
T / K	100(2)	173(2)	100(2)
Z	2	2	2
R [F > 4σ (F)][a]	0.0292	0.0324	0.0221
R_w[b]	0.0524	0.073	0.045
GOF[c]	0.926	0.921	0.984
Δρ max and min/ eÅ^{-3}	2.010 and -1.610	1.734 and -1.466	1.287 and -0.795

[a] $R = \Sigma||Fo| - |Fc||/\Sigma|Fo|$. [b] $R_w = [\Sigma w(Fo^2 - Fc^2)^2/\Sigma wFo^2)]^{1/2}$. [c] GOF = $[\Sigma w(Fo^2 – Fc^2)^2/(n-p)]^{1/2}$. Where n = number of reflections and p = number of parameters.

Table 4.2. Selected bond lengths (Å) and angles (°). (A) Iodido complexes [Os(η^6-bip)(2-Cl-Azpy)I]PF_6 (**13**), [Os(η^6-*p*-cym)(2-Cl-Azpy)I]PF_6 (**14**), [Os(η^6-*p*-cym)(2-Br-Azpy)I]PF_6 (**18**) and [Os(η^6-*p*-cym)(3-Cl-Azpy)I]PF_6 (**24**). (B) Chlorido complexes [Os(η^6-bip)(1-Cl-Azpy)Cl]PF_6 (**7**), [Os(η^6-bip)(2-F-Azpy)Cl]PF_6 (**10**), [Os(η^6-*p*-cym)(2-Cl-Azpy)Cl]PF_6 **(16)**, [Os(η^6-bip)(2-Br-Azpy)Cl]PF_6 (**19**), [Os(η^6-*p*-cym)(2-Br-Azpy)Cl]PF_6 (**20**) and [Os(η^6-*p*-cym)(3-Cl-Azpy)Cl]PF_6 (**26**).

(A) Iodido complexes

bond length/angle	**13**	**14**	**18**	**24**
Os(1)-N(8)	2.006(3)	2.033(4)	2.033(3)	2.009(3)
Os(1)-N(1)	2.057(3)	2.065(4)	2.051(3)	2.053(3)
Os(1)-C(15)	2.219(3)	2.213(5)	2.210(4)	2.228(4)
Os(1)-C(19)	2.261(3)	2.230(5)	2.220(4)	2.245(4)
Os(1)-C(18)	2.172(3)	2.240(5)	2.245(4)	2.190(4)
Os(1)-C(16)	2.221(3)	2.239(5)	2.243(4)	2.226(4)
Os(1)-C(20)	2.313(3)	2.219(5)	2.216(4)	2.284(4)
Os(1)-C(17)	2.203(3)	2.260(5)	2.268(4)	2.247(4)
Os(1)-I(1)	2.7063(2)	2.7002(4)	2.7056(3)	2.7007(3)
N(7)-N(8)	1.293(4)	1.296(5)	1.290(5)	1.284(4)
N(8)-Os(1)-N(1)	74.94(10)	75.47(16)	75.15(13)	74.41(13)
N1-Os-I	84.72(7)	84.98(11)	84.91(9)	82.36(9)
I-Os-N8	87.31(7)	88.76(11)	89.49(9)	87.76(9)

Table 4.2. Selected bond lengths (Å) and angles (°). (A) Iodido complexes [Os(η^6-bip)(2-Cl-Azpy)I]PF_6 (**13**), [Os(η^6-*p*-cym)(2-Cl-Azpy)I]PF_6 (**14**), [Os(η^6-*p*-cym)(2-Br-Azpy)I]PF_6 (**18**) and [Os(η^6-*p*-cym)(3-Cl-Azpy)I]PF_6 (**24**). (B) Chlorido complexes [Os(η^6-bip)(1-Cl-Azpy)Cl]PF_6 (**7**), [Os(η^6-bip)(2-F-Azpy)Cl]PF_6 (**10**), [Os(η^6-*p*-cym)(2-Cl-Azpy)Cl]PF_6 **(16)**, [Os(η^6-bip)(2-Br-Azpy)Cl]PF_6 (**19**), [Os(η^6-*p*-cym)(2-Br-Azpy)Cl]PF_6 (**20**) and [Os(η^6-*p*-cym)(3-Cl-Azpy)Cl]PF_6 (**26**).

(B) Chlorido complexes

bond length/angle	**7**	**10**	**16**	**19**	**20**	**26**
Os(1)-N(8)	2.007(7)	2.023(3)	2.012(2)	2.039(3)	2.024(2)	2.0067(17)
Os(1)-N(1)	2.124(9)	2.053(3)	2.059(2)	2.055(3)	2.047(2)	2.0638(18)
Os(1)-C(15)	2.173(10)	2.233(3)	2.227(3)	2.242(4)	2.238(3)	2.246(2)
Os(1)-C(19)	2.227(9)	2.233(3)	2.218(3)	2.181(4)	2.208(3)	2.217(2)
Os(1)-C(18)	2.225(12)	2.239(3)	2.227(3)	2.204(4)	2.228(3)	2.221(2)
Os(1)-C(16)	2.255(10)	2.212(3)	2.173(3)	2.215(4)	2.187(3)	2.177(2)
Os(1)-C(20)	2.230(10)	2.233(3)	2.263(3)	2.278(4)	2.259(3)	2.286(2)
Os(1)-C(17)	2.257(11)	2.242(4)	2.226(3)	2.215(4)	2.238(3)	2.231(2)
Os(1)-Cl(1)	2.387(3)	2.3727(8)	2.3954(6)	2.3896(9)	2.3880(7)	2.3915(5)
N(7)-N(8)	1.276(11)	1.287(4)	1.295(3)	1.283(5)	1.295(3)	1.292(2)
N(8)-Os(1)-N(1)	73.8(3)	74.52(11)	74.96(9)	74.32(13)	74.88(10)	74.68(7)
N1-Os-Cl	83.5(3)	82.24(8)	84.88(6)	84.69(9)	85.11(7)	84.45(5)
Cl-Os-N8	89.6(2)	88.36(8)	87.82(6)	88.86(9)	86.44(7)	89.63(5)

4.3.2 Stability and Hydrolysis

The hydrolysis (aquation) of two azopyridine complexes were investigated since this is a potential mechanism for activation of halido osmium arene complexes in their interactions with biological targets such as DNA.[19] The aqueous behaviour of the highly active complex **9** [Os(η^6-bip)(2-F-Azpy)I]PF_6 and moderately active complex **23** [Os(η^6-bip)(3-Cl-Azpy)I]PF_6 was studied at 310 K. The UV-Vis spectra, showed no change after 24 h, (Fig 4.2) indicating that complexes **9** and **23** remained stable and did not hydrolyze over that period, similar to the highly active azopyridine complexes containing unsubstituted pyridine rings that studied in the previous chapter.[6]

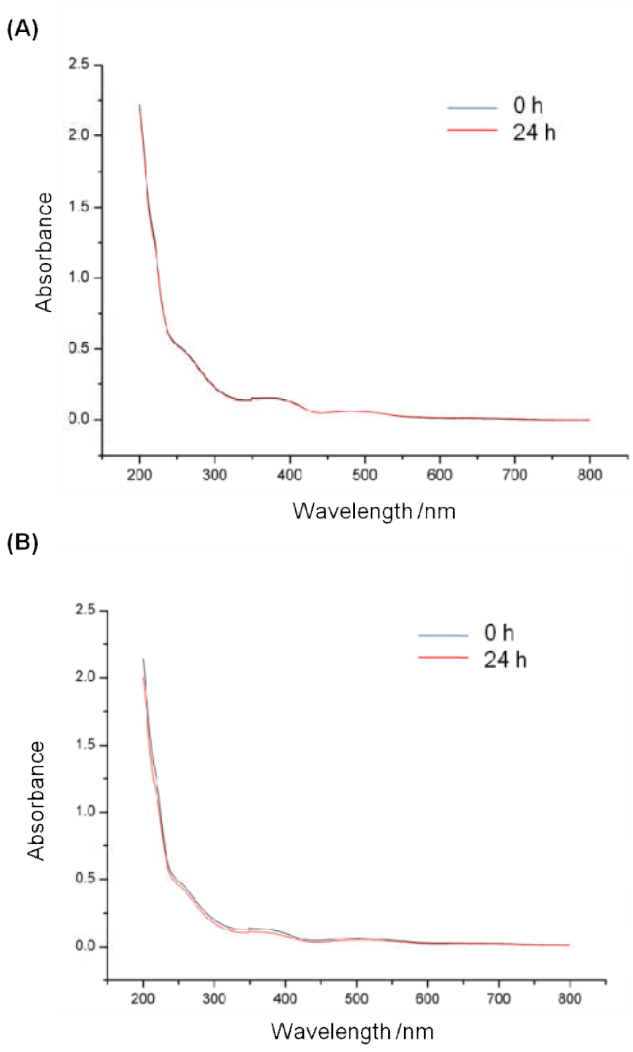

Figure 4.2. UV-Vis spectra for complexes **9** (A) and **23** (B) before and after incubation for 24 h at 310 K in a solution of methanol/ water (5:95 v/v).

4.3.3 Structure-Activity Relationships Based on Bioisosteres

The effect of F, Cl, Br, I and CF_3 substituents in the R_1-R_4 positions of the pyridine ring of the azopyridine chelating ligand (Chart 4.1) on the cytotoxicity of the complexes towards human ovarian A2780 cancer cells was investigated (Table 4.3 A).

Their potency covers a wide range of concentrations, from very high potency with an IC_{50} of 220 nM for complex **21**, $[Os(\eta^6\text{-bip})(2\text{-I-Azpy})I]PF_6$, to >100 μM and inactivity for complexes **10**, **25**, **26** and **30** (Table 4.3). The following trends are observed:

(1) Complexes containing iodide as the monodentate ligand have a higher activity compared to the chlorido complexes (Table 4.3 B).

(2) Biphenyl complexes are, in general, 10 times more active than *p*-cymene complexes (Table 4.3 C).

(3) The effect of chloride as an electron-withdrawing group on the pyridine ring depends on its position. Within the most active series, which contain biphenyl as the arene and iodide as the monodentate ligand, anticancer activity decreases with pyridine ring substitution position in the order $R_2 > R_1 > R_3$, with $[Os(\eta^6\text{-bip})(2\text{-Cl-Azpy})I]PF_6$ (**13**) being the most active, (IC_{50}= 1 μM) (Fig. 4.3 A).

(4) Changing the electron-withdrawing group at the R_2 position leads to increases in activity in the order $Cl < Br \leq F < I$ (Fig. 4.3 B).

(5) Changing the phenyl ring in the azopyridine chelating ligand to pyridine, does not improve the anticancer activity (Table 4.3). Also it is notable that that the osmium(II) chlorido and iodido complexes with 5-hydroxy-2-(4-nitrophenylazo)pyridine as the chelating ligand showed similar activity (Table 4.3 A).

Table 4.3. (A) IC_{50} values for A2780 cells for complexes **1-32**. **(B)** Comparison of IC_{50} values for A2780 cells for monodentate ligand = Cl or I. **(C)** Comparison of IC_{50} values for A2780 cells for arene - *p*-cym or bip.

(A)

Complex	IC_{50} (μM)
(**1**) $[Os(\eta^6\text{-bip})(1\text{-}CF_3\text{-}4\text{-Cl-Azpy})I]PF_6$	5.7(±1.0)
(**2**) $[Os(\eta^6\text{-}p\text{-cym})(1\text{-}CF_3\text{-}4\text{-Cl-Azpy})I]PF_6$	10.9(±0.3)
(**3**) $[Os(\eta^6\text{-bip})(1\text{-}CF_3\text{-}4\text{-Cl-Azpy})Cl]PF_6$	25.2(±0.1)
(**4**) $[Os(\eta^6\text{-}p\text{-cym})(1\text{-}CF_3\text{-}4\text{-Cl-Azpy})Cl]PF_6$	38.2(±2.8)
(**5**) $[Os(\eta^6\text{-bip})(1\text{-Cl-Azpy})I]PF_6$	3.7(±0.3)
(**6**) $[Os(\eta^6\text{-}p\text{-cym})(1\text{-Cl-Azpy})I]PF_6$	9.0(±4.5)
(**7**) $[Os(\eta^6\text{-bip})(1\text{-Cl-Azpy})Cl]PF_6$	42.9(±5.4)
(**8**) $[Os(\eta^6\text{-}p\text{-cym})(1\text{-Cl-Azpy})Cl]PF_6$	24.0(±0.1)
(**9**) $[Os(\eta^6\text{-bip})(2\text{-F-Azpy})I]PF_6$	0.63(±0.1)
(**10**) $[Os(\eta^6\text{-bip})(2\text{-F-Azpy})Cl]PF_6$	>100
(**11**) $[Os(\eta^6\text{-}p\text{-cym})(2\text{-F-Azpy})I]PF_6$	6.0(±0.4)
(**12**) $[Os(\eta^6\text{-}p\text{-cym})(2\text{-F-Azpy})Cl]PF_6$	13.3(±0.7)
(**13**) $[Os(\eta^6\text{-bip})(2\text{-Cl-Azpy})I]PF_6$	1.0(±0.1)
(**14**) $[Os(\eta^6\text{-}p\text{-cym})(2\text{-Cl-Azpy})I]PF_6$	33.6(±2.0)
(**15**) $[Os(\eta^6\text{-bip})(2\text{-Cl-Azpy})Cl]PF_6$	>50
(**16**) $[Os(\eta^6\text{-}p\text{-cym})(2\text{-Cl-Azpy})Cl]PF_6$	30.2(±12.4)
(**17**) $[Os(\eta^6\text{-bip})(2\text{-Br-Azpy})I]PF_6$	0.59(±0.02)
(**18**) $[Os(\eta^6\text{-}p\text{-cym})(2\text{-Br-Azpy})I]PF_6$	36.6(±0.9)
(**19**) $[Os(\eta^6\text{-bip})(2\text{-Br-Azpy})Cl]PF_6$	>50
(**20**) $[Os(\eta^6\text{-}p\text{-cym})(2\text{-Br-Azpy})Cl]PF_6$	>50
(**21**) $[Os(\eta^6\text{-bip})(2\text{-I-Azpy})I]PF_6$	0.22(±0.02)
(**22**) $[Os(\eta^6\text{-}p\text{-cym})(2\text{-I-Azpy})I]PF_6$	2.4(±0.5)
(**23**) $[Os(\eta^6\text{-bip})(3\text{-Cl-Azpy})I]PF_6$	22.0(±2.0)
(**24**) $[Os(\eta^6\text{-}p\text{-cym})(3\text{-Cl-Azpy})I]PF_6$	48.4(±6.1)
(**25**) $[Os(\eta^6\text{-bip})(3\text{-Cl-Azpy})Cl]PF_6$	>100
(**26**) $[Os(\eta^6\text{-}p\text{-cym})(3\text{-Cl-Azpy})Cl]PF_6$	>100
(**27**) $[Os(\eta^6\text{-bip})(Abpy))I]PF_6$	21.3(±6.2)
(**28**) $[Os(\eta^6\text{-}p\text{-cym})(Abpy))I]PF_6$	10.8(±0.11)
(**29**) $[Os(\eta^6\text{-bip})(Abpy)Cl]PF_6$	22.4(±11.8)
(**30**) $[Os(\eta^6\text{-}p\text{-cym})(Abpy))Cl]PF_6$	>100
(**31**) $[Os(\eta^6\text{-}p\text{-cym})(OH\text{-Azpy-}NO_2)I]PF_6$	0.29(±0.04)
(**32**) $[Os(\eta^6\text{-}p\text{-cym})(OH\text{-Azpy-}NO_2)Cl]PF_6$	0.30(±0.05)

Table 4.3. (A) IC_{50} values for A2780 cells for complexes **1-32**. **(B)** Comparison of IC_{50} values for A2780 cells for monodentate ligand = Cl or I. **(C)** Comparison of IC_{50} values for A2780 cells for arene - *p*-cym or bip.

(B)

Cl complex / I complex	**IC_{50} (Cl) / IC_{50} (I)**
3/1	4.4
4/2	3.5
7/5	11.6
8/6	2.7
10/9	>159
12/11	2.2
15/13	>50
16/14	0.9
19/17	>85
20/18	>1.4
25/23	>4.5
26/24	>2.1
29/27	1.0

(C)

***p*-Cym Complex / Bip Complex**	**IC_{50} (*p*-Cym) / IC_{50} (Bip)**
2/1	1.91
4/3	1.52
6/5	2.43
8/7	0.56
12/10	>7.5
14/13	33.6
18/17	62.0
22/21	10.9
24/23	2.20
28/27	0.51

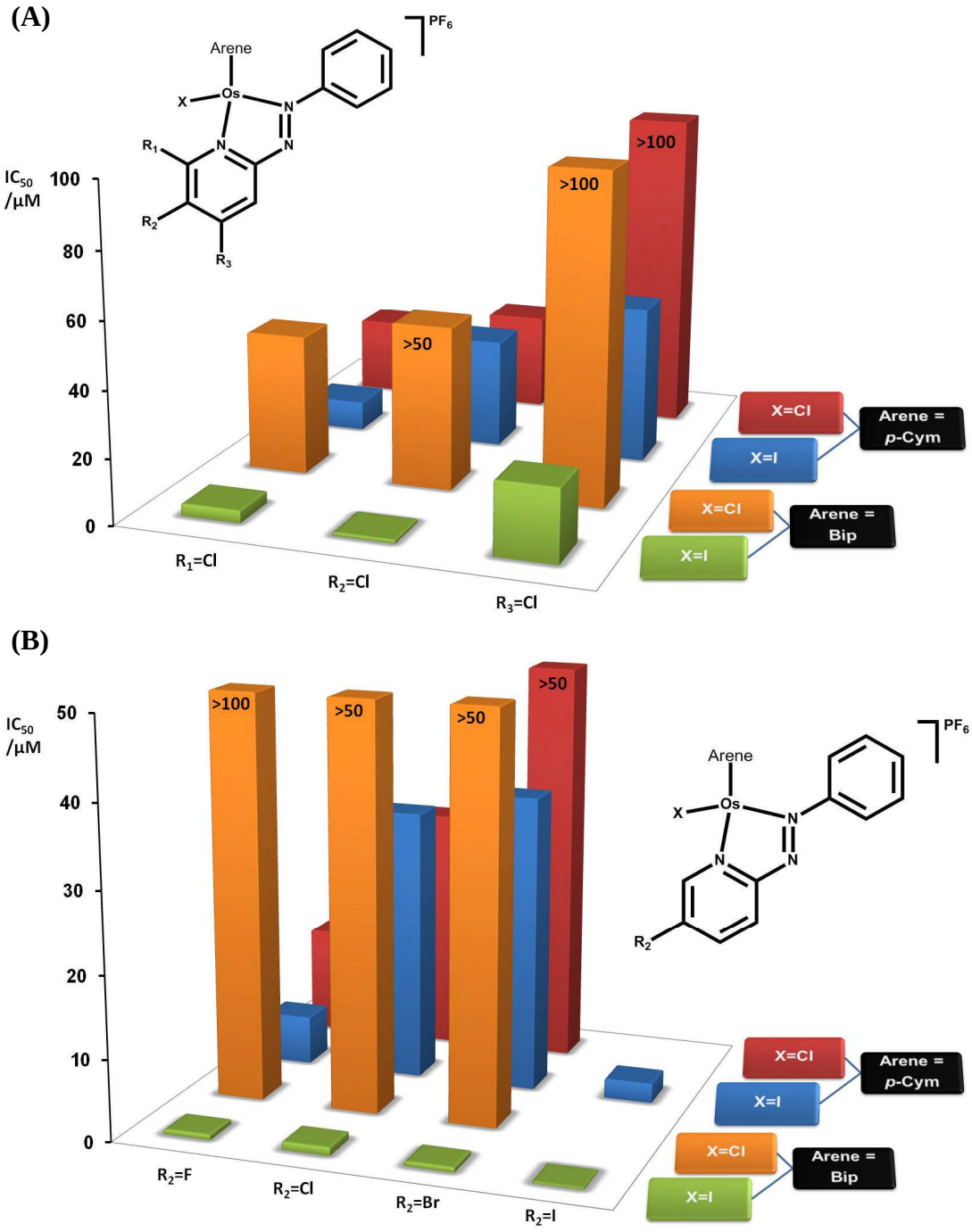

Figure 4.3. Comparision of the effect of different pyridine ring substitutions on IC_{50} values for A2780 cells. Different colours are employed to show different sub-families of these complexes: green (arene = biphenyl, monodentate ligand=iodide), orange (arene = biphenyl, monodentate ligand = chloride), blue (arene = *para*-cymene, monodentate ligand = iodide), red (arene = *para*-cymene, monodentate ligand = chloride). **(A)** Chloride substituent at R_1, R_2 and R_3 positions. **(B)** Fluoride, chloride, bromide or iodide substituent at R_2 position.

4.3.4 Partition Coefficients (Log P)

Octanol/water partition coefficients (log P values) provide a measure of the lipophilicity of compounds and are often a useful indication of the likely extent of drug uptake by cells.[20] The log P values for four iodido biphenyl complexes **9** (2-F), **13** (2-Cl), **17** (2-Br), and **23** (3-Cl), and two chlorido complexes **19** (2-Br), and **25** (3-Cl) were studied by using the "shake tube method". The log P values for these complexes (Table 4.4) decrease along the series: complex **19** (monodentate ligand Cl/substituent 2-Br) > **17** (I/2-Br) > **13** (I/2-Cl) > **23** (I/3-Cl) > **9** (I/2-F)> **25** (Cl/3-Cl) (Fig. 4.4), ranging from 0.1330 (partitioning preferentially into octanol) to -1.446 (partitioning preferentially into water).

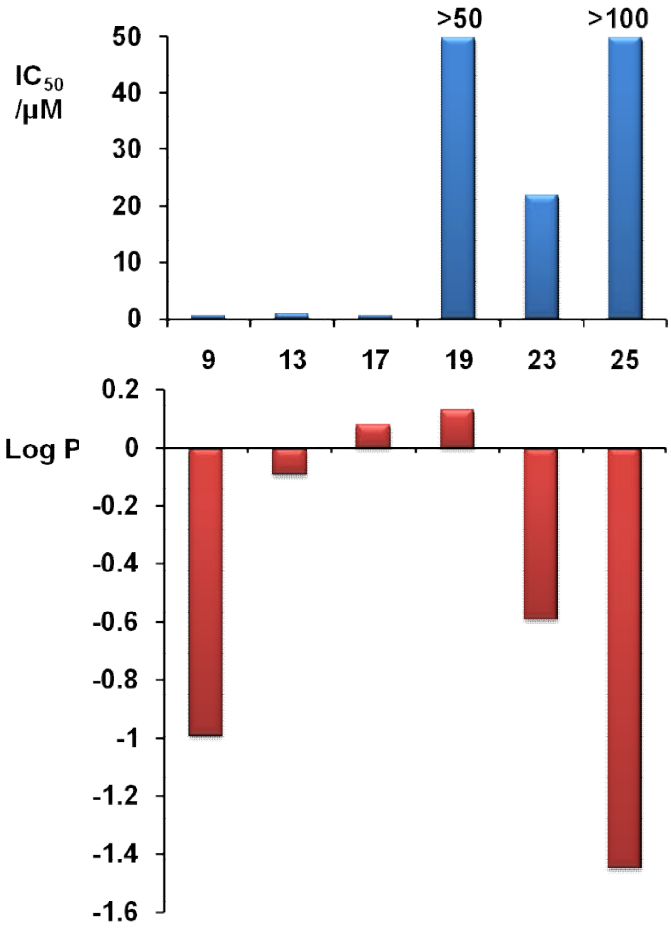

Figure 4.4. Comparison of octanol/water partition coefficients (log P values) and cytotoxicity towards A2780 cells.

Table. 4.4. Comparison of octanol/water partition coefficients (log P values) and cytotoxicity towards A2780 cells. Data are the mean of three experiments and are reported as mean ± standard error of the mean (SEM).

Complex	Log P	IC_{50}/μM
9	-0.99 (± 0.28)	0.63 (±0.1)
13	-0.09 (± 0.06)	1.0 (±0.1)
17	0.08 (± 0.07)	0.59 (±0.02)
19	0.13 (± 0.06)	>50
23	-0.59 (± 0.32)	22.0 (±2.0)
25	-1.45 (± 0.37)	>100

4.3.5 Cellular Uptake and Distribution in A2780 Cells

Time-dependent cellular uptake studies of the biphenyl/iodido complexes **9** [Os(bip)(2-F-Azpy)I]PF_6 and **23** [Os(bip)(3-Cl-Azpy)I]PF_6 showed that the accumulation of osmium from **9** is much higher than that of **23** after 24 h (Table 4.5 and Fig. 4.6 A) The distribution of Os in A2780 cells was investigated after incubation with 4 μM complex **9** or **23** (the concentration was selected based on the IC_{50} values of **9** and **23** against A2780 cells)**.** The cytosol, membrane-plus-particulate fraction, nucleus and cytoskeleton fractions were separated and their Os contents were determined by ICP-MS (Fig. 4.5 and Fig 4.6 B). Complex **9** gave rise an uptake of osmium into the cytosol, membrane plus particulate fraction and nucleus ca. 23 times higher than for **23** (Fig. 4.6 B). It is interesting that for **23** there is a very high percentage of osmium in the cytoskeleton, up to 43 % of the total cellular Os (Fig 4.5).

Table 4.5. Time dependent accumulation of Os from complexes **9** and **23** in A2780 human ovarian cancer cells.

Time / h	**9**/ppt Os/10^4 cells	**23**/ppt Os/10^4 cells
0.5	40.6 (±1.6)	64.8 (±5.6)
1	51.8 (±2.8)	67.4 (±0.3)
4	263.8 (±12.7)	67.9 (±1.8)
24	399.4 (±20.9)	35.1 (±2.2)

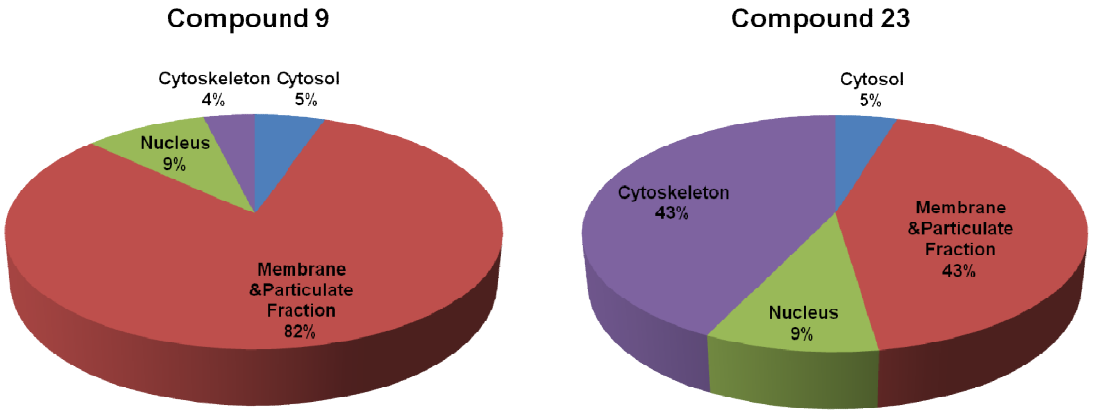

Figure. 4.5 Distribution of osmium in A2780 cells as a percentage of total osmium for compounds **9** and **23**. All data are the mean of three experiments and are reported as mean ± standard error of the mean (SEM)

(A)

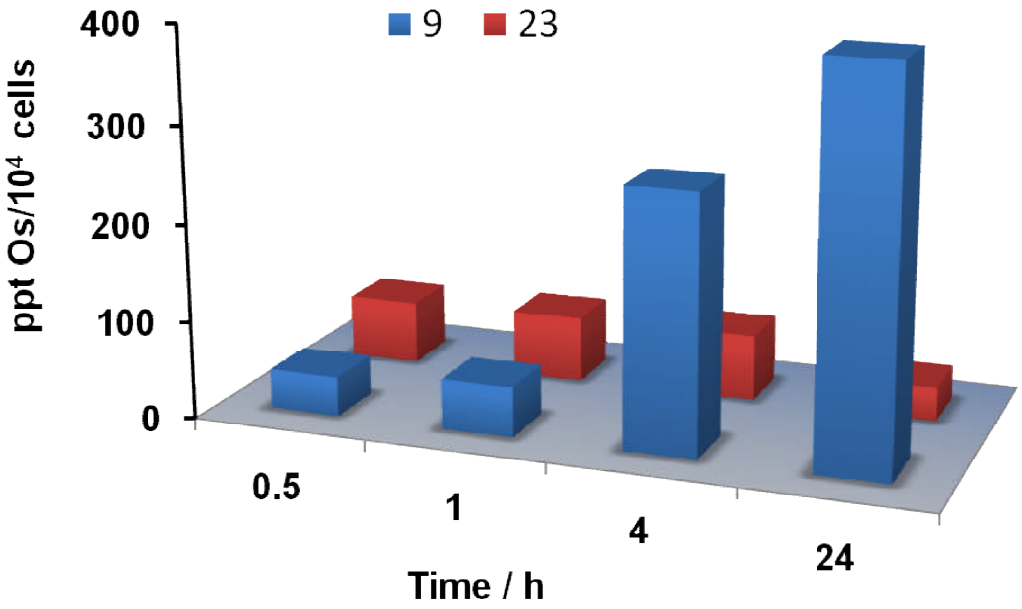

(B)

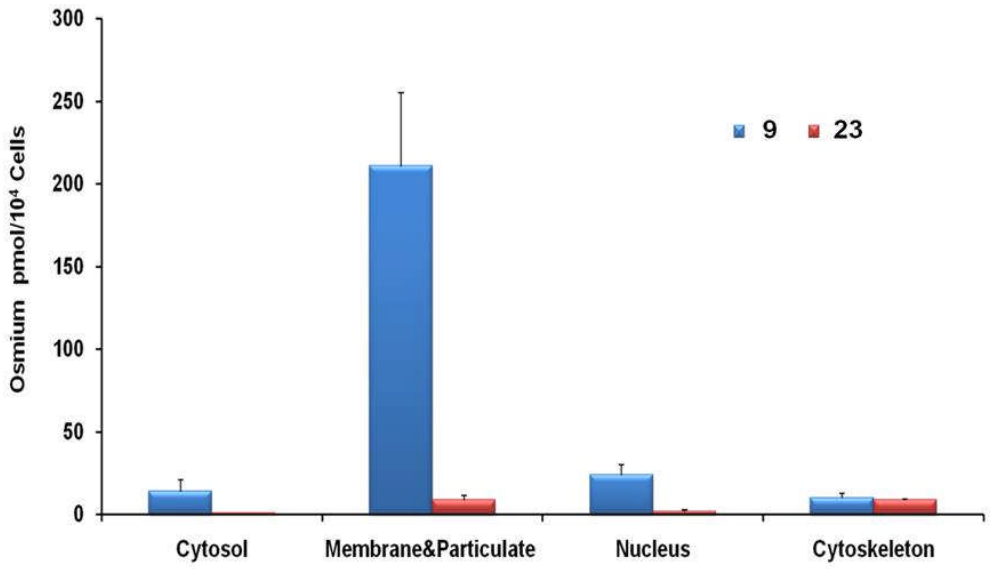

Figure 4.6. Uptake of osmium into A2780 human ovarian cancer cells. **(A)** Time dependence for complexes **9** and **23** **(B)** Osmium distribution of Os from complexes **9** and **23** in cell fractions: cytosol, membrane plus particulate fraction, nucleus and cytoskeleton. Data are the mean of three experiments and are reported as mean ± standard error of the mean (SEM).

4.3.6 Detection of ROS in A2780 Cancer Cells

To detect changes in general oxidative stress,[21] the level of reactive oxygen species (ROS, including O_2^-, $OH^{\cdot}$, H_2O_2) in A2780 cells was determined by using the probe 2′,7′-dichlorodihydrofluorescein-diacetate (DCFH-DA). When taken up by live cells, DCFH-DA hydrolyzes to 2′,7′-dichlorodihydrofluorescein (DCFH), which in turn is oxidized to 2′,7′-dichlorofluorescein (DCF) in the presence of ROS and detected by its intense fluorescence.[22, 23] The change in ROS level induced by **9** was monitored, $[Os(\eta^6\text{-bip})(2\text{-F-Azpy})I]PF_6$, one of the most active compounds. The relative increase in DCF fluorescence was detected over time after exposure to **9** alone (1 μM), **9** (1 μM) with L-buthionine sulfoximine (Chart 4.2, 50 μM, an inhibitor of glutamylcysteine synthetase),[24] and, for comparison, H_2O_2 (50 μM). For **9**, an increase in intracellular ROS level was observed, but it was lower than that observed for H_2O_2 (50 μM) after 4 h of incubation.

Chart 4.2. Structure of L-buthionine sulfoximine (L-BSO).

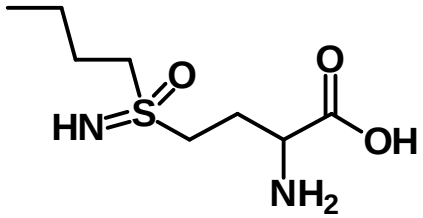

L-BSO

Exposure of A2780 cells to **9** (1 μM) in the presence of the antioxidant thiol N-acetyl-L-cysteine (NAC, 50 μM)[25] gave no increase in ROS level compared to the control. However, for **9** (1 μM) with L-BSO (50 μM), the increase in ROS level was even higher than that for H_2O_2 (50 μM) (Fig 4.7A). The increase of fluorescence over time after exposure of A2780 cells preloaded with DCFH-DA to 1 μM of **9**, indicates that **9** causes a build-up of ROS inside A2780 cancer cells.

(A)

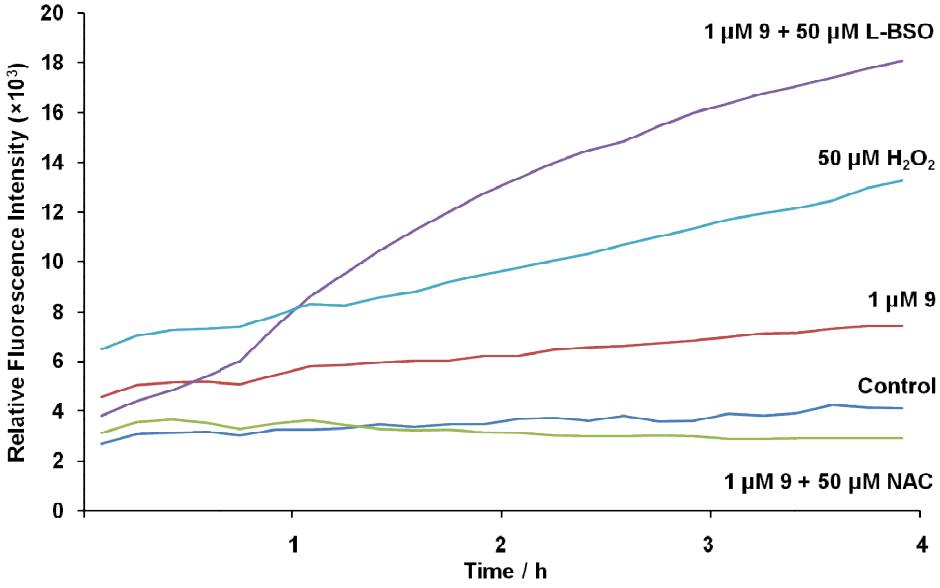

(B)

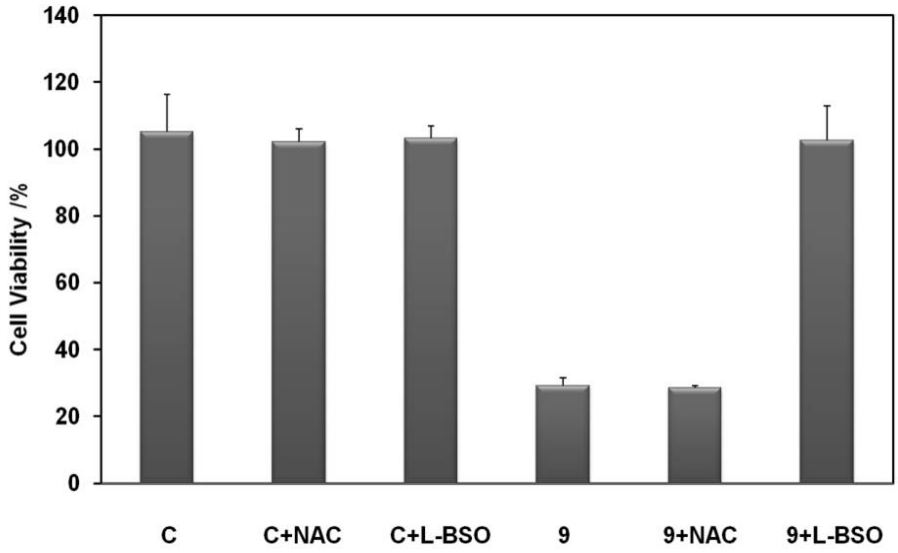

Figure 4.7. (**A**) Relative changes in DCF fluorescence detected over time after exposure to 1 μM **9**, 1 μM **9** with 50 μM NAC, 1 μM **9** with 50 μM L-BSO, or 50 μM H_2O_2. For each compound, the fluorescence was averaged over 6 wells (n = 6). (**B**) Percentage cell survival after 24 h exposure to 50 μM NAC (C+NAC), 50 μM L-BSO (C+L-BSO), 1 μM **9** (9), 1 μM **9** with 50 μM NAC (**9**+NAC), 1 μM **9** with 50 μM L-BSO (**9**+ L-BSO) and 96 h recovery for A2780 ovarian cancer cells; effects of combination treatment of complex [Os(η^6-bip)(2-F-Azpy)I]PF_6 (**9**) or [Os(η^6-bip)(2-Br-Azpy)I]PF_6 (**17**) with NAC or L-BSO.

4.3.7 Relationship of Cytotoxicity to ROS

In order to further investigate the possible involvement of ROS in the cytotoxicity of the azopyridine osmium arene complexes studied here, the combined effects of either complex **9** or **17** with the reductant NAC which can deplete ROS or with L-BSO which depletes glutathione levels and can lead to an increase in levels of ROS in cells were investigated.

The cytotoxicity assays showed that complex **9** (1 μM) in combination with the reductant (antioxidant) NAC (50 μM) did not increase the survival of A2780 cells compared to those treated with **9** alone for 24 h (Fig 4.7 B). This suggests that ROS are not implicated in cell death induced by complex **9**. In contrast, combination treatment of **9** with the oxidant L-BSO, which resulted in an increase in the ROS level, blocked the anticancer activity.

The effect of combination treatment with the reductant (antioxidant) NAC (50 μM) on IC_{50} values for complex **9** was investigated for both A2780 (ovarian) and A549 (lung) human cancer cell lines (Table 4.6). A2780 cells were treated with various concentrations of **9** or **17** together with NAC (50 μM). Combination treatment with NAC decreased the cytotoxicity of both **9** and **17**, slightly. However, combination treatment with L-BSO raised the IC_{50} values for **9** and **17** more than 10 times for A2780 cells. For the A549 cell line, the IC_{50} value of **9** was raised from 1.8 μM to more than 100 μM, and for **17** the IC_{50} values increased more than 70-fold (Table 4.6). Although the combination treatment of **9** or **17** with L-BSO then increase ROS block the anticancer acitivty is still need further investigations, these data resemble those reported for the effects of combination treatment on the organic drug Paclitaxel (Taxol) intriguingly which is in clinical use for the treatment of ovarian, breast and non-small cell lung cancer. Taxol is known to target tubulin in microtubules.[14]

Table 4.6. IC_{50} values of combination treatment with NAC or L-BSO. **(A)** Effect of L-BSO treatment (24 h) on IC_{50} values for A549 human lung cancer cells. **(B)** Effect of L-BSO and NAC treatment (24 h) on IC_{50} values for IC_{50} values for A2780 human ovarian cancer cells. The error bars are standard deviations from an average of three wells.

(A)

Complex	IC_{50}/μM	+ L-BSO IC_{50} /μM
9	1.8 (±1.4)	>100
17	3.6 (±0.2)	30.5 (±2.6)

(B)

Complex	IC_{50}/μM	+ L-NAC IC_{50} /μM	+ L-BSO IC_{50} /μM
9	0.63 (±0.10)	0.97 (±0.01)	12.6 (±1.9)
17	0.59 (±0.02)	1.14 (±0.22)	8.4 (±0.9)

4.3.8 Prevention of the Polymerization of Tubulin *in Vitro*

In order to investigate whether the osmium azopyridine complexes can influence the polymerization process of tubulin, a variety of osmium complexes (**1, 5, 9, 10** and **23)** were incubated with purified and unpolymerized tubulin, the polymerization processes of tubulin were monitored at 37°C for 60 min. Taxol (microtubule stabilizer) and colchicine (microtubule de-stabilizer) were used as comparisons. The process of polymerization was facilitated with the treatment of taxol but completely halted by clochicine`s inhibition on the contrary. It was found that **9** was able to reduce the total amount of polymerization of tubulin in a dose-dependent manner during the 1h incubation time, the IC_{50} of tubulin polymerization of **9** is ca. 20 μM (Figure 4.8 A). With the treatment with **9** at 20 μM, the tubulin polymerization process had one elongated nucleation phase which lasted for 14 min (Figure 4.8 A). All the osmium anticancer complexes which were tested for tubulin polymerization showed the inhibitive effect at different extents; among them, complex **9** demonstrated the most potent inhibition to the polymerization process of tubulin (Fig. 4.8 B).

(A)

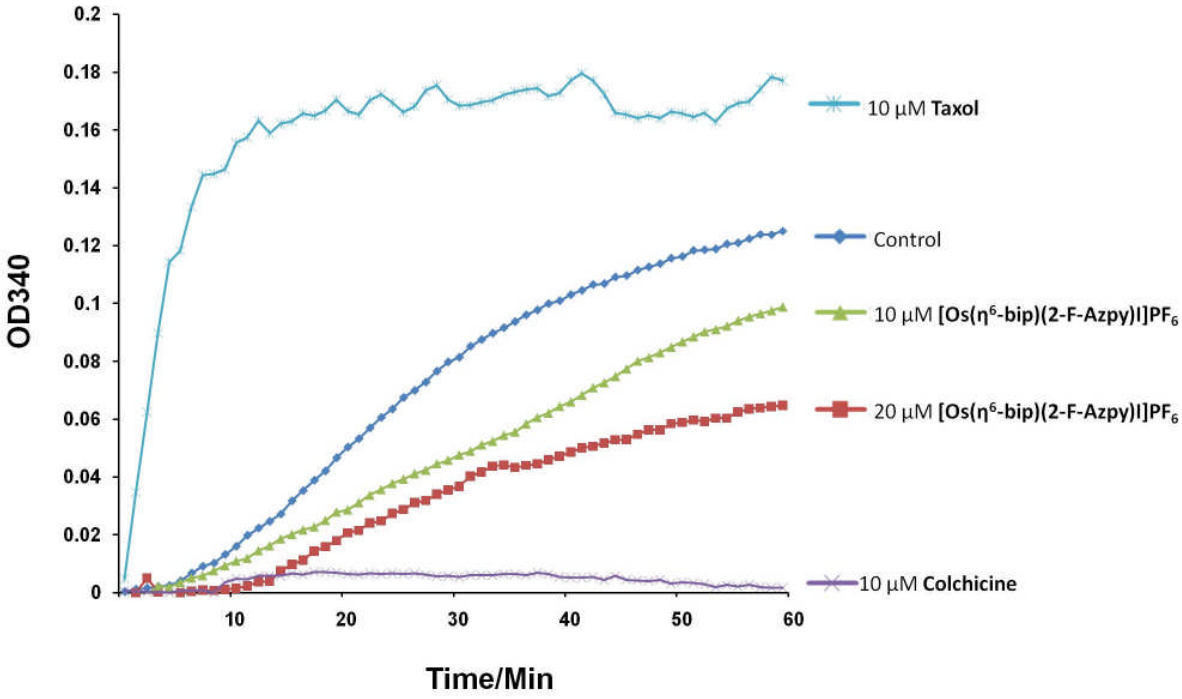

(B)

Osmium Compounds at 10 μM	Inhibition of Tubulin Polymerisation/%
1	**12.96**
5	**11.36**
9	**20.96**
10	**8.08**
23	**19.68**

Figure 4.8. Inhibition of tubulin polymerization by osmium complexes *in vitro*. (A) Inhibition of [Os(η^6-bip)(2-F-Azpy)I]PF (**9**) on tubulin polymerization over a period of 1 hour at 310 K. (2) The inhibition extents of tubulin polymerization after 1 h incubation at 310 K for different osmium complexes: **1**, **5**, **9**, **10** and **23**.

4.3.9 Complex 9 Inhibits the Formation of Microtubules in Cells

The microtubule assembly status in A2780 cells was examined by confocal microscopy after the treatment with various concentrations of **9** at different time points (2h and 24h)**.** The A2780 cells were fixed, then the microtubules were stained by anti-α-tubulin-Alexa 488 (monoclonal antibody which can react with all forms of alpha tubulin with a conjugation of green-fluorescent dye) and nuclei were counterstained with propidium iodide (DNA intercalating agent and red-fluorescent dye). After 2 h incubation with **9** at high concentrations (10 μM and 20 μM), chromosome separation disruption in A2780 cells was observed (Fig 4.9 A). After 24 h of treatment, most of the cells have long microtubule fragments scattered throughout the cytoplasm in the control cells; however, the inhibition of forming microtubules were even observed with the incubation with **9** at low concentrations (1 μM), moreover there was a complete loss of microtubules with only a diffuse stain visible throughout the cytoplasm at higher concentrations (5, 10 and 20 μM).

(A)

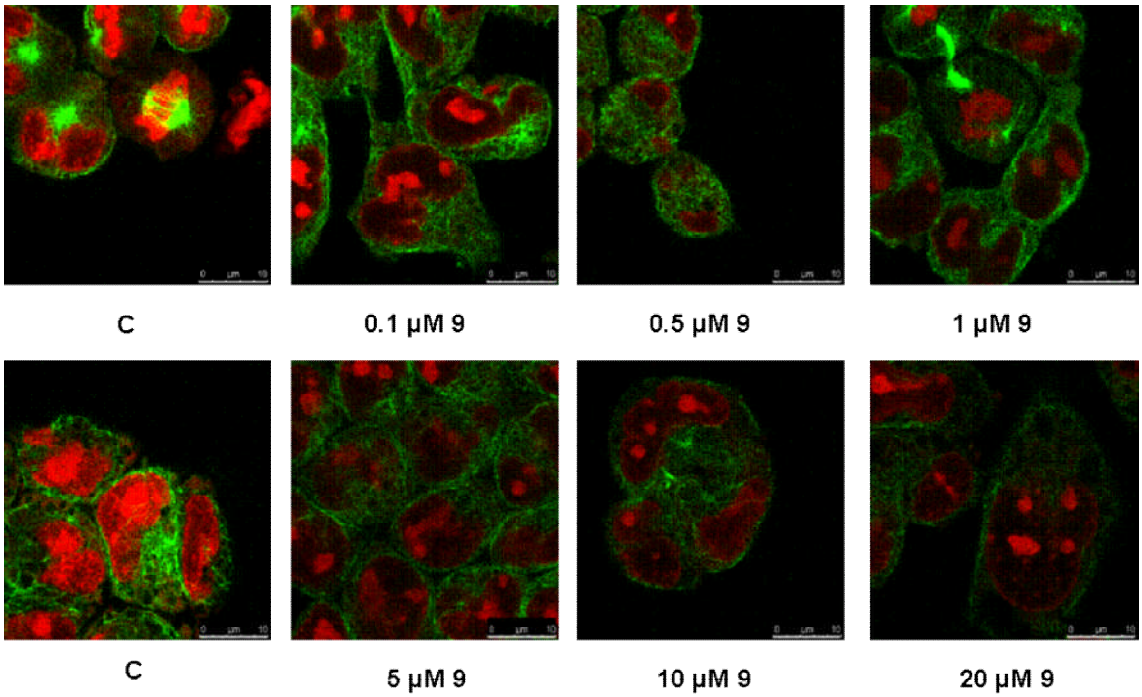
C
0.1 μM 9
0.5 μM 9
1 μM 9
C
5 μM 9
10 μM 9
20 μM 9

(B)

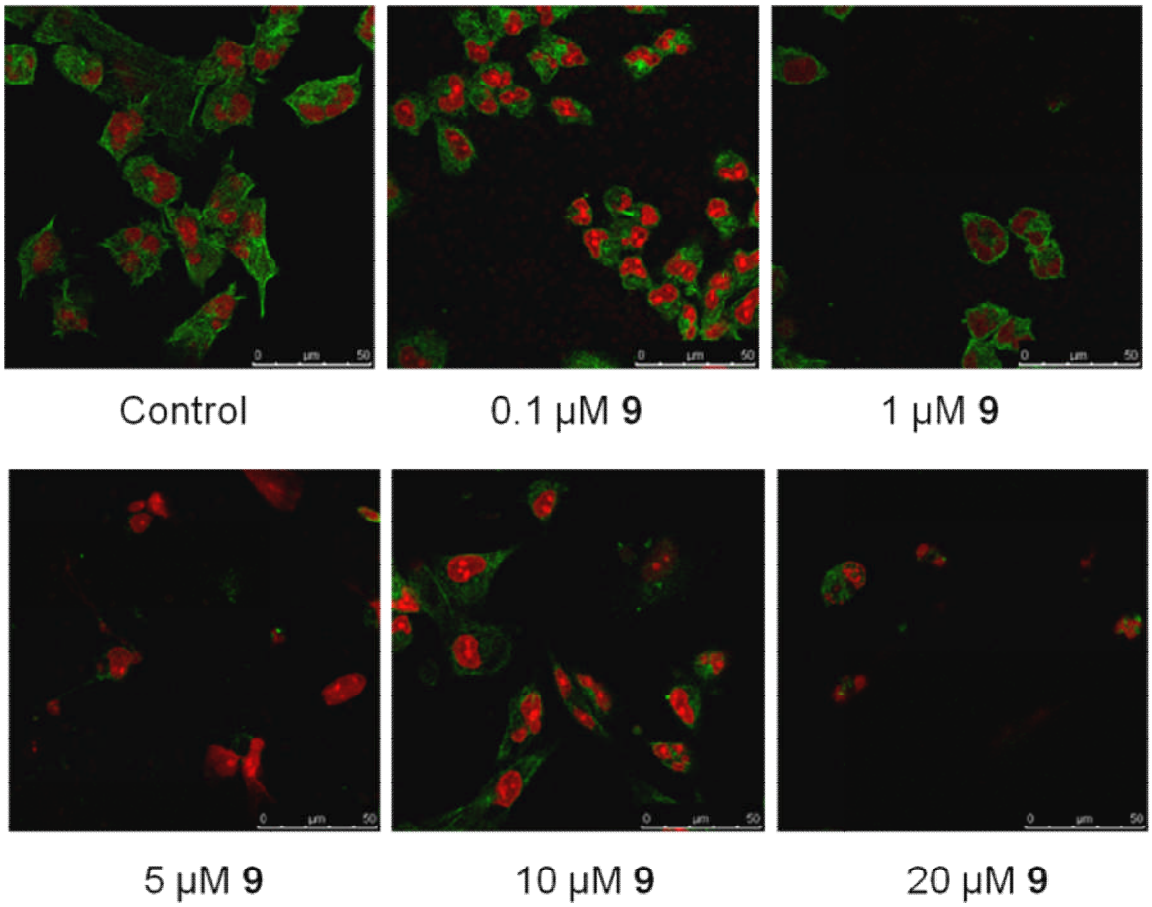
Control
0.1 μM 9
1 μM 9
5 μM 9
10 μM 9
20 μM 9

(C)

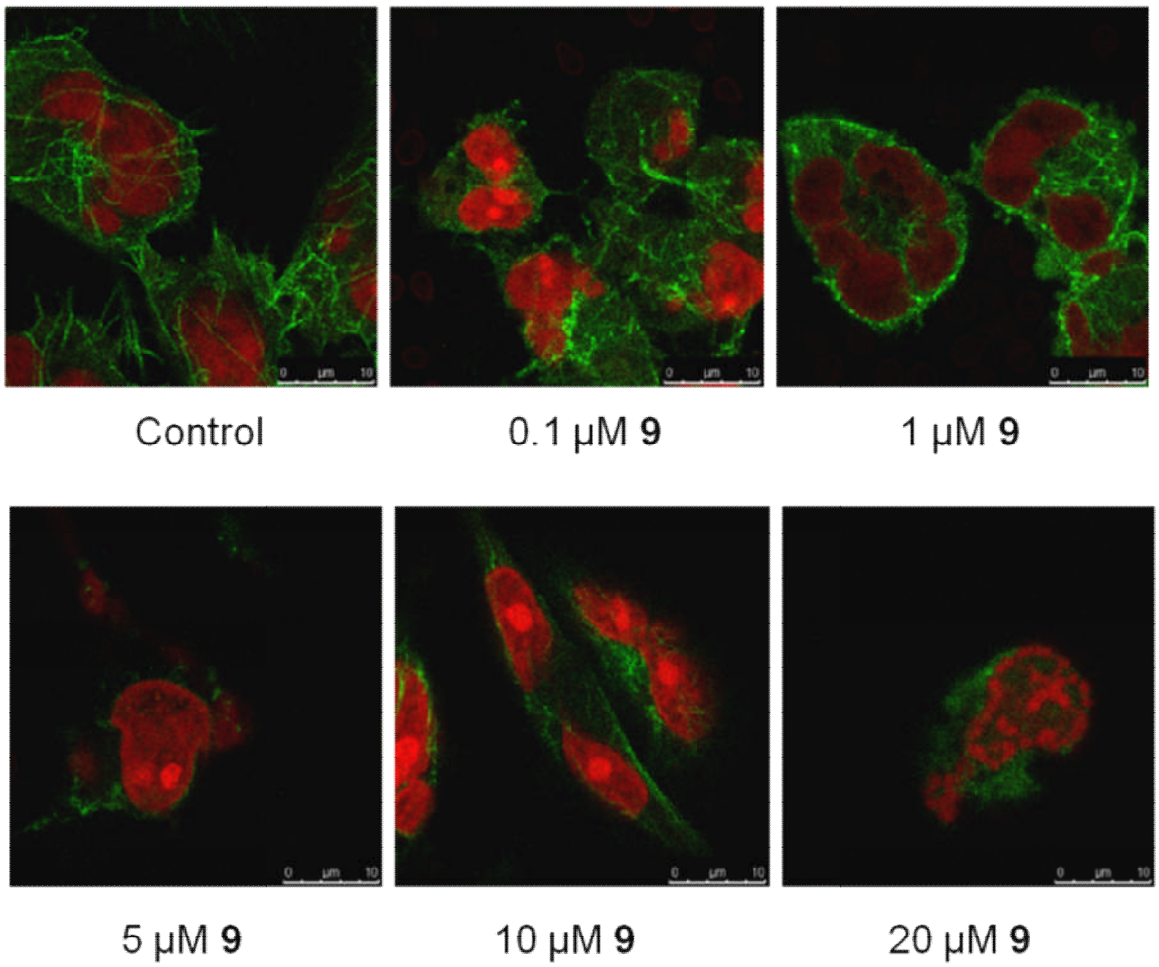

Figure 4.9. Confocal microscopy of A2780 cells treated with different concentrations of **9**. (A) 2 h of treatment under 100× objective plus 4× magnification; (B) 24 h treatment and under 100× objective; (C) 24 h treatment and under 100× objective plus 4× magnification. Microtubules were stained by anti-α-tubulin-Alexa 488 (green) and nuclei were dyed with propidium iodide (red). Results are representative of two independent experiments.

4.3.10 Complexes 9 and 23 Induce G_2/M Phase Cell Cycle Arrest

Since inhibition of forming microtubules can affect the cell divisions in mitosis phase, the changes of distributions in different cell cycle phases on A2780 cells after incubated with **9** or **23** were monitored by using flow cytometer. The A2780 cells were incubated with **9** or **23** at different concentrations which were selected to be comparable to their IC_{50} values respectively (Table 4.3). A dose-dependent accumulation of A2780 cells with G_2/M phase (4N DNA content) and a concomitant decrease with G_0/G_1 phase (2N DNA content) were found after the treatment with **9** or **23** for 24 h (Fig. 4.10). Together with the accumulation of cells in G_2/M phase, an increase in subdiploid cells at highest concentrations for both **9** and **23** was also observed (Fig 4.10). An S phase arrest induced by **9** was also observed during the cell cycle which is not observed after the treatment with **23**.

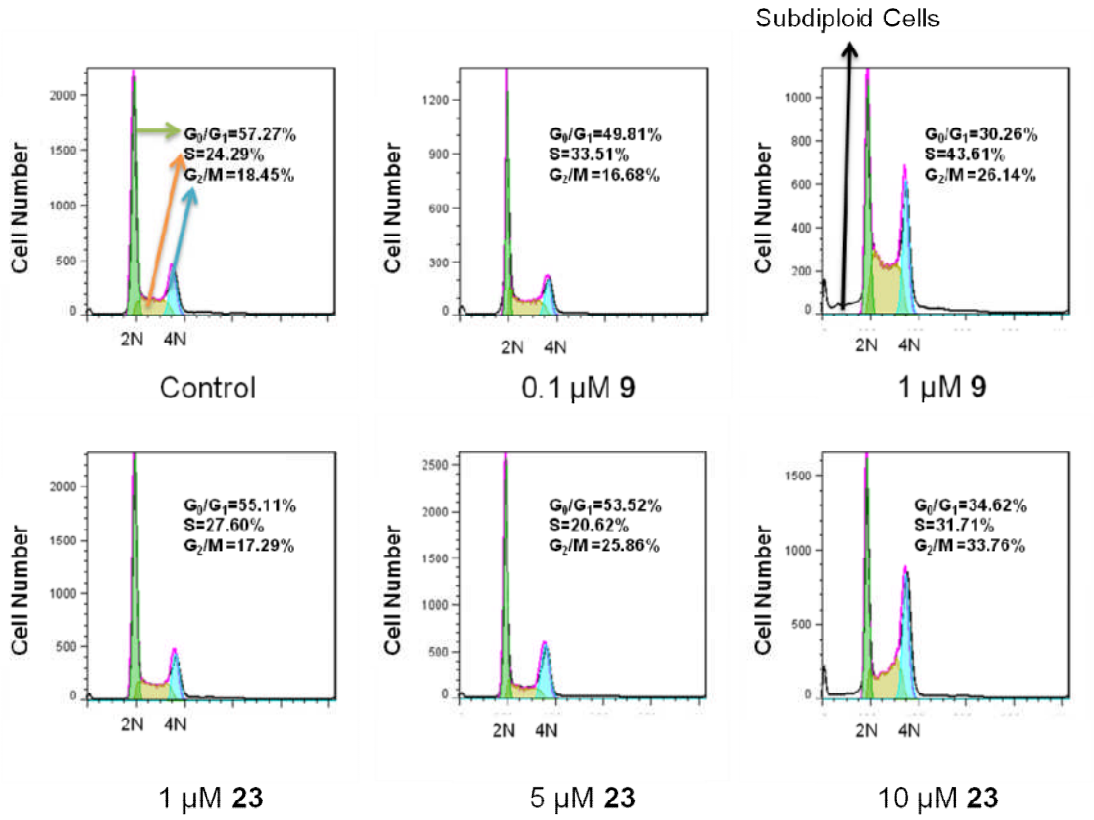

Figure 4.10. (A) Cell cycle distributions of A2780 cells after the treatment of various concentrations of **9** or **23** for 24 h.

4.4 Discussions

The replacement of the N,N-chelating ligand ethylenediamine (en) by azopyridine in $[Ru(\eta^6\text{-arene})(N,N)X]^+$ complexes introduced some dramatic changes in their chemical and biological properties was already found.[8] Azopyridine ligands are not only σ-donors (like en), but also strong π-acceptors. The chlorido azopyridine complexes $[Ru(\eta^6\text{-arene})(Azpy)Cl]^+$ (arene: *p*-cymene (*p*-cym), benzene (bz), or biphenyl (bip)) readily underwent slow decomposition via hydrolysis and/or arene loss. They were inactive (non-cytotoxic) towards cancer cells but activated by the introduction of electron-donating substituents into the phenyl ring, e.g. OH and NMe_2. The π-acceptor property of the azopyridine ligand results in highly acidic aqua complexes. For example, the pK_a of the coordinated water in $[Ru(\eta^6\text{-}p\text{-cym})(Azpy\text{-}NMe_2)OH_2]^{2+}$ is 4.60.[26] Most dramatic was the effect of changing the monodentate leaving group from chloride to iodide which conferred on the complexes remarkable inertness towards ligand substitution.[8] Moreover these iodido complexes with substituents on the phenyl ring were highly cytotoxic to A2780 human ovarian and A549 human lung cancer cell lines with IC_{50} values of 2 - 6 μM. The mechanism of cytotoxicity appeared to involve ligand-based redox reactions.[8]

These findings for Ru^{II} complexes appear to be mirrored to some extent for Os^{II} complexes. The chlorido Os^{II} azopyridine complex $[Os(\eta^6\text{-}p\text{-cym})(Azpy)Cl]PF_6$ is inactive towards A2780 human ovarian cancer cells but active with electron-donor NMe_2 or OH substituents on the phenyl ring.[6] The iodido complexes are more active and complexes with moderate activity e.g. $[Os(\eta^6\text{-}p\text{-cym})(Azpy)I]PF_6$ (IC_{50} = 10.3 μM in A2780 cell line) become potently cytotoxic at nanomolar concentrations towards a panel of human cancer cell lines when substituents are introduced into the phenyl ring, e.g. IC_{50} = 140 nM for $[Os(\eta^6\text{-bip})(Azpy\text{-}NMe_2)I]PF_6$ towards A2780 ovarian cancer cells.[6]

The aim of this chapter was to investigate the effects on anticancer activity of introducing substituents into the pyridine ring especially when the phenyl ring is left unsubstituted. 32 novel organometallic osmium azopyridine complexes were synthesized and characterized (Chart 4.1). All the osmium complexes adopted the familiar piano-stool geometry in the crystalline state, with bond lengths and angles within the expected ranges.[6] X-ray crystallographic data, selected bond lengths and angles for these structures are listed in table 4.1 and table 4.2. For the iodido osmium complexes, the Os-C (arene) bond lengths are in the range of 2.172-2.284 Å, and the Os-I bond lengths from 2.7002-2.7063 Å (Table 4.2). For the chlorido osmium complexes, the Os-C (arene) bond lengths are in the range of 2.173-2.286 Å, and Os-Cl bond lengths are 2.3727-2.3954 Å (Table 4.2). A relatively longer bond length for Os(1)-N(1)(pyridine) compared to Os(1)-N(8)(azo) was observed in all the 10 crystal structures. This can be attributed to the back-bonding competition for the osmium $5d^6$ electron density by the azopyridine and arene -acceptor ligands. A similar trend was also observed for ruthenium arene azopyridine complexes.[26]

Three of the structures show π-π stacking. [Os(η^6-bip)(2-F-Azpy)Cl]PF_6 (**10**) exhibits intramolecular π-π stacking between the phenyl ring of the biphenyl arene ligand and the phenyl ring of the 2-F-Azpy ligand. There is also intermolecular π-π stacking involving the same groups, but between symmetry-related molecules. For [Os(η^6-*p*-cym)(3-Cl-Azpy)I]PF_6 (**24**), there is π-π stacking between the *p*-cymene and a phenyl ring in a symmetry-related molecule. There is an intermolecular π-π stacking interaction between 2-Cl-Azpy ligands that lie in a head-to-tail dimer fashion related by an inversion centre in [Os(η^6-*p*-cym)(2-Cl-Azpy)I]PF_6 (**14**). The distances between the planes of the stacked rings (ca. 3.3 Å) are within the normal range for such interactions.[27]

Remarkably electron-withdrawing substituents on the pyridine ring can give rise to highly potent complexes with IC_{50} values in the nano-molar range (Table

4.3 and Fig. 4.3). The structure-activity relationships show that potency is higher for biphenyl versus *p*-cymene as the arene (Table 4.3 C), and for iodide compared to chloride as the monodenate ligand (Table 4.3 B). Biphenyl is a stronger π-acceptor than *p*-cymene (back-donation of electron density from Ru^{II}) whereas *p*-cym is the stronger electron donor. When Ru^{II} arene complexes bind to DNA, the uncoordinated phenyl ring of bip can intercalate between DNA bases whereas DNA distortions caused by *p*-cymene are steric in origin.[28] The arene can also have a major effect on interactions with protein targets, as demonstrated for interactions between serum albumin and biphenyl and *p*-cymene Ru^{II} complexes.[29]

The inertness of the most active complexes to hydrolysis suggests direct binding to DNA is not the major mechanism of action and that a novel target for these metal arene complexes is involved. Studies on Os^{II} azopyridine complexes containing unsubstituted pyridine and substitutions of the phenyl ring also lead to the same conclusion.

Reactive oxygen species (ROS) play important roles in regulating cell proliferation, death, and senescence, they can also play significant roles in the mechanism of action of anticancer agents.[30] The cytotoxicity mechanism for osmium arene azopyridine iodido complexes containing unsubstituted ($R_1 - R_4$ = H) pyridine rings and their ruthenium analogues was found to be related to ROS generation.[8] However, the complexes investigated in this chapter containing substituted pyridine rings do not appear to share a mechanism dependent to the formation of ROS. Down-regulation of ROS by increasing intracellular GSH, does not block the anticancer activity of **9** and **17** (Table 4.6). It is also known that cisplatin resistance is partly related to an increase of GSH levels,[31] and the data for complexes **9** and **17** suggests that they have potential for the treatment of cisplatin-resistant tumours.[32]

The mechanism of action of complexes **9** and **17** appears to be GSH-dependent. L-buthionine sulfoximine (L-BSO) depletes intracellular glutathione levels by inhibiting the enzyme glutamylcysteine synthetase. L-BSO is on clinical trial for combination treatment with Melphalan,[33] and increases the cytotoxicity of a number of therapeutic agents, including cisplatin, especially towards resistant cancer cell lines.[34, 35] The only reported exception in which the L-BSO can block the cytotoxicity of a drug appears to be taxol.[14]

For the structure activity relationships, it is evident that when biphenyl is the arene and iodide is the monodentate ligand, the osmium complexes in this class show the highest anticancer activity towards A2780 cells, consistent with our previous work on azopyridine complexes with unsubstituted pyridine rings.[6] Introducing biphenyl as the arene instead of *p*-cymene not only provides a potential DNA intercalator but also increases the hydrophobicity for interaction with proteins which may contribute to the increased activity.[36, 37]

Consideration of the substituents on the pyridine ring shows that changing from chloride at R_3 to fluoride causes the cellular accumulation of osmium to increase dramatically and is accompanied by an improvement in anticancer activity. The difference in the extent of cellular accumulation within this family may contribute to the observed variations in anticancer activity, as may interactions with targets (which may be proteins) .[37]

To investigate whether there is a link between lipophilicity and anticancer activity for these complexes. The log P values were determined; they cover a broad range from -1.446 to 0.1330 (Table 4.4). These values can be compared to those for the less lipophilic clinical Pt^{II} drug cisplatin (log P = -2.36)[38] and to the Ru^{III} drug NAMI-A (log P = -0.25)[39] which is on clinical trials as an antimetastatic agent. The sequence of potency towards A2780 human ovarian cancer cells for the osmium azopyridine complexes is: **17** > **9** > **13** > **23** > 1**9** > **25**,

whereas lipophilicity decreases in the order **9** (monodentate ligand Cl/ pyridine substituent 2-Br) > **17** (I/2-Br) > **13** (I/2-Cl) > **23** (I/3-Cl) > **9** (I/2-F)> **25** (Cl/3-Cl). Hence there appears to be little correlation between lipophilicity (log P), and anticancer activity (Fig. 4.4 and Table. 4.4). The introduction of bioisosterism into the design has led to the discovery of compounds with different pharmaceutical properties, potential candidates for further pharmacokinetic studies.

The cell distribution studies showed a dramatic increase in accumulation of osmium in the membrane and particulate fraction of A2780 cells for **9** compared to **23**, and **9** is > 50 times more active than **23** (Fig. 4.5 and 4.6). Whether the critical target site is in the membrane and particulate fraction remains to be investigated further. However, to identify and determine the contribution of the individual binding sites is a complex task, for example, only ca. 1 % of Pt from intracellular cisplatin binds to its target, DNA,[40,41] Further work is required to validate the target for this sub-family of osmium arene azopyridine complexes.

Since the anticancer activity of osmium arene azopyridine complexes can be blocked by the combination treatment with L-BSO, a similar effect which was only observed on the combination treatment of L-BSO with taxol which can show its anticancer effect through affecting the polymerization of tubulin, osmium arene complexes were studied on the influence of the formation of microtubules for the first time. There are two common types of tubulins (α-tubulin and β-tubulin) which are able to polymerize to form microtubules; they and their inherent dynamicity is vital for the cell division process especially in G_2/M cell cycle phase. Two classes of drugs which are targeting the polymerization process of tubulin are now in clinical uses: (1) microtubule stabilizers (eg. taxol); (2) microtubule de-stabilizers like *Vinca* alkaloids (eg. vincristine, vinblastine, and vinorelbine). Both of these two types of anticancer drugs work by interfering with the cell's ability to form mitotic spindles appropriately by inducing or preventing

the normal polymerization of microtubules in the G_2/M phase during the cell cycle process.[42] The design of tubulin-targeting anticancer drugs was mainly based on natural products (eg. taxol and vinca alkaloids) with more than 30 drug candidates in different phases of clinical trials now.[43] A lot of progresses have also been made based on organic structures to design new tubulin polymerization inhibitors,[44-48] however, there is still no report showing any organometallic complex can inhibit the polymerization of tubulin, although an osmium carbonyl cluster was found to hyperstabilize microtubules in 2009.[49]

The results showed an inhibition effect of osmium arene complexes on the tubulin polymerization process which was determined *in vitro* (Fig. 4.8). Complex **9** which showed the best inhibition effect *in vitro* and was selected for a further cellular test in A2780 cells, the confocal microscopy images showed less microtubules formed in A2780 cells after the treatment with **9** in a dose-dependent manner (Fig. 4.9). However, for complex **9**, the IC_{50} value of polymerization of tubulin (ca. 20 μM) is much higher than the IC_{50} of anticancer activity (0.63 μM). It is also noted that an S phase arrest together with G_2/M phase arrest was induced by complex **9**, it suggested another anticancer mechanism involved for complex **9** which should be investigated in the future (Fig. 4.10).

The substitution of hydrogen by fluorine (most electronegative element) is one of the most commonly employed monovalent isosteric replacements (e.g. 5-fluorouracil) to improve the pharmacological properties.[13] The major reason is that fluorine substitution may cause an interaction with a biological target (for example: hydrogen bond) as well as its effect on the metabolism of the drug *in vivo*. Following this design, the osmium complex **9** was developed and showed nanomolar anticancer activity, the mechanism for anti-proliferation is found through cell cycle arrest and apoptosis. The mechanism of action of **9** involves the inhibition of tubulin polymerization. Tubulin is possibly not the only target in this case; more work will be carried out to search for the target(s) of osmium arene

azopyridine complexes with potent anticancer activity. However, complex **9** demonstrated the first example of an organometallic complex which inhibits tubulin polymerization.

4.5 Summary

The synthesis and characterisation of 32 half sandwich azopyridine Os^{II} arene complexes $[Os(\eta^6\text{-arene})(\text{azopyridine})X]^+$ in which X is chloride or iodide, the arene is *p*-cymene or biphenyl and the pyridine and phenyl rings contain a variety of substituents (F, Cl, Br, I, CF_3, OH or NO_2) were reported. Ten X-ray crystal structures have been determined. Cytotoxicity towards A2780 human ovarian cancer cells ranges from high potency at nanomolar concentrations to inactivity. In general the introduction of an electron-withdrawing group (e.g. F, Cl, Br or I) at specific positions on the pyridine ring significantly increases cytotoxic activity and aqueous solubility. Changing the arene from *p*-cymene to biphenyl and the monodentate ligand X from chloride to iodide also increases the activity significantly. Activation by hydrolysis and DNA binding appears not to be the major mechanism of action since both the highly active complex $[Os(\eta^6\text{-bip})(2\text{-F-Azpy})I]PF_6$ (**9**) and the moderately active complex $[Os(\eta^6\text{-bip})(3\text{-Cl-Azpy})I]PF_6$ (**23**) are very stable and inert towards aquation. Studies of octanol/water partition coefficients (log P) and subcellular distributions of osmium in A2780 human ovarian cancer cells suggested that cell uptake and targeting to cellular organelles play important roles in determining activity. Although complex **9** induced the production of reactive oxygen species (ROS) in A2780 cells, the ROS level did not appear to play a role in the mechanism of anticancer activity. This class of organometallic osmium complexes has new and unusual features worthy of further exploration for the design of novel anticancer drugs, their mechanism of action may involve the inhibition of forming microtubules.

4.6 References

1. D. J. W. H. SHEPPEARD, *Rheumatology*, 1980, **19**, 25-29.
2. F. E. Berglof, *Scand. J. Rheumatol.*, 1959, **5**, 70-74.
3. C. J. MENKES, *Rheumatology*, 1979, **18**, 65-77.
4. Platinum, Gold, and Other Metal Chemotherapeutic Agents (ACS symposium series), ed. C. Hinckley, C. N. Bemiller, L. J. E. Strack and L. D. Russell, American Chemical Society, 1983, vol. 209.
5. W.-X. Ni, W.-L. Man, M. T.-W. Cheung, R. W.-Y. Sun, Y.-L. Shu, Y.-W. Lam, C.-M. Che and T.-C. Lau, *Chem. Commun.*, 2011, **47**, 2140-2142.
6. Y. Fu, A. Habtemariam, A. M. Pizarro, S. H. van Rijt, D. J. Healey, P. A. Cooper, S. D. Shnyder, G. J. Clarkson and P. J. Sadler, *J. Med. Chem.*, 2010, **53**, 8192-8196.
7. S. D. Shnyder, Y. Fu, A. Habtemariam, S. H. van Rijt, P. A. Cooper, P. M. Loadman and P. J. Sadler, *Med. Chem. Commun.*, 2011, **2**, 666–668
8. S. J. Dougan, A. Habtemariam, S. E. McHale, S. Parsons and P. J. Sadler, *Proc. Natl. Acad. Sci. U. S. A.*, 2008, **105**, 11628-11633.
9. S. H. van Rijt, A. Mukherjee, A. M. Pizarro and P. J. Sadler, *J. Med. Chem.*, 2009, **53**, 840-849.
10. D. F. Veber, S. R. Johnson, H.-Y. Cheng, B. R. Smith, K. W. Ward and K. D. Kopple, *J. Med. Chem.*, 2002, **45**, 2615-2623.
11. Y. C. Martin, *J. Med. Chem.*, 1981, **24**, 229-237.
12. K. Birchall, V. J. Gillet, P. Willett, P. Ducrot and C. Luttmann, *J. Chem. Inf. Model.*, 2009, **49**, 1330-1346.
13. G. A. Patani and E. J. LaVoie, *Chem. Rev.*, 1996, **96**, 3147-3176.
14. J. E. Liebmann, S. M. Hahn, J. A. Cook, C. Lipschultz, J. B. Mitchell and D. C. Kaufman, *Cancer Res.*, 1993, **53**, 2066-2070.
15. *CrysAlis PRO, Oxford Diffraction Ltd., Abington, Oxfordshire, U.K., 2007.*

16. G. M. Sheldrick, Acta Crystallogr., Sect. A: Found. Crystallogr., 1990, **46**, 467–473

17. G. M. Sheldrick, SHELX97, Programs for Crystal Structure Analysis (Release 97-92), University of Göttingen, Germany, 1997.

18. V. Vichai and K. Kirtikara, *Nat. Protocols*, 2006, **1**, 1112-1116.

19. S. H. van Rijt, A. J. Hebden, T. Amaresekera, R. J. Deeth, G. J. Clarkson, S. Parsons, P. C. McGowan and P. J. Sadler, *J. Med. Chem.*,2009, **52**, 7753-7764.

20. M. J. McKeage, S. J. Berners-Price, P. Galettis, R. J. Bowen, W. Brouwer, L. Ding, L. Zhuang and B. C. Baguley, *Cancer Chemother. Pharmacol*.,2000, **46**, 343-350.

21. B. Halliwell and M. Whiteman, *Br. J. Pharmacol.*, 2004, **142**, 231-255.

22. H. Wang and J. A. Joseph, *Free Radical Biol. Med.*, 1999, **27**, 612-616.

23. A. Gomes, E. Fernandes and J. L. F. C. Lima, *J. Biochem. Biophys. Methods*, 2005, **65**, 45-80.

24. R. F. Ozols, K. G. Louie, J. Plowman, B. C. Behrens, R. L. Fine, D. Dykes and T. C. Hamilton, *Biochem. Pharmacol*., 1987, **36**, 147-153.

25. O. I. Aruoma, B. Halliwell, B. M. Hoey and J. Butler, *Free Radical Biol. Med*., 1989, **6**, 593-597.

26. S. J. Dougan, M. Melchart, A. Habtemariam, S. Parsons and P. J. Sadler, *Inorg. Chem.*, 2006, **45**, 10882-10894.

27. C. A. Hunter and J. K. M. Sanders, *J. Am. Chem. Soc*., 1990, **112**, 5525-5534.

28. O. Novakova, H. Chen, O. Vrana, A. Rodger, P. J. Sadler and V. Brabec, *Biochemistry*, 2003, **42**, 11544-11554.

29. W. Hu, Q. Luo, X. Ma, K. Wu, J. Liu, Y. Chen, S. Xiong, J. Wang, P. J. Sadler and F. Wang, *Chem.--Eur. J.*, 2009, **15**, 6586-6594.

30. D. Trachootham, J. Alexandre and P. Huang, *Nat. Rev. Drug Discov.*, 2009, **8**, 579-591.

31. L. K. Hosking, R. D. H. Whelan, S. A. Shellard, P. Bedford and B. T. Hill, *Biochem. Pharmacol*., 1990, **40**, 1833-1842.

32. Z. H. Siddik, *Oncogene*, **22**, 7265-7279.

33. H. H. Bailey, R. T. Mulcahy, K. D. Tutsch, R. Z. Arzoomanian, D. Alberti, M. B. Tombes, G. Wilding, M. Pomplun and D. R. Spriggs, *J. Clin. Oncol.*, 1994, **12**, 194-205.

34. T. C. Hamilton, M. A. Winker, K. G. Louie, G. Batist, B. C. Behrens, T. Tsuruo, K. R. Grotzinger, W. M. McKoy, R. C. Young and R. F. Ozols, *Biochem. Pharmacol*., 1985, **34**, 2583-2586.

35. H. Maeda, S. Hori, H. Ohizumi, T. Segawa, Y. Kakehi, O. Ogawa and A. Kakizuka, *Cell Death Differ.*, 2004, **11**, 737-746.

36. R. E. Morris, R. E. Aird, P. del Socorro Murdoch, H. Chen, J. Cummings, N. D. Hughes, S. Parsons, A. Parkin, G. Boyd, D. I. Jodrell and P. J. Sadler, *J. Med. Chem.*, 2001, **44**, 3616-3621.

37. E. A. Meyer, R. K. Castellano and F. o. Diederich, *Angew. Chem., Int. Ed.*, 2003, **42**, 1210-1250.

38. J. A. Platts, D. E. Hibbs, T. W. Hambley and M. D. Hall, *J. Med. Chem.*, 2000, **44**, 472-474.

39. M. Groessl, E. Reisner, C. G. Hartinger, R. Eichinger, O. Semenova, A. R. Timerbaev, M. A. Jakupec, V. B. Arion and B. K. Keppler, *J. Med. Chem.*, 2007, **50**, 2185-2193.

40. F. Yu, J. Megyesi and P. M. Price, *Am. J. Physiol.: Renal Physiol.*, 2008, **295**, F44-52.

41. E. R. Jamieson and S. J. Lippard, *Chem. Rev.*, 1999, **99**, 2467-2498.

42. J. R. Jackson, D. R. Patrick, M. M. Dar and P. S. Huang, *Nat. Rev. Cancer.*, 2007, **7**, 107-117.

43. I. E. L. M. Kuppens, *Curr. Clin. Pharmacol.*, 2006, **1**, 57-70.

44. T. Beckers, T. Reissmann, M. Schmidt, A. M. Burger, H. H. Fiebig, U. Vanhoefer, H. Pongratz, H. Hufsky, J. Hockemeyer, M. Frieser and S. Mahboobi, *Cancer Res.*, 2002, **62**, 3113-3119.

45. J.-D. Jiang, L. Denner, Y.-H. Ling, J.-N. Li, A. Davis, Y. Wang, Y. Li, J. Roboz, L.-G. Wang, R. Perez-Soler, M. Marcelli, G. Bekesi and J. F. Holland, *Cancer Res.*, 2002, **62**, 6080-6088.

46. A. Wienecke and G. Bacher, *Cancer Res.*, 2009, **69**, 171-177.

47. J.-D. Jiang, A. S. Davis, K. Middleton, Y.-H. Ling, R. Perez-Soler, J. F. Holland and J. G. Bekesi, *Cancer Res.*, 1998, **58**, 5389-5395.

48. A. M. McElligott, E. N. Maginn, L. M. Greene, S. McGuckin, A. Hayat, P. V. Browne, S. Butini, G. Campiani, M. A. Catherwood, E. Vandenberghe, D. C. Williams, D. M. Zisterer and M. Lawler, *Cancer Res.*, 2009, **69**, 8366-8375.

49. K. V. Kong, W. K. Leong and L. H. K. Lim, *Chem. Res. Toxicol.*, 2009, **22**, 1116-1122.

Chapter 5
Os^{II} Arene Iminopyridine Complexes

5.1 Introduction

Recently, non-organometallic osmium (VI) complexes were reported to show good anticancer activity *in vivo*.[1] Certain half-sandwich organometallic iodido osmium (II) arene azopyridine complexes were also found to exhibit potent *in vitro* and *in vivo* anticancer activity (Chapter 2).[2, 3] The mechanism of action is different from that found previously for osmium(II) arene picolinate complexes which can hydrolyze and then bind to DNA bases,[4] with DNA believed to be the target as is it for cisplatin.[5, 6]

Anticancer agents which target DNA will encounter an activated DNA repair system which is driven by ATP energy.[7] Reduced nicotinamide adenine dinucleotide (NADH) is an important intermediate for energy metabolism (through glycolysis and mitochondrial respiration[8]) and is therefore vital for DNA-damage repair. Therefore, the depletion of NADH may have severe effects on the bioenergetics of cells. NADH is not only an important intermediate in mitochondrial respiration and glycolysis which can provide energy for cancer cells, but also together with nicotinamide adenine dinucleotide (NAD^+) is a part of redox balance system.[9] Under physiological conditions, the ratio of free [NADH]/[NAD^+] in cells is very low (in Hela cells, it was found to be 0.0016) and the free NADH has cellular concentration in the range of nano molar,[10] which makes it a potential target in cancer cells.

Early work by Steckhan's group[11] and Fish's group[12] reported on an economical process for regeneration of NADH from NAD^+ by rhodium catalysts. In previous work from Sadler's group, ruthenium arene anticancer complexes were found to regioselectively reduce NAD^+ to NADH through hydrogenation transfer under physiological conditions in the presence of formate as hydride donor.[13] Though osmium is in the same group of ruthenium, no osmium complexes have been reported to catalytically react with NAD^+ or NADH to the best of my knowledge.

There are some intriguing differences between the chemical properties of organometallic Ru^{II} and Os^{II} arene complexes even though their three-dimensional structures can be almost identical.[14] For example, osmium complexes are often considered to be relatively inert (a common characteristic of low-spin d^6 metal ions and especially 3rd row transition metals).[4, 15] Probably due to the intriguing difference between ruthenium and osmium, several organometallic osmium anticancer complexes have been designed based on their ruthenium analogues.[6, 16]

However, the osmium complexes in this chapter were not designed based on the work on ruthenium.[2] Osmium(II) arene azopyridine complexes [Os(η^6-arene)(Azpy-R)X]PF_6 (arene = biphenyl, *p*-cymene; X= Cl, I) were found to show anticancer activity in nanomolar range *in vitro*,[2] and resulted in the first organometallic osmium complex ([Os(η^6-*p*-cym)(Azpy-NMe_2)I]PF_6, **FY026**) showing anticancer activity *in vivo*.[3] An efficient approach to the study of the anticancer activity[17] of osmium arene complexes employed here uses bioisosterism, which is a term coined to describe the wide application of modifying biological activity by isosterism. The different biological behaviours achieved by changing from the azo bond (N=N) to the imine bond (C=N) on the osmium arene azopyridine complexes are explored. With this aim, derivatives of osmium arene complexes containing iminopyridine as the N, N-chelating ligand were prepared and the iodido and chlorido analogues of **FY026** were mainly studied in this chapter. The results indicate higher anticancer activity for the iminopyridine complexes which also show good anticancer activity in the NCI 60 cell lines screen. Additionally, unlike the azopyridine complexes, the iminopyridine complexes do not only undergo hydrolysis and then bind with 9-ethylguanine, but also they can catalytically oxidize NADH to NAD^+. For that reason, the combination of both processes could contribute to the enhanced anticancer activity of these complexes. It is therefore conceivable to develop a strategy to combine both the nucleobase binding capability with NADH oxidizing ability in one compound to improve its anticancer activity.

5.2 Experimental

5.2.1 Synthesis of Iminopyridine ligands. Syntheses of iminopyridine ligand were based on literature reports.[18]

5.2.2 Syntheses of Osmium Iminopyridine Complexes

(1) [Os(η^6-bip)(Impy)I]PF_6. $[Os(\eta^6\text{-bip})I_2]_2$ (50.0 mg, 0.042 mmol) was dissolved in methanol (30 mL) at 353 K. Ligand Impy (15.3mg, 0.84 mmol) in methanol (10 mL) was added drop-wise, the solution-colour changed from orange to red immediately. The solution was stirred at 353 K for 3 h. The volume was reduced to about 10 mL by removal of methanol on a rotary evaporator, and ammonium hexafluorophosphate (27.4 mg. 0.17 mmol) was added. Then the solution was left in the freezer (253K) for 24 h. Dark coloured powder was precipitated which was collected by filtration, washed with cold ethanol and diethyl ether, then finally dried in vacuum. Yield: 51.0 mg (78.1%) ESI-MS Calcd for $C_{24}H_{20}IN_2Os$: m/z 655.0, found 655.3. ^{1}H NMR($(CD_3)_2CO$): δ 9.38 (d, 1H, J=5 Hz), 9.19 (s, 1 H), 8.55 (d, 1H, J=8 Hz), 8.25 (t, 1H, J=8 Hz), 7.70 (d, 2H, J=9 Hz),7.55-7.48 (m, 7H). 7.40 (d, 2H, J=9 Hz), 6.68 (d, 1H, J=6 Hz), 6.63 (t, 1H, J=6 Hz), 6.58 (t, 1H, J=6 Hz), 6.47 (t, 1H, J=6 Hz),), 6.34 (t, 1H, J=6 Hz), CHN analysis: Found: C 34.91%, H 2.41%, N 3.34%. Calcd. for $C_{24}H_{20}F_6IN_2OsP$: C 36.10%, H 2.52%, N 3.51%.

(2) [Os(η^6-p-cym)(Impy)I]PF_6. $[Os(\eta^6\text{-}p\text{-cym})I_2]_2$ (30.0 mg, 0.026 mmol) was dissolved in methanol (20 mL) at 313 K. Ligand Impy (9.4mg, 0.052 mmol) in methanol (10 mL) was added drop-wise, the solution-colour changed from orange to red immediately. The solution was stirred at ambient temperature for 2 h. The volume was reduced to about 10 mL by removal of methanol on a rotary evaporator, and ammonium hexafluorophosphate (17.0 mg. 0.1 mmol) was added. Then the solution was left in the freezer (253K) for 24 h. Dark coloured powder was precipitated which was collected by filtration, washed with cold ethanol and diethyl ether, then finally dried in vacuum. Yield: 30.2 mg (74.8 %). ESI-MS

Calcd for $C_{22}H_{24}IN_2Os$: m/z 635.1, found 635.0. ^{1}H NMR($(CD_3)_2CO$): δ 9.65 (d, 1H, J=6 Hz), 9.31 (s, 1 H), 8.59 (d, 1H, J=8 Hz), 8.32 (t, 1H, J=8 Hz), 7.97-7.95 (m, 2H), 7.86 (t, 1H, J=8 Hz), 7.68-7.65 (m, 2H), 6.37 (d, 1H, J=8 Hz), 6.08 (d, 1H, J=6 Hz), 5.98 (d, 1H, J=6 Hz), 5,83 (d, 1H, J=6 Hz), 2.81 (s, 3H), 2.75-2.68 (m, 1H), 2.63 (s, 6H), 1.09 (d, 3H, J=7 Hz) 1.07 (d, 3H, J=7 Hz). CHN analysis: Found: C, 34.29%; H, 3.10%; N, 3.57%. Calcd for $C_{22}H_{24}F_6IN_2OsP$: C, 33.94% H, 3.11% N, 3.60%.

(3) [Os(η^6-bip)(Impy-OH)I]PF_6. [Os(η^6-bip)I_2]$_2$ (50.0 mg, 0.042 mmol) was dissolved in methanol (30 mL) and water (10 mL) mixture at 353 K. Ligand Impy-OH (16.6 mg, 0.084mmol) in methanol (10 mL) was added drop-wise, The solution was stirred at 353 K for 4 h. The volume was reduced to about 10 mL by removal of methanol on a rotary evaporator, and ammonium hexafluorophosphate (52.2 mg. 0.32 mmol) was added. Then the solution was left in the fridge (277K) for 24 h. Dark coloured powder was precipitated which was collected by filtration, washed with cold ethanol and diethyl ether, then finally dried in vacuum. Yield: 29.0 mg (17.2 %). ESI-MS Calcd for $C_{22}H_{24}IN_2OOs$: m/z 651.0, found 651.0. ^{1}H NMR($(CD_3)_2CO$): δ 9.37 (d, 1H, J=6 Hz), 9.10 (s, 1 H), 8.49 (d, 1H, J=8 Hz), 8.20 (t, 1H, J=8 Hz), 7.66 (t, 1H, J=9 Hz),7.59 (d, 2H, J=8 Hz), 7.49-7.41 (m, 5H), 6.91 (d, 2H, J=9 Hz), 6.89 (d, 1H, J=6 Hz), 6.65 (t, 1H, J=6 Hz), 6.55 (d, 1H, J=6 Hz), 6.48 (t, 1H, J=6 Hz), 6.34 (t, 1H, J=6 Hz), CHN analysis: Found: C, 34.92%; H, 2.65%; N, 3.29%. Calcd for $C_{22}H_{24}F_6IN_2OOsP$: C, 35.39% H, 2.47% N, 3.44%.

(4) [Os(η^6-p-cym)(Impy-OH)I]PF_6. [Os(η^6-*p*-cym)I_2]$_2$ (50.0 mg, 0.043 mmol) was dissolved in methanol (30 mL) at 313 K. Ligand Impy-OH (17.1 mg, 0.086 mmol) in methanol (10 mL) was added drop-wise, the solution-colour changed from orange to red immediately. The solution was stirred at ambient temperature for 48 h. The volume was reduced to about 10 mL by removal of methanol on a rotary evaporator, and ammonium hexafluorophosphate (26.1 mg. 0.16 mmol)

was added. Then the solution was left in the freezer (253K) for 24 h. Dark coloured powder was precipitated which was collected by filtration, washed with cold ethanol and diethyl ether, then finally dried in vacuum. Yield: 43.7 mg (64.0 %). ESI-MS Calcd for $C_{22}H_{24}IN_2OOs$: m/z 651.0, found 651.1. ^1H NMR($(CD_3)_2CO$): δ 9.61 (d, 1H, J=5 Hz), 9.22 (s, 1 H), 8.51 (d, 1H, J=7 Hz), 7.85(t, 1H, J=6 Hz), 7.80 (t, 1H, J=7 Hz), 7.07 (d, 2H, J=9 Hz), 6.40 (d, 1H, J=6 Hz),, 6.07 (d, 1H, J=6 Hz), 5.97 (d, 1H, J=6 Hz), 5.88 (d, 1H, J=6 Hz), 5.66 (s, 1H), 2.81 (s, 3H), 2.74-2.66 (m, 1H), 2.09 (s, 6H), 1.13 (d, 3H, J=7 Hz) 1.09 (d, 3H, J=7 Hz).. CHN analysis: Found: C, 33.01%; H, 3.15%; N, 3.41%. Calcd for $C_{22}H_{24}F_6IN_2OOsP$: C, 33.26% H, 3.04% N, 3.53%. Crystals for X-ray diffreaction were obtained by crystallization of a concentrated solution of [(η^6-p-cym)Os(Impy-OH)I]PF_6 in a mixture of DCM and MeOH at 253K.

(5) [Os(η^6-bip)(Impy-NMe_2)I]PF_6. [Os(η^6-bip)I_2]$_2$ (50.0 mg, 0.042 mmol) was dissolved in methanol (30 mL) at 353 K. Ligand Impy-NMe_2 (18,8mg, 0.84 mmol) in methanol (10 mL) was added drop-wise, the solution-colour changed from orange to red immediately. The solution was stirred at 353K for 4 h. The volume was reduced to about 10 mL by removal of methanol on a rotary evaporator, and ammonium hexafluorophosphate (27.3 mg. 0.17 mmol) was added. Then the solution was left in the freezer (253K) for 24 h. red coloured powder was precipitated which was collected by filtration, washed with cold ethanol and diethyl ether, then finally dried in vacuum. Yield: 35.1 mg (49.8 %). ESI-MS Calcd for $C_{26}H_{25}IN_3Os$: m/z 698.1, found 698.1. ^1H NMR($(CD_3)_2CO$): δ 9.29 (d, 1H, J=5 Hz), 9.02 (s, 1 H), 8.42 (d, 1H, J=8 Hz), 8.18 (t, 1H, J=8 Hz), 7.65 (d, 2H, J=9 Hz), 7.51-7.38 (m, 7H). 6.88 (d, 1H, J=6 Hz), 6.74 (d, 2H, J=9 Hz), 6.62 (t, 1H, J=6 Hz), 6.55 (d, 1H, J=6 Hz), 6.50 (t, 1H, J=6 Hz), 6.34 (t, 1H, J=6 Hz), CHN analysis: Found: C, 41.54%; H, 3.31%; N, 5.61%. Calcd for $C_{24}H_{29}ClF_6N_3OsP$: C, 41.63% H, 3.36% N, 5.60%.

(6) [Os(η^6-*p*-cym)(Impy-NMe$_2$)I]PF$_6$. [Os(η^6-*p*-cym)I$_2$]$_2$ (50.0 mg, 0.043 mmol) was dissolved in methanol (30 mL) at 313 K. Ligand Impy-NMe$_2$ (19.5mg, 0.086 mmol) in methanol (10 mL) was added drop-wise, the solution-colour changed from orange to red immediately. The solution was stirred at ambient temperature for 2 h. The volume was reduced to about 10 mL by removal of methanol on a rotary evaporator, and ammonium hexafluorophosphate (141.8 mg. 0.87 mmol) was added. Then the solution was left in the freezer (253K) for 24 h. Dark coloured powder was precipitated which was collected by filtration, washed with cold ethanol and diethyl ether, then finally dried in vacuum. Yield: 50.7 mg (72.9 %). ESI-MS Calcd for $C_{24}H_{28}IN_3Os$: m/z 678.1, found 678.0. ^{1}H NMR($(CD_3)_2CO$): δ 9.55 (d, 1H, J=5 Hz), 9.12 (s, 1 H), 8.45 (d, 1H, J=7 Hz), 8.24 (t, 1H, J=7 Hz), 7.83 (d, 2H, J=9 Hz), 7.73 (t, 1H, J=5 Hz), 6.89 (d, 2H, J=9 Hz), 6.38 (d, 1H, J=6 Hz), 6.04 (d, 1H, J=6 Hz), 5.92-5.87 (m, 2H), 3.15 (s, 6H), 2.65 (s, 3H), 2.21-2.13 (m, 1H), 1.09 (d, 3H, J=6 Hz) 1.07 (d, 3H, J=6 Hz). CHN analysis: Found: C, 34.53%; H, 3.36%; N, 5.06%. Calcd for $C_{24}H_{28}F_6IN_3OsP$: C, 35.08% H, 3.56% N, 5.11%.

(7) [Os(η^6-bip)(OMe-Impy-NMe$_2$)I]PF$_6$. [Os(η^6-bip)I$_2$]$_2$ (50.0 mg, 0.042 mmol) was dissolved in methanol (30 mL) and water (10 mL) mixture at 353 K. Ligand OMe-Impy-NMe$_2$ (21.3 mg, 0.84 mmol) in methanol (10 mL) was added drop-wise, the solution-colour changed from orange to red immediately. The solution was stirred at 353K for 4 h. The volume was reduced to about 10 mL by removal of methanol on a rotary evaporator, and ammonium hexafluorophosphate (27.3 mg. 0.17 mmol) was added. Then the solution was left in the freezer (253K) for 24 h. red coloured powder was precipitated which was collected by filtration, washed with cold ethanol and diethyl ether, then finally dried in vacuum. Yield: 18.0 mg (24.0 %). ESI-MS Calcd for $C_{27}H_{27}IN_3OOs$: m/z 728.08, found 727.9. ^{1}H NMR($(CD_3)_2CO$): δ 9.00 (s, 1H), 8.18 (t, 1H, J=8 Hz), 7.99 (d, 1H, J=8 Hz), 7.60 (d, 2H, J=9 Hz), 7.49-7.39 (m, 5H), 7.34 (d, 1H, J=8 Hz), 6.91 (d, 1H, J=6 Hz),

6.74 (d, 2H, J=9 Hz), 6.56 (d, 1H, J=6 Hz), 6.51 (d, 1H, J=6 Hz), 6.48 (d, 1H, J=6 Hz), 6.21 (d, 1H, J=6 Hz), 4.10 (s, 3H), 3.12 (s, 6H), CHN analysis: Found: C, 37.17%; H, 2.98%; N, 5.04%. Calcd for $C_{27}H_{27}F_6IN_3OOsP$: C, 37.21% H, 3.12% N, 4.82%.

(8) [Os(η^6-*p*-cym)(OMe-Impy-NMe$_2$)I]PF$_6$. [Os(η^6-*p*-cym)I$_2$]$_2$ (50.0 mg, 0.043 mmol) was dissolved in methanol (30 mL) at 313 K. Ligand OMe-Impy-NMe$_2$ (22.0 mg, 0.086 mmol) in methanol (10 mL) was added drop-wise, the solution-colour changed from orange to red immediately. The solution was stirred at ambient temperature for 2 h. The volume was reduced to about 10 mL by removal of methanol on a rotary evaporator, and ammonium hexafluorophosphate (28.0 mg. 0.172 mmol) was added. Then the solution was left in the freezer (253K) for 24 h. Dark coloured powder was precipitated which was collected by filtration, washed with cold ethanol and diethyl ether, then finally dried in vacuum. Yield: 35.2 mg (49.2 %). ESI-MS Calcd for $C_{25}H_{31}IN_3OOs$: m/z 708.1, found 708.0. ^{1}H NMR($(CD_3)_2CO$): δ 9.10 (s, 1 H), 8.23 (t, 1H, J=8 Hz), 8.03 (d, 1H, J=8 Hz), 7.83 (d, 2H, J=8 Hz), 7.64 (d, 1H, J=8 Hz), 6.89 (d, 2H, J=8 Hz), 6.51 (d, 1H, J=6 Hz), 5.96 (d, 1H, J=6 Hz), 5.91(d, 1H, J=6 Hz), 5.75 (d, 1H, J=6 Hz), 4.40 (s, 3H), 3.16 (s, 6H), 2.84 (s, 3H), 2.70-2.61 (m, 1H), 1.11 (d, 3H, J=6 Hz) 1.09 (d, 3H, J=6 Hz).. CHN analysis: Found: C 35.20%, H 3.61%, N 5.01%. Calcd for $C_{25}H_{31}F_6IN_3OOsP$: C, 35.26 % H, 3.67 % N, 4.93 %.

(9) [Os(η^6-bip)(Impy)Cl]PF$_6$. [Os(η^6-bip)Cl$_2$]$_2$ (50.0 mg, 0.060 mmol) was dissolved in methanol (30 mL) at 353 K. Ligand Impy (21.9mg, 0.12 mmol) in methanol (10 mL) was added drop-wise, the solution-colour changed from orange to red immediately. The solution was stirred at 353 K for 4 h. The volume was reduced to about 10 mL by removal of methanol on a rotary evaporator, and ammonium hexafluorophosphate (39.1 mg. 0.24 mmol) was added. Then the solution was left in the freezer (253K) for 24 h. Dark coloured powder was precipitated which was collected by filtration, washed with cold ethanol and

diethyl ether, then finally dried in vacuum. Yield: 64.0 mg (75.3 %). ESI-MS Calcd for $C_{24}H_{20}ClN_2Os$: m/z 563.1, found 563.0. ^{1}H NMR($(CD_3)_2CO$): δ 9.42 (d, 1H, J=5 Hz), 9.28 (s, 1 H), 8.53 (d, 1H, J=8 Hz), 8.34 (t, 1H, J=8 Hz), 7.80 (t, 1H, J=8 Hz), 7.62 (d, 2H, J=9 Hz), 7.58(d, 2H, J=9 Hz), 7.54-7.45 (m, 6H). 6.71 (d, 1H, J=6 Hz), 6.45 (d, 1H, J=6 Hz), 5.45-5.40 (m, 2H). 6.36 (t, 1H, J=6 Hz), CHN analysis: Found: C, 40.77%; H, 2.79%; N, 3.91%. Calcd for $C_{24}H_{20}ClF_6N_2OsP$: C, 40.77% H, 2.85% N, 3.96%.

(10) [Os(η^6-*p*-cym)(Impy)Cl]PF$_6$. [Os(η^6-*p*-cym)Cl$_2$]$_2$ (30.0 mg, 0.042 mmol) was dissolved in methanol (30 mL) at 313 K. Ligand Impy (15.2mg, 0.085 mmol) in methanol (10 mL) was added drop-wise, the solution-colour changed from yellow to red immediately. The solution was stirred at ambient temperature for 2 h. The volume was reduced to about 10 mL by removal of methanol on a rotary evaporator, and ammonium hexafluorophosphate (27.6 mg. 0.17 mmol) was added. Then the solution was left in the freezer (253K) for 24 h. Dark coloured powder was precipitated which was collected by filtration, washed with cold ethanol and diethyl ether, then finally dried in vacuum. Yield: 27.4 mg (77.4%). ESI-MS Calcd for $C_{22}H_{24}ClN_2Os$: m/z 543.1, found 543.1. ^{1}H NMR($(CD_3)_2CO$): δ 9.63 (d, 1H, J=6 Hz), 9.37 (s, 1 H), 8.54 (d, 1H, J=8 Hz), 8.37 (t, 1H, J=8 Hz), 7.90 (d, 2H, J=9 Hz), 7.66 (d, 2H, J=8 Hz), 7.86 (d, 2H, J=8 Hz), 6.44 (d, 1H, J=6 Hz), 6.02 (d, 1H, J=6 Hz), 5,96 (d, 1H, J=6 Hz), 5,79 (d, 1H, J=6 Hz), 2.79 (s, 3H), 2.69-2.55 (m, 1H), 2.39 (s, 6H), 1.09 (d, 3H, J=7 Hz) 1.07 (d, 3H, J=7 Hz). CHN analysis: Found: C 38.44%, H 3.38%, N 4.06% Calcd. for $C_{22}H_{24}ClF_6N_2OsP$: C 38.46%, H 3.52%, N 4.08%.

(11) [Os(η^6-bip)(Impy-OH)Cl]PF$_6$. [Os(η^6-bip)Cl$_2$]$_2$ (50.0 mg, 0.060 mmol) was dissolved in methanol (20 mL) and water (10 mL) mixture at 353 K. Ligand Impy-OH (23.8mg, 0.012mmol) in methanol (10 mL) was added drop-wise, The solution was stirred at 353 K for 4 h. The volume was reduced to about 10 mL by removal of methanol on a rotary evaporator, and ammonium hexafluorophosphate

(97.8 mg. 0.6 mmol) was added. Then the solution was left in the freezer (253K) for 24 h. Dark coloured powder was precipitated which was collected by filtration, washed with cold ethanol and diethyl ether, then finally dried in vacuum. Yield: 15.3 mg (17.2 %). ESI-MS Calcd for $C_{24}H_{20}ClN_2OOs$: m/z 579.1, found 579.0. ^{1}H NMR($(CD_3)_2CO$): δ 9.36 (d, 1H, J=6 Hz), 9.18 (s, 1 H), 8.47 (d, 1H, J=8 Hz), 8.29 (t, 1H, J=8 Hz), 7.76 (t, 1H, J=9 Hz),7.58 (d, 2H, J=8 Hz), 7.54-7.43 (m, 5H), 6.92 (d, 2H, J=9 Hz), 6.74 (d, 1H, J=6 Hz), 6.64 (d, 1H, J=6 Hz), 6.45 (t, 1H, J=6 Hz), 6.42 (t, 1H, J=6 Hz), 6.35 (t, 1H, J=6 Hz), CHN analysis: Found: C, 39.44%; H, 2.84%; N, 3.71%. Calcd for $C_{24}H_{20}ClF_6N_2OOsP$: C, 39.87% H, 2.79% N, 3.87%.

(12) [Os(η^6-p-cym)(Impy-OH)Cl]PF$_6$. [Os(η^6-*p*-cym)Cl$_2$]$_2$ (50.0 mg, 0.063 mmol) was dissolved in methanol (30 mL) at 313 K. Ligand Impy-OH (25.0 mg, 0.12 mmol) in methanol (10 mL) was added drop-wise, the solution-colour changed from orange to red immediately. The solution was stirred at ambient temperature for 2 h. The volume was reduced to about 10 mL by removal of methanol on a rotary evaporator, and ammonium hexafluorophosphate (41.2 mg. 0.25 mmol) was added. Then the solution was left in the freezer (253K) for 24 h. Dark coloured powder was precipitated which was collected by filtration, washed with cold ethanol and diethyl ether, then finally dried in vacuum. Yield: 53.8 mg (63.7 %). ESI-MS Calcd for $C_{22}H_{24}ClN_2OOs$: m/z 559.1, found 559.1. ^{1}H NMR($(CD_3)_2CO$): δ 9.60 (d, 1H, J=5 Hz), 9.35 (s, 1 H), 8.50 (d, 1H, J=7 Hz), 8.34 (t, 1H, J=7 Hz), 7.84(t, 1H, J=6 Hz), 7.75 (d, 2H, J=9 Hz), 7.08 (d, 2H, J=9 Hz), 6.46 (d, 1H, J=6 Hz), 6.00 (d, 1H, J=6 Hz), 5.84 (d, 1H, J=6 Hz), 2.81 (s, 3H), 2.65-2.55 (m, 1H), 2.41 (s, 6H), 1.10 (d, 3H, J=7 Hz) 1.08 (d, 3H, J=7 Hz). CHN analysis: Found: C, 37.82%; H, 3.33%; N, 3.91%. Calcd for $C_{22}H_{24}ClF_6N_2OOsP$: C, 37.58% H, 3.44% N, 3.98%.

(13) [Os(η^6-bip)(Impy-NMe$_2$)Cl]PF$_6$. [Os(η^6-bip)Cl$_2$]$_2$ (50.0 mg, 0.060 mmol) was dissolved in methanol (20 mL) at 313 K. Ligand Impy-NMe$_2$ (27.1mg, 0.12

mmol) in methanol (10 mL) was added drop-wise, the solution-colour changed from orange to red immediately. The solution was stirred at 353K for 12 h. The volume was reduced to about 10 mL by removal of methanol on a rotary evaporator, and ammonium hexafluorophosphate (39.1 mg. 0.24 mmol) was added. Then the solution was left in the freezer for 24 h. red coloured powder was precipitated which was collected by filtration, washed with cold ethanol and diethyl ether, then finally dried in vacuum. Yield: 52.0 mg (57.8 %). ESI-MS Calcd for $C_{24}H_{20}ClN_2Os$: m/z 563.1, found 563.0. ^{1}H NMR($(CD_3)_2CO$): δ 9.31 (d, 1H, J=5 Hz), 9.09 (s, 1 H), 8.39 (d, 1H, J=8 Hz), 8.25 (t, 1H, J=8 Hz), 7.70 (t, 1H, J=9 Hz),7.61-7.44 (m, 7H). 6.77 (d, 2H, J=9 Hz), 6.74 (d, 1H, J=6 Hz), 6.62 (d, 1H, J=6 Hz), 6.63-6.45 (m, 2H), 6.34 (t, 1H, J=6 Hz), CHN analysis: Found: C, 41.54%; H, 3.31%; N, 5.61%. Calcd for $C_{24}H_{20}ClF_6N_2OsP$: C, 41.63% H, 3.36% N, 5.60%.

(14) [Os(η^6-*p*-cym)(Impy-NMe_2)Cl]PF_6. [Os(η^6-*p*-cym)Cl_2]$_2$ (50.0 mg, 0.063 mmol) was dissolved in methanol (30 mL) at 313 K. Ligand Impy-NMe_2 (28.5mg, 0.126 mmol) in methanol (10 mL) was added drop-wise, the solution-colour changed from orange to red immediately. The solution was stirred at ambient temperature for 2 h. The volume was reduced to about 10 mL by removal of methanol on a rotary evaporator, and ammonium hexafluorophosphate (41.2 mg. 0.253 mmol) was added. Then the solution was left in the freezer for 24 h. Dark coloured powder was precipitated which was collected by filtration, washed with cold ethanol and diethyl ether, then finally dried in vacuum. Yield: 67.2 mg (85.6 %). ESI-MS Calcd for $C_{24}H_{29}ClN_3Os$: m/z 586.2, found 586.1. ^{1}H NMR($(CD_3)_2CO$): δ 9.55 (d, 1H, J=5 Hz), 9.20 (s, 1 H), 8.44 (d, 1H, J=7 Hz), 8.31 (t, 1H, J=7 Hz), 7.82(t, 1H, J=6 Hz), 7.76 (d, 2H, J=9 Hz), 6.92 (d, 2H, J=9 Hz), 6.44 (d, 1H, J=6 Hz), 6.04 (d, 1H, J=6 Hz), 5.97 (d, 1H, J=6 Hz), 5.85 (d, 1H, J=6 Hz), 3.16 (s, 6H), 2.42 (s, 3H), 2.21-2.11 (m, 1H), 1.09 (d, 3H, J=7 Hz) 1.07

(d, 3H, J=7 Hz). CHN analysis: Found: C 39.43%, H 3.89%, N 5.75%. Calcd. for $C_{24}H_{29}ClF_6N_3OsP$: C 39.48%, H 4.00%, N 5.75%.

(15) [Os(η^6-bip)(OMe-Impy-NMe$_2$)Cl]PF$_6$. [Os(η^6-bip)Cl$_2$]$_2$ (50.0 mg, 0.060 mmol) was dissolved in methanol (20 mL) and water (10 mL) at 313 K. Ligand OMe-Impy-NMe$_2$ (30.6 mg, 0.12 mmol) in methanol (10 mL) was added drop-wise, the solution-colour changed from orange to red immediately. The solution was stirred at 353K for 12 h. The volume was reduced to about 10 mL by removal of methanol on a rotary evaporator, and ammonium hexafluorophosphate (39.1 mg. 0.24 mmol) was added. Then the solution was left in the freezer (253K) for 24 h. red coloured powder was precipitated which was collected by filtration, washed with cold ethanol and diethyl ether, then finally dried in vacuum. Yield: 72.1 mg (77.0 %). ESI-MS Calcd for $C_{27}H_{27}ClN_3OOs$: m/z 636.2, found 636.0. ^{1}H NMR($(CD_3)_2CO$): δ 9.00 (s, 1H), 8.24 (t, 1H, J=8 Hz), 7.95 (d, 1H, J=8 Hz), 7.60-7.56 (m, 5H), 7.50-7.41 (m, 5H), 6.77 (d, 2H, J=9 Hz), 6.60 (d, 1H, J=6 Hz), 6.37-6.32 (m, 2H), 4.14 (s, 3H), 3.12 (s, 6H), CHN analysis: Found: C, 41.04%; H, 3.32%; N, 5.28%. Calcd for $C_{27}H_{27}ClF_6N_3OOsP$: C, 41.57 % H, 3.49 % N, 5.39 %.

(16) [Os(η^6-*p*-cym)(OMe-Impy-NMe$_2$)Cl]PF$_6$. [Os(η^6-*p*-cym)Cl$_2$]$_2$ (50.0 mg, 0.063 mmol) was dissolved in methanol (30 mL) at 313 K. Ligand OMe-Impy-NMe$_2$ (32.2 mg, 0.126 mmol) in methanol (10 mL) was added drop-wise, the solution-colour changed from orange to red immediately. The solution was stirred at ambient temperature for 2 h. The volume was reduced to about 10 mL by removal of methanol on a rotary evaporator, and ammonium hexafluorophosphate (41.2 mg. 0.253 mmol) was added. Then the solution was left in the freezer (253K) for 24 h. Dark coloured powder was precipitated which was collected by filtration, washed with cold ethanol and diethyl ether, then finally dried in vacuum. Yield: 58.7 mg (61.3 %). ESI-MS Calcd for $C_{25}H_{31}ClN_3OOs$: m/z 616.2, found 616.0. ^{1}H NMR($(CD_3)_2CO$): δ 9.10 (s, 1 H), 8.25 (t, 1H, J=8 Hz), 7.98 (d,

1H, J=8 Hz), 7.72 (d, 2H, J=8 Hz), 7.53 (d, 1H, J=8 Hz), 6.90 (d, 2H, J=8 Hz), 6.54 (d, 1H, J=6 Hz), 5.98 (d, 1H, J=6 Hz), 5.82 (dd, 2H, J=6 Hz), 4.38 (s, 3H), 2.86 (s, 6H), 2.61-2.51 (m, 1H), 2.38 (s, 3H), 1.11 (d, 3H, J=7 Hz) 1.08 (d, 3H, J=7 Hz). CHN analysis: Found: C 38.66%, H 4.00%, N 5.29%. Calcd. for $C_{25}H_{31}ClF_6N_3OOsP$: C 39.50%, H 4.11%, N 5.53%.

(14A) [Os(η^6-*p*-cym)(Impy-NMe$_2$)OH]PF$_6$. [Os(η^6-*p*-cym)Cl$_2$]$_2$ (100.0 mg, 0.126 mmol) and AgNO3 (85.9 mg, 0.506 mmol) was stirred in water (20 mL) at 313 K for 12h, a white precipitate was filtered off. Ligand Impy-NMe$_2$ (57.0 mg, 0.25 mmol) was added to the yellow clear solution, the solution-colour changed from yellow to red immediately. The solution was stirred at ambient temperature for 12 h. Ammonium hexafluorophosphate (205 mg. 1.26 mmol) was added. Then the solution was left in the fridge (277K) for 24 h. Dark coloured powder was precipitated which was collected by filtration, washed with cold ethanol and diethyl ether, then finally dried in vacuum. Yield: 105 mg (58.5 %). ESI-MS Calcd for $C_{24}H_{31}N_3OOs$: m/z 569.2, found 569.1. ^{1}H NMR(D_2O): δ 9.29 (d, 1H, J=5 Hz), 8.98 (s, 1 H), 8.15 (d, 1H, J=7 Hz), 8.12 (t, 1H, J=7 Hz), 7.67 (t, 1H, J=6 Hz), 7.52 (d, 2H, J=9 Hz), 6.96 (d, 2H, J=9 Hz), 6.17 (d, 1H, J=6 Hz), 5.81 (d, 1H, J=6 Hz), 5.66 (d, 1H, J=6 Hz), 5.54 (d, 1H, J=6 Hz), 2.98 (s, 6H), 2.25 (s, 3H), 2.23-2.16 (m, 1H), 0.83 (d, J=7 Hz, 3H), 0.74 (d, J=7 Hz, 3H). CHN analysis: Found: C 39.59%, H 3.87%, N 6.23%. Calcd. for $C_{24}H_{30}F_6N_3OOsP$: C 40.50%, H 4.25%, N 5.90%.

5.2.3 X-ray Crystallography. X-ray diffraction data for [Os(η^6-*p*-cym)(Impy-OH)I]PF$_6$ (**3**), was obtained on an Oxford Diffraction Gemini four-circle system with a Ruby CCD area detector using Mo Kα radiation.[19] Absorption corrections were carried out using ABSPACK. The crystals were mounted in oil and held at 100(2) K with the Oxford Cryosystem Cryostream Cobra. The structures were

solved by direct methods using SHELXS (TREF) with additional light atoms found by Fourier methods.[20] Refinement used SHELXL 97.[21]

5.2.4 NCI Cell Tests. The cells were treated for 48 h at five concentrations ranging from 0.01 to 100 μM. Three endpoints were determined: IC_{50} (the concentration that inhibits cell growth by 50 %); TGI (the concentration that inhibits cell growth by 100 %); LC_{50} (the concentration that kills original cells by 50 %). Cisplatin data are from NCI/DTP screening: Oct 2009.

5.2.5 Hydrolysis. A solution of **6** or **14** in 10% MeOD-d_4/90% D_2O phosphate buffer (v/v) was prepared by dissolution in MeOD-d_4 followed by a dilution with D_2O phosphate buffer (pH^*=7.2). NMR spectra were recorded after 24 h incubation at 310K. The extent of hydrolysis was determined from ^1H NMR peak integrals.

5.2.6 pH^* Measurements. The pH^* values of NMR samples in D_2O (pH meter reading without correction for effects of deuterium on glass electrode) were measured at 298 K using a chloride-free electrode calibrated with Sigma-Aldrich buffer solutions at pH 4, 7 and 10.

5.2.7 Determination of pK_a^* Value of 14. The pK_a^* value (pK_a value in D_2O solution) was determined by pH^* titration of **14A** with diluted solutions of NaOH and $HClO_4$ in D_2O. The ^1H NMR spectra at different pH^* values ranging from c.a. 1.5 to 13 were recorded and chemical shifts against pH^* values were plotted. The pH titration curves were fitted according to the Henderson-Hasselbalch equation with the assumption that the observed chemical shifts are weighted averages

according with the populations of the protonated and deprotonated species. This work was helped by Dr. Maria. J. Romero-Castro (Chemistry Department, University of Warwick).

5.2.8 Interaction with 9-Ethylguanine. 14A and 9-Ethylguanine (1 equiv) were mixed in D_2O phosphate buffer (pH^*=7.4) and incubated at 310 K. The ^1H NMR spectra were recorded after different time intervals. This work was helped by Dr. Maria. J. Romero-Castro (Chemistry Department, University of Warwick).

5.2.9 Catalytic Reaction with NADH. Osmium iminopyridine complexes: **6**, **8**, **14**, **14A** and **16** were incubated with different equivalents of NADH in a solution of 10% MeOD-d_4/90% D_2O phosphate buffer (pH*=7.4). ^1H-NMR spectra were recorded at different time intervals under incubations at 310 K. The analysis using UV-Vis spectroscopy was carried out under similar conditions but with non-deuterated solvents.

5.2.10 ROS Detection in A549 Cells. The ROS accumulation induced by complex **6** (4 μM) and **14** (4 μM) without or with L-BSO (50 μM) was monitored by using a method reported in chapter 3.[22]

5.2.11 Combination Treatment with L-BSO. To determine the effect of decreased GSH levels on the cytotoxicity of osmium iminopyridine complexes, A549 human lung cancer cells were co-incubated with 50 μM L-BSO and various concentrations of complexes for 24 h, then followed by 72 h recovery. Cell viability was then determined by using the sulforhodamine (SRB) assay (details in chapter 3).

5.2.12 Electrochemistry. The electrochemical study was carried out using the similar conditions as for the ruthenium azopyridine analogues reported previously:[22] Electrochemical studies were performed with a CHI730A bipotentiostat (CH Instrument, USA) system. All of the electrochemical techniques used a three-electrode configuration with all the electrodes in solution. A 2 mm diameter platinum disc electrode was used as the working electrode with a chloridized silver wire as the quasi-reference electrode and a Pt counter electrode (CH Instrument, USA). The reference electrode was Ag/AgCl in a solution of 0.1 M [TBA][BF_4] in DMF against which $E_{1/2}$ for the ferrocinium/ferrocene couple was measured to be +0.55 V.

5.2.13 Liquid Chromatography–Mass Spectrometry Analysis. NADH (0.5 mM) with or without complex **14A** (0.5 mM) were incubated at 310 K for 24 h, NADH and NAD^+ were incubated under the same conditions and LC-MS was employed to analyze the 3 samples.

5.2.14 Detection of H_2 by Gas Chromatography (GC). Solutions containing complex **14** [(η^6-*p*-cym)Os(Impy-NMe_2)OH]PF_6 and NADH (Os, 100 µM, NADH, 2 mM, 100 mM phosphate buffer, pH 7.4, 10% MeOH/90% H_2O) was incubated at 310 K for 18 h before sampling. Aliquot of the head space (10 µl) was removed by using a gas-tight syringe and analyzed on an Agilent GC 7890A instrument equipped with a thermal conductivity detector, using N_2 as the carrier gas. Under these conditions H_2 had a retention time of 0.4 min and O_2 a retention time of 0.8 min. This work was helped by Dr. Andrew Crombie and Prof. Colin Murrell (Biology Department, University of Warwick).

5.2.15 Cell Cycle Analysis. A2780 cells were incubated with complex **14** at various concentrations for 24 h and then harvested. Detached and adherent cells were washed with PBS and fixed in 70% ethanol (253 K). The fixed cells were centrifuged and washed once with PBS, followed by resuspension in PBS containing 7.5 µM propidium iodide (PI) and 100 µg/ml RNase A. They were analyzed by flow cytometry (FACS-Calibur, Beckton Dickenson). The cell cycle distribution was evaluated using the Flow Jo (Version 7.6, Software from Tree Star).

5.3 Results

5.3.1 Synthesis and Characterization

Sixteen osmium(II) arene iminopyridine complexes (Chart 5.1) of general formula $[Os(\eta^6\text{-arene})(R_1\text{-Impy-}R_2)X]PF_6$ (arene = biphenyl or *p*-cymene; X = Cl or I) containing different chelating iminopyridine ligands (Impy, Impy-OH, Impy-NMe_2 and OMe-Impy-NMe_2) were synthesized. The general method involves stirring the mixture of osmium dimer and appropriate chelating iminopyridine ligand which was synthesized following a method based on literature[18] in a methanol solution, which is similar to that reported before for the synthesis of their azopyridine analogues.[2] In general, the iminopyridine complexes were obtained in good yields and well characterized by ^{1}H-NMR spectroscopy, mass spectrometry and CHN elemental analysis.

For organometallic metal arene complex with the piano-stool structure which contains an unsymmetrical chelating ligand and another monodentate ligand, the metal atom is a chiral centre.[23] ^{1}H NMR spectra ($CDCl_3$, 298 K) were taken before and after adding the chiral anionic chiral shift-reagent (Δ–trisphat) to the solution of complex **14** in chloroform-d. The even splits of peaks were observed (Fig. 5.1) which indicated that there were two osmium enantiomers in ca. 1:1 ratio, consistent with the previous report on osmium/ruthenium arene anticancer complexes.[5]

Recrystallization of $[Os(\eta^6\text{-}p\text{-cym})(Impy\text{-}OH)I]PF_6$ (**4)** in DCM and methanol mixed solvent (Fig 5.2) gave purple single crystals corresponding to **4**·$0.5CH_2Cl_2$·H_2O (Fig 5.3) suitable for the study by X-ray diffraction. Crystallographic data are listed in Table 5.1 and selected bond lengths and angles in Table 5.2. The asymmetric unit comprises a mixture of enantiomers of the cation $[Os(\eta^6\text{-}p\text{-cym})(Impy\text{-}OH)I]^+$ with (R)- and (S)- configuration respectively at the metal centre (Fig. 5.3) and two molecules of PF_6^- acting as counterions. Cahn–Ingold–Prelog priority rules (CIP system**)** were used to define the priority sequence of ligands attached to osmium: I > η^6-C_6 > N (imine) > N (pyridine).

Additionally, the two enantiomers are solvated by one dichloromethane and two water molecules. The osmium complex shows the usual pseudo-octahedral "piano-stool" structure with the *p*-cymene ligand π-bonded to the metal ion and the iminopyridine chelating ligand Impy-OH coordinated through the pyridine and imine nitrogen atoms. The imine bond in the chelating ligand Impy-OH adopts an *E* conformation to minimise the steric hindrance with the bulky phenol group. The coordination sphere of the osmium(II) ion is completed with a terminal iodide atom behaving as monodentate ligand. The Os-N, Os-I and Os-arene bond lengths in this complex are similar to those found in the azopyridine analogues previously reported.[2] The crystal structure of complex **4**·0.5CH_2Cl_2·H_2O shows dissimilarities with the crystal structure of [Os(η^6-bip)(Azpy-OH)I]PF_6 which was reported previously in Chapter 3. In complex **4**·0.5CH_2Cl_2·H_2O there is no deprotonation of the hydroxyl group on the chelating ligand which allows each enantiomer to establish an intramolecular hydrogen bond between the phenol OH group of the iminopyridine ligand and one water molecule [O115-H11H···O400 1.84 Å, O215-H21H···O300 1.89 Å] as shown in Figure 5.3 B. Additional intermolecular hydrogen bonds are observed between one water molecule and both PF_6^- counterions [O300-H30A···F33 2.10(3) Å, x+1, y, z; O300-H30B···F21 2.36(3) Å, -x+1, -y, -z].

Chart 5.1. Osmium (II) arene iminopyridine complexes synthesized and studied in this chapter.

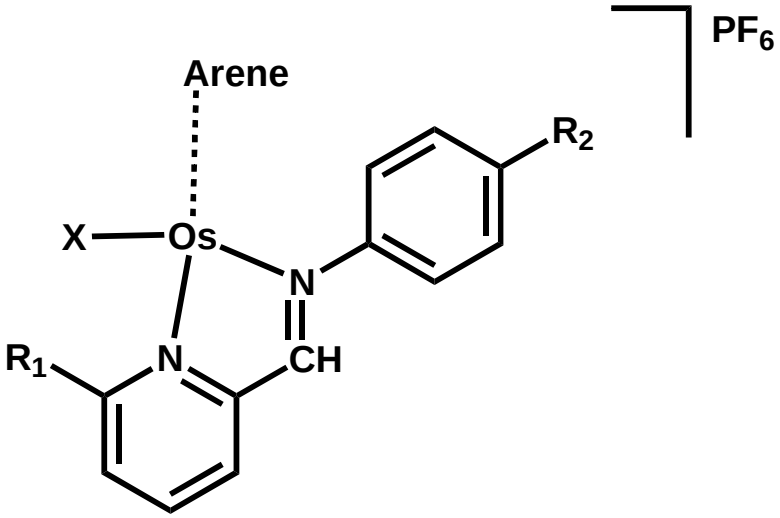

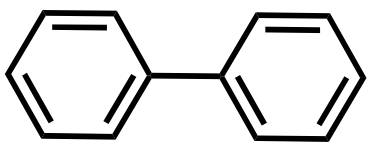

bip

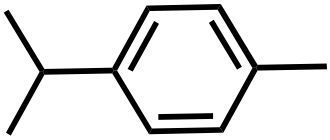

p-cym

Complex	Arene	R_1	R_2	X	Chelating ligand
1	bip	H	H	I	Impy
2	*p*-cym	H	H	I	Impy
3	bip	H	OH	I	Impy-OH
4	*p*-cym	H	OH	I	Impy-OH
5	bip	H	NMe_2	I	Impy-NMe_2
6	*p*-cym	H	NMe_2	I	Impy-NMe_2
7	bip	OMe	NMe_2	I	OMe-Impy-NMe_2
8	*p*-cym	OMe	NMe_2	I	OMe-Impy-NMe_2
9	bip	H	H	Cl	Impy
10	*p*-cym	H	H	Cl	Impy
11	bip	H	OH	Cl	Impy-OH
12	*p*-cym	H	OH	Cl	Impy-OH
13	bip	H	NMe_2	Cl	Impy-NMe_2
14	*p*-cym	H	NMe_2	Cl	Impy-NMe_2
15	bip	OMe	NMe_2	Cl	OMe-Impy-NMe_2
16	*p*-cym	OMe	NMe_2	Cl	OMe-Impy-NMe_2

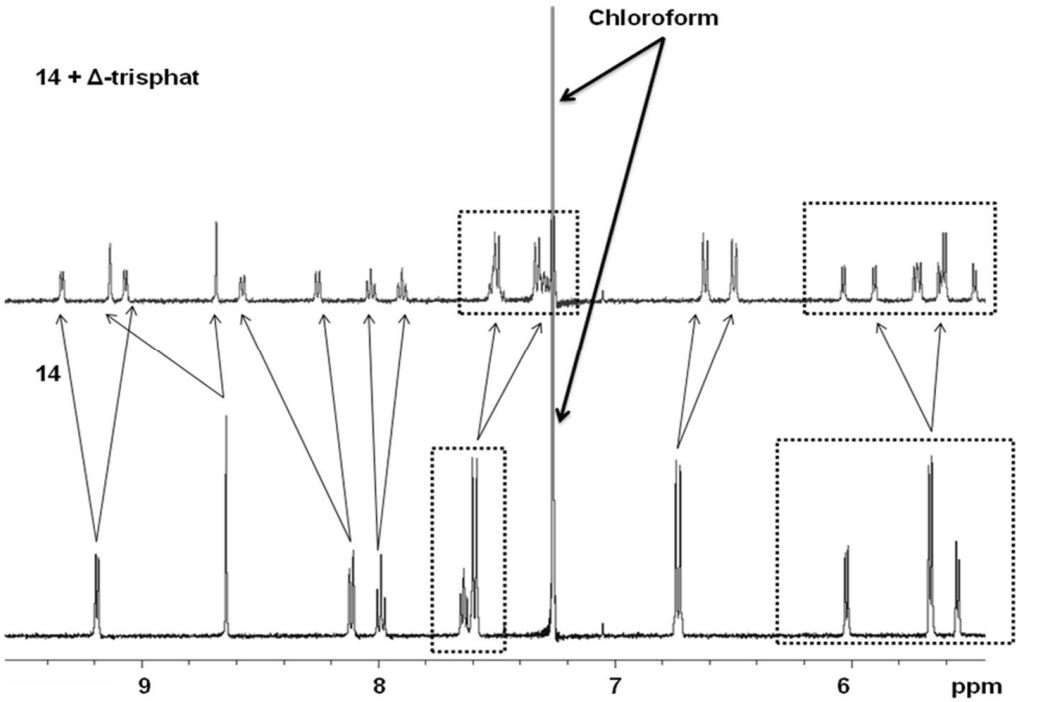

Figure 5.1. ^{1}H NMR spectrum before and after adding 2 mol equivalents of Δ-trisphat in chloroform-d.

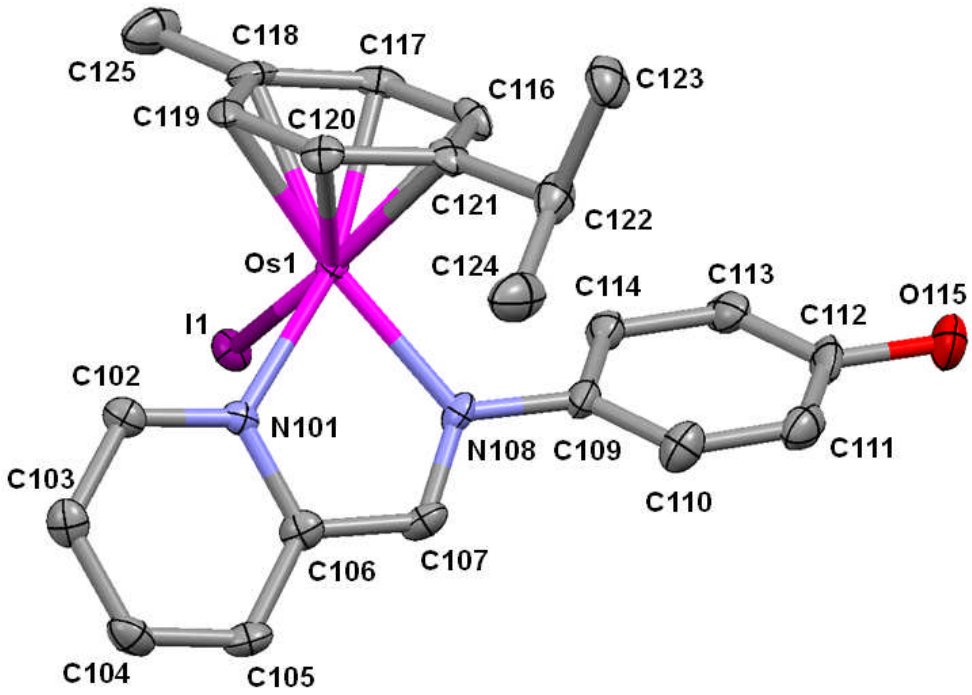

Figure 5.2. X-ray crystal structure of the cation of the enantiomer (S)-[Os(η^6-*p*-cym)(Impy-OH)I]PF_6 **(4)** showing the atomic numbering scheme. The thermal ellipsoids are drawn at 50% probability. The hydrogen atoms, counterion (PF_6^-) and solvent molecules have been omitted for clarity.

(A)

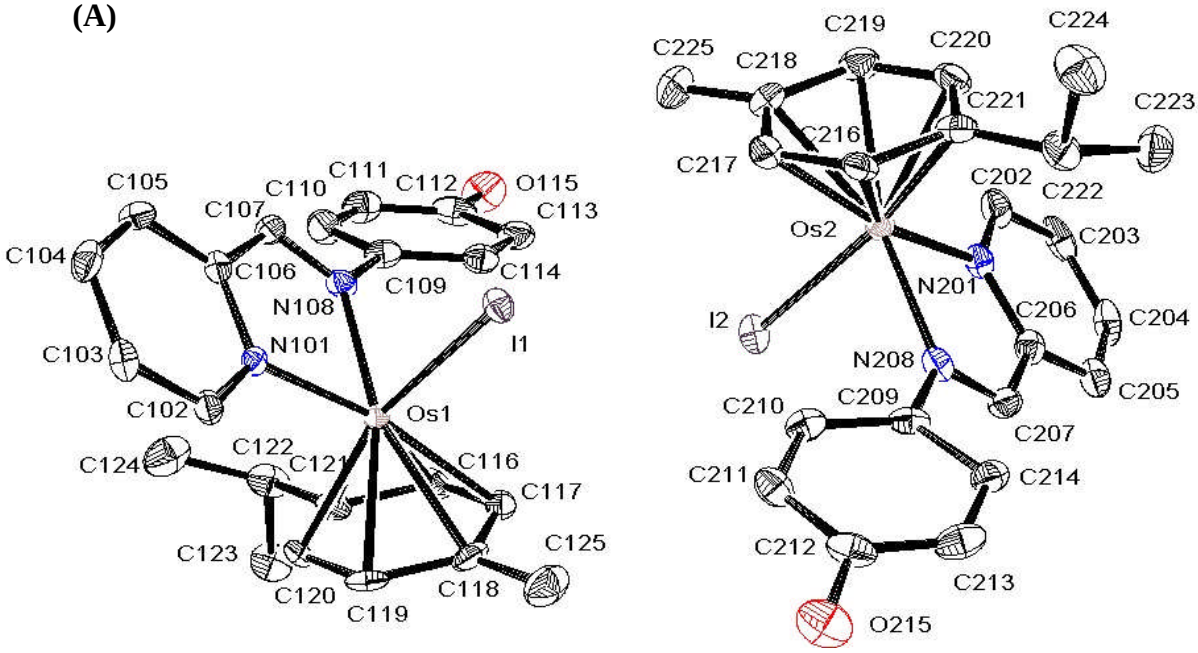

(B)

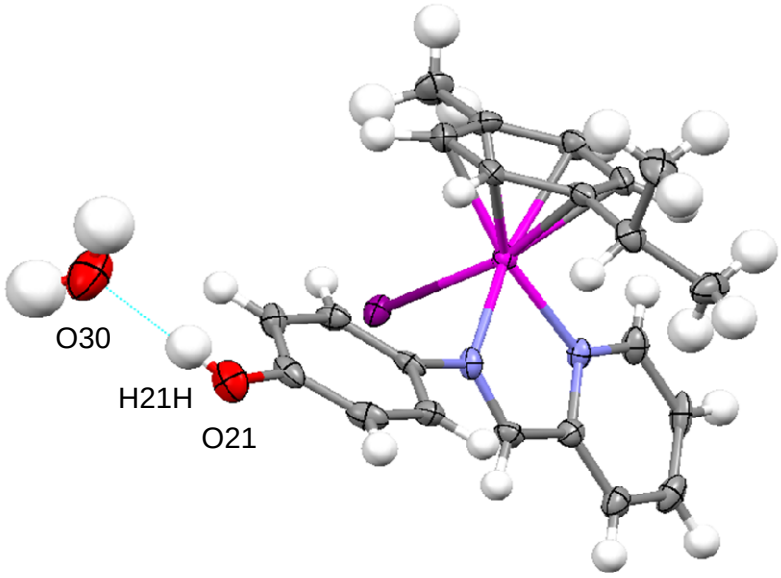

Figure 5.3. (A) Crystal structures of the enantiomers (S)-[Os(η^6-*p*-cym)(Impy-OH)I]PF_6 (left) and (R)-[Os(η^6-*p*-cym)(Impy-OH)I]PF_6 (right) of complex **4** ·0.5CH_2Cl_2·H_2O showing the atomic numbering scheme. Thermal ellipsoids are drawn at the 50% probability level. Lattice CH_2Cl_2 and H_2O molecules are not shown. Hydrogen atoms and PF_6^- counterions are omitted for clarity. **(B)** There is an hydrogen bond interaction between the phenol group of the chelating iminopyridine ligand in the enantiomer (R)-[Os(η^6-*p*-cym)(Impy-OH)I]PF_6 and one water molecule.

Table 5.1. Crystal data and structure refinement for [Os(η^6-*p*-cym)(Impy-OH)I]$PF_6 \cdot 0.5CH_2Cl_2 \cdot H_2O$ **(4** $\cdot 0.5CH_2Cl_2 \cdot H_2O$ **)**

	4 $\cdot 0.5CH_2Cl_2 \cdot H_2O$
Empirical formula	$C_{22.50}H_{27}ClF_6IN_2O_2OsP$
Crystal size [mm]	0.20×0.20×0.20
Formula weight	854.98
Crystal system	Triclinic
Space group	P-1
a [Å]	11.3168(3)
b [Å]	13.0498(3)
c [Å]	19.2278(4)
α [º]	95.3980(19)
β [º]	103.654(2)
γ [º]	97.2625(19)
Volume [Å^3]	2714.50(11)
Temperature [K]	100(2)
Z	4
μ [mm^{-1}]	6.057
Reflections collected	12572
Independent reflections [Rint]	9981 [0.0222]
*R*1, *wR*2 [$I>2\sigma(I)$]	0.0332, 0.0793
*R*1, *wR*2 (all data)	0.0450, 0.0817

Table 5.2. Selected bond lengths [Å] and angles [º] for [Os(η^6-*p*-cym)(Impy-OH)I]$PF_6 \cdot \cdot 0.5CH_2Cl_2 \cdot H_2O$ **(4** $\cdot 0.5CH_2Cl_2 \cdot H_2O$ **)**

4 $\cdot 0.5CH_2Cl_2 \cdot H_2O$					
Os1-N108	2.077(4)	Os2-N208	2.078(4)	Os1- η^6-arene centroid	1.6962(2)
Os1-N101	2.087(4)	Os2-N201	2.080(4)	Os2- η^6-arene centroid	1.6845(2)
Os1-C120	2.182(5)	Os2-C220	2.169(5)	N108-Os1-N101	76.05(14)
Os1-C116	2.189(5)	Os2-C216	2.184(5)	N101-Os1-I1	84.80(11)
Os1-C117	2.206(5)	Os2-C221	2.201(6)	N208-Os2-N201	76.59(15)
Os1-C121	2.209(5)	Os2-C217	2.209(5)	N208-Os2-I2	85.06(12)
Os1-C119	2.219(4)	Os2-C219	2.212(5)		
Os1-C118	2.256(4)	Os2-C218	2.245(5)		
Os1-I1	2.7091(4)	Os2-I2	2.7247(4)		

5.3.2 Hydrolysis and Binding with 9-Ethylguanine

The possible activation of these complexes by hydrolysis and their interaction with 9-ethylguanine (9-EtG) which is a DNA nucleobase model were studied by following the reactions by ^{1}H NMR. The osmium iminopyridine complexes [Os(η^6-*p*-cym)(Impy-NMe_2)I]PF_6 (**6)** and [Os(η^6-*p*-cym)(Impy-NMe_2)Cl]PF_6 (**14)** which are mainly studied here can undergo hydrolysis, after incubation of the samples at 310 K for 24 h in D_2O, they can reach the hydrolysis extent of 49.5 % and 99.5%, respectively. The formation of the aqua product (**14A**) was confirmed by the presence of new signals in the ^{1}H NMR spectra shifted with respect to the signals observed for **6** and **14**.

To study the potential of DNA binding, the reaction of the hydrolyzed product of **14** (**14A**) with 9-ethylguanine (9-EtG) was monitored at different time intervals by ^{1}H NMR after incubation of the solution at 310 K in 0.1 M phosphate buffer (D_2O, pH^* = 7.4). The 9-EtG binding was evidenced by the appearance of new signals assignable to the **14**-9-EtG adduct which are shifted in comparison with the signals of **14A** and the free nucleobase. The binding extent reached only 14% after 18 hours and the ratio increase slightly to 19% after another 20 h of incubation at 310 K (Fig. 5.4 A).

5.3.3 pK_a Measurement

The pK_a value for the hydrolysed product of **6** and **14** (**14A)** was determined by ^{1}H NMR spectroscopy after variations of the pH^* values of a solution of **14A** in D_2O (Fig. 5.4 B). The chemical shifts of the ^{1}H NMR signals were gradually shifted upfield after increasing the pH^* value from c.a. pH^* 1.5 to 13 which is consistent with the behaviour of an aqua adduct. Plots of the chemical shifts of the pyridine proton Ha against pH^* were fitted to the Henderson-Hasselbalch equation, giving a pK_a^* value of 5.1 (pK_a= 5.2) corresponding to the coordinated water molecule. The low value of pK_a found in the aqua adduct indicates that the hydroxy adduct is possibly the predominant species in aqueous solution under

physiological conditions. The pK_a value of the dimethylamine substituent on the iminopyridine chelating ligand Impy-NMe_2 (pK_a^*=2.3, pK_a= 2.6) which is the first reported pK_a for this type of ligand bound to metal.

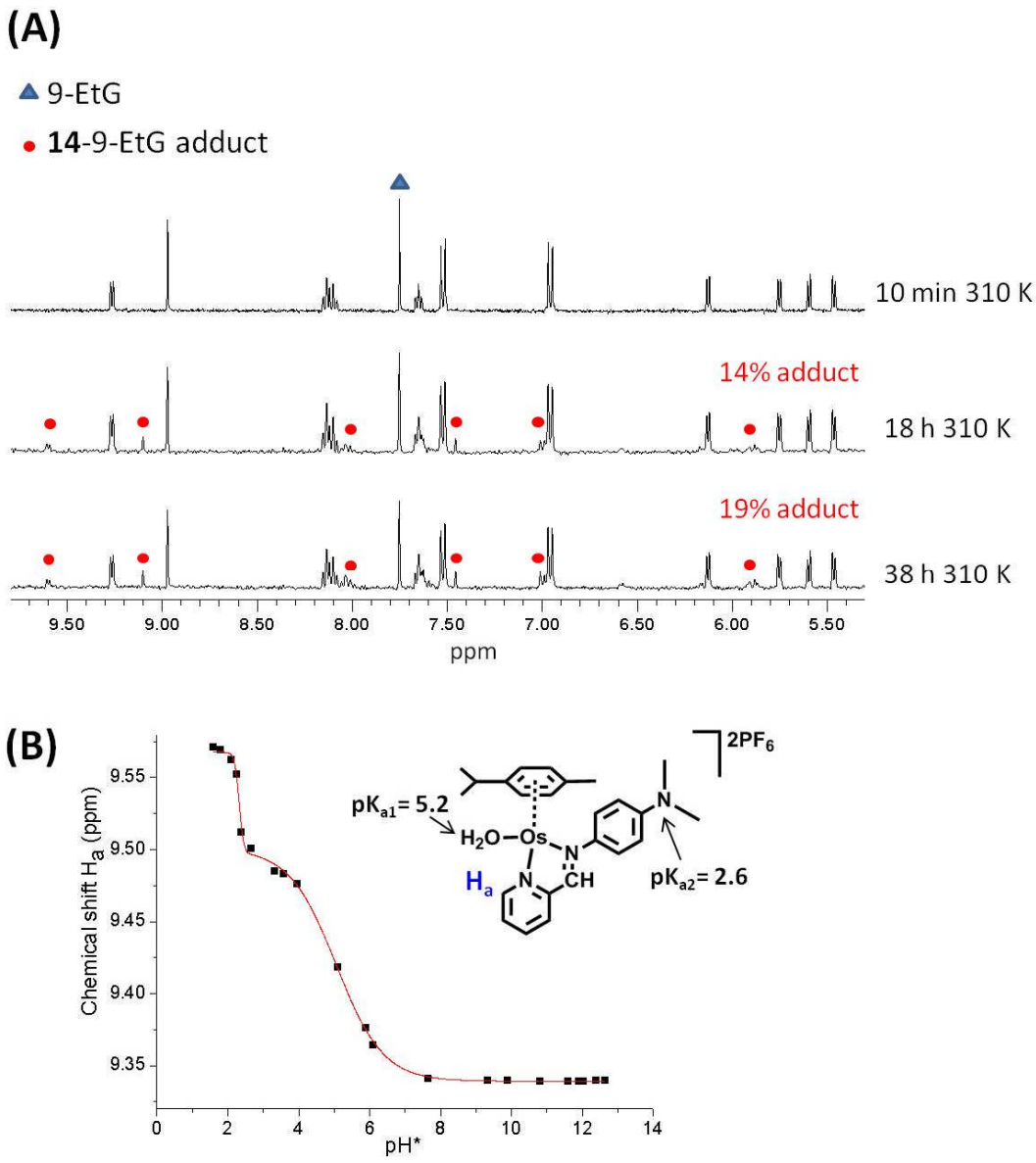

Figure 5.4. **(A)** Interaction of the hydroxo complex **14A** (1 mM) with the 9-ethylguanine (2 mM, 2 equiv.) followed by ^{1}H NMR. The spectra were recorded 10 min after preparing the mixture in a 10%D_2O/90%H_2O phosphate buffer solution (pH^*=7.4) and after incubation of the sample during 18 h and 38 h at 310 K; **(B)** Dependence of the ^{1}H NMR chemical shifts with pH* for the pyridine proton H_a in the complex **14A**. The pK_a^* values were determined by fitting the data points to the Henderson-Hasselbalch equation, corresponding to pK_{a1}^* = **5.1** for the coordinated water and pK_{a2}^* = **2.3** for the dimethylamine substituent. These values were converted to pK_a values (pK_{a1}=5.2, pK_{a2}= 2.6) using the equation $pK_a = 0.929pK_a^*+0.42$.

5.3.4. Anticancer Activity

All the sixteen osmium arene iminopyridine complexes were tested on the A2780 cell line and some were tested on the A549 human lung cancer cell line (Table 5.3). The results showed they had a broad range of anticancer activity from 0.14 μM to 35.5 μM (IC_{50} values) to A2780 cells (Table 5.3A). Anticancer efficacy was also seen on A549 cells and a significant increase of anticancer activity by combination treatment enhancement with L-buthionine-sulfoximine (L-BSO, a specific inhibitor of gamma-glutamylcysteinesynthetase, depletes intracellular glutathione which plays important role for maintaining the redox balance in cancer cells) was achieved (Table 5.3B).

The complexes $[Os(\eta^6\text{-}p\text{-cym})(Impy\text{-}NMe_2)I]PF_6$ (**6)** and $[Os(\eta^6\text{-}p\text{-cym})(Impy\text{-}NMe_2)Cl]PF_6$ (**14)** showed anticancer activity in the same range of cisplatin against A2780 cancer cells. Moreover, complexes **6** and **14** were selected for the study of anticancer activity screening towards the human tumour 60-cell line panel of the Developmental Therapeutics Program of the National Cancer Institute (DTP of NCI) which includes nine tumour type subpanels. The mean values of IC_{50} (the concentration that inhibits cell growth by 50 %), TGI (the concentration which that cell growth by 100 %) and LC_{50} (the concentration that kills original cells by 50 %) are listed in Table 5.3C. Both of them showed anticancer activity within the same range of cisplatin.

Table 5.3. *In vitro* anticancer activity towards A2780 human ovarian cancer cells (A); A549 human lung cancer cells and combination treatment with 50 μM L-BSO (B); 60-cell line screening results from the NCI (C).

(A)

Complex	IC_{50}(μM)
(**1**) $[Os(\eta^6\text{-bip})(Impy)I]PF_6$	18.6(±0.9)
(**2**) $[Os(\eta^6\text{-}p\text{-cym})(Impy)I]PF_6$	29.4(±5.3)
(**3**) $[Os(\eta^6\text{-bip})(Impy\text{-}OH)I]PF_6$	5.4(±1.1)
(**4**) $[Os(\eta^6\text{-}p\text{-cym})(Impy\text{-}OH)I]PF_6$	31.8(±3.8)
(**5**) $[Os(\eta^6\text{-bip})(Impy\text{-}NMe_2)I]PF_6$	0.14(±0.01)
(**6**) $[Os(\eta^6\text{-}p\text{-cym})(Impy\text{-}NMe_2)I]PF_6$	0.80(±0.05)
(**7**) $[Os(\eta^6\text{-bip})(Ome\text{-}Impy\text{-}NMe_2)I]PF_6$	9.14(±0.93)
(**8**) $[Os(\eta^6\text{-}p\text{-cym})(Ome\text{-}Impy\text{-}NMe_2)I]PF_6$	35.5(±3.2)
(**9**) $[Os(\eta^6\text{-bip})(Impy)Cl]PF_6$	4.6(±0.4)
(**10**) $[Os(\eta^6\text{-}p\text{-cym})(Impy)Cl]PF_6$	26.2(±2.8)
(**11**) $[Os(\eta^6\text{-bip})(Impy\text{-}OH)Cl]PF_6$	2.4(±1.1)
(**12**) $[Os(\eta^6\text{-}p\text{-cym})(Impy\text{-}OH)Cl]PF_6$	5.5(±0.6)
(**13**) $[Os(\eta^6\text{-bip})(Impy\text{-}NMe_2)Cl]PF_6$	0.44(±0.01)
(**14**) $[Os(\eta^6\text{-}p\text{-cym})(Impy\text{-}NMe_2)Cl]PF_6$	1.5(±0.047)
(**15**) $[Os(\eta^6\text{-bip})(Ome\text{-}Impy\text{-}NMe_2)Cl]PF_6$	9.5(±0.22)
(**16**) $[Os(\eta^6\text{-}p\text{-cym})(Ome\text{-}Impy\text{-}NMe_2)Cl]PF_6$	32.9(±1.2)
Cisplatin	1.8(±0.1)

(B)

Complex	IC_{50}(μM)	IC_{50}(μM) with L-BSO
(**3**) $[Os(\eta^6\text{-bip})(Impy\text{-}OH)I]PF_6$	4.55(±1.09)	1.59(±0.36)
(**6**) $[Os(\eta^6\text{-}p\text{-cym})(Impy\text{-}NMe_2)I]PF_6$	3.7(±0.2)	0.73(±0.10)
(**9**) $[Os(\eta^6\text{-bip})(Impy)Cl]PF_6$	>100	25.88(±12.29)
(**10**) $[Os(\eta^6\text{-}p\text{-cym})(Impy)Cl]PF_6$	0.9(±0.09)	NA
(**13**) $[Os(\eta^6\text{-bip})(Impy\text{-}NMe_2)Cl]PF_6$	2.55(±1.35)	NA
(**14**) $[Os(\eta^6\text{-}p\text{-cym})(Impy\text{-}NMe_2)Cl]PF_6$	8.68(±2.11)	2.34(±1.18)
Cisplatin	6.65(±0.06)	NA

Table 5.3. *In vitro* anticancer activity towards A2780 human ovarian cancer cells (A); A549 human lung cancer cells and combination treatment with 50 μM L-BSO (B); 60-cell line screening results from the NCI (C).

(C)

Complex	IC_{50}(μM)	TGI(μM)	LC_{50}(μM)
(6) $[Os(\eta^6\text{-}p\text{-cym})(Impy\text{-}NMe_2)I]PF_6$	3.72	13.2	49
(14) $[Os(\eta^6\text{-}p\text{-cym})(Impy\text{-}NMe_2)Cl]PF_6$	8.3	33.9	75.8
Cisplatin[*]	10.3	50.7	90.5

[*] Data from NCI/DTP screening. **6** = NSC755639; **14** = NSC755640. Mean-graph midpoint (MG-MID) for IC_{50}, TGI and LC_{50} values of NCI all cell panels.

5.3.5. Accumulations of Reactive Oxygen Species (ROS)

In Chapter 3, osmium(II) arene azopyridine complexes were found to cause an increase in ROS levels in cancer cells. For comparison, whether the cellular ROS level was affected by iminopyridine complexes was also investigated. The level of ROS was monitored in A549 human lung cancer cells induced by osmium complexes (**6** and **14**) using the probe 2,7-dichlorodihydrofluorescein-diacetate (DCFH-DA). It can be hydrolyzed to 2,7-dichlorodihydrofluorescein (DCFH) in live cells, which in turn is oxidized to 2,7-dichlorofluorescein (DCF) in the presence of ROS and exhibits a green fluorescence. Using this probe, the level of general oxidative stress induced in A549 cells by **6** and **14** was determined. The ROS accumulations of combined exposure to **6** or **14** with L-BSO were also studied. In A549 cells, the relative increase in DCF fluorescence was detected over a period of 4 h after treating the cells with **6** (4 μM), **14** (4 μM), **6** (4 μM) plus L-BSO (50 μM), **14** (4 μM) plus L-BSO (50 μM) or 10 μM H_2O_2 (Fig. 5.5). After a treatment only with **6** or **14**, the ROS level increased dramatically compared to the control and even the positive control (H_2O_2, 10μM). This level increased further in the presence of L-BSO in addition to **6** or **14**. The further increase of ROS by the combination treatment may explain why L-BSO can enhance the cytotoxicity of complex **6** and **14** towards A549 cancer cells significantly (Table 5.3B). L-BSO alone at a dose of 50 μM had no significant effect on the increase of ROS and the growth of A549 cancer cells, but greatly enhanced the cytotoxicity of osmium iminopyridine complexes to A549 cancer cells. These data implied the increasing ROS might be the basis of combination treatment strategy of **6** or **14** with L-BSO which is opposite to our recent report on azopyridine complexes with substituent on the pyridine ring in Chapter 4.[24]

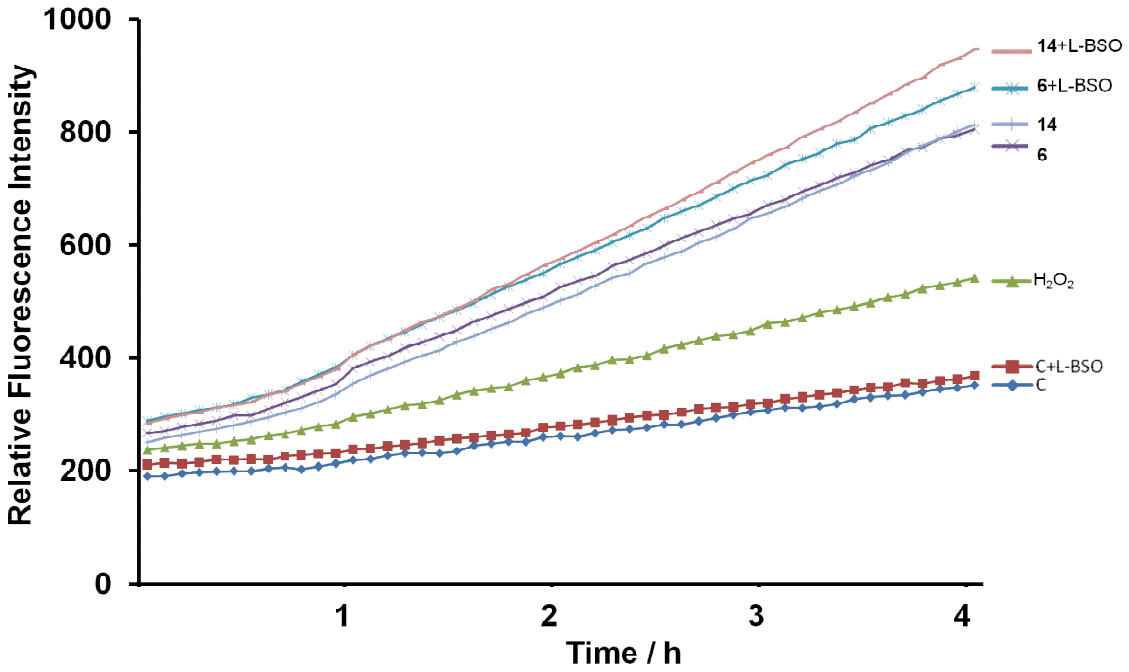

Figure 5.5. Changes of ROS levels in A549 human lung cancer cells after the treatment of **6** (4 μM), **14** (4 μM), L-BSO (50 μM), **6** or **14** combined with L-BSO (50 μM), and H_2O_2 (10 uM, positive control) during 4 h at 310 K.

5.3.6. Catalytic Oxidation of NADH

Following the indication of an increase of ROS in cells induced by osmium iminopyridine complexes, whether they can react with important cellular reducing agents directly was examined. It was found that **6** and **14** could not catalytically oxidize GSH which is different from their ruthenium azopyrdine iodido analogues.[22] Since NADH forms a redox pair with NAD^+ to play an important role in maintaining the redox balance in cells, the reaction with NADH was also studied. The reactions of NADH with complexes **6**, **8**, **14**, **14A** and **16** were followed by ^{1}H NMR spectroscopy. They were found to catalytically oxidize NADH to NAD^+ to different extents after incubation in a 10%MeOD/90%D_2O phosphate buffer solution (pH^*=7.4) over 24 h at 310 K (Fig. 5.6 and Fig. 5.7), whereas the control (NADH) was stable towards the NAD^+ formation under the same conditions. More than one equivalent of NADH was found to be oxidized by osmium complexes; it implies that this is a catalytic oxidation. The recording of the ^{1}H NMR spectra for the reaction with **14A** after 3 h and 6 h of incubation at 310 K (10%D_2O/90%H_2O phosphate buffer) in lead to the detection of a weak hydride signal at –4.20 ppm, as shown in Figure 5.8. This signal is indicative of the formation of an osmium hydride adduct during the catalytic reaction.

(A)

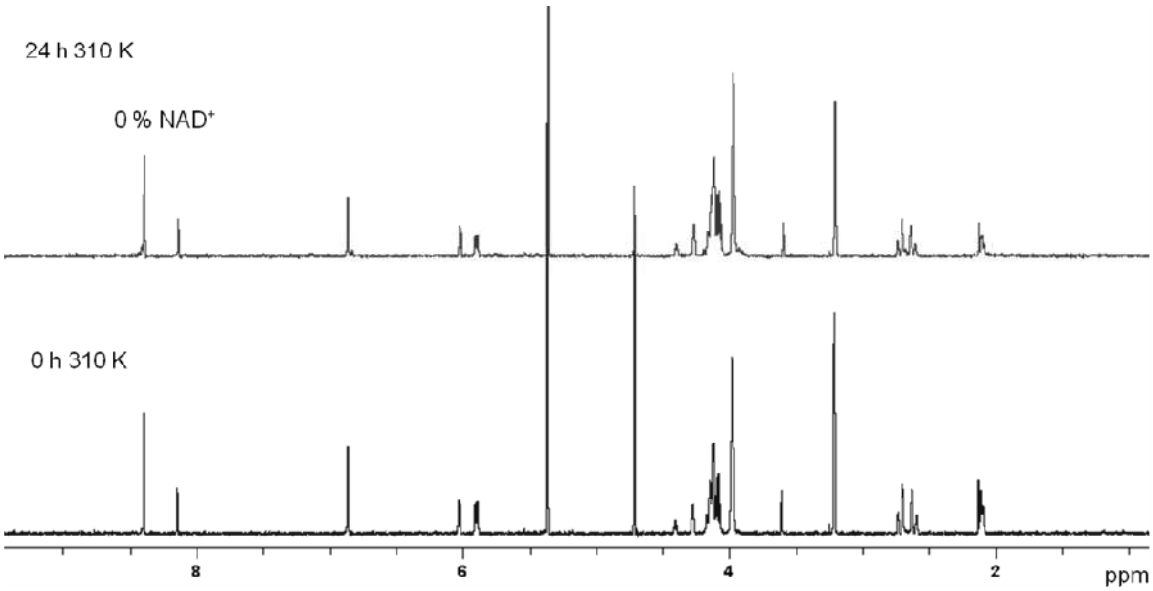

(B)

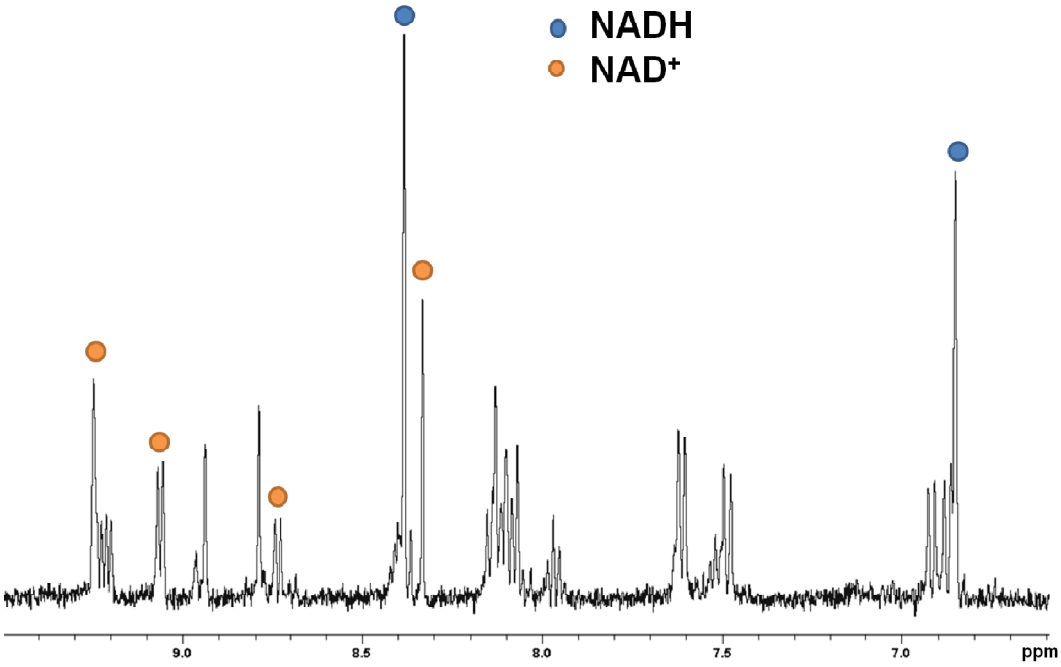

(C)

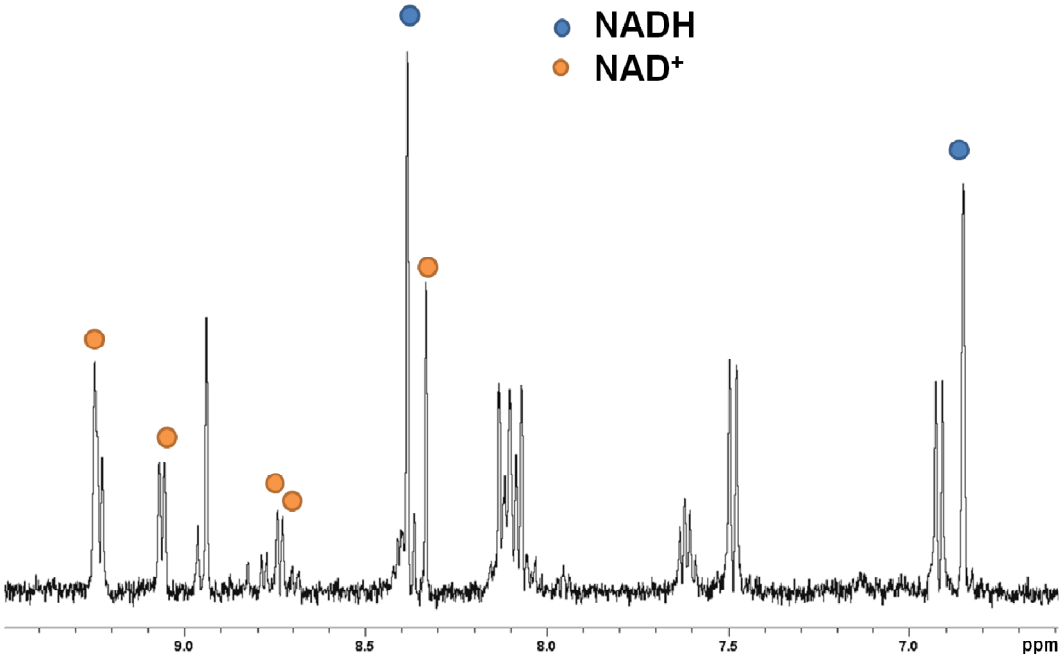

(D)

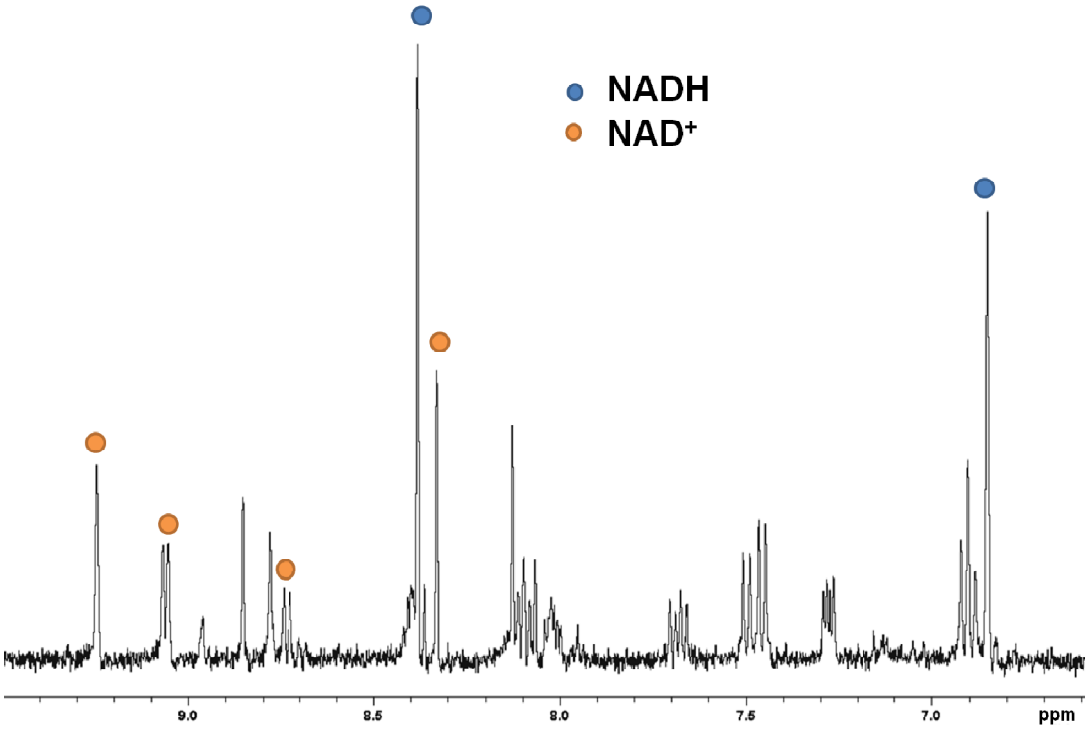

(E)

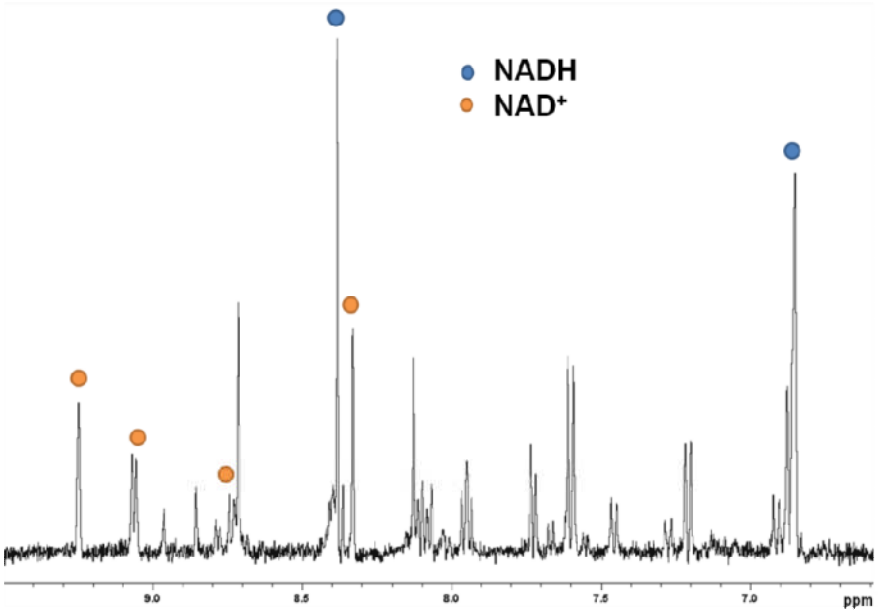

(F)

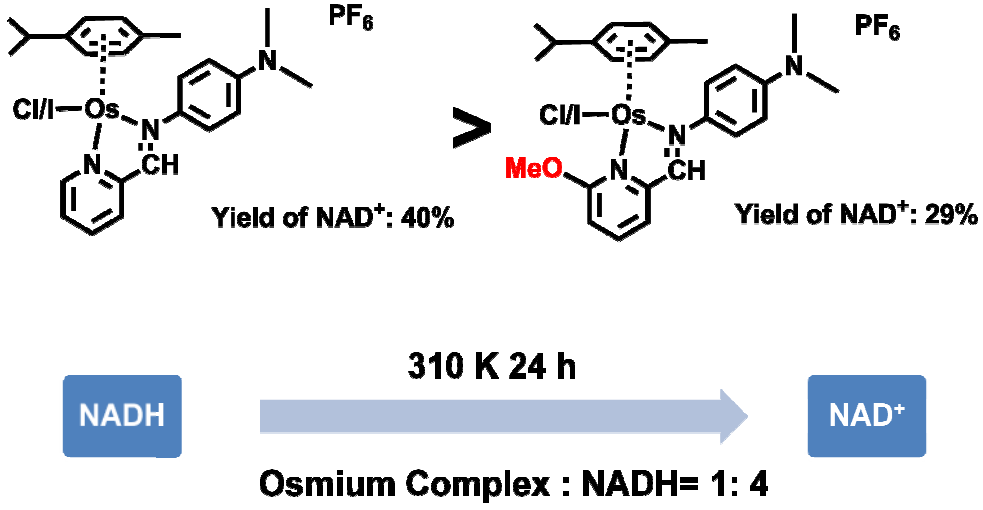

Figure 5.6. ^{1}H NMR spectra corresponding to the reaction between the osmium complex (0.1 mM) and NADH (0.4 mM, 4 equivalents). The spectra were recorded in a 10%MeOD /90%D_2O phosphate buffer solution (pH*=7.4) after 24 h of incubation of the sample at 310 K. (A) Control: NADH at time 0 and time 24 h (310 K oven) (B) (**6**) [Os(η^6-*p*-cym)(Impy-NMe_2)I]PF_6. (C) (**14**) [Os(η^6-*p*-cym)(Impy-NMe_2)Cl]PF_6. (D) (**8**) [Os(η^6-*p*-cym)(Ome-Impy-NMe_2)I]PF_6. (E) (**16**) [Os(η^6-*p*-cym)(OMe-Impy-NMe_2)Cl]PF_6. (F) Summary of extent of NADH catalytic oxidation by osmium iminopyridine complexes: **6**, **8**, **14**, and **16**. The ^{1}H NMR spectra at 0 h were NMR recorded immediately after preparing the samples.

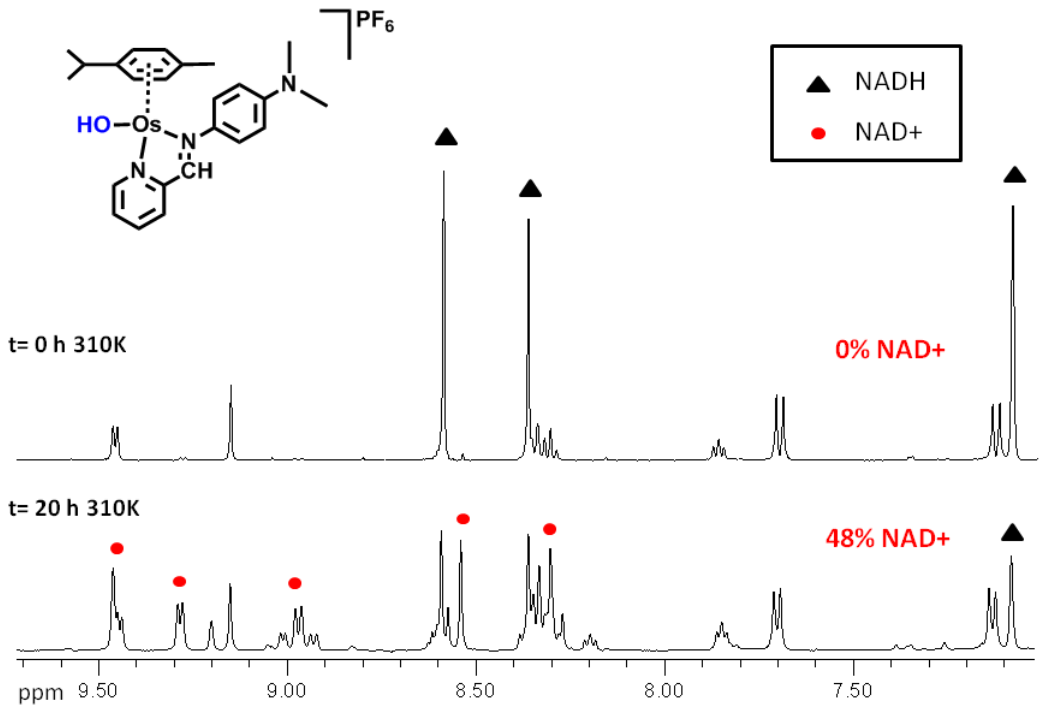

Figure 5.7. ^{1}H NMR spectra corresponding to the reaction between the hydroxo complex **14A** (2 mM) and NADH (8 mM, 4 mol equivalents). The spectra were recorded in a 10%D_2O/90%H_2O phosphate buffer solution (pH* 7.4) at t = 0 h and after 20 h of incubation of the sample at 310 K. The ^{1}H NMR spectra at 0 h were NMR recorded immediately after preparing the samples.

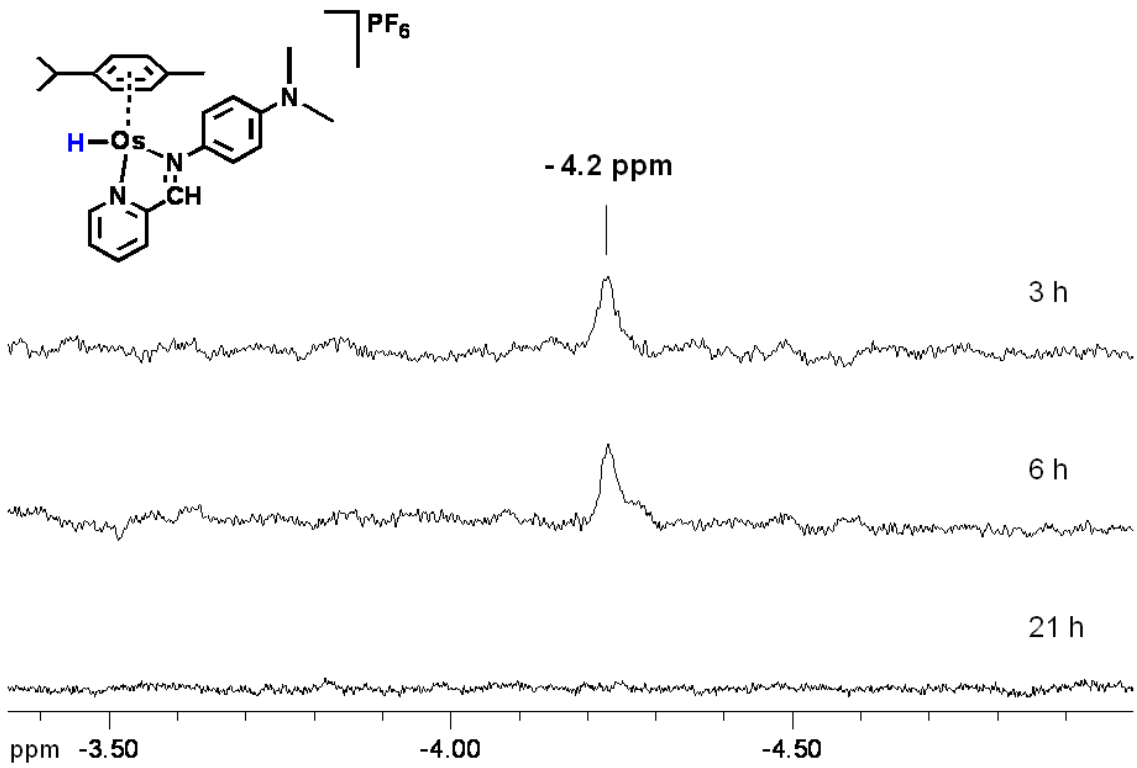

Figure 5.8. Detection of hydride signals by ^{1}H NMR for the reaction of 4 mol equivalents of NADH with the hydroxo complex **14A** (2.5 mM) at different time points.

LC-MS was also employed to analyse the reaction between NADH (0.5 mM) and **14A** (0.5 mM) after the incubation at 310 K for 24 h. The decrease of the peak with a retention time 11-12 min (identified by MS as NADH) and the appearance of a new peak with a retention time at 4.8-5.2 min (identified by MS as NAD^+ and also comfirmed by a comparison with the retention time of NAD^+ control) were observed by LC after the treatment with **14A** (Fig. 5.9A). The MS results showed the correct masses of NADH (Calcd for $C_{21}H_{30}N_7O_{14}P_2$: m/z = 666.1 and found m/z = 666.1) and NAD^+ (Calcd for $C_{21}H_{28}N_7O_{14}P_2$: m/z = 664.1 and found m/z = 664.1) which is consistent with the LC results. The MS results of the two controls (NADH and NAD^+) are also shown in Figure 5.9 D and E, respectively, other than the MS of **14A**, a phosphate adduct was also detected by MS (Fig. 5.9 F and 5.9 G).

(A)

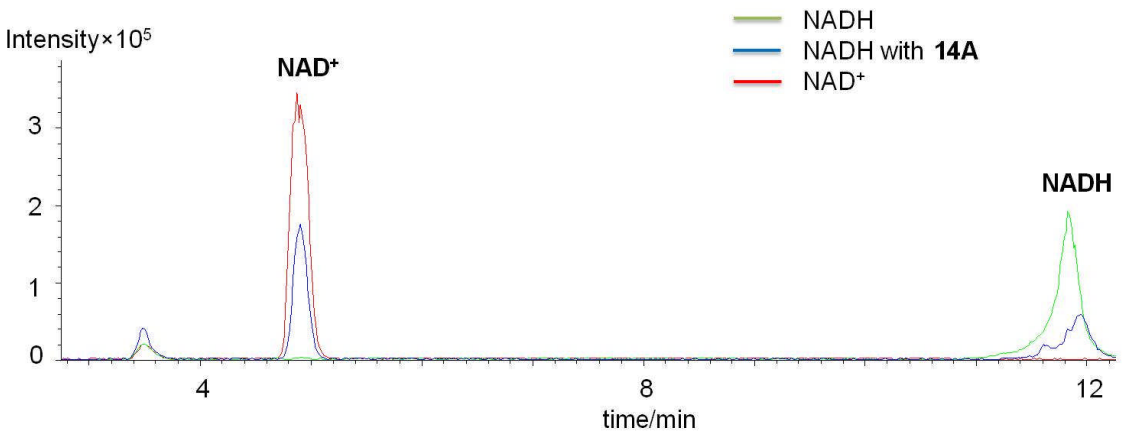

(B)

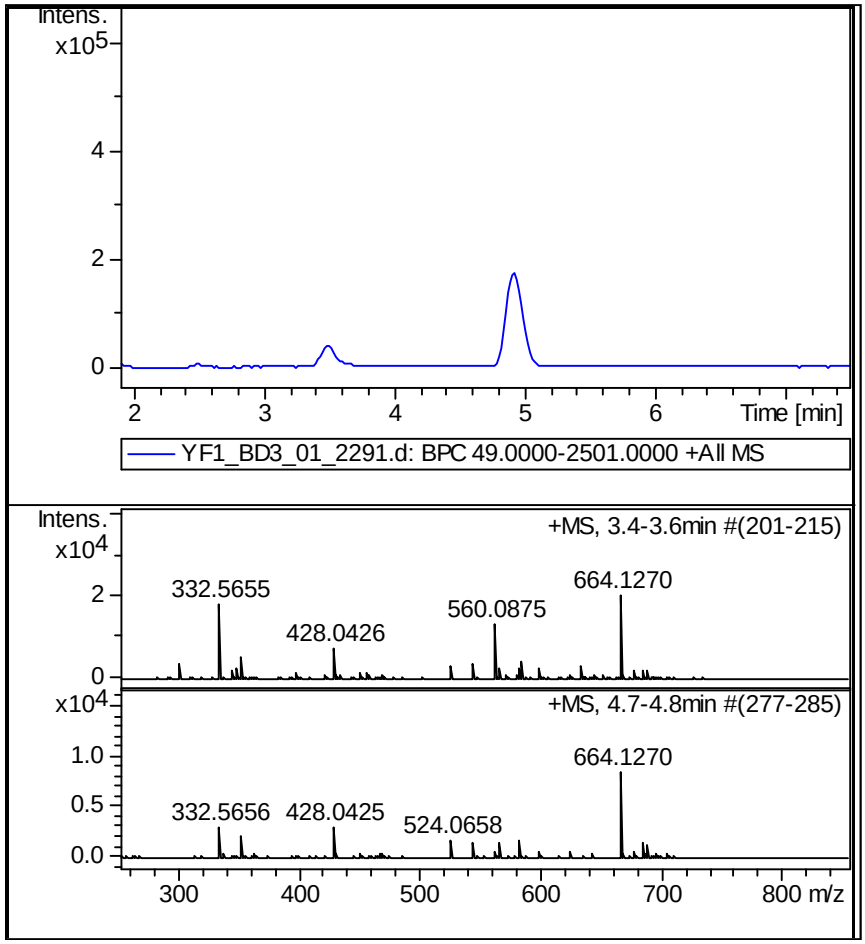
Intens.
x10^5
4
2
0
2
3
4
5
6
Time [min]
YF1_BD3_01_2291.d: BPC 49.0000-2501.0000 +All MS
Intens.
x10^4
+MS, 3.4-3.6min #(201-215)
332.5655
428.0426
560.0875
664.1270
x10^4
+MS, 4.7-4.8min #(277-285)
1.0
0.5
0.0
332.5656
428.0425
524.0658
664.1270
300
400
500
600
700
800 m/z

(C)

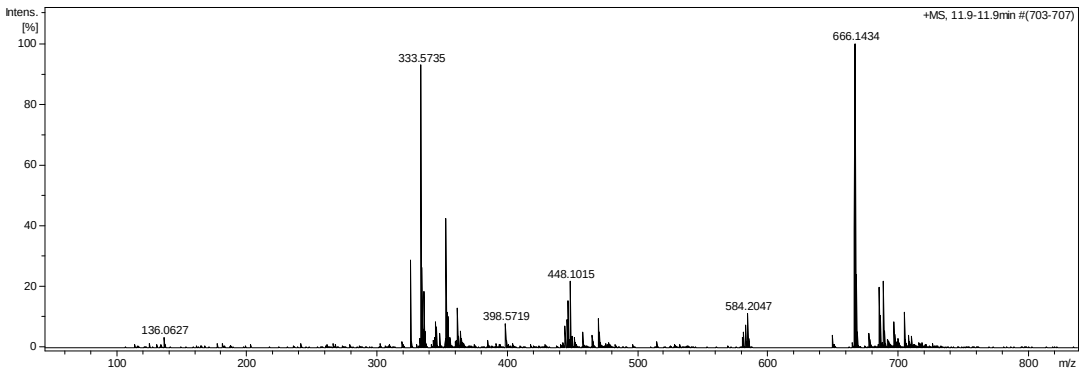
Intens.
[%]
+MS, 11.9-11.9min #(703-707)
100
80
60
40
20
0
333.5735
666.1434
448.1015
584.2047
398.5719
136.0627
100
200
300
400
500
600
700
800
m/z

(D)

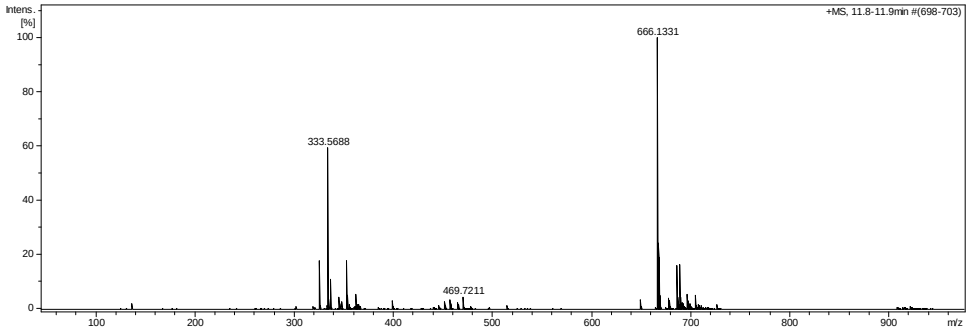
Intens.
[%]
+MS, 11.8-11.9min #(698-703)
666.1331
333.5688
469.7211
m/z

(E)

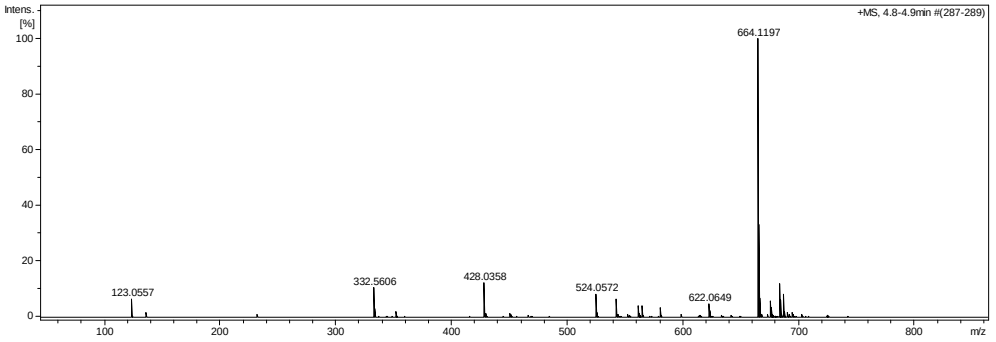
Intens.
[%]
+MS, 4.8-4.9min #(287-289)
664.1197
123.0557
332.5606
428.0358
524.0572
622.0649
m/z

(F)

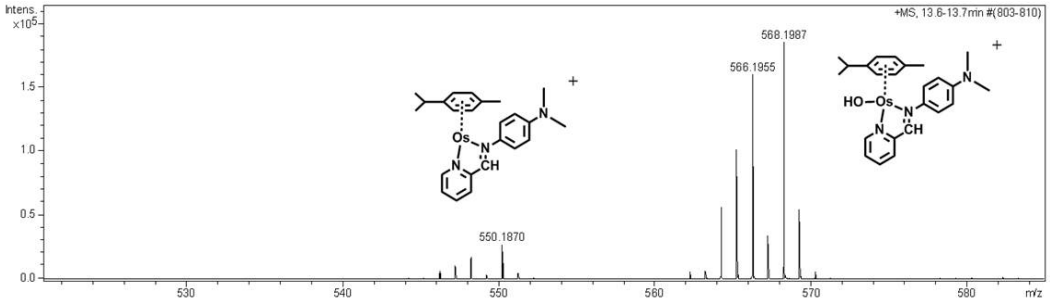
Intens.
x10^5
+MS, 13.6-13.7min #(803-810)
568.1987
566.1955
HO–Os
N
CH
Os
N
CH
550.1870
m/z

(G)

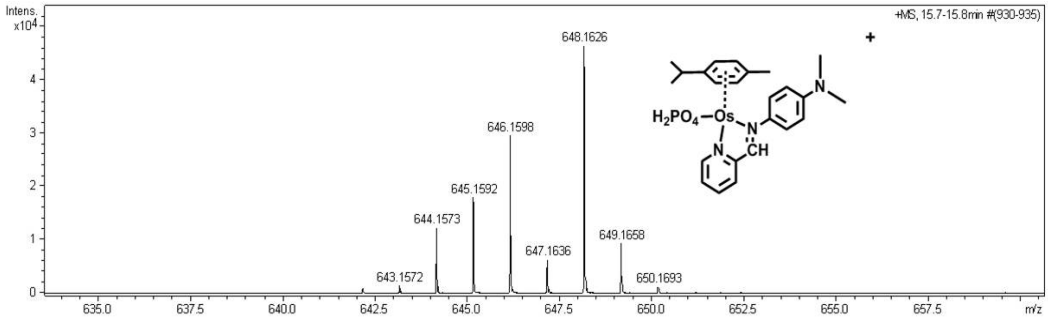
Intens.
x10^4
+MS, 15.7-15.8min #(930-935)
648.1626
646.1598
645.1592
644.1573
649.1658
647.1636
643.1572
650.1693
H2PO4–Os
N
CH
m/z

Figure 5.9. NADH (0.5 mM) with or without Complex **14A** (0.5 mM) were incubated at 310 K for 24 h, NAD^+ were incubated under the same conditions and LC-MS was employed to analyze the 3 samples. (A) HPLC separation of NADH (0.5 mM, green line), NADH with complex **14A** (blue line) and NAD^+ (0.5 mM, red line). (B) MS of first two appearing peaks from HPLC of NADH with complex **14A** (blue line). (C) MS of second appearing peak from HPLC (green line). (D) MS of third appearing peak from HPLC of NADH with Complex **14A** (blue line). (E) MS of NAD^+. (F) MS of **14A**. (G) MS of phosphate adduct of **14A**.

The catalytic reaction of the chlorido complex **14** with NADH (8 mol equiv) was monitored by UV-Vis over 18 h at 310 K using a phosphate buffer solution in H_2O (pH = 7.4, Fig. 5.10A). The kinetic experiment showed one isosbestic point at 300 nm corresponding to the oxidation from NADH to NAD^+ and another isosbestic point at 432 nm due to the hydrolysis of **14** in an aqueous solution, suggesting that the hydrolysis of the chloride complex **14** occurred during the catalytic reaction. The formation of NAD^+ was confirmed by the decrease of the characteristic band of the NADH at 338 nm and the simultaneous increase of the band at 260 nm. Additionally, the dependence of the catalytic activity of **14** on the concentration of NADH in solution was studied by following the conversion of 2 and 8 mol equivalents of NADH into NAD^+ (Fig. 5.10B) under the same conditions described above. The results indicate that in the presence of 25 μM of **14**, the conversion of NADH into NAD^+ is slightly higher for 2 equiv than for 8 equiv of NADH. In these experiments a slight decomposition of the NADH control was observed under these conditions due to the effect of phosphate buffer which is consistent with previous reports.[25, 26]

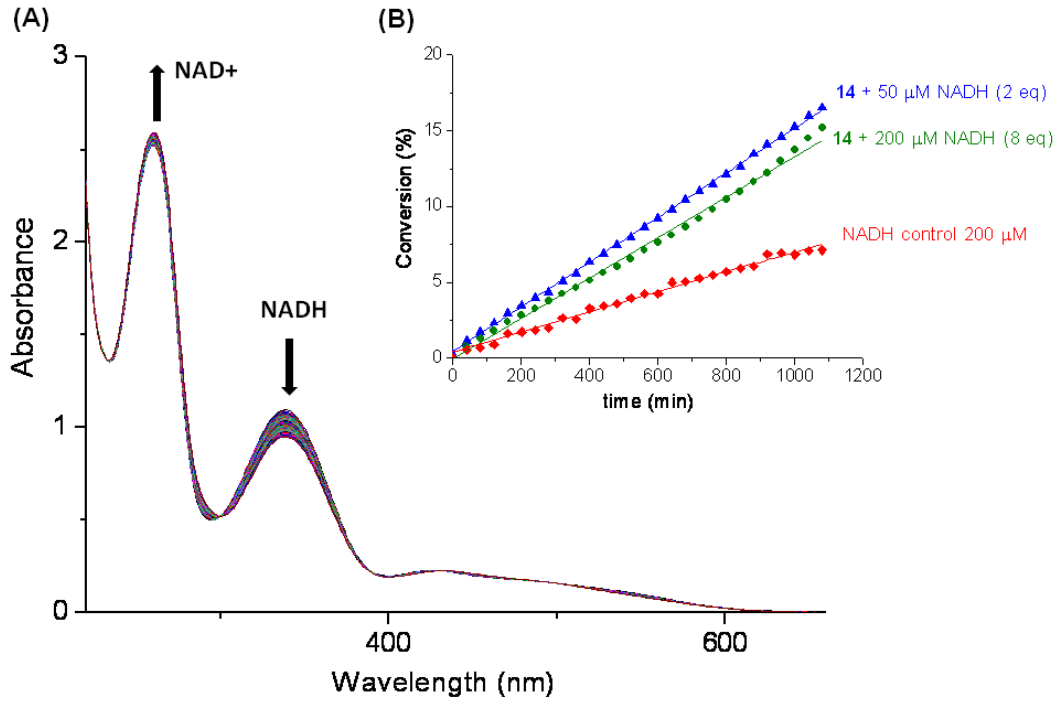

Figure 5. 10. **(A)** Monitored UV-Vis spectra corresponding to the reaction between the chlorido complex **14** (0.025 mM) and NADH (0.2 mM, 8 equiv). The spectra were recorded in phosphate buffer solution (pH* 7.4) during 18h at 310 K. Inset: **(B)** Conversion of 2 and 8 mol equiv of NADH into NAD^+ in the presence of complex **14** (0.025 mM) plotted versus time during 18 h.

To elucidate the mechanism of the catalytic of action of these compounds, the step following the formation of the osmium-hydride adduct was investigated. Gas chromatography (GC) was used for the detection of H_2 gas which could be a potential product from osmium hydride. However, no H_2 peak was detected by GC, indicating that the hydride is not transferred from the osmium-hydride adduct to the medium to form hydrogen gas.

The reaction between the osmium complex **14** (0.1 mM) and NADH (0.4 mM) was studied under aerobic condition or after degassing with argon for 10 min, the corresponding ^{1}H NMR spectra were recorded after 18 h of incubation at 310 K in a 10%MeOD/90%D_2O phosphate buffer solution (pH* = 7.4). A decrease in the NAD^+ product from 17% to 3% under argon atmosphere was observed (Fig. 5.11).

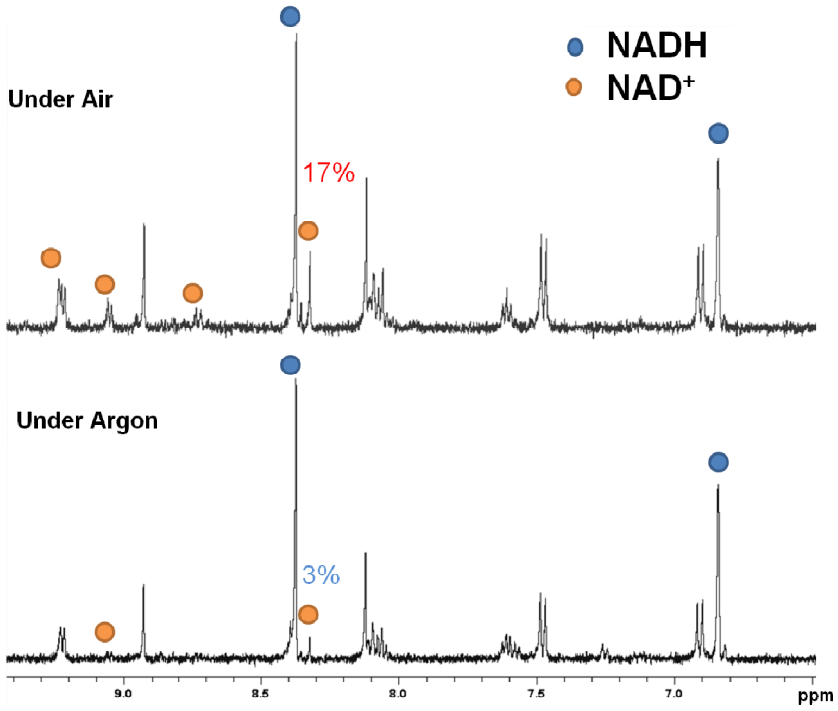

Figure 5.11. ^{1}H NMR spectra corresponding to the reaction between the osmium complex **14** (0.1 mM) and NADH (0.4 mM, 4 equivalents) under aerobic conditions (top spectrum) or degassed (bottom spectrum) with argon for 10 min. The spectra were recorded in a 10%MeOD /90%D_2O phosphate buffer solution (pH*=7.4) after 18 h incubation of the sample at 310 K.

When the reaction between **14** (0.1 mM) and NADH (0.5 mM) was performed after the oxygen saturation for 10 min. the NAD^+ product increased from 10% (reaction under aerobic condition) to 25% (saturated oxygen condition) whereas the control had no obvious NAD^+ formation (under oxygen saturation for 10 min without osmium complex, then incubate for 18 h at 310K) (Fig. 5.12).

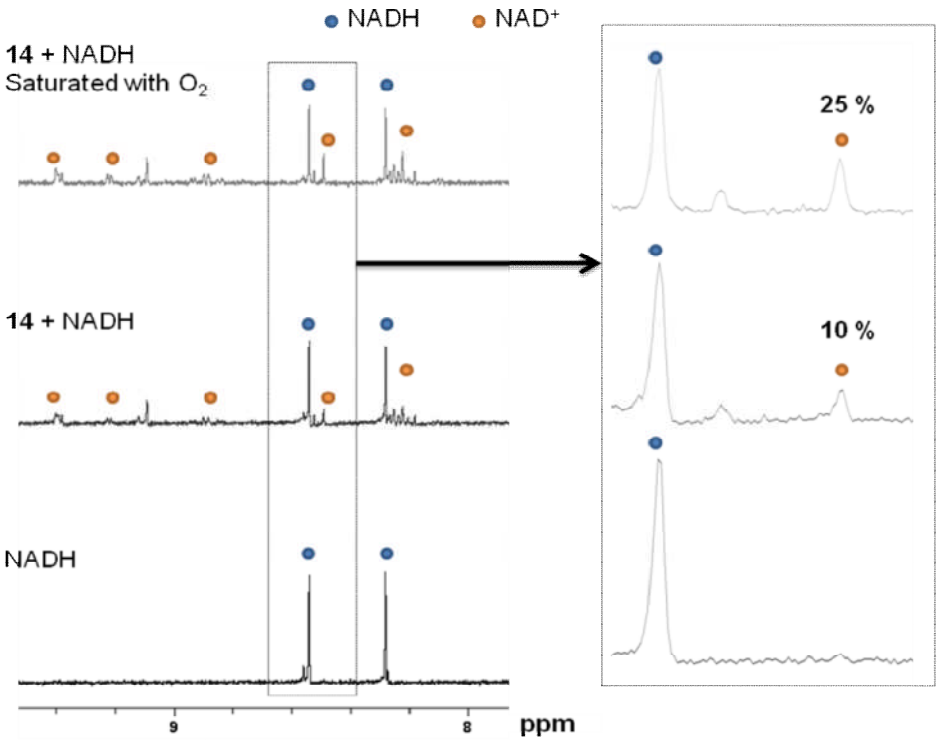

Figure 5.12. ^1H NMR spectra corresponding to the reaction between the osmium complex **14** (0.1 mM) and NADH (0.5 mM, 5 equivalents) under oxygen saturation condition (top spectrum), aerobic condition (middle spectrum) and the NADH control under oxygen saturation condition (bottom spectrum). The spectra were recorded in a 10%MeOD /90%D_2O phosphate buffer solution (pH*=7.4) after 18 h incubation of the sample at 310 K.

5.4. Discussions

5.4.1. Hydrolysis and Binding with 9-Ethylguanine

The chlorido complex (**14**) achieved higher hydrolysis extent than the iodido complex (**6**), which is in agreement with the more inert character of iodide as a ligand for osmium. To study the potential of DNA binding, the reaction of the hydrolyzed product of **14** (**14A**) with 9-EtG (model DNA nucleobase) was monitored at different time intervals by ^{1}H NMR. The binding process with 9-EtG was found to be much slower than the previously reported osmium DNA-targeted complexes[4] probably due to the low pK_a value (pK_a = 5.2) found in this complex. This value indicates the tendency of compound **14** to form the hydroxyl adduct **14A** under physiological conditions. For this reason, the predominant inert hydroxyl adduct (**14A**) interacts slowly with DNA nucleobases and consequently slows down the reaction[4] with 9-EtG reaching only 14% of binding with 9-EtG after 18 hours of incubation at 310K; the binding ratio only increased to 19% after another 20 h of incubation at 310K.

5.4.2. Structure Activity Relationships (SARs) on A2780 Cell Line

Comparing the anticancer activity of osmium arene iminopyridine complexes with their azopyridine analogues, the correlation coefficient of SAR is low (R^2= 0.0673), which indicates that the mechanism of action could be different for these two families of osmium anticancer complexes (Fig. 5.13). The major differences between them are: (1) the iminopyridine complexes can hydrolyze and bind to a DNA base; (2) the iminopyridine complexes can catalytically oxidize NADH to NAD^+.

It was found that all the iminopyridine complexes bearing biphenyl arene showed better anticancer activity to A2780 cells than their *p*-cymene analogues. The reasons might be the intercalation of the extended biphenyl arene with the DNA and/or the increase of hydrophobility which can facilitate the cellular uptake. In general, the chlorido complexes showed better or similar anticancer

activity compared to iodido analogues which is contrary to the trend observed for their azopyridine analogues except for those with a $–NMe_2$ electron withdrawing substituent in the phenyl moiety of the iminopyridine ligand. The functionalization of these compounds with a methoxy group in the ortho position on the pyridine ring of iminopyridine ligand decreased the anticancer activity significantly. This effect may due to the steric effect introduced by the methoxy group, and indicates that the binding site on osmium of the monodentate ligand is important for the mechanism of action.

It was noted that the anticancer activity of **6** and **14** is better than those obtained for ruthenium and osmium anticancer complexes reported previously[4, 27] which could bind DNA bases to greater extents and/or in faster speeds. This suggests that a different mechanism of action is involved in the biological activity of these iminopyridine complexes other than targeting DNA.

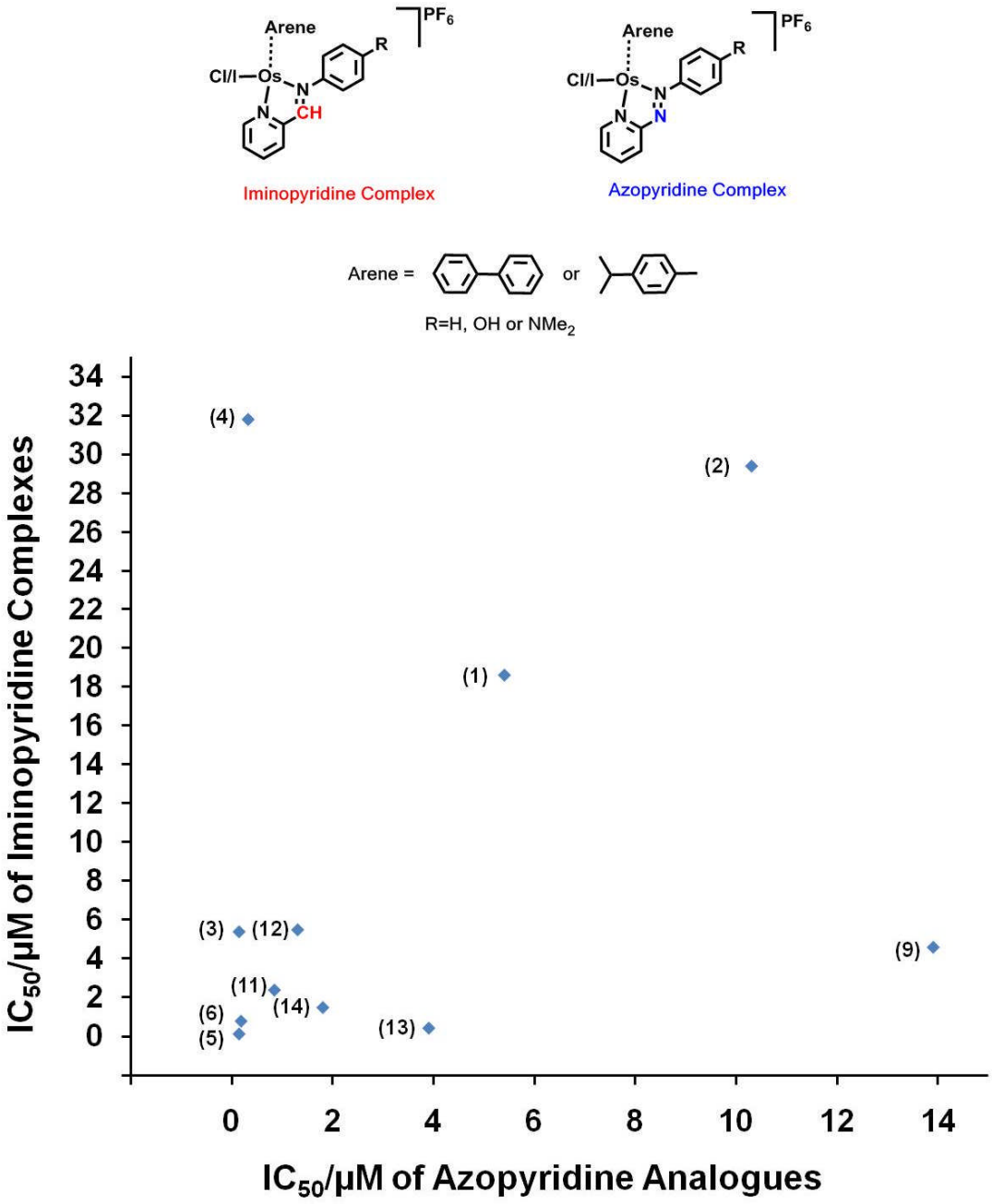

Figure 5.13. Correlations of structure-activity-relationships of osmium arene iminopyridine complexes with their azopyridine analogues. Each plot represents the IC_{50} value of one iminopyridine complex (y axis) labelled with number and its azopyridine analog (x axis).

5.4.3. Accumulations of Reactive Oxygen Species (ROS)

ROS are highly reactive O_2 metabolites that include superoxide radicals ($O_2^{-}\cdot$), hydrogen peroxide (H_2O_2) and hydroxyl radicals ($OH\cdot$).[28] Because cancerous cells have increased ROS levels compared to normal cells, this difference can be exploited as a biochemical basis for therapeutic selectivity.[29, 30] Increasing the ROS level in cancer cells can reach the threshold to induce cell death but can be tolerated by normal cells.[30] Because the GSH concentration is higher (100-10,000 fold) compared to other reductants (NADH, NADPH and thioredoxin) of redox couples in cells, the level of GSH usually determines the steady-state value of intracellular redox potentials.[31] However, it was found that **6** and **14** cannot catalytically oxidize GSH similarly as their ruthenium azopyridine analogues. The cyclic voltammetry studies of **6** and **14** together with **3** and **10** showed that these compounds underwent an irreversible electrochemical reduction in dimethylformamide. Two reduction peaks during cyclic voltammetry study were found for all the four complexes, the first from –0.58 to –0.76 V and the second from –0.82 to –1 V. All the reduction peaks are more negative than -0.5 V and the processes are not reversible (no reverse scan peak at 0.1 Vs^{-1} as shown in figure 5.14). The overlapped reduction peaks make it hard to identify whether there is a one-electron reduction and calculate the redox potentials. However the reduction peaks are more negative than the ruthenium azopyridine complexes, indicating that the imine bonds in the osmium complexes are harder to reduce than the azo bonds within ruthenium azopyridine complexes. These results might explain why no GSH oxidation was observed for osmium arene iminopyridine complexes.[22]

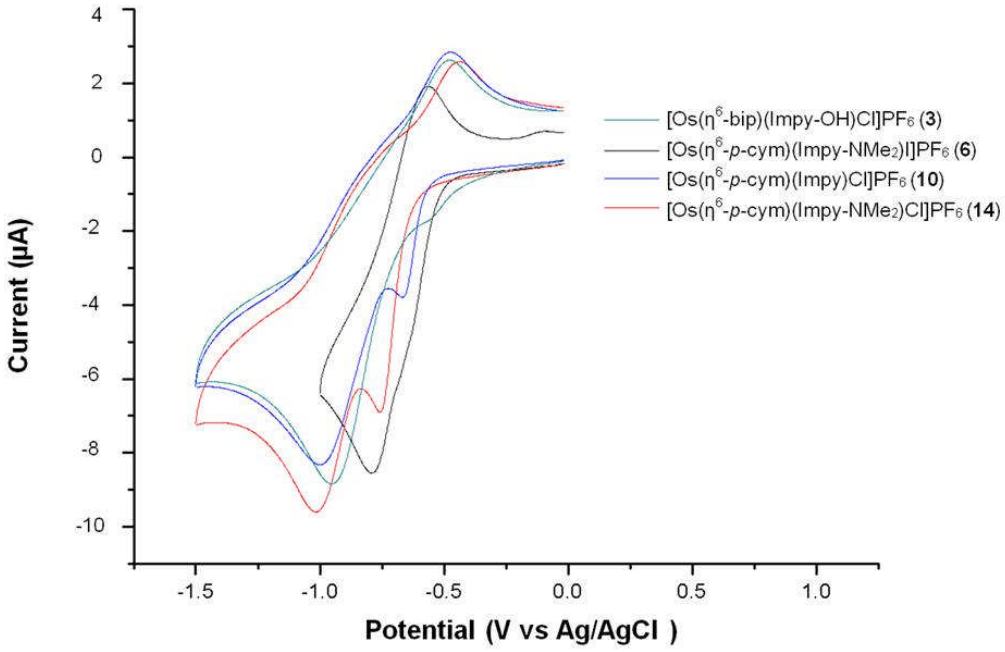

Complex	Reduction Peak /V
(**3**) [Os(η^6-bip)(Impy-OH)I]PF_6	-0.58 and -0.95
(**6**) [Os(η^6-*p*-cym)(Impy-NMe_2)I]PF_6	-0.65 and -0.82
(**10**) [Os(η^6-*p*-cym)(Impy)Cl]PF_6	-0.67 and -1.0
(**14**) [Os(η^6-*p*-cym)(Impy-NMe_2)Cl]PF_6	-0.76 and -1.0

Figure 5.14. Cyclic voltammograms for **3**, **6**, **10** and 1**4** (in 0.1 M tetrabutylammonium BF_4 DMF, sweep from 0 to -1.5 to 0 V or 0 to -1.0 to 0 V at scan rate 0.1 V/s). Reduction peaks were also listed in the table.

5.4.4. Catalytic Oxidation of NADH

Following the evidence for generation of ROS and with the aim of rationalizing the surprisingly good anticancer activity of these osmium (II) iminopyridine complexes, a catalytic reaction employing the reducing agent NADH was discovered. The reaction between the iminopyridine complexes and NADH was monitored by ^{1}H NMR for **6**, **8**, **14** and **16**, LC-MS for **14A** and UV-Vis spectroscopy for **14**. All these data consistently showed the oxidation of NADH and their behaviours as catalysts.

The ^{1}H NMR studies show that **6** and **14** can oxidize a greater amount of NADH than **8** and **16** after 24 h incubation at 310K. This could be due to the steric hindrance exerted by the methoxy substituent on the ortho-position of the iminopyridine chelating ligand for **8** and **16** (Fig. 5.6). This trend is also in agreement with the anticancer activity of these compounds (**6** and **14** are more active than **8** and **16)**. It was noted that the complexes with the methoxy substituent exhibit 20 times less anticancer activity than **8** and **16**, indicating that the catalytic reaction with NADH is involved in the mechanism of action for osmium iminopyridine anticancer complexes.

During the catalytic conversion from NADH to NAD^+ in the presence of **14A**, an osmium-hydride peak was detected by ^{1}H NMR at –4.20 ppm. This value is in agreement with previous reports of osmium-hydride peaks identified at similar chemical shifts by NMR.[32] Although several examples of hydride transfer have been published for osmium(II) complexes, this is still the first time an osmium(II) hydride peak has been detected in an aqueous solution by NMR. This is also the first example of an osmium compound which is able to transfer the hydride from a biomolecule as one hydride source (NADH). This evidence indicated the potency of using osmium complexes as catalysts to interfere in biological systems. The hydride transfer initiated by **14A** during the reaction with NADH was demonstrated with the detection of the Os(II)-hydride signal after 3 h and 6 h by ^{1}H NMR experiment, using a sample preincubated for 24 h at 310 K. However,

no hydride peak was detected after 21 h, which indicated that the hydride adduct is not stable enough but its formation is important for the catalytic oxidation reaction with NADH.

LC-MS was also performed to determine the product of **14A** with NADH after 24 hours of incubation at 310 K. NADH and NAD^+ references were incubated under the same conditions for comparison. For the sample of NADH with **14A**, one peak appeared at the same retention time of NAD^+ reference and also the mass spectrum showed one peak at 664.1 m/z corresponding to the NAD^+ which confirmed the oxidation of the NADH. It must be noticed that a small peak appeared before the appearance of the NAD^+ peak, which follows the same pattern of NAD^+ in the MS suggesting an isomer of NAD^+, but further tests are needed to confirm its chemical structure (Fig. 5.9). Further investigation of the chlorido complex **14** showed that it can catalytically oxidize NADH even when sodium chloride was added to suppress its hydrolysis. This study demonstrated that the Os-Cl complex can transfer hydride directly and that hydrolysis is not a prerequisite step for the formation of osmium hydride using NADH as a hydride source (Fig. 5.15).

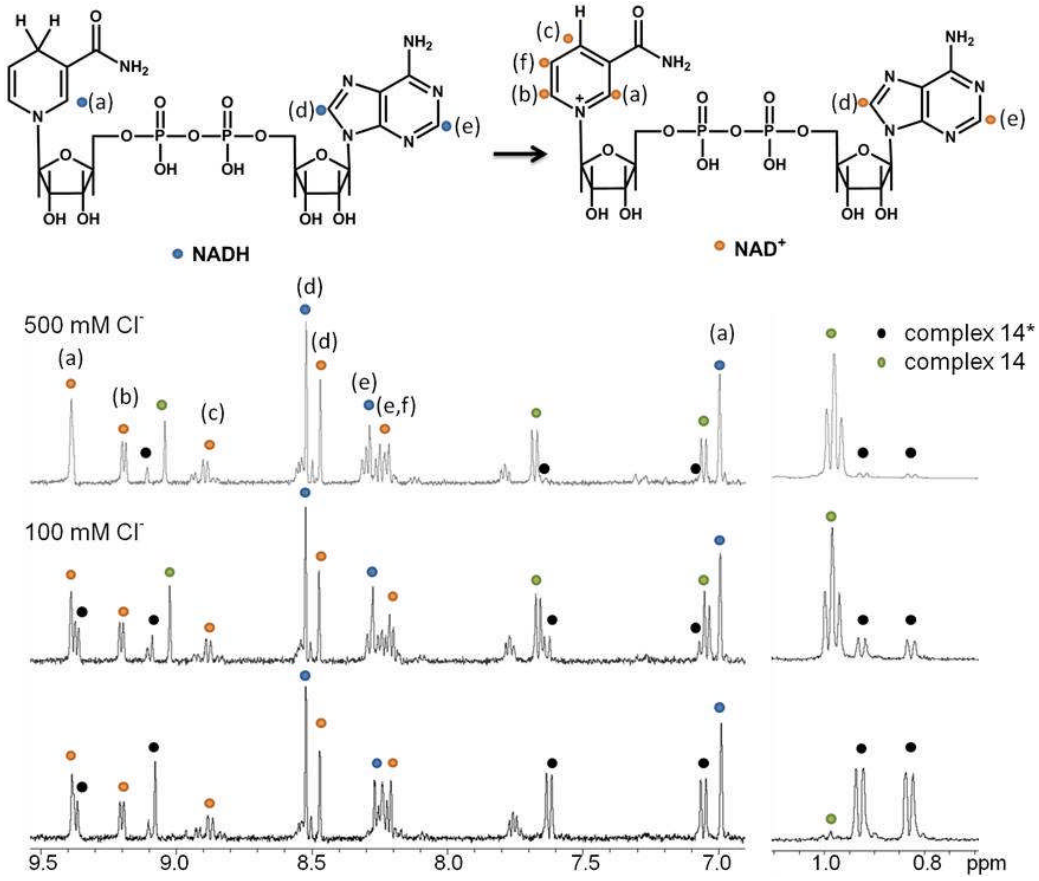

Figure 5.15. Effect of adding Cl^- on NADH catalytic oxidation by complex **14** in a solution of 10% MeOD-d_4/90% D_2O phosphate buffer (pH*=7.4) after 24 h incubation at 310 K.

For the elucidation of the catalytic mechanism, it was firstly checked whether the osmium hydride can form hydrogen gas, but no H_2 was detected after the incubation of NADH with **14** or **14A** after 24 h at 310 K. It was also studied whether air was involved in the catalytic reaction. ^{1}H-NMR experiments were used to monitor the influence of the aerobic atmosphere on the catalytic reaction. It was found that the catalytic oxidation of NADH by **14** is significantly depressed after degassing the solution with argon (Fig 5.11). On the contrary, oxidation of NADH by **14** was facilitated in oxygen-saturated solution (Fig. 5.12). This suggested the involvement of oxygen in the oxidation of NADH, and it is very likely to be oxygen in the air who takes part in this catalytic reaction facilitating the generation of ROS. Taking all this evidence into account, A possible catalytic mechanism of action was proposed based in the interaction of these compounds with the NADH through a hydride transfer process with the concomitant formation of a osmium-hydride adduct and NAD^+ (Chart 5.2), the regeneration of the osmium iminopyridine catalyst would take place after the hydrogenation of dissolved molecular oxygen to produce H_2O_2. Further investigations will be necessary to uncover the details of this mechanism of action.[33-35]

Finally, a concentration dependent cell cycle arrest on S phase (increase from 10% to 21%) was also detected on A2780 cancer cells induced by complex **14** (Fig. 5.16). This indicated that a consequence after DNA was damaged; the cancer cells will be halted at S phase for DNA repairs.

Under physiological conditions, the aqua osmium complex has a tendency to form the Os-OH hydroxyl adduct, which is an inert ligand that can stop the poisoning of the catalyst for NADH oxidation. With DNA nucleobase (9-ethylguanine) binding and a catalytic NADH oxidation induced by the osmium iminopyridine complexes, the combined mechanism may explain the reason why this family of osmium complexes showed good anticancer activity.

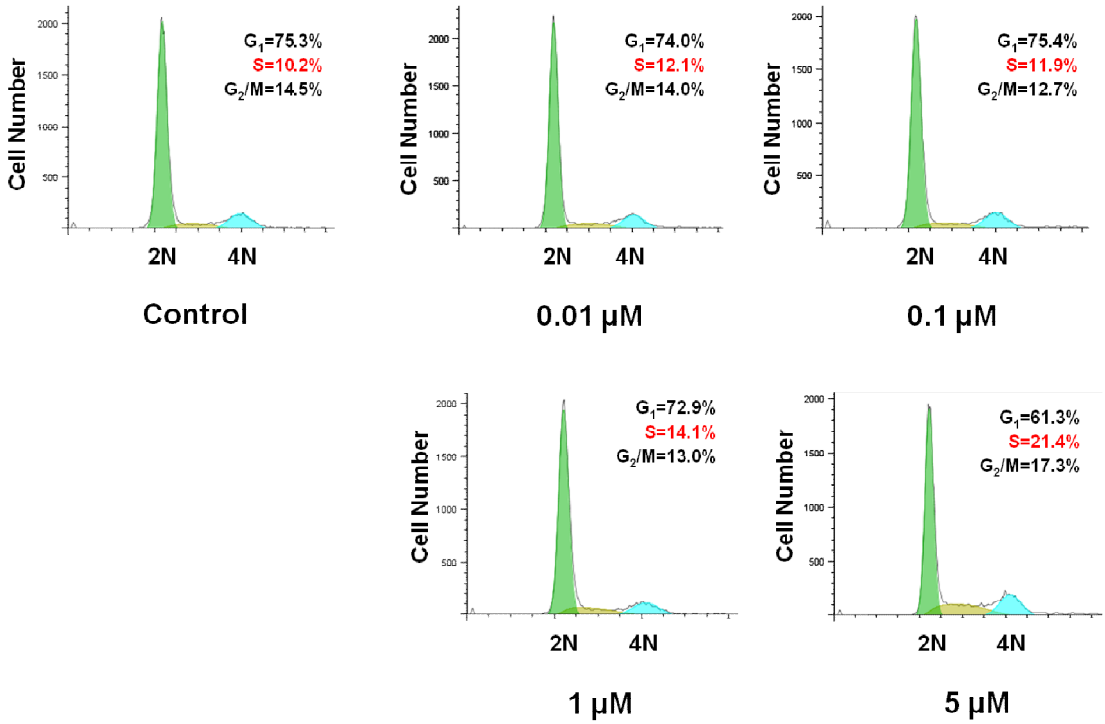

Figure 5.16. S phase cell cycle arrest induced complex **14** at different concentrations after incubation of 24 h on A2780 human ovarian cancer cell line**.**

Chart 5.2. Proposed catalytic mechanism for the oxidation of NADH to NAD$^+$.

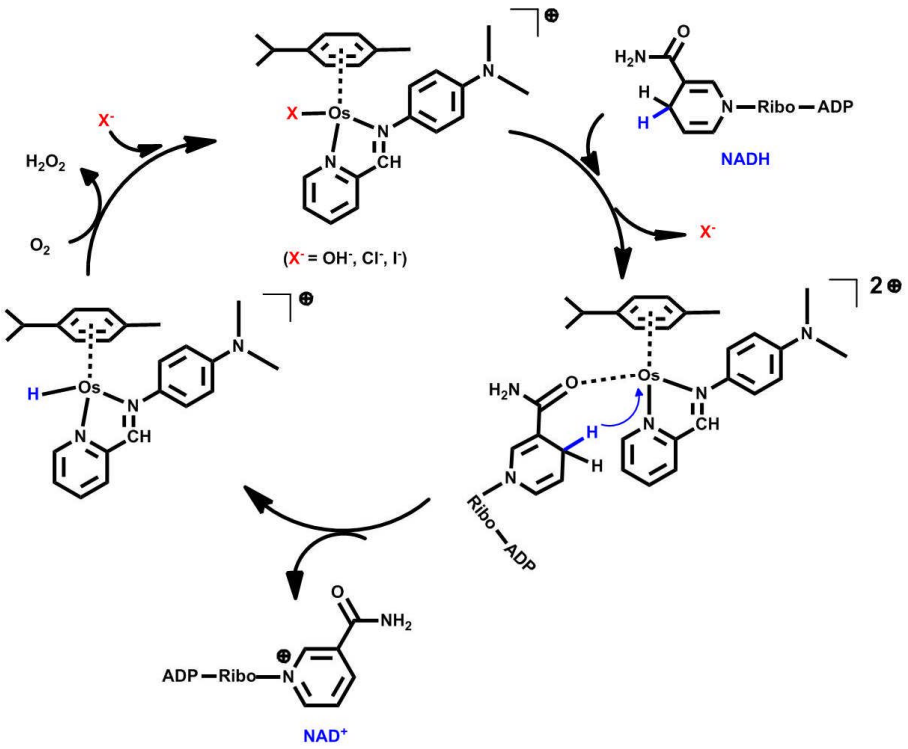

5.5. Conclusions

Based on the previous work on osmium azopyridine complexes, the iminopyridine complexes were designed and were found to show a good potential for anticancer activity. However, different from their azopyridine analogues, they can hydrolyze and bind to 9-EtG, the mechanism involves DNA base binding and a novel catalytic oxidation of NADH. This is the first example of an osmium compound showing the capability to transfer hydride from a biomolecule: NADH. This evidence indicated the potency of using osmium complexes as catalysts to interfere in biological systems.

5.6 Summary

Previously, the first organometallic osmium arene complex [Os(η^6-*p*-cym)(Azpy-NMe_2)I]PF_6 (FY026) showing potent anticancer activity *in vivo* was reported. In this work, its bioisosteres by changing the azopyridine chelating ligand to iminopyridine were mainly investigated. Sixteen osmium arene iminopyridine complexes were synthesized, well characterized and showed anticancer activity in the same range of cisplatin against A2780 cancer cells. Totally different structure-activity relationships comparing iminopyridine complexes with azopyridine complexes were identified which suggested a different anticancer mechanism. Dissimilarly from FY026, [Os(η^6-*p*-cym)(Impy-NMe_2)I]PF_6 (**6)** and [Os(η^6-*p*-cym)(Impy-NMe_2)Cl]PF_6 (**14)** were found to be able to undergo hydrolysis and the binding of the hydrolyzed product (**14A**) to 9-ethylguanine was observed. Moreover, an osmium hydride intermediate in a catalytic process to form NAD^+ was discovered. This process might be involved in the anticancer mechanism of action. A mechanism of action based in the interaction of these compounds with DNA nucleobase and catalytically oxidizing NADH is proposed.

5.7 References

1. W.-X. Ni, W.-L. Man, M. T.-W. Cheung, R. W.-Y. Sun, Y.-L. Shu, Y.-W. Lam, C.-M. Che and T.-C. Lau, *Chem. Commun.*, 2011, **47**, 2140-2142.
2. Y. Fu, A. Habtemariam, A. M. Pizarro, S. H. van Rijt, D. J. Healey, P. A. Cooper, S. D. Shnyder, G. J. Clarkson and P. J. Sadler, *J. Med. Chem.*, 2010, **53**, 8192-8196.
3. S. D. Shnyder, Y. Fu, A. Habtemariam, S. H. van Rijt, P. A. Cooper, P. M. Loadman and P. J. Sadler, *MedChemComm.*, 2011, **2**, 666–668..
4. A. F. A. Peacock, S. Parsons and P. J. Sadler, *J. Am. Chem. Soc.*, 2007, **129**, 3348-3357.
5. S. H. van Rijt, A. J. Hebden, T. Amaresekera, R. J. Deeth, G. J. Clarkson, S. Parsons, P. C. McGowan and P. J. Sadler, *J. Med. Chem.*, 2009, **52**, 7753-7764.
6. H. Kostrhunova, J. Florian, O. Novakova, A. F. A. Peacock, P. J. Sadler and V. Brabec, *J. Med. Chem.*, 2008, **51**, 3635-3643.
7. C. Bernstein, H. Bernstein, C. M. Payne and H. Garewal, *Mutat. Res-rev. Mutat.*, 2002, **511**, 145-178.
8. H. Pelicano, D. S. Martin, R. H. Xu and P. Huang, *Oncogene*, 2006, **25**, 4633-4646.
9. W. Ying, *Antioxid. Redox Signaling*, 2008, **10**, 179-206.
10. Q. Zhang, D. W. Piston and R. H. Goodman, *Science*, 2002, **295**, 1895-1897.
11. E. Steckhan, S. Herrmann, R. Ruppert, E. Dietz, M. Frede and E. Spika, *Organometallics*, 1991, **10**, 1568-1577.
12. H. C. Lo, C. Leiva, O. Buriez, J. B. Kerr, M. M. Olmstead and R. H. Fish, *Inorg. Chem.*, 2001, **40**, 6705-6716.
13. Y. Yan, M. Melchart, A. Habtemariam, A. Peacock and P. Sadler, *J. Biol. Inorg. Chem.*, 2006, **11**, 483-488.

14. M. Jasna, S. W. Douglas , G. E. Atilla-Gokcumen, S. M. S. Keiran , J. C. Patrick , D. W. Richard , F. Panagis, K. Stefan, H. Meenhard and M. Eric, *Chem.--Eur. J.*, 2008, **14**, 4816-4822.
15. A. Dorcier, W. H. Ang, S. Bolaño, L. Gonsalvi, L. Juillerat-Jeannerat, G. Laurenczy, M. Peruzzini, A. D. Phillips, F. Zanobini and P. J. Dyson, *Organometallics*, 2006, **25**, 4090-4096.
16. A. F. A. Peacock, A. Habtemariam, S. A. Moggach, A. Prescimone, S. Parsons and P. J. Sadler, *Inorg. Chem.*, 2007, **46**, 4049-4059.
17. Y. C. Martin, *J. Med. Chem.*, 1981, **24**, 229-237.
18. S. S. Hindo, A. M. Mancino, J. J. Braymer, Y. Liu, S. Vivekanandan, A. Ramamoorthy and M. H. Lim, *J. Am. Chem. Soc.*, 2009, **131**, 16663-16665.
19. *CrysAlis PRO, Oxford Diffraction Ltd., Abington, Oxfordshire, U.K., 2007.*
20. G. M. Sheldrick, Acta Crystallogr., Sect. A: Found. Crystallogr., 1990, 46, 467–473.
21. G. M. Sheldrick, SHELX97, Programs for Crystal Structure Analysis (Release 97-92), University of Göttingen, Germany, 1997.
22. S. J. Dougan, A. Habtemariam, S. E. McHale, S. Parsons and P. J. Sadler, *Proc. Natl. Acad. Sci. U. S. A.*, 2008, **105**, 11628-11633.
23. H. Brunner, *Eur. J. Inorg. Chem.*, 2001, 905-912.
24. Y. Fu, A. Habtemariam, A. M. B. H. Basri, D. Braddick, G. J. Clarkson and P. J. Sadler, *Dalton Transactions*, 2011, **40**, 10553-10562.
25. J. Wu, L. Wu and J. Knight, *Clin Chem.*, 1986, **32**, 314-319.
26. R. M. Burton and N. O. Kaplan, *Arch. Biochem. Biophys.*, 1963, **101**, 139-149.
27. H.-K. Liu and P. J. Sadler, *Acc. Chem. Res.*, 2011, **44**, 349-359.
28. V. J. Thannickal and B. L. Fanburg, *Am. J. Physiol. Lung Cell Mol. Physiol.*, 2000, **279**, 1005-1028.

29. E. Hileman, J. Liu, M. Albitar, M. Keating and P. Huang, *Cancer Chemoth. Pharm.*, 2004, **53**, 209-219.

30. J. W. a. J. Yi, *Cancer Bio. Ther.*, 2008, **7**, 1875-1884.

31. F. Q. Schafer and G. R. Buettner, *Free Radical Biol. Med.*, 2001, **30**, 1191-1212.

32. T. Bolaño, R. Castarlenas, M. A. Esteruelas, F. J. Modrego and E. Oñate, *J. Am. Chem. Soc.*, 2005, **127**, 11184-11195.

33. T. Matsuo and J. M. Mayer, *Inorg. Chem.*, 2005, **44**, 2150-2158.

34. S. Fukuzumi, K. Ohkubo, Y. Tokuda and T. Suenobu, *J. Am. Chem. Soc.*, 2000, **122**, 4286-4294.

35. S. Fukuzumi, Y. Tokuda, T. Kitano, T. Okamoto and J. Otera, *J. Am. Chem. Soc.*, 1993, **115**, 8960-8968.

Chapter 6
Chiral Osmium Iminopyridine Complexes

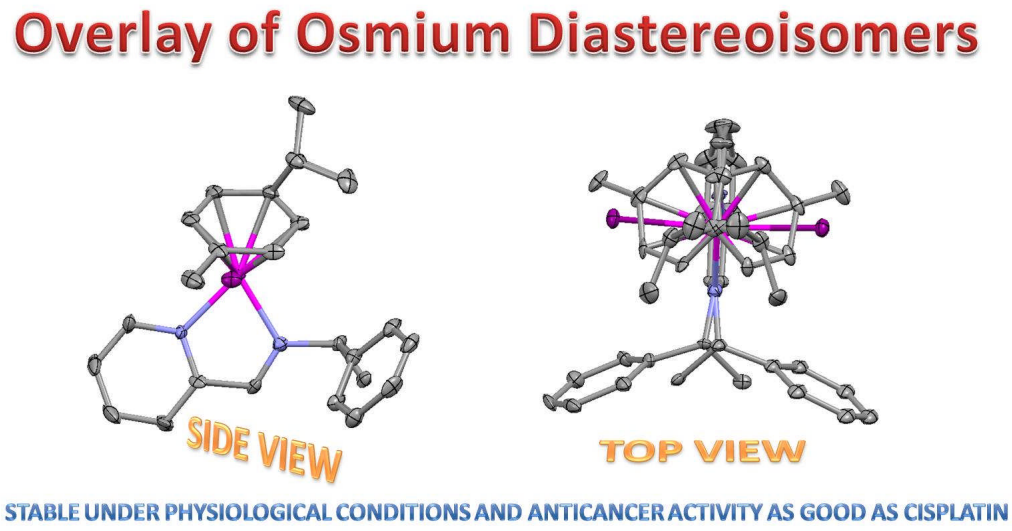

6.1 Introduction

After the tragedy of severe birth defects caused by the S isomer of thalidomide in the 1950s (thalidomide was originally used as a sedative drug then found to be an inhibitor of angiogenesis in recent years),[1, 2] it had been compulsory for all the drug candidates to purify the isomers and identify their toxicities. For organometallic arene complexes with the three-legged piano-stool structure which contain an unsymmetrical chelating ligand and an additional monodentate ligand, the metal atom becomes a chiral centre.[3] It is also necessary to investigate the stability, biological activity and toxicity of chiral-at-metal[4] organometallic drug candidates. Some early work has been done: the chirality of a ruthenium centre was found to be able to affect the inhibition of glycogen synthease kinase 3β;[5] the first purification of Z/E isomers of chiral osmium arene paullone complexes by crystallization demonstrated that Z/E isomers are able to undergo an exchange in solution.[6]

In 1911, Werner successfully isolated the first enantiomerically pure metal complex,[4] this discovery paved the way for the study on chiral metal complexes in enantioselective catalysis over the last 40 years.[7-9] Nevertheless, reports on the stabilities and anticancer activites of chiral osmium arene complexes are scarce. The reasons may be chiral enantiomers are not easy to purify, chiral columns are expensive with relatively small yield and chirality-selective synthesis for a metal centre is still not always easily applicable.

In this Chapter, two chiral iminopyridine chelating ligands were used: N-(2-pyridylmethylene)-(S)-1-phenylethylamine (Impy-S) and N-(2-pyridylmethylene)-(R)-1-phenylethylamine (Impy-R) (Fig. 6.1), chiral osmium complexes obtained were isolated by crystallizations and were studied for anticancer activity against A2780 human ovarian cancer cell line; in addition, the NCI 60-cell line screening results were also reported.

6.2 Experimental

6.2.1 Materials

$OsCl_3 \cdot 3H_2O$ was purchased from Alfa-Aesar. Ethanol and methanol were dried over Mg/I_2 or anhydrous quality was used (Aldrich). All other reagents used were obtained from commercial suppliers and used as received. The preparation of the starting material $[Os(\eta^6\text{-}p\text{-cym})Cl_2]_2$ has been previously reported.[10] The synthesis of the chirally pure iminopyridine ligands was carried out as reported.[11] The A2780 human ovarian carcinoma cell line was purchased from European Collection of Animal Cell Cultures (Salisbury, UK), RPMI-1640 media and trypsin were purchased from Invitrogen, bovine serum from Biosera, penicillin, streptomycin, trichloroacetic acid (TCA) and sulforhodamine B (SRB) from Sigma-Aldrich, and tris[hydroxymethyl]aminomethane from Formedium.

6.2.2 Syntheses

$[Os(\eta^6\text{-}p\text{-cym})(Imine\text{-}S)Cl]PF_6$ (1). $[Os(\eta^6\text{-}p\text{-cym})Cl_2]_2$ (50.0 mg, 0.063 mmol) was dissolved in methanol (20 mL) at 313 K. Imine-S (26.9 mg, 0.12 mmol) in methanol (10 mL) was added drop-wise; the solution-colour changed from orange to red immediately. The solution was stirred at ambient temperature for 2 h. Ammonium hexafluorophosphate (41.2 mg. 0.24 mmol) was added. Then the solution was left in the fridge (277 K) for 24 h. Dark coloured crystals precipitated which were collected by filtration, washed with diethyl ether, finally dried in vacuum. Yield: 54.0 mg (58.7 %). ESI-MS Calcd for $C_{24}H_{28}ClN_2Os$: m/z 571.2, found 571.1. ^{1}H NMR($(CD_3)_2CO$): δ 9.59 (d, 1H, J = 6 Hz), 9.32 (s, 1 H), 8.47 (d, 1H, J = 8 Hz), 8.32 (t, 1H, J = 6 Hz), 7.73 (t, 2H, J = 6 Hz), 7.62-7.55 (m, 3H), 6.55 (d, 1H, J = 6 Hz), 6.16 (d, 1H, J= 6 Hz), 6.06 (qd, 1H, J = 6 Hz), 5.89 (d, 2H, J = 6 Hz), 2.65 (s, 3H), 2.54-2.42 (m, 1H), 2.38 (s, 6H), 1.93 (d, 3H, J = 6 Hz), 1.07 (d, 3H, J = 7 Hz), 0.94 (d, 3H, J = 7 Hz). CHN analysis: Found: C,

40.30%; H, 3.87%; N, 3.90%. Calcd for $C_{24}H_{28}ClF_6N_2OsP$: C, 40.31% H, 3.95% N, 3.92%.

[Os(η^6-*p*-cym)(Imine-S)I]PF$_6$ (2). [Os(η^6-*p*-cym)I$_2$]$_2$ (50.0 mg, 0.043 mmol) was dissolved in methanol (20 mL) at 313 K. Imine-S (19.3 mg, 0.086 mmol) in methanol (10 mL) was added drop-wise, the solution-colour changed from orange to red immediately. The solution was stirred at ambient temperature for 24 h. Ammonium hexafluorophosphate (28.0 mg. 0.17 mmol) was added. Then the solution was left in the fridge (277 K) for 24 h. Dark coloured crystals precipitated which were collected by filtration, washed with diethyl ether, finally dried in vacuum. Yield: 28.9 mg (33.8 %). ESI-MS Calcd for $C_{24}H_{28}IN_2Os$: m/z 663.1, found 663.0. ^{1}H NMR($(CD_3)_2CO$): δ 9.57 (d, 1H, J = 6 Hz), 9.43 (s, 1 H), 8.48 (d, 1H, J = 8 Hz), 8.25 (t, 1H, J = 6 Hz), 7.77 (t, 2H, J = 6 Hz), 7.52-7.48 (m, 3H), 6.49 (d, 1H, J = 6 Hz), 6.26 (d, 1H, J= 6 Hz), 6.08 (qd, 1H, J = 6 Hz), 6.04 (d, 1H, J = 6 Hz), 5.83 (d, 1H, J= 6 Hz), 2.84 (s, 3H), 2.67-2.602 (m, 1H), 2.65 (s, 6H), 2.13 (d, 3H, J = 7 Hz), 1.09 (d, 3H, J = 7 Hz), 0.96 (d, 3H, J = 7 Hz). CHN analysis: Found: C, 35.76%; H, 3.53%; N, 3.36%. Calcd for $C_{24}H_{28}F_6IN_2OsP$: C, 35.74 % H, 3.50 % N, 3.47 %.

[Os(η^6-*p*-cym)(Imine-R)Cl]PF$_6$ (3). [Os(η^6-*p*-cym)Cl$_2$]$_2$ (50.0 mg, 0.063 mmol) was dissolved in methanol (20 mL) at 313 K. Imine-R (26.9 mg, 0.12 mmol) in methanol (10 mL) was added drop-wise, the solution-colour changed from orange to red immediately. The solution was stirred at ambient temperature for 2 h. Ammonium hexafluorophosphate (41.2 mg. 0.24 mmol) was added. Then the solution was left in the fridge (277K) for 24 h. Dark coloured crystals precipitated which were collected by filtration, washed with diethyl ether, finally dried in vacuum. Yield: 25.5 mg (27.7 %). ESI-MS Calcd for $C_{24}H_{28}ClN_2Os$: m/z 571.2, found 571.1. ^{1}H NMR($(CD_3)_2CO$): δ 9.59 (d, 1H, J = 6 Hz), 9.32 (s, 1 H), 8.47 (d, 1H, J = 8 Hz), 8.32 (t, 1H, J = 6 Hz), 7.73 (t, 2H, J = 6 Hz), 7.62-7.55 (m, 3H), 6.55 (d, 1H, J = 6 Hz), 6.16 (d, 1H, J= 6 Hz), 6.06 (qd, 1H, J = 6 Hz), 5.89 (d, 2H,

J = 6 Hz), 2.65 (s, 3H), 2.54-2.42 (m, 1H), 2.38 (s, 6H), 1.93 (d, 3H, J = 6 Hz), 1.07 (d, 3H, J = 7 Hz), 0.94 (d, 3H, J = 7 Hz).. CHN analysis: Found: C, 40.16 %; H, 3.80%; N, 3.90%. Calcd for $C_{24}H_{28}ClF_6N_2OsP$: C, 40.31% H, 3.95% N, 3.92%.

[Os(η^6-*p*-cym)(Imine-R)I]PF_6 (4). [Os(η^6-*p*-cym)I_2]$_2$ (50.0 mg, 0.043 mmol) was dissolved in methanol (20 mL) at 313 K. Imine-R (19.3 mg, 0.086 mmol) in methanol (10 mL) was added drop-wise, the solution-colour changed from orange to red immediately. The solution was stirred at ambient temperature for 24 h. Ammonium hexafluorophosphate (28.0 mg. 0.17 mmol) was added. Then the solution was left in the fridge (277K) for 24 h. Dark coloured crystals precipitated which were collected by filtration, washed with diethyl ether, finally dried in vacuum. Yield: 25.2 mg (35.6 %). ESI-MS Calcd for $C_{24}H_{28}IN_2Os$: m/z 663.1, found 663.0. ^{1}H NMR($(CD_3)_2CO$): δ 9.57 (d, 1H, J = 6 Hz), 9.43 (s, 1 H), 8.48 (d, 1H, J = 8 Hz), 8.25 (t, 1H, J = 6 Hz), 7.77 (t, 2H, J = 6 Hz), 7.52-7.48 (m, 3H), 6.49 (d, 1H, J = 6 Hz), 6.26 (d, 1H, J= 6 Hz), 6.08 (qd, 1H, J = 6 Hz), 6.04 (d, 1H, J = 6 Hz), 5.83 (d, 1H, J= 6 Hz), 2.84 (s, 3H), 2.67-2.602 (m, 1H), 2.65 (s, 6H), 2.13 (d, 3H, J = 7 Hz), 1.09 (d, 3H, J = 7 Hz), 0.96 (d, 3H, J = 7 Hz). CHN analysis: Found: C, 35.63%; H, 3.47%; N, 3.33%. Calcd for $C_{24}H_{28}F_6IN_2OsP$: C, 35.74 % H, 3.50 % N, 3.47 %.

6.2.3 Circular Dichroism (CD). The CD spectra of 0.5 mM solutions (MeOH) of **1**, **2**, **3** or **4** at ambient temperature in CD cuvettes (path: 1mm, Starna, UK) were recorded on J-815 circular dichroism spectropolarimeter (Jasco, UK).

6.2.4 Stability and Hydrolysis. A 100 μM solution of **1**, **2**, **3** or **4** in 10% MeOD-d_4/90% D_2O phosphate buffer (v/v) was prepared by dissolution of **1**, **2**, **3** or **4** in MeOD-d_4 followed by a dilution with D_2O/100 mM phosphate buffer (pH*=7.4). The NMR spectra were recorded after 24 h incubation at 310 K in an oven. The extent of hydrolysis was determined by ^{1}H NMR peak integrals.

6.2.5 Data Evaluation and Mean Graph Analysis of NCI Screening. Complexes **2** and **4** (Fig. 6.1) were selected for study for activity towards the human tumour 60-cell line panel of the Developmental Therapeutics Program of the National Cancer Institute (DTP of NCI, USA) which includes nine tumour type subpanels (leukemia, lung, colon, central nervous system, melanoma, ovarian, renal, prostate, and breast cancer). The cells were treated for 48 h at five concentrations ranging from 0.01 to 100 μM. Three endpoints were calculated: IC_{50} (the concentration that inhibits cell growth by 50 %); TGI (the concentration that inhibits cell growth by 100 %) and LC_{50} (the concentration that kills original cells by 50 %).

6.3 Results and Discussions

6.3.1 Syntheses and Cyrstallizations

In Chapter 5, it was found that two osmium arene iminopyridine enantiomers coexisted in a ca. 1:1 ratio. In this chapter, in order to isolate chirally pure chiral-at-metal iminopyridine complexes, a classical resolution was employed by introducing an additional carbon chiral centre in the chelating iminopyridine ligand. By doing this, a racemic mixture is converted into a pair of diastereoisomers. The solubility difference between the diastereoisomers may be used for the isolation of optically pure products by crystallization. Since diastereomers usually show different ^{1}H NMR spectra, the purification process can be easily monitored without the need of chiral shift-reagents (eg. Δ-trisphat: [Tetrabutylammonium] [Δ-tris(tetrachloro-1,2-benzenediolato)phosphate(V)]). In this Chapter, all the four osmium complexes were synthesized and crystallized to obtain pure chirality at the osmium centre (Fig. 6.1).

For the two osmium iminopyridine iodido complexes **2** and **4**, the synthesis and crystallization were reproduced more than three times, and single crystals (Fig. 6.1) of chirally pure osmium complex were grown overnight in the fridge from a concentrated methanol solution of **2** and **4** respectively. The crystallographic data and selected bond lengths are summarized in Table 6.1 and Table 6.2. Although similar method has been widely used for organometallic chiral catalysts,[7, 12-14] the application to metal arene anticancer complexes is demonstrated for the first time in this Chapter.

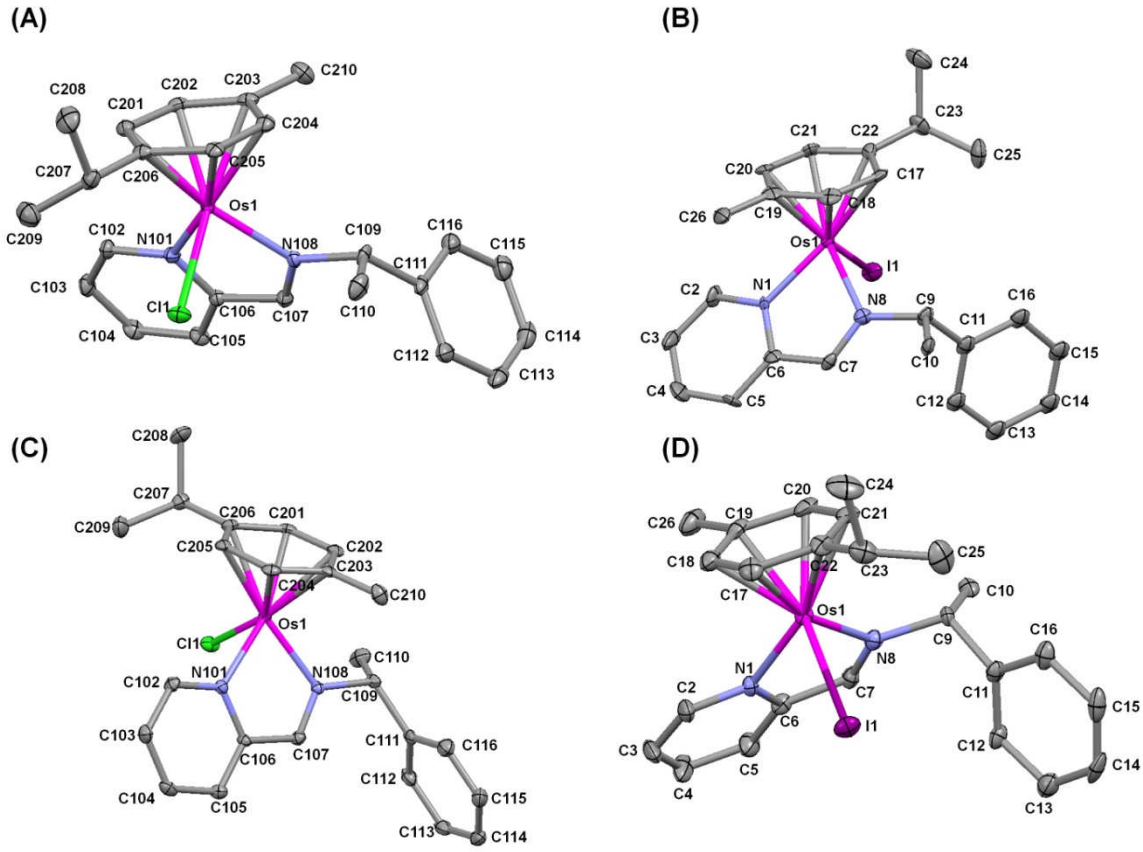

Figure 6.1. Solid state structure of one of the crystallographically independent molecules of (S_{Os}, S_C)-**1** (A), (S_{Os}, S_C)-**2** (B), (R_{Os}, R_C)-**3** (C) and (R_{Os}, R_C)-**4** (D) with atom numbering (PF_6 counter ion is omitted for clarity).

Table 6.1. X-ray crystallographic data for complexes (A) **1** and **3**; (B) **2** and **4**.

(A)

	1	**3**
Formula	$C_{24}H_{28}ClF_6N_2OsP$	$C_{24}H_{28}ClF_6N_2OsP$
Molar mass	715.1	715.1
Crystal system	Monoclinic	Monoclinic
Crystal size /mm	0.25 x 0.18 x 0.16	0.24 x 0.20 x 0.20
Space group	P2(1)	P2(1)
Crystal	brown block	orange block
a / Å	10.19773(12)	10.19210(18)
b / Å	11.79001(13)	11.78829(18)
c / Å	10.99917(13)	10.99531(18)
α / deg	90	90
β / deg	103.0453(12)	103.0937(17)
γ / deg	90	90
T / K	100(2)	100(2)
Z	2	2
R [F > 4σ (F)][a]	0.0241	0.0184
R_w[b]	0.0526	0.0391
GoF[c]	1.017	1.022
Δρ max and min/ eÅ^{-3}	1.217 and -0.796	1.046 and -0.718

(B)

	2	**4**
Formula	$C_{24}H_{28}F_6IN_2Os$ P	$C_{24}H_{28}F_6IN_2OsP$
Molar mass	806.55	806.55
Crystal system	Monoclinic	Monoclinic
Crystal size /mm	0.18 x 0.18 x 0.06 mm	0.35 x 0.35 x 0.12
Space group	P2(1)	P2(1)
Crystal	brown block	brown block
a / Å	9.1232(2)	9.1232(2)
b / Å	15.0439(4)	15.0439(4)
c / Å	9.6304(2)	9.6304(2)
α / deg	90	90
β / deg	97.591(3)	97.591(3)
γ / deg	90	90
T / K	100(2)	100(2)
Z	2	2
R [F > 4σ (F)][a]	0.0427	0.028
R_w[b]	0.0992	0.0698
GoF[c]	1.02	1.03
Δρ max and min/ eÅ^{-3}	2.220 and -1.676	1.904 and -1.058

[a] $R = \Sigma||Fo| - |Fc||/\Sigma|Fo|$.

[b] $Rw = [\Sigma w(Fo^2 - Fc^2)^2/\Sigma wFo^2)]^{1/2}$.

[c] $GoF = [\Sigma w(Fo^2 - Fc^2)^2/(n-p)]^{1/2}$

where n = number of reflections and p = number of parameters.

Table 6.2. Selected bond lengths (Å) and angles (°) for complexes **1**, **3**, **2** and **4**.

(A)

bond length/angle	**1**	**3**
Os(01)-N(101)	2.082(3)	2.086(2)
Os(01)-N(108)	2.124(9)	2.086(2)
Os(01)-Arene Centroid	1.685	1.682
Os(1)-Cl(1)	2.3913(8)	2.3892(7)
N(101)-Os(01)-N(108)	76.61(10)	76.43(9)

(B)

bond length/angle	**2**	**4**
Os(1)-N(1)	2.084(6)	2.090(4)
Os(1)-N(8)	2.089(7)	2.074(5)
Os(01)-Arene Centroid	1.689	1.695
Os(1)-I(1)	2.7068(6)	2.7078(4)
N(1)-Os(1)-N(8)	75.9(3)	76.17(17)

All the four osmium complexes were well characterized by NMR, MS and CHN analysis. However, these techniques could not provide evidence for the purity of the two pairs of diastereoisomers. In that, X-ray crystallography was used to determine the chirality at the osmium centre. Only one type of osmium chirality was found in cubic single crystals for all the four osmium complexes which were different from that found for iminopyridine osmium complexes in Chapter 5. A type of intermolecular interaction was found for both of the chiral chlorido complexes (**1** and **3**) between the chloride (monodentate lignad) and nitrogen in the pyridine ring of the chiral chelating iminopyrdine ligand (Fig. 6.2).

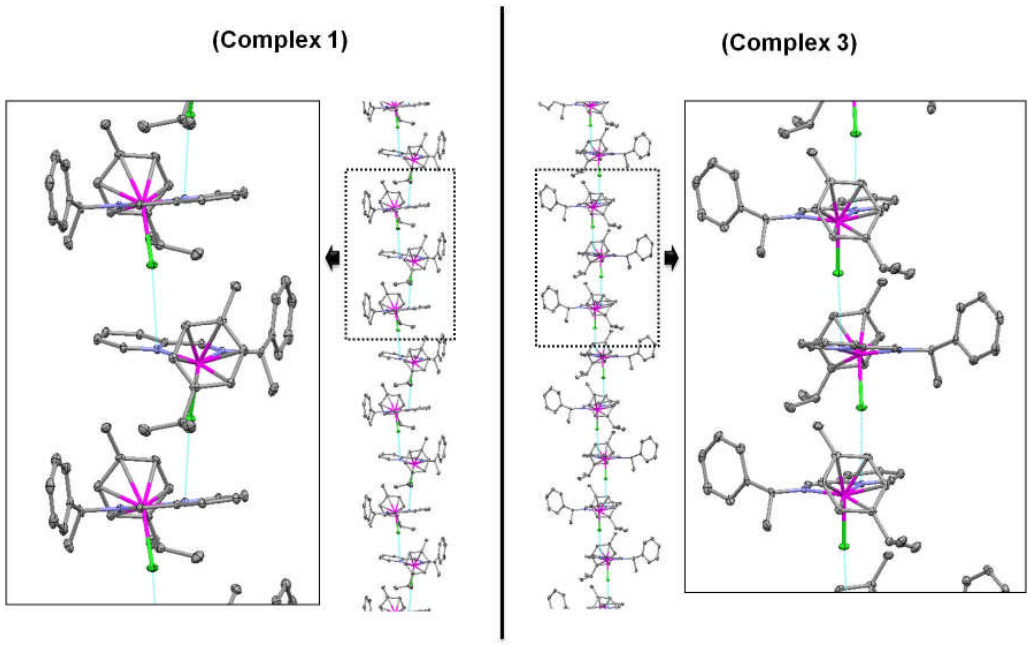

Figure 6.2. Similar intermolecular interaction within the crystal structures of complexes **1** (left) and **3** (right), the distance between chloride (monodentate lignad) and nitrogen in the pyridine ring of chelating iminopyrdine ligand is 3.279 Å for **1** and 3.388 Å for **3**.

To assign the chirality at the metal centre, Cahn–Ingold–Prelog priority rules (CIP system**)** were used to define the priority sequence of ligands attached on the osmium centre: η^6-C_6 > Cl > N (imine) > N (pyridine) or I > η^6-C_6 > N (imine) > N (pyridine). According to the sequence rule of the R/S system, the configurations of the osmium centre in these four chiral osmium arene iminopyridine complexes are: **1** = S_{Os}, **2** = S_{Os}, **3** = R_{Os} and **4** = R_{Os}. It was noticed that there are two pairs of osmium diastereoisomers among the 4 complexes: (S_{Os}, S_C)-**1**/(R_{Os}, R_C)-**3** and (S_{Os}, S_C)-**2**/(R_{Os}, R_C)-**4**.

Circular dichroism which can give rise to absorption bands for optically active chiral molecules was used to compare the two pairs of osmium complexes which are mirror images. The results show complementary CD spectra recorded at ambient temperature for **1** versus **3** and **2** versus **4** indicating the presence of mirror images, which is consistent with the crystal structure data (Fig. 6.3).

During the synthesis of chiral iodido complexes, two complexes with chiral-at-osmium of R or S can co-exist. However, only one isomer is crystallized under the conditions used in this chapter, another type of crystals was observed after leaving the solutions of **2** or **4** in fridge for another several days, which indicates antoher isomer co-existed for both of **2** and **4**. DFT geometry optimizations and energy calculations (by Dr. Luca Salassa, University of Warwick) were performed on the iodido osmium complexes **2** and **4** and their corresponding enantiomers. Such calculations were run at the b3lyp/LANL2DZ/6-31G** level in gas phase using the program Gaussian 03. The sequence of thermodynamic stability is: (S_{Os}, R_C) > (R_{Os}, S_C) > (S_{Os}, S_C)-**2** = (R_{Os}, R_C)-**4**. According to computational results, the (R_{Os}, S_C) configuration is only 0.0015753 KJ/mol less stable than the (S_{Os}, R_C) configuration, while (S_{Os}, S_C)-**2** and (R_{Os}, R_C)-**4** are 10.0627518 KJ/mol less stable than the (S_{Os}, R_C) configuration. On the basis of the computational results, **2** and **4** are not thermodymanic favoured isomers. Since complexes **2** and **4** were still reproducibly obtained and crystallized, suggesting that they are the kinetically

favoured isomers in the reactions between osmium dimer with the chiral iminopyridine ligands.

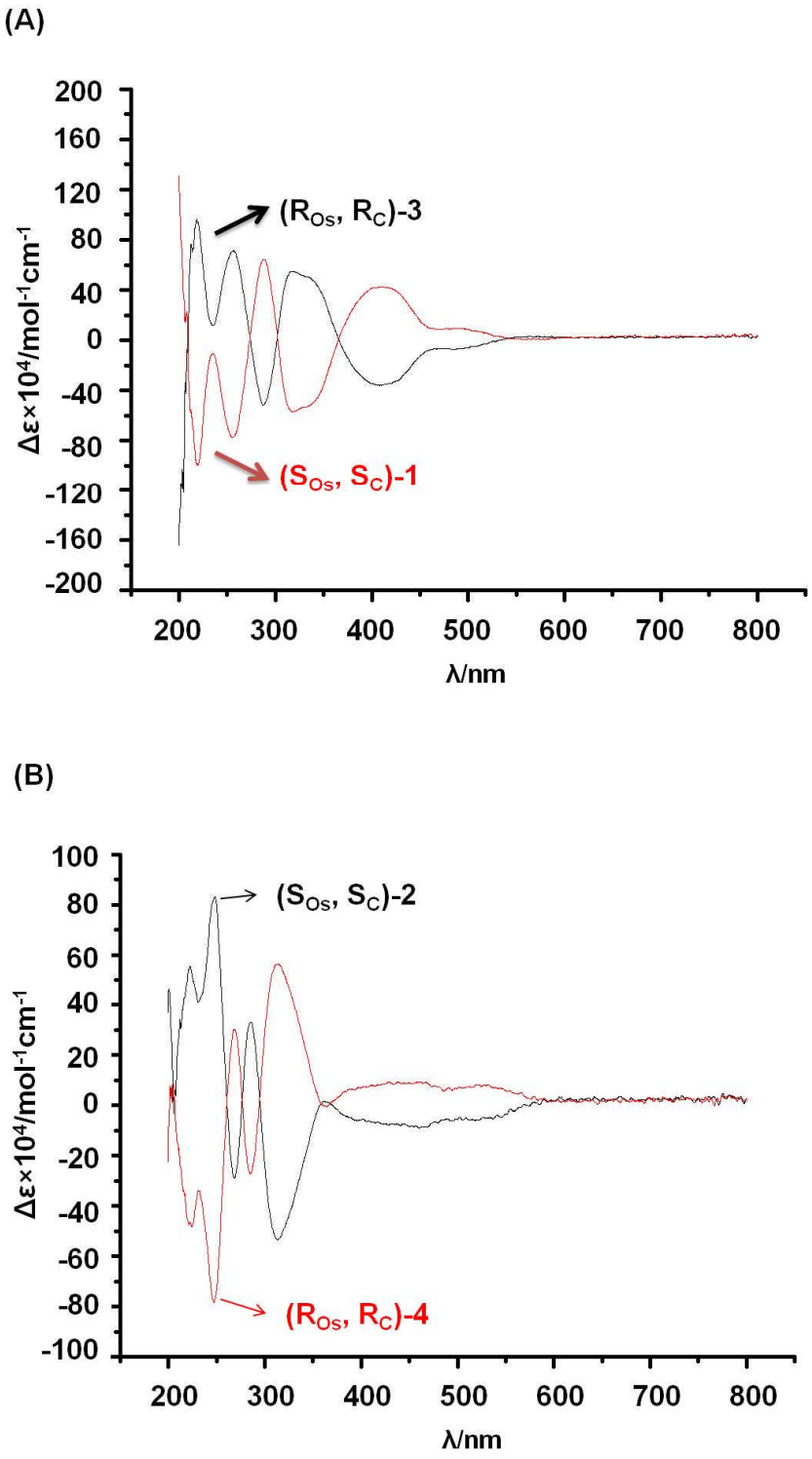

Figure 6.3. CD spectra for the two pairs of osmium arene iminopyridine complexes. (A) **1** and **3**; (B) **2** and **4** in methanol.

6.3.2 Stability and Hydrolysis

Although chiral metal centres are usually stable in the solid state at ambient temperature and physiological temperature, they can still behave differently in solutions: some are configurationally stable whereas others are very labile.[4, 15, 16] Early work on the ruthenium iodido complexes [Ru(η^6-*p*-cym)(LL^*)I] (LL^*=(S_C)-(-)-dimethyl(1-phenylethyl)amine) showed that they were even more configurationally labile than their chlorido analogues.[17] Considering the possiblilites of different bahaviors in solutions between chlorido and iodide complexes and there is still no report on the the comparisions on osmium complexes, it is therefore necessary to study the stability of the osmium complexes in this chapter especially under biologically-relevant conditions.

Since hydrolysis followed by targeting DNA is an important mechanism for the ruthenium and osmium arene anticancer complexes, the hydrolysis of all the four complexes was also studied in 10% MeOD/90% D_2O phosphate buffer (pH^*= 7.4). About 10 % hydrolysis was observed after 24 h at 310 K for chlorido complexes **1** and **3**, which can be suppressed by the presence of excess Cl^- (Fig 6.4). After incubation for 24 h at 310 K, the two idodido complexes (**2** and **4**) were found to be very stable in water and no hydrolysis was observed by ^{1}H NMR. Since there is a very high chloride concentration ca. 10 mM in human blood, it was investigated whether the iodide ligand can be replaced by choride. Even if at very high concentration of Cl^- (5000 mol equivalent) present, no replacement of iodide by chloride was observed for both **2** and **4** (Fig 6.4). In summary, there is no isomerisation at the osmium centre during an incubation time of 24 h at 310 K for both the osmium arene chlorido and iodido osmium iminopyridine complexes; it indicates good stability on the chiral osmium centre for these complexes under physiological conditions.

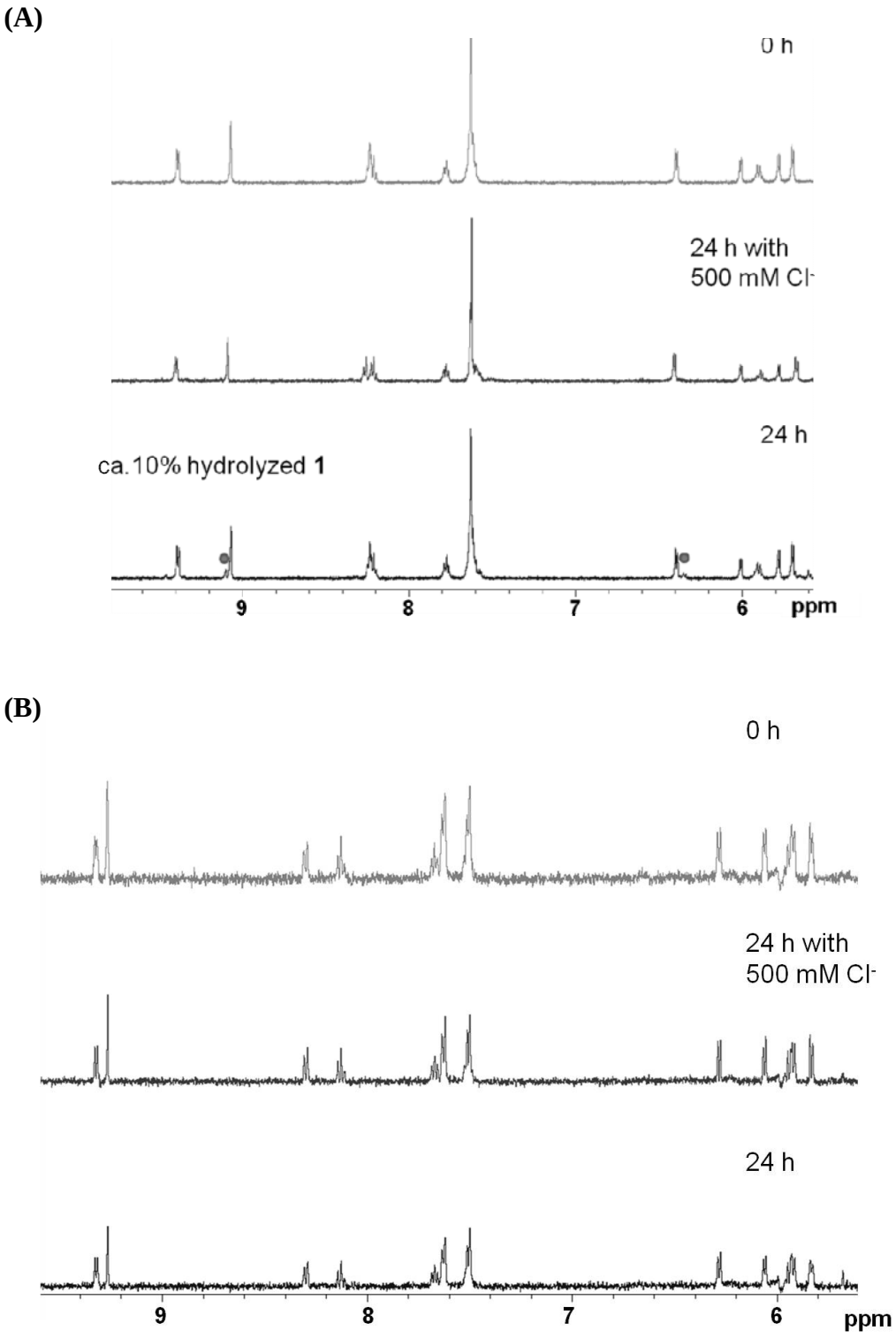

Figure 6.4. ^{1}H NMR spectra of complexes **1** (A), **2** (B), **3** (C) and **4** (D) in 10% MeOD/90% D_2O phosphate buffer (pH^{*}= 7.4) after incubation for 24 h at 310 K. The time 0 h NMR spectra were recorded immediately (within 10 min) after preparation of the samples.

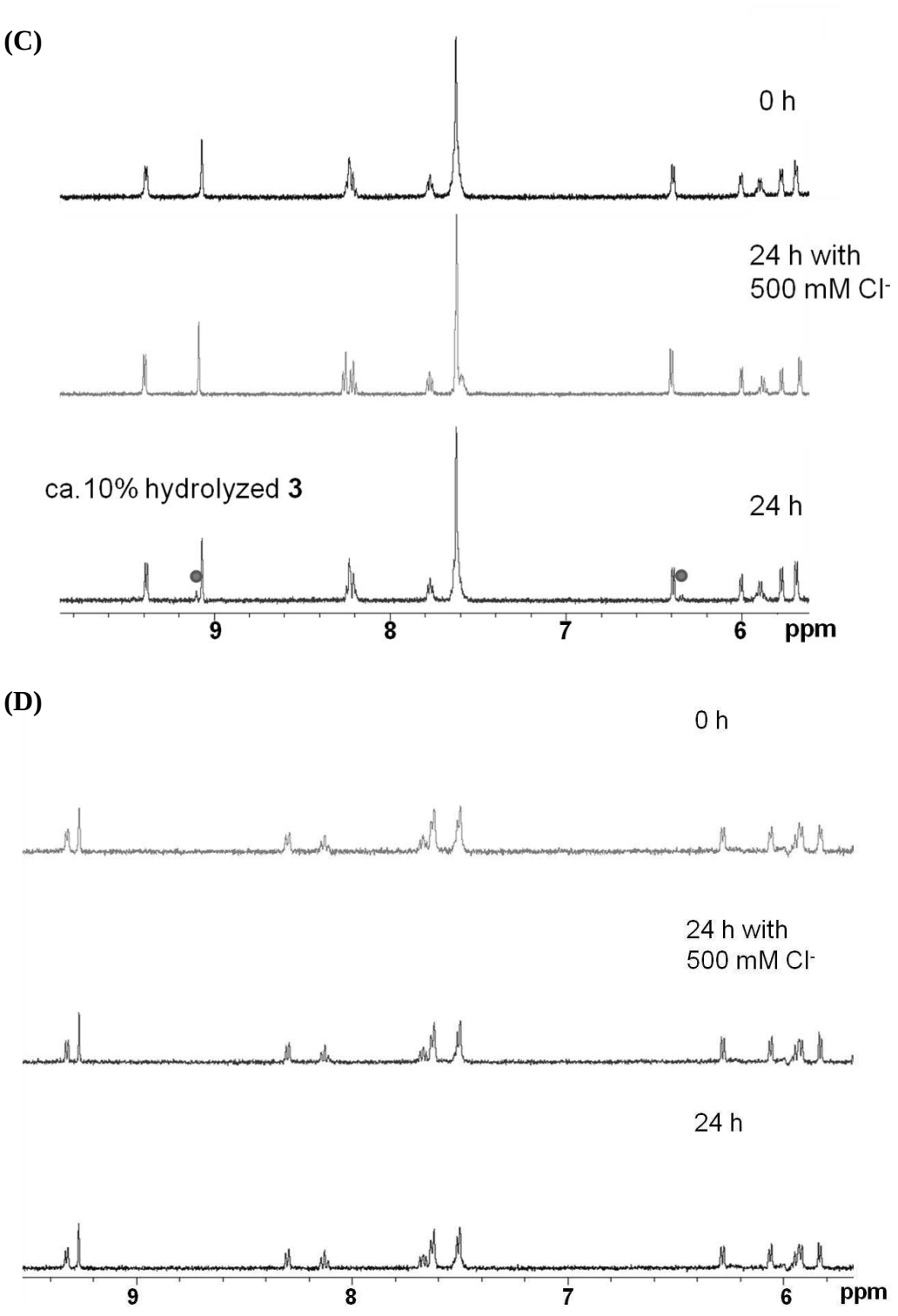

Figure 6.4. ^{1}H NMR spectra of complexes **1** (A), **2** (B), **3** (C) and **4** (D) in 10% MeOD/90% D_2O phosphate buffer (pH^{*}= 7.4) after incubation for 24 h at 310 K. The time 0 h NMR spectra were recorded immediately (within 10 min) after preparation of the samples.

6.3.3 Anticancer Activity

The anticancer activity *in vitro* of the four chiral osmium arene iminopyrdine complexes was studied. After 24 h incubation followed by 72 h recovery, the two chlorido osmium complexes (**1** and **3**) did not show very good anticancer activity (their IC_{50} values are larger than 10 μM (Table 6.3) and are significantly higher than that of cisplatin (2 μM). On the contrary, the two iodido osmium complexes (**2** and **4**) showed anticancer activity in the same range of cisplatin (Table 6.3). The two iodido complexes were selected by NCI (National Cancer Institute of USA) for 60 cell line screening. Both **2** and **4** showed anticancer activity as good as cisplatin over the average of all the cell lines screened. The results of MG-MID (full-panel mean-graph midpoint) values of IC_{50} (the concentration inhibits cell growth by 50 %): TGI (the concentration inhibits cell growth by 100 %) and LC_{50} (the concentration kills original cells by 50 %) are listed in Table 6.3B. The details for each cell line are shown in Table 6.4. As opposed to cisplatin, these two osmium complexes showed a broad range of anticancer activity towards different cell lines, with IC_{50} values ranging from nanomolar to 100 micromolars.

Further analysis of the *in vitro* anticancer efficacy of complexes **2** and **4** by the NCI revealed a selectivity pattern reflecting a characteristic distribution of sensitive and resistant tumours. Complex **2** and **4** showed a broad spectrum of activity and a particular selectivity for melanoma and breast cancer, with particular activity against MDA-MB-468 breast cancer cell line giving IC_{50} values in the nanomolar range (703 nM for **2** and 530 nM for **4**). It was also noted that complexes **2** and **4** are highly inactive towards renal cancer cell lines with IC_{50} values larger than 100 μM towards most of the renal cancer cell lines.

Table 6.3. IC_{50} values against A2780 ovarian cancer cell line.

(A)

Complex	IC_{50}(μM)
[Os(η^6-*p*-cym)(Impy-S)Cl]PF_6 **(1)**	22.3 (± 1.6)
[Os(η^6-*p*-cym)(Impy-S)I]PF_6 **(2)**	1.9 (± 0.2)
[Os(η^6-*p*-cym)(Impy-R)Cl]PF_6 **(3)**	18.3 (± 1.7)
[Os(η^6-*p*-cym)(Impy-R)I]PF_6 **(4)**	0.60 (± 0.02)
Cisplatin	2.0 (± 0.2)

(B)

Compound	IC_{50}/ μM	TGI/ μM	LC_{50}/ μM
[Os(η^6-*p*-cym)(Impy-S)I]PF_6 **(2)**	9.55	61.7	91.2
[Os(η^6-*p*-cym)(Impy-R)I]PF_6 **(4)**	7.58	53.7	89.1
Cisplatin	10.3	50.7	90.5

Cisplatin Data from NCI/DTP screening: **Oct 2009**, 48 h incubation.

6.4 Conclusions

In this chapter, four chiral-at-osmium arene iminopyridine complexes were synthesized. All of them showed good configurational stability under physiological conditions, with no isomerisation observed at the chiral metal centre over 24 h at 310 K. The two iodido complexes, [Os(η^6-*p*-cym)(Imine-S)I]PF_6 **(2)** and [Os(η^6-*p*-cym)(Imine-R)I]PF_6 (**4)** showed promising anticancer activity, as good as or better than cisplatin. From the 60-cell line screening of National Cancer Institute (NCI), the two iodide complexes, **2** (FY175A, NSC: D-758116/1) and **4 (**FY178A, NSC: D-758118/1) also showed promising anticancer activity and dramatic selectivity between different cell lines. However, further work is also needed to investigate the difference in pharmacological action, metabolism, toxicity, plasma disposition, and urinary excretion kinetics of the osmium diastereoisomers.[18]

Table 6.4. Anticancer activity in the NCI 60-cell line screen. (A) complex **2**, (B) complex **4**. The meanings of GI_{50} and IC_{50} value are the same: the concentration that inhibits cell growth by 50 %.

(A) Complex **2**

National Cancer Institute Developmental Therapeutics Program
In-Vitro Testing Results

NSC : D - 758116 / 1	Experiment ID : 1106NS66	Test Type : 08	Units : Molar
Report Date : August 29, 2011	Test Date : June 20, 2011	QNS :	MC :
COMI : FY175A (105701)	Stain Reagent : SRB Dual-Pass Related	SSPL : 0Y4T	

			Log10 Concentration												
	Time		Mean Optical Densities					Percent Growth							
Panel/Cell Line	Zero	Ctrl	-8.0	-7.0	-6.0	-5.0	-4.0	-8.0	-7.0	-6.0	-5.0	-4.0	GI50	TGI	LC50
Leukemia															
HL-60(TB)	0.836	2.721	2.765	2.886	2.834	1.095	0.503	102	109	106	14	-40	4.04E-6	1.80E-5	> 1.00E-4
MOLT-4	0.495	2.013	2.008	2.002	2.010	1.558	0.589	100	99	100	70	6	2.06E-5	> 1.00E-4	> 1.00E-4
SR	0.409	1.836	1.688	1.633	1.554	1.025	0.422	90	86	80	43	1	6.54E-6	> 1.00E-4	> 1.00E-4
Non-Small Cell Lung Cancer															
A549/ATCC	0.264	1.402	1.384	1.301	1.247	0.867	0.491	98	91	86	53	20	1.23E-5	> 1.00E-4	> 1.00E-4
EKVX	0.774	1.837	1.803	1.728	1.658	1.202	0.936	97	90	83	40	15	5.91E-6	> 1.00E-4	> 1.00E-4
HOP-62	0.479	1.362	1.362	1.364	1.308	0.827	0.618	100	100	94	39	16	6.38E-6	> 1.00E-4	> 1.00E-4
HOP-92	1.062	1.466	1.470	1.494	1.391	1.086	0.617	101	107	82	6	-42	2.61E-6	1.32E-5	> 1.00E-4
NCI-H226	0.558	1.441	1.391	1.377	1.363	1.172	0.806	94	93	91	70	28	2.95E-5	> 1.00E-4	> 1.00E-4
NCI-H23	0.486	1.697	1.690	1.677	1.661	1.074	0.575	99	98	97	49	7	9.33E-6	> 1.00E-4	> 1.00E-4
NCI-H322M	0.705	1.703	1.594	1.583	1.634	1.608	0.979	89	88	93	90	27	4.38E-5	> 1.00E-4	> 1.00E-4
NCI-H460	0.246	2.527	2.635	2.638	2.522	0.823	0.361	105	105	100	25	5	4.66E-6	> 1.00E-4	> 1.00E-4
NCI-H522	0.526	1.267	1.219	1.262	1.176	0.603	0.240	94	99	88	10	-54	3.07E-6	1.45E-5	8.56E-5
Colon Cancer															
COLO 205	0.240	1.400	1.447	1.396	1.096	0.080	0.084	104	100	74	-67	-65	1.48E-6	3.35E-6	7.59E-6
HCC-2998	0.539	2.052	1.939	1.948	1.874	1.053	0.573	93	93	88	34	2	5.06E-6	> 1.00E-4	> 1.00E-4
HCT-116	0.226	1.675	1.716	1.714	1.576	0.577	0.303	103	103	93	24	5	4.23E-6	> 1.00E-4	> 1.00E-4
HCT-15	0.301	1.793	1.843	1.864	1.733	1.843	1.545	103	105	96	103	83	> 1.00E-4	> 1.00E-4	> 1.00E-4
HT29	0.175	1.115	1.159	1.140	1.133	0.529	0.200	105	103	102	38	3	6.42E-6	> 1.00E-4	> 1.00E-4
KM12	0.441	2.391	2.421	2.443	2.344	1.007	0.570	102	103	98	29	7	4.95E-6	> 1.00E-4	> 1.00E-4
SW-620	0.199	1.349	1.370	1.373	1.317	0.747	0.329	102	102	97	48	11	8.96E-6	> 1.00E-4	> 1.00E-4
CNS Cancer															
SF-268	0.360	1.296	1.300	1.311	1.332	0.752	0.521	100	102	104	42	17	7.38E-6	> 1.00E-4	> 1.00E-4
SF-295	0.860	2.494	2.359	2.291	2.350	2.272	1.010	92	88	91	86	9	2.96E-5	> 1.00E-4	> 1.00E-4
SF-539	0.572	1.550	1.613	1.598	1.591	1.049	0.696	106	105	104	49	13	9.49E-6	> 1.00E-4	> 1.00E-4
SNB-19	0.503	1.641	1.542	1.529	1.466	0.858	0.736	91	90	85	31	20	4.45E-6	> 1.00E-4	> 1.00E-4
SNB-75	0.771	1.288	1.213	1.195	1.220	0.813	0.527	85	82	87	8	-32	2.94E-6	1.60E-5	> 1.00E-4
U251	0.239	1.064	1.056	1.043	0.960	0.481	0.325	99	97	87	29	10	4.40E-6	> 1.00E-4	> 1.00E-4
Melanoma															
LOX IMVI	0.214	1.406	1.377	1.309	1.269	0.536	0.228	98	92	89	27	1	4.23E-6	> 1.00E-4	> 1.00E-4
MALME-3M	0.626	1.007	0.974	0.962	0.928	0.734	0.414	91	88	79	28	-34	3.74E-6	2.85E-5	> 1.00E-4
M14	0.405	1.617	1.647	1.692	1.609	1.310	0.457	102	106	99	75	4	2.24E-5	> 1.00E-4	> 1.00E-4
MDA-MB-435	0.416	2.005	1.945	1.872	1.778	0.637	0.266	96	92	86	14	-36	3.14E-6	1.90E-5	> 1.00E-4
SK-MEL-2	0.883	1.929	1.986	2.067	1.976	1.096	0.344	105	113	105	20	-61	4.44E-6	1.78E-5	7.31E-5
SK-MEL-28	0.484	1.298	1.294	1.318	1.238	0.865	0.311	100	102	93	47	-36	8.50E-6	3.69E-5	> 1.00E-4
SK-MEL-5	0.517	2.279	2.208	2.134	1.938	0.394	0.009	96	92	81	-24	-98	1.96E-6	5.91E-6	2.24E-5
UACC-257	0.628	1.415	1.362	1.384	1.256	0.683	0.396	93	96	80	7	-37	2.57E-6	1.44E-5	> 1.00E-4
UACC-62	0.701	2.474	2.328	2.298	2.130	1.201	0.221	92	90	81	28	-69	3.83E-6	1.96E-5	6.43E-5
Ovarian Cancer															
IGROV1	0.425	1.468	1.502	1.445	1.402	0.933	0.393	103	98	94	49	-8	9.34E-6	7.35E-5	> 1.00E-4
OVCAR-3	0.455	1.472	1.518	1.492	1.338	0.676	0.489	105	102	87	22	3	3.68E-6	> 1.00E-4	> 1.00E-4
OVCAR-4	0.677	1.724	1.711	1.760	1.571	0.827	0.672	99	103	85	14	-1	3.14E-6	8.93E-5	> 1.00E-4
OVCAR-5	0.487	1.148	1.157	1.145	1.106	0.984	0.561	101	100	94	75	11	2.48E-5	> 1.00E-4	> 1.00E-4
OVCAR-8	0.321	1.343	1.309	1.331	1.304	0.693	0.408	97	99	96	36	8	5.92E-6	> 1.00E-4	> 1.00E-4
NCI/ADR-RES	0.467	1.528	1.507	1.501	1.504	1.534	1.548	98	97	98	101	102	> 1.00E-4	> 1.00E-4	> 1.00E-4
SK-OV-3	0.485	1.258	1.201	1.222	1.233	1.156	0.695	93	95	97	87	27	4.14E-5	> 1.00E-4	> 1.00E-4
Renal Cancer															
786-0	0.595	1.950	1.957	1.973	1.896	2.023	0.952	100	102	96	105	26	5.02E-5	> 1.00E-4	> 1.00E-4
A498	1.041	2.028	2.013	2.027	1.995	1.970	1.516	98	100	97	94	48	9.12E-5	> 1.00E-4	> 1.00E-4
ACHN	0.410	1.630	1.587	1.681	1.570	1.543	1.234	96	104	95	93	68	> 1.00E-4	> 1.00E-4	> 1.00E-4
CAKI-1	0.760	2.257	2.189	2.162	2.167	2.231	2.275	95	94	94	98	101	> 1.00E-4	> 1.00E-4	> 1.00E-4
RXF 393	0.282	0.749	0.744	0.751	0.722	0.698	0.329	99	101	94	89	10	3.12E-5	> 1.00E-4	> 1.00E-4
SN12C	0.524	1.993	1.834	1.898	1.771	1.089	0.676	89	94	85	38	10	5.64E-6	> 1.00E-4	> 1.00E-4
TK-10	0.583	1.405	1.440	1.443	1.466	1.368	0.861	104	105	107	95	34	5.46E-5	> 1.00E-4	> 1.00E-4
UO-31	0.535	1.488	1.374	1.324	1.333	1.422	1.399	88	83	84	93	91	> 1.00E-4	> 1.00E-4	> 1.00E-4
Prostate Cancer															
PC-3	0.493	1.665	1.664	1.620	1.542	0.797	0.550	100	96	90	26	5	4.18E-6	> 1.00E-4	> 1.00E-4
DU-145	0.410	1.631	1.710	1.667	1.710	1.146	0.766	106	103	106	60	29	2.14E-5	> 1.00E-4	> 1.00E-4
Breast Cancer															
MCF7	0.549	2.170	2.092	2.092	2.102	0.918	0.640	95	95	96	23	6	4.24E-6	> 1.00E-4	> 1.00E-4
MDA-MB-231/ATCC	0.465	1.121	1.095	1.121	1.089	0.766	0.366	96	100	95	46	-21	8.24E-6	4.82E-5	> 1.00E-4
HS 578T	0.722	1.541	1.559	1.566	1.584	1.368	0.958	102	103	105	79	29	3.77E-5	> 1.00E-4	> 1.00E-4
BT-549	0.750	1.565	1.583	1.583	1.566	0.986	0.709	102	102	100	29	-5	5.06E-6	6.94E-5	> 1.00E-4
T-47D	0.518	1.169	1.173	1.167	1.069	0.692	0.580	101	100	85	27	10	3.96E-6	> 1.00E-4	> 1.00E-4
MDA-MB-468	0.569	1.477	1.397	1.354	0.963	0.508	0.163	91	87	43	-11	-71	7.03E-7	6.32E-6	4.44E-5

(B) Complex **4**

National Cancer Institute Developmental Therapeutics Program
In-Vitro Testing Results

NSC : D - 758118 / 1	Experiment ID : 1106NS66	Test Type : 08	Units : Molar
Report Date : August 29, 2011	Test Date : June 20, 2011	QNS :	MC :
COMI : FY178A (105704)	Stain Reagent : SRB Dual-Pass Related	SSPL : 0Y4T	

Log10 Concentration

Panel/Cell Line	Time Zero	Mean Optical Densities Ctrl	-8.0	-7.0	-6.0	-5.0	-4.0	Percent Growth -8.0	-7.0	-6.0	-5.0	-4.0	GI50	TGI	LC50
Leukemia															
HL-60(TB)	0.836	2.696	2.687	2.602	2.287	0.912	0.397	99	95	78	4	-53	2.39E-6	1.18E-5	9.01E-5
MOLT-4	0.495	1.972	1.919	1.903	1.838	1.168	0.629	96	95	91	46	9	7.99E-6	> 1.00E-4	> 1.00E-4
SR	0.409	1.757	1.686	1.574	1.499	0.594	0.375	95	86	81	14	-8	2.88E-6	4.19E-5	> 1.00E-4
Non-Small Cell Lung Cancer															
A549/ATCC	0.264	1.381	1.317	1.302	1.316	0.737	0.414	94	93	94	42	13	7.12E-6	> 1.00E-4	> 1.00E-4
EKVX	0.774	1.827	1.806	1.709	1.589	1.113	0.945	98	89	77	32	16	4.03E-6	> 1.00E-4	> 1.00E-4
HOP-62	0.479	1.320	1.291	1.270	1.281	0.788	0.494	97	94	95	37	2	5.94E-6	> 1.00E-4	> 1.00E-4
HOP-92	1.062	1.449	1.462	1.429	1.433	0.911	0.547	103	95	96	-14	-49	2.61E-6	7.43E-6	> 1.00E-4
NCI-H226	0.558	1.452	1.397	1.393	1.363	1.144	0.777	94	93	90	66	25	2.39E-5	> 1.00E-4	> 1.00E-4
NCI-H23	0.486	1.662	1.616	1.612	1.580	0.858	0.524	96	96	93	32	3	5.02E-6	> 1.00E-4	> 1.00E-4
NCI-H322M	0.705	1.773	1.705	1.635	1.627	1.491	0.870	94	87	86	74	15	2.55E-5	> 1.00E-4	> 1.00E-4
NCI-H460	0.246	2.506	2.649	2.590	2.495	0.812	0.356	106	104	100	25	5	4.62E-6	> 1.00E-4	> 1.00E-4
NCI-H522	0.526	1.261	1.185	1.241	1.057	0.542	0.185	90	97	72	2	-65	2.07E-6	1.08E-5	6.01E-5
Colon Cancer															
COLO 205	0.240	1.309	1.309	1.310	1.071	0.065	0.083	100	100	78	-73	-66	1.53E-6	3.28E-6	7.04E-6
HCC-2998	0.539	1.834	1.785	1.829	1.731	0.866	0.471	96	100	92	25	-13	4.26E-6	4.64E-5	> 1.00E-4
HCT-116	0.226	1.735	1.775	1.805	1.696	0.552	0.283	103	105	97	22	4	4.22E-6	> 1.00E-4	> 1.00E-4
HCT-15	0.301	1.877	1.769	1.862	1.874	1.881	1.689	93	99	100	100	88	> 1.00E-4	> 1.00E-4	> 1.00E-4
HT29	0.175	1.073	1.081	1.132	1.076	0.376	0.178	101	107	100	22	.	4.42E-6	> 1.00E-4	> 1.00E-4
KM12	0.441	2.358	2.398	2.440	2.208	0.907	0.554	102	104	92	24	6	4.18E-6	> 1.00E-4	> 1.00E-4
SW-620	0.199	1.345	1.363	1.338	1.327	0.692	0.377	102	99	98	43	16	7.47E-6	> 1.00E-4	> 1.00E-4
CNS Cancer															
SF-268	0.360	1.254	1.301	1.330	1.282	0.636	0.449	105	109	103	31	10	5.43E-6	> 1.00E-4	> 1.00E-4
SF-295	0.860	2.358	2.257	2.195	2.225	2.128	0.956	93	89	91	85	6	2.77E-5	> 1.00E-4	> 1.00E-4
SF-539	0.572	1.618	1.663	1.643	1.636	0.933	0.691	104	102	102	34	11	5.88E-6	> 1.00E-4	> 1.00E-4
SNB-19	0.503	1.708	1.646	1.643	1.518	0.843	0.737	95	95	84	28	19	4.09E-6	> 1.00E-4	> 1.00E-4
SNB-75	0.771	1.244	1.165	1.215	1.149	0.736	0.549	83	94	80	-5	-29	2.25E-6	8.83E-6	> 1.00E-4
U251	0.239	1.032	0.982	0.974	0.876	0.400	0.274	94	93	80	20	4	3.20E-6	> 1.00E-4	> 1.00E-4
Melanoma															
LOX IMVI	0.214	1.364	1.281	1.305	1.242	0.425	0.205	93	95	89	18	-4	3.58E-6	6.38E-5	> 1.00E-4
MALME-3M	0.626	1.035	1.009	0.974	0.911	0.652	0.350	94	85	70	6	-44	2.04E-6	1.33E-5	> 1.00E-4
M14	0.405	1.590	1.617	1.598	1.542	1.272	0.642	102	101	96	73	20	2.72E-5	> 1.00E-4	> 1.00E-4
MDA-MB-435	0.416	2.000	1.932	1.883	1.678	0.573	0.296	96	93	80	10	-29	2.66E-6	1.80E-5	> 1.00E-4
SK-MEL-2	0.883	1.889	1.949	2.025	1.995	1.013	0.290	106	114	111	13	-67	4.17E-6	1.45E-5	6.11E-5
SK-MEL-28	0.484	1.208	1.223	1.258	1.152	0.782	0.277	102	107	92	41	-43	6.69E-6	3.09E-5	> 1.00E-4
SK-MEL-5	0.517	2.156	2.098	2.089	1.700	0.276	0.006	96	96	72	-47	-99	1.54E-6	4.05E-6	1.16E-5
UACC-257	0.628	1.368	1.282	1.277	1.169	0.607	0.415	88	88	73	-3	-34	2.01E-6	9.02E-6	> 1.00E-4
UACC-62	0.701	2.381	2.278	2.300	2.044	1.134	0.322	94	95	80	26	-54	3.57E-6	2.10E-5	8.89E-5
Ovarian Cancer															
IGROV1	0.425	1.457	1.523	1.462	1.364	0.821	0.316	106	100	91	38	-26	6.00E-6	3.97E-5	> 1.00E-4
OVCAR-3	0.455	1.456	1.502	1.527	1.327	0.620	0.442	105	107	87	16	-3	3.35E-6	7.04E-5	> 1.00E-4
OVCAR-4	0.677	1.661	1.795	1.744	1.503	0.794	0.634	114	108	84	12	-6	2.96E-6	4.46E-5	> 1.00E-4
OVCAR-5	0.487	1.201	1.183	1.190	1.188	0.927	0.523	98	99	98	62	5	1.60E-5	> 1.00E-4	> 1.00E-4
OVCAR-8	0.321	1.363	1.300	1.316	1.272	0.779	0.379	94	96	91	44	6	7.44E-6	> 1.00E-4	> 1.00E-4
NCI/ADR-RES	0.467	1.460	1.529	1.468	1.468	1.514	1.497	107	101	101	105	104	> 1.00E-4	> 1.00E-4	> 1.00E-4
SK-OV-3	0.485	1.215	1.191	1.209	1.187	1.033	0.555	97	99	96	75	10	2.41E-5	> 1.00E-4	> 1.00E-4
Renal Cancer															
786-0	0.595	1.965	2.003	1.970	1.979	2.056	1.259	103	100	101	107	48	9.39E-5	> 1.00E-4	> 1.00E-4
A498	1.041	2.009	1.921	1.989	2.006	1.956	1.537	91	98	100	94	51	> 1.00E-4	> 1.00E-4	> 1.00E-4
ACHN	0.410	1.618	1.638	1.681	1.662	1.687	1.413	102	105	104	106	83	> 1.00E-4	> 1.00E-4	> 1.00E-4
CAKI-1	0.760	2.236	2.157	2.140	2.130	2.284	2.380	95	93	93	103	110	> 1.00E-4	> 1.00E-4	> 1.00E-4
RXF 393	0.282	0.701	0.704	0.693	0.688	0.685	0.390	101	98	97	96	26	4.53E-5	> 1.00E-4	> 1.00E-4
SN12C	0.524	1.943	1.867	1.888	1.772	0.870	0.645	95	96	88	24	9	3.95E-6	> 1.00E-4	> 1.00E-4
TK-10	0.583	1.358	1.392	1.392	1.390	1.359	0.924	104	104	104	100	44	7.81E-5	> 1.00E-4	> 1.00E-4
UO-31	0.535	1.535	1.389	1.359	1.369	1.421	1.380	85	82	83	89	85	> 1.00E-4	> 1.00E-4	> 1.00E-4
Prostate Cancer															
PC-3	0.493	1.626	1.661	1.610	1.367	0.691	0.511	103	99	77	17	2	2.85E-6	> 1.00E-4	> 1.00E-4
DU-145	0.410	1.609	1.735	1.723	1.666	0.999	0.696	111	110	105	49	24	9.65E-6	> 1.00E-4	> 1.00E-4
Breast Cancer															
MCF7	0.549	2.063	1.997	2.018	1.945	0.741	0.537	96	97	92	13	-2	3.39E-6	7.13E-5	> 1.00E-4
MDA-MB-231/ATCC	0.465	1.169	1.141	1.129	1.049	0.648	0.333	96	94	83	26	-28	3.78E-6	3.01E-5	> 1.00E-4
HS 578T	0.722	1.577	1.597	1.561	1.592	1.232	0.925	102	98	102	60	24	1.86E-5	> 1.00E-4	> 1.00E-4
BT-549	0.750	1.573	1.614	1.632	1.616	0.918	0.754	105	107	105	20	.	4.48E-6	> 1.00E-4	> 1.00E-4
T-47D	0.518	1.166	1.139	1.108	1.007	0.605	0.514	96	91	75	13	-1	2.57E-6	8.69E-5	> 1.00E-4
MDA-MB-468	0.569	1.483	1.373	1.371	0.895	0.489	0.145	88	88	36	-14	-75	5.30E-7	5.20E-6	3.93E-5

6.5 References

1. R. J. D'Amato, M. S. Loughnan, E. Flynn and J. Folkman, *Proc. Natl. Acad. Sci. U. S. A.*, 1994, **91**, 4082-4085.

2. S. Singhal, J. Mehta, R. Desikan, D. Ayers, P. Roberson, P. Eddlemon, N. Munshi, E. Anaissie, C. Wilson, M. Dhodapkar, J. Zeldis, D. Siegel, J. Crowley and B. Barlogie, *N. Engl. J. Med.*, 1999, **341**, 1565-1571.

3. H. Brunner, *Eur. J. Inorg. Chem.*, 2001, **2001**, 905-912.

4. C. Ganter, *Chem. Soc. Rev.*, 2003, **32**, 130-138.

5. G. Atilla-Gokcumen, L. Di Costanzo and E. Meggers, *J. Biol. Inorg. Chem.*, 2011, **16**, 45-50.

6. W. F. Schmid, R. O. John, G. Mühlgassner, P. Heffeter, M. A. Jakupec, M. Galanski, W. Berger, V. B. Arion and B. K. Keppler, *J. Med. Chem.*, 2007, **50**, 6343-6355.

7. R. Noyori and S. Hashiguchi, *Acc. Chem. Res.*, 1997, **30**, 97-102.

8. H. C. Kolb, M. S. VanNieuwenhze and K. B. Sharpless, *Chem. Rev.*, 1994, **94**, 2483-2547.

9. W. S. Knowles, *Acc. Chem. Res.*, 1983, **16**, 106-112.

10. A. F. A. Peacock, A. Habtemariam, S. A. Moggach, A. Prescimone, S. Parsons and P. J. Sadler, *Inorg. Chem.*, 2007, **46**, 4049-4059.

11. S. Nieto, J. M. Dragna and E. V. Anslyn, *Chem.--Eur. J.*, 2010, **16**, 227-232.

12. H. Brunner, T. Zwack, M. Zabel, W. Beck and A. Böhm, *Organometallics*, 2003, **22**, 1741-1750.

13. H. Brunner, M. Muschiol, I. Bernal and G. M. Reisner, *J. Organomet. Chem.*, 1980, **198**, 169-178.

14. G. Consiglio and F. Morandini, *Chem. Rev.*, 1987, **87**, 761-778.

15. H. Brunner, *Angew. Chem., Int. Ed.*, 1999, **111**, 1248-1263.

16. H. Chen, J. A. Parkinson, O. Nováková, J. Bella, F. Wang, A. Dawson, R. Gould, S. Parsons, V. Brabec and P. J. Sadler, *Proc. Natl. Acad. Sci. U. S. A.*, 2003, **100**, 14623-14628.

17. H. Brunner and T. Zwack, *Organometallics*, 2000, **19**, 2423-2426.

18. I. W. Wainer and C. P. Granvil, *Ther. Drug Monit.*, 1993, **15**, 570-575.

Chapter 7
Future Work

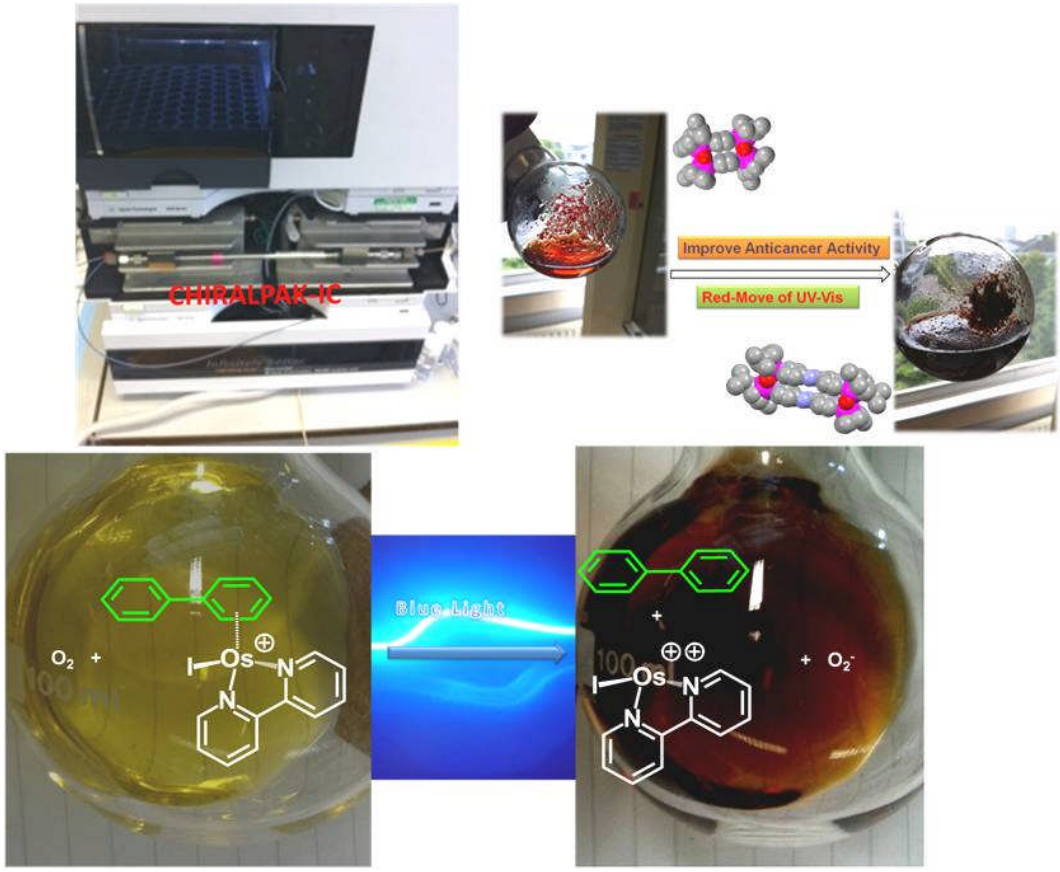

This chapter explores possible areas of future work for this project which has the potential to provide an osmium anticancer complex as a candidate for clinical trials. This chapter is mainly based on the results described in the previous chapters or preliminary data obtained which is not included in previous chapters.

7.1 Absorption, Distribution, Metabolism, and Excretion Analysis

In Chapter 3 and 4, the drug properties of osmium (II) arene azopyridine complexes were evaluated *in vitro* and *in vivo*. In the future work, more absorption, distribution, metabolism, and excretion (ADME) studies should be carried on with two purposes: (1) to tune the drug properties without losing the anticancer activity; (2) to obtain a lead compound for further testing and even clinical trials. In order to setup one sensitive method for analysis, LC/MS/MS was employed and the response of the osmium azopyridine compounds was analyzed. Then it is possible to analyze, evaluate and optimize the most important pharmaceutical indexes of osmium (II) arene azopyridine anticancer complexes. For example, the *in vitro* intrinsic clearance (CLint) values and the inhibition of cytochrome P450 (CYP) are very important indices. The CLint values of drug candidates are helpful to confirm whether metabolism is the main clearance pathway and to project the metabolic clearance of drug candidates in humans.[1] Investigations of whether the drug candidates have the effect of decreasing the activity of various CYP isozymes are also important for evaluations of drug candidates. Because inhibitions of CYP enzymes activity may affect the metabolism and clearance of various other drugs and result in drug accumulation and reaching toxic levels; this CYP enzyme inhibition test is also important for selection of drugs for combination therapy in the future. After the screening of ADME *in vitro*, the ADME study of the promising complexes from screening *in vitro* should be explored *in vivo*.

7.2 Designs for Improved Anticancer Activity

Based on knowledge of structure activity relationships (SARs) gained in the study of osmium azopyridine complexes, the preliminary conclusions are that the anticancer activity can be increased dramatically with extended arene, fluoride and dimethylamino substituents at specific position in the pyridine ring and phenyl ring of the chelating ligand respectively. The most active osmium complex achieved so far is $[Os(\eta^6\text{-bip})(Azpy\text{-}NMe_2)I]PF_6$ which was selected and screened by NCI. Its IC_{50} value is 60 nM (mean value for 60 cell lines). Following the SARs, one osmium complex can be proposed to have even better anticancer activity (Fig. 7.1A). For comparison, its iminopyridine analogue and phenyldiazenyl benzothiazole[2] analogues should be investigated as well (Fig. 7.1).

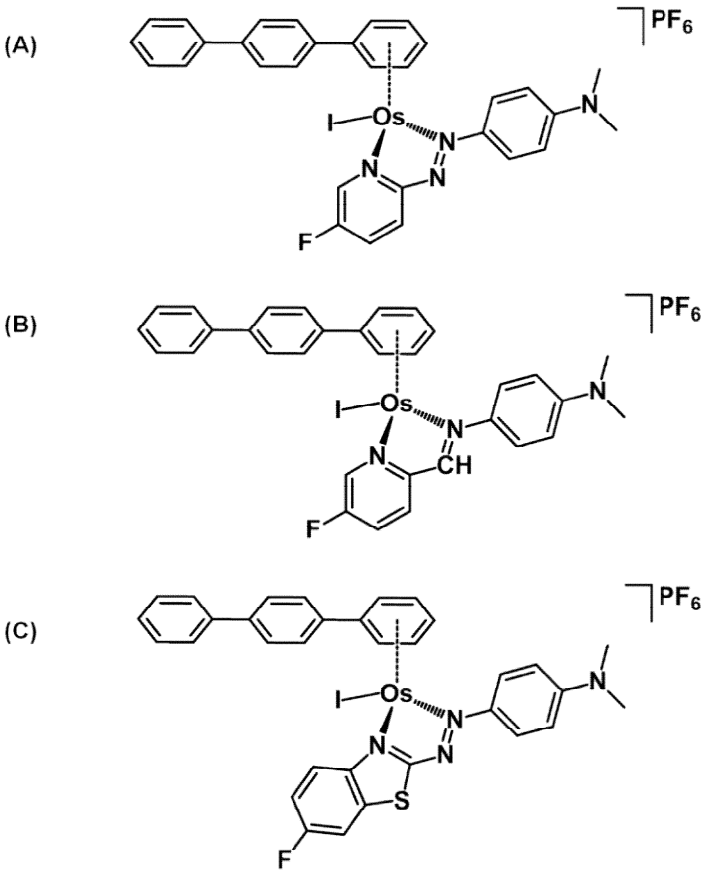

Figure 7.1. Osmium azopyridine (A), iminopyridine (B) and phenyldiazenyl benzothiazole (C) complexes which may obtain improved anticancer activity based on the knowledge of SARs.

7.3 Separation of Enantiomers of Osmium Anticancer Complexes

The most common chiral centre is carbon, however, it is notable that a chiral osmium centre is created when four non-identical atoms or groups are attached to osmium. The two osmium complexes with non-superimposable mirror-image structures are called enantiomers. In Chapter 5, it was found that two enantiomers of osmium arene iminopyridine complex exist in ca 1:1 ratio (a racemic misture). The requirement of resolving chiral racemic mixtures for drugs is compulsory after the thalidomide tragedy.[3] Thalidomide, (+)(R)-thalidomide in the racemic mixtures is the effective pharmaceutical part, is a sedative drug mainly used by pregnant women. However, thalidomide can cause a notorious dysmelia (stunted limb growth) side effect in humans due to the (-)(S)-thalidomide component in the racemic mixtures (Fig. 7.2).[3]

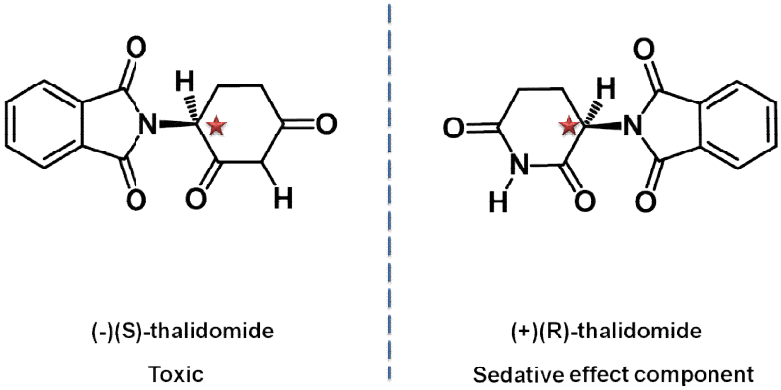

Figure 7.2. Structures of the enantiomers of thalidomide (the chiral carbon centre is labelled with red star).

There are mainly two types of methods commonly used for the separation of chiral drugs: (1) fractional crystallization (2) chromatography on a chiral column. In Chapter 6, one possible simple way of synthesizing and purifying chiral pure osmium arene anticancer complexes was demonstrated by crystallization. However, that method was based on useing a chiral ligand, and is not generally applicable to osmium arene enantiomers. In that, there is an unmet need to purify the osmium complexes which are already been made and proven to show good anticancer activities as racemic mixtures. A preliminary chiral purification

screening has been carried out by CHIRAL TECHNOLOGIES EUROPE in France on FY026. Three types of chiral column were screened. CHIRALPAC-IC was found to be the most suitable chiral column for FY026 that giving the best separation; it also suggested that CHIRALPAK-IC might be the most suitable chiral separation column for osmium arene iodido azopyridine complexes (Fig. 7.3).

CHIRALPAK® IC (250mmL x 4.6 ID)

Eluent:	n-Heptane/Ethanol/TEA/TFA 50:50:0.5:0.3
Flow Rate:	1.0mL/min
Temperature:	25°C
Sample solution:	~ 1mg/mL in EtOH/MeOH 50:50

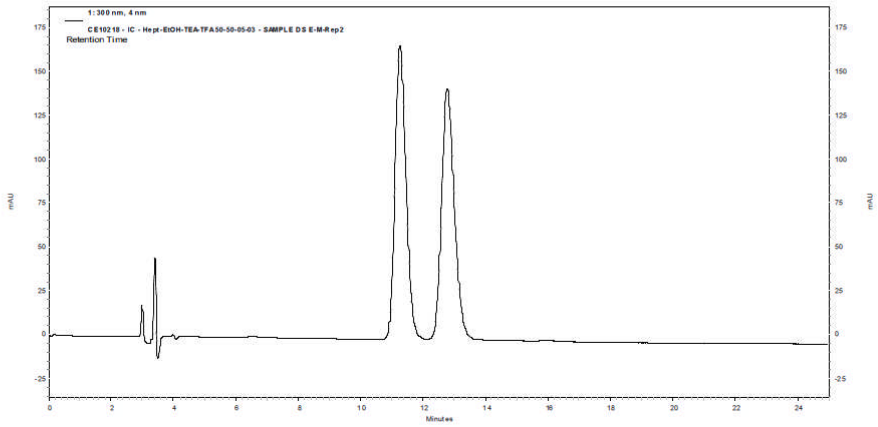

Figure 7.3. Separation of enantiomers of [Os(η^6-*p*-cym)(Azpy-NMe_2)I]PF_6 **(FY026)**.

7.4 Polymerization of Tubulin as Anticancer Target

In Chapter 4, a surprising inhibition of tubulin polymerization by osmium iodido azopyridine complexes was identified which may involve the mechanism of action. Investigations of the tubulin binding site of osmium complexes should be continued by competitions study with known microtubule inhibitors. (eg. vinca alkaloid). However, the anticancer activity was not improved along with the increase of effect on inhibition of tubulin polymerization. Therefore, a possible second mechanism of action is likely to be involved (section 4.3.9). Other than G_2/M phase cell cycle arrest which is possibly induced by inhibition of tubulin

polymerization, S phase cell cycle arrest was also observed (section 4.3.10), it indicated a DNA damage response. Further work should be done to investigate whether DNA damage is also involved in the mechanism of action. Since the osmium iodide azopyridine complexes cannot create a binding site by hydrolysis, the potential interaction with DNA is possibly through the intercalation of the aromatic arene or the chelating azopyridine ligand.

7.5 Mechanism of Catalytic Reaction with NADH

In Chapter 5, the osmium iminopyridine complexes were found to oxidize NADH catalytically. The mechanism appears to be novel and involves oxygen. To elucidate the mechanism of action, more work should be done including detecting the intermediate product during the catalytic reaction with NADH. From the proposed mechanism (Chart 7.1), H_2O_2 can form as a product, so further tests should be done to detect H_2O_2. Consider the instability of H_2O_2, a very sensitive enzyme detection kit (Hydrogen Peroxide Assay Kit, Biovision, USA) was tried initially for H_2O_2 detection. This involves of action of horse radish peroxidase (HRP), substrate in the presence of H_2O_2 can produce a coloured (λmax = 570 nm) and red-fluorescent (Ex/Em = 535/587 nm) product.

Chart 7.1. Proposed catalytic mechanism for the oxidation of NADH to NAD^+.

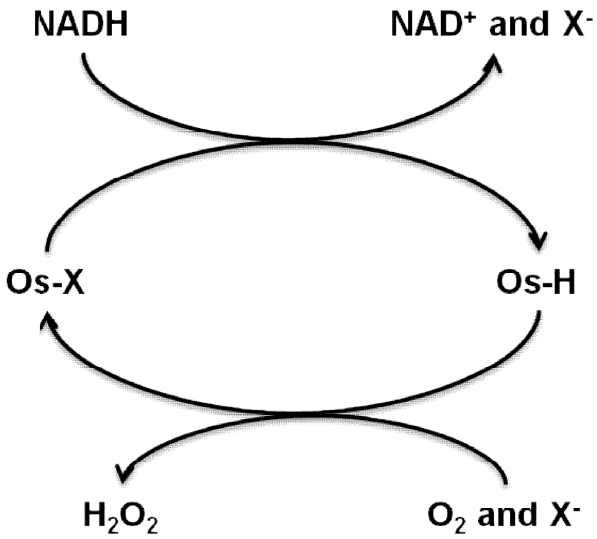

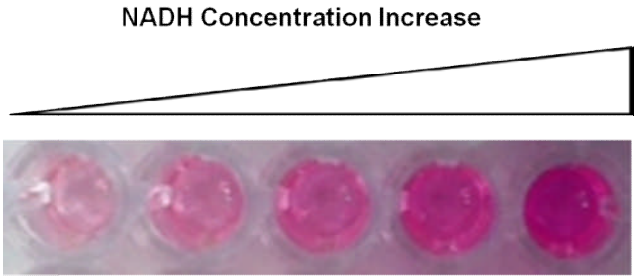

Fig. 7.4. NADH Instability under the hydrogen peroxide assay.

The negative controls were examined firstly: different concentrations of NADH alone at 0.1, 0.2, 0.4, 0.8 and 1.6 mM were incubated for 1h at 310K, then the H_2O_2 detection assay was performed following the protocol for the kit. The increasing red colour with a concentration dependent manner indicated that the NADH was not to be stable under the conditions of this enzyme assay (Fig 7.4). It might due to the organic solvent (DMSO) used in the assay. In order to avoid the similar affect introduced by detecting agents, electrode detection of H_2O_2 can be employed based on using a conventional platinum microelectrode, though the sensitivity of this method is relatively low: 0.05 mM.[4] The ability of transfer hydride can also be extended to catalyze imine reduction as well; it makes a possibility to explore the capability of becoming hydrogen transfer catalysts for osmium iminopyridine complexes. Further work should be done to explore the hydrogen transfer efficiency to different imine subtracts.

7.6 Tetranuclear Osmium Azopyridine Complexes

This work was encouraged by work on macrocyclic polynuclear platinum complexes from Fujita`s group[5, 6] such as self-assembled platinum molecular square $[Pt(en)(4,4'\text{-dipyridyl})]_4$ which showed G-quadruplex binding selectivity[7] and anticancer activity.[8]

Self-assembly of both polynuclear platinum complexes and arene ruthenium polynuclear complexes with anticancer activity had received a lot of attention in recent years.[9-11] Early work from Therrien`s group established an interesting size dependence for the anticancer activity of ruthenium metalla-rectangles though the mechanism of action is not completely clear yet.[12] Later on, the osmium analogues were also found to show anticancer activity.[13] It should also be noted that the scarcity of such reports is striking in contrast to the relative abundance of papers on Pt-based[14] and Ru-Based[15] macromolecules.

Preliminary data showed that when the linker was changed from pyrazine to 4-4`-azopyridine, a 10-fold increase in anticancer activity was achieved (Fig. 7.5). Further investigations to uncover the mechanism of action should be carried out.

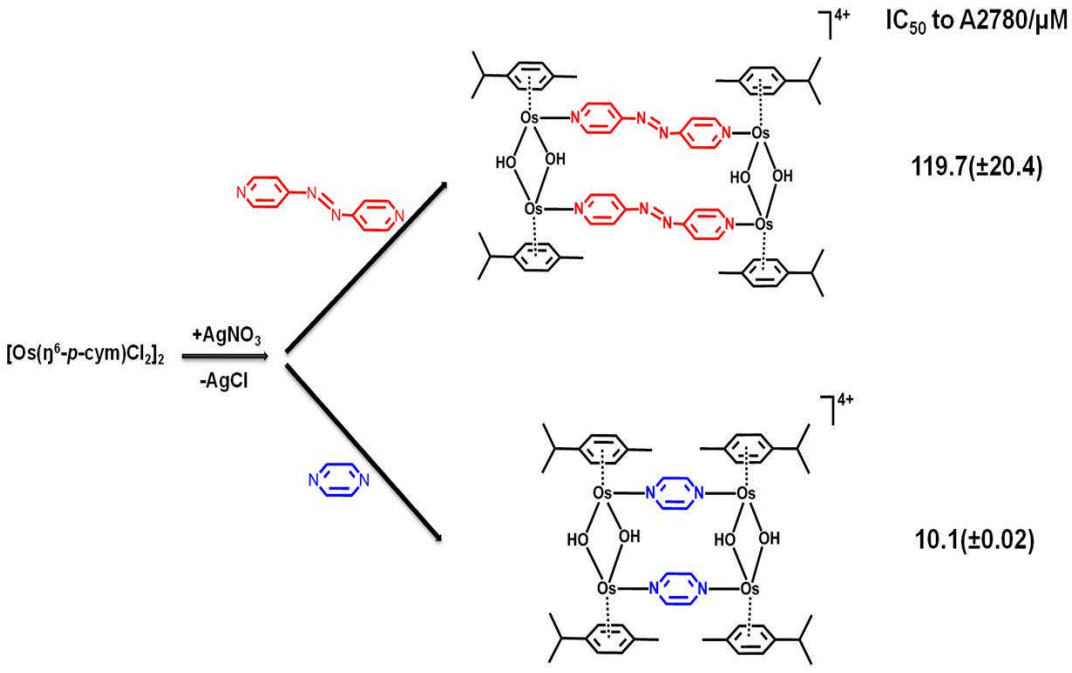

Figure 7.5. Synthetic routes for tetranuclear osmium complexes.

7.7 Osmium Complexes for Photodynamic Therapy

Ruthenium and osmium polypyridyl complexes have demonstrated interesting photophysical properties[16, 17] which can be employed for anticancer treatment.

Two types of photochemistry can be expected. (1) Photo-substitution of a ligand by a biomolecule such as a nucleobase; this type of photochemistry can be developed for photoactivated chemotherapy (PACT)[18-21] which has recently been highlighted.[21, 22] (2) Photo-redox processes with biomolecules such as DNA; complexes with this type of photochemistry have the potential to become candidates for photodynamic therapy[23] (PDT) which makes use of reactive oxygen species produced by excited photosensitizer.[24, 25]

The photochemical properties of osmium arene iodido complexes were investigated. Osmium compounds with biphenyl arene and iodide as ligands were found to undergo a arene dissociation after light irradiation. Photocatalysis of glutathione oxidation by the osmium derivative was also observed which indicated a production of ROS. A further work should be done to study the improvement of anticancer activity under light irradiation. The mechanism of action was proposed below in Figure 7.6.

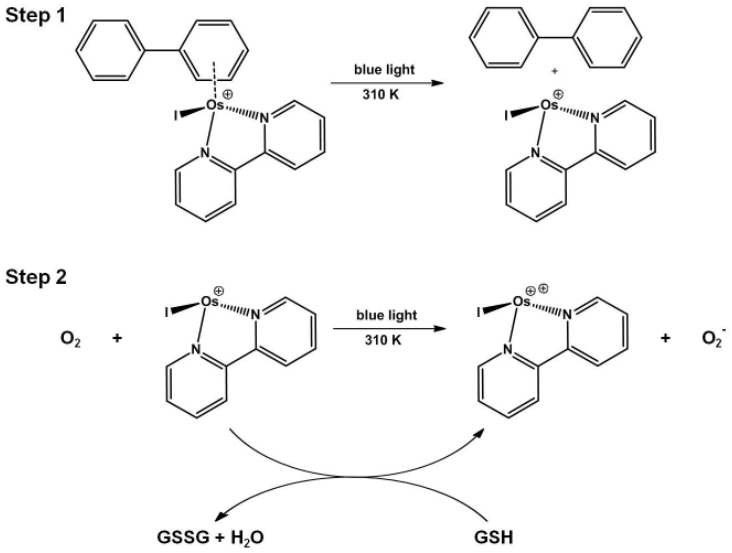

Figure 7.6. Proposed mechanism for the oxidation of GSH by osmium (II) arene iodido complexes in the presence of oxygen.

7.8 References

1. C. Lu, P. Li, R. Gallegos, V. Uttamsingh, C. Q. Xia, G. T. Miwa, S. K. Balani and L.-S. Gan, *Drug Metab. Dispos.*, 2006, **34**, 1600-1605.
2. K. Matsumura, M. Ono, S. Hayashi, H. Kimura, Y. Okamoto, M. Ihara, R. Takahashi, H. Mori and H. Saji, *MedChemComm*, 2011, **2**, 596-600.
3. R. J. D'Amato, M. S. Loughnan, E. Flynn and J. Folkman, *Proc. Natl. Acad. Sci. U. S. A.*, 1994, **91**, 4082-4085.
4. S. A. G. Evans, J. M. Elliott, L. M. Andrews, P. N. Bartlett, P. J. Doyle and G. Denuault, *Anal. Chem.*, 2002, **74**, 1322-1326.
5. M. Fujita, J. Yazaki and K. Ogura, *J. Am. Chem. Soc.*, 1990, **112**, 5645-5647.
6. M. Fujita, M. Tominaga, A. Hori and B. Therrien, *Acc. Chem. Res.*, 2005, **38**, 369-378.
7. R. Kieltyka, P. Englebienne, J. Fakhoury, C. Autexier, N. Moitessier and H. F. Sleiman, *J. Am. Chem. Soc.*, 2008, **130**, 10040-10041.
8. M. Mounir, J. Lorenzo, M. Ferrer, M. J. Prieto, O. Rossell, F. X. Avilès and V. Moreno, *J. Inorg. Biochem.*, 2007, **101**, 660-666.
9. F. Schmitt, P. Govindaswamy, G. Süss-Fink, W. H. Ang, P. J. Dyson, L. Juillerat-Jeanneret and B. Therrien, *J. Med. Chem.*, 2008, **51**, 1811-1816.
10. V. Vajpayee, Y. J. Yang, S. C. Kang, H. Kim, I. S. Kim, M. Wang, P. J. Stang and K.-W. Chi, *Chem. Commun.*, 2011, **47**, 5184-5186.
11. F. T. Linares, M. A. Galindo, S. Galli, M. A. Romero, J. A. R. Navarro and E. Barea, *Inorg. Chem.*, 2009, **48**, 7413-7420.
12. J. Mattsson, P. Govindaswamy, A. K. Renfrew, P. J. Dyson, P. Štěpnička, G. Süss-Fink and B. Therrien, *Organometallics*, 2009, **28**, 4350-4357.
13. N. P. E. Barry, F. Edafe, P. J. Dyson and B. Therrien, *Dalton Trans.*, 2010, **39**, 2816-2820.

14. J. Zehnulova, J. Kasparkova, N. Farrell and V. Brabec, *J. Biol. Chem.*, 2001, **276**, 22191-22199.
15. B. Therrien, G. Süss-Fink, P. Govindaswamy, A. K. Renfrew and P. J. Dyson, *Angew. Chem., Int. Ed.*, 2008, **47**, 3773-3776.
16. H.-J. Yu, H. Chao, L. Jiang, L.-Y. Li, S.-M. Huang and L.-N. Ji, *Inorg. Chem. Commun.*, 2008, **11**, 553-556.
17. S. Dhar, D. Senapati, P. K. Das, P. Chattopadhyay, M. Nethaji and A. R. Chakravarty, *J. Am. Chem. Soc.*, 2003, **125**, 12118-12124.
18. R. R. Allison, G. H. Downie, R. Cuenca, X.-H. Hu, C. J. H. Childs and C. H. Sibata, *Photodiagnosis Photodyn. Ther*., 2004, **1**, 27-42.
19. D. Kessel, *Photodiagnosis Photodyn. Ther*., 2004, **1**, 3-7.
20. R. R. Allison, H. C. Mota and C. H. Sibata, *Photodiagnosis Photodyn. Ther*., 2004, **1**, 263-277.
21. N. J. Farrer, L. Salassa and P. J. Sadler, *Dalton Trans.*, 2009, 10690-10701.
22. C. Moucheron, A. Kirsch-De Mesmaeker and J. M. Kelly, *J. Photochem. Photobiol. B.*, 1997, **40**, 91-106.
23. S. B. Brown, E. A. Brown and I. Walker, *Lancet Oncol.*, 2004, **5**, 497-508.
24. A. A. Holder, D. F. Zigler, M. T. Tarrago-Trani, B. Storrie and K. J. Brewer, *Inorg. Chem*., 2007, **46**, 4760-4762.
25. S.-W. Lai, Q. K. W. Chan, N. Zhu and C.-M. Che, *Inorg. Chem*., 2007, **46**, 11003-11016.

Appendix:

Summary of 4 classes of osmium complexes with different chelating ligands (azopyridine-R, R-azopyridine, Iminopyridine and Chiral Iminopyridine) in this thesis, this table is made according to the observation for the tested osmium iodido complexes within this thesis. (N/A= not avaialbe)

	Azopyridine-R	R-azopyridine	Iminopyridine	Chiral Iminopyridine
Hydrolysis	No	No	Yes	No
Binding with 9-EtG	No	No	Yes	N/A
Catalytically Oxidize NADH	No	N/A	Yes	No
Catalytically Oxidize GSH	No	N/A	No	N/A
Prevent Polymerisation of Tubulin	Yes	Yes	No	No
Effect of NAC on Anticancer Activity	Decrease	Decrease	N/A	N/A
Effect of L-BSO on Anticancer Activity	Increase	Decrease	Increase	N/A